NOVA SCHOOL OF SCIENCE & TECHNOLOGY

DEPARTMENT OF CHEMISTRY

DEVELOPMENT OF CHITOSAN BIONANOCOMPOSITES REINFORCED WITH NANOCELLULOSE EXTRACTED FROM ENERGY CROPS

CHARACTERIZATION AND APPLICATION AS ACTIVE PACKAGING

JOÃO RICARDO AFONSO PIRES

Master in Food Technology and Safety

DOCTORATE IN BIOENERGY

NOVA University Lisbon

July, 2023

DEPARTMENT OF
CHEMISTRY

DEVELOPMENT OF CHITOSAN BIONANOCOMPOSITES REINFORCED WITH NANOCELLULOSE EXTRACTED FROM ENERGY CROPS

CHARACTERIZATION AND APPLICATION AS ACTIVE PACKAGING

JOÃO RICARDO AFONSO PIRES

Master in Food Technology and Safety

Adviser: Ana Luísa Almaça da Cruz Fernando
Associate Professor, FCT-NOVA University Lisbon

Co-advisers: Maria Helena Figueiredo Godinho
Associate Professor with Aggregation, FCT-NOVA University Lisbon

Victor Gomes Lauriano de Souza
Researcher, International Iberian Nanotechnology Laboratory

Examination Committee:

Chair: Eurico José da Silva Cabrita,
Full Professor, FCT-NOVA University Lisbon

Rapporteurs: Ana Vera Alves Machado Nóbrega,
Associate Professor with Aggregation, Minho University

Vítor Manuel Delgado Alves,
Assistant Professor, ISA-Lisbon University

Adviser: Ana Luísa Almaça da Cruz Fernando
Associate Professor, FCT-NOVA University Lisbon

Members: Dilpreet Bajwa,
Full Professor, Montana State University

Ana Teresa Sanches Silva,
Assistant Professor, Coimbra University

Eurico José da Silva Cabrita,
Full Professor, FCT-NOVA University Lisbon

Isabel Maria Rôla Coelhoso,
Associate Professor, FCT-NOVA University Lisbon

Maria Margarida Boavida Pontes Gonçalves,
Associate Professor, FCT-NOVA University Lisbon

Miguel Ângelo Parente Ribeiro Cerqueira,
Researcher, International Iberian Nanotechnology Laboratory

DOCTORATE IN BIOENERGY

NOVA University Lisbon
July, 2023

Development of Chitosan Bionanocomposites Reinforced with Nanocellulose Extracted from Energy Crops - Characterization and Application as Active Packaging

Dedicated to my family.

ACKNOWLEDGMENTS

The realization of this doctoral thesis is due to all the people and institutions that believed in me and supported this project, which I name below.

First of all, to my teacher, advisor and friend, Professor Ana Luísa Fernando, for accompanying my growth from the beginning of my master's degree to the end of my doctorate. Thank you very much for all the knowledge transmitted both in teaching and in work methodologies and for having believed in my abilities from the first moment. And of course, for allowing me to travel and make contacts in the scientific world with people of excellence. I would also like to thank my co-advisors, Doctor Victor Souza, who, in addition to being an advisor, was my laboratory companion and a friend always available to help me whenever I had doubts, and Professor Doctor Maria Helena Godinho, who promptly accepted the invitation to help in the realization of this thesis, making itself available to provide essential equipment and laboratory conditions for conducting many laboratory assays. Thank you very much and I know I still have a lot to learn about bioenergy, energy crops, food packaging, materials science and of course nanocellulose from you.

Thanks to "FCT - Fundação para a Ciência e a Tecnologia" for granting me a PhD scholarship, without this financial support it would be practically impossible to achieve this dream. Thanks to "NOVA School of Science and Technology", my home in the last decade, and to the two research centers that supported my candidature for the FCT doctoral scholarship. Thanks to "Metrics" through its president, Professor Doctor José Carlos Teixeira, and to "Cenimat - I3N" through its president, Professor Doctor Rodrigo Martins. I would also like to give a special appreciation to all the professors who helped with their knowledge or willingness to contribute to this work, Professor Doctor Nuno Lapa, Professor Doctor Paula Duarte, Professor Doctor Margarida Gonçalves, Professor Doctor Benilde Mendes, Professor Doctor Isabel Coelhoso. I also carry in my heart three fantastic ladies who help always run the laboratory and the department that I was present, Dona Lurdes, Dona Rita, and Dona Rosa.

While conducting this doctoral work, I was faced with many moments of frustration, anxiety, and stress, difficult to overcome. Fortunately, I was incredibly lucky to have by my side people who were there with friendship, helping me to surpass these less enjoyable moments. Leandro Gomes, a great Brazilian fellow, I hope future Portuguese, and citizen of the world, we shared so many moments in that office over these 5 years, thank you for having been there with me on so many crazy adventures. I wish you the best, whatever the part of the world and laboratory you may be in. Carolina Rodrigues, a companion, and a special friend since the first year of the master's, with many hours, shared in classes, work, and laboratory. And of course, my coffee partner Catarina Nobre, who taught me so much about the life of a Ph.D. student, and a nerd like me, is always available to discuss the hottest topics in pop culture. Many thanks to everyone else who shared laboratory and office moments with me during this time. Also, a big thanks to all the students that I had the pleasure of guiding or helping in the development of their bachelor's and master's work.

Finally, I dedicate this doctoral work to all my family and close friends who put up with my bad temper at certain points in the thesis. A special thanks to my father Ilídio and my mother Liliana for all the values transmitted and for always supporting me unconditionally in all aspects of my life. To my brothers Diogo and Beatriz who are also finishing their first university adventures, which I hope to be an inspiration for them. To my grandmother Maria and my late grandparents Manuel, José, and Lisete for always giving me their all, you are always present in my memory. Last but not least, to my girlfriend, friend, and companion Rute Cardoso, who with her joy and constant optimism helps me every day to strive for more and to be a better person. I love you all very much and I hope you are proud of me.

"There is plenty of room at the bottom." (Richard P. Feynman).

ABSTRACT

The renewable and biodegradable materials are crucial in combating the environmental impacts of fossil-based products. Lignocellulosic feedstocks, abundant in cellulose, hemicellulose, and lignin, can yield valuable products. Cellulose Nanocrystals (CNCs) exemplify bioproducts with diverse applications. Moreover, incorporating CNCs into chitosan (Ch) films presents a promising approach to enhance bioplastics.

This doctoral thesis focuses on developing a high-value bionanocomposite for fully biodegradable and active food packaging, contributing to the circular economy. Firstly, Cellulose was sustainably isolated from three lignocellulosic biomasses (*Miscanthus* × *giganteus* Greef et Deuter, *Arundo donax* L., and *Hibiscus cannabinus* L.) and converted into CNCs through acid hydrolysis. The CNCs exhibited a rod-like shape but formed strong aggregates, hindering individual observation and aspect ratio quantification due to less effective dispersion. The second phase involved incorporating CNCs into chitosan bio-based films to determine the optimal formulation. The nanocellulose significantly improved the film's mechanical, thermal, and barrier properties, as well as U.V. light resistance, without altering color and opacity. Bionanocomposites with 2.5% CNCs from any biomass showed the best overall properties. In the final stage, the optimized bionanocomposites were used for active food packaging, with novel formulations incorporating salvia essential oil (SEO) to enhance antimicrobial and antioxidant activities. The results demonstrated reduced microbiological degradation and lipid oxidation in meat packaged with bionanocomposites compared to unpackaged meat. However, the addition of SEO did not significantly improve the bionanocomposites' active properties as expected. The "*in vitro*" migration tests suggested that CNCs entrapped the phenolic compounds, resulting in decreased migration of SEO active compounds from the packaging. In conclusion, this thesis successfully demonstrated the potential of reusing lignocellulosic biomass to isolate and convert cellulose into nanocellulose. Incorporating CNCs into chitosan films yielded functional, renewable, and biodegradable bionanocomposites with active properties, offering a sustainable alternative to traditional fossil-based plastic food packaging.

Keywords: Energy Crops, Nanocellulose, Chitosan, Bionanocomposite, Salvia Essential Oil, Food Packaging

RESUMO

Os materiais renováveis e biodegradáveis são cruciais no combate aos impactos ambientais associados aos produtos de origem fóssil. As matérias-primas lenhocelulósicas, abundantes em celulose, hemicelulose e lenhina, podem produzir produtos de valor acrescentado. Os nanocristais de celulose (CNCs) exemplificam bioprodutos com diversas aplicações. Além disso, a incorporação de CNCs em filmes de quitosano (Ch) representa uma abordagem promissora para melhorar as propriedades dos bioplásticos.

Esta tese de doutoramento foca-se no desenvolvimento de um bionanocompósito para embalagens de alimentos totalmente biodegradável e ativo, contribuindo para a economia circular. Primeiramente, a celulose foi isolada de forma sustentável de três biomassas lenhocelulósicas (*Miscanthus* × *giganteus* Greef et Deuter, *Arundo donax* L. e *Hibiscus cannabinus* L.) e convertida em CNCs por meio de hidrólise ácida. Os CNCs exibiram uma forma de bastão, mas formaram agregados fortes, dificultando a observação individual e a quantificação da razão de aspecto devido à dispersão menos efetiva. A segunda fase envolveu a incorporação de CNCs em filmes de quitosano para determinar a formulação ideal. A nanocelulose melhorou significativamente as propriedades mecânicas, térmicas e de barreira do filme, bem como a proteção UV, resistência à luz, sem alterar a sua cor e a opacidade. Os bionanocompósitos com 2.5 % de CNCs de qualquer biomassa apresentaram as melhores propriedades. Na etapa final, os bionanocompósitos otimizados foram usados para embalagens ativas de alimentos, com novas formulações incorporando óleo essencial de sálvia (SEO) para aumentar as atividades antimicrobianas e antioxidantes. Os resultados demonstraram degradação microbiológica e oxidação lipídica reduzida em carne embalada em comparação com a carne não embalada. No entanto, a adição de SEO não melhorou significativamente as propriedades ativas dos bionanocompósitos como era esperado. Os testes de migração "*in vitro*" sugeriram que os CNCs aprisionaram os compostos fenólicos, resultando numa diminuição da migração de compostos ativos do óleo. Em conclusão, esta tese demonstrou com sucesso o potencial de reutilização de biomassa lignocelulósica para isolar e converter celulose em nanocelulose. A incorporação de

CNCs em filmes de quitosano produziu bionanocompósitos funcionais, renováveis e biodegradáveis com propriedades ativas, oferecendo uma alternativa sustentável às tradicionais embalagens plásticas de alimentos de origem fóssil.

Palavras chave: Culturas Energéticas, Nanocelulose, Quitosano, Biocompósito, Óleo Essencial de Sálvia, Embalagem Alimentar

CONTENTS

LIST OF FIGURES

LIST OF TABLES

ACRONYMS

AFM	Atomic Force Microscopy.
AOAC	Association of Official Analytical Chemists.
ASTM	American Society for Testing and Materials.
ATR	Attenuated Total Reflectance.
BF	Bleached Fiber.
BNCs	Bacterial Nanocellulose.
CFU	Colony Forming Units.
Ch	Chitosan.
CI	Cristallinity Index.
CK	Creatine Kinase
CMC	Carboxymethyl Cellulose.
CNFs	Cellulose Nanofibers.
CNCs	Cellulose Nanocrystals.
CNCC	Commercial Cellulose Nanocrystals.
CNWs	Cellulose Nanowhiskers.
CSA	Canadian Standards Association.
DD	Degree of Deacetylation.
DNA	Deoxyribonucleic Acid.
DPPH	2,2-Diphenyl-1-picrylhydrazyl.

DSC	Differential Scanning Calorimetry.
DTG	Derivative Thermogravimetric Curve (DTG).
EAB	Elongation at Break.
EM	Elastic Modulus.
EO	Essential Oil
EU	European Union.
FCT	Faculdade de Ciência e Tecnologia/ NOVA School of Science and Technology.
FDA	Food and Drug Administration.
FFD	Film-Forming Dispersion.
FTIR	Fourier-Transform Infrared Spectroscopy.
GAE	Gallic Acid Equivalent.
GEO	Ginger Essential Oil.
GHG	Greenhouse Gases.
G	Giant Reed.
GRAS	Generally Recognized As Safe.
HDPE	High-Density Polyethylene.
ICDD	International Centre for Diffraction Data.
ILs	Ionic Liquids.
ILUC	Indirect Land-use Change.
ISO	International Organization for Standardization.
K	Kenaf.
LCC	Lignin–Carbohydrate Complexes.
M	Miscanthus.
MCCs	Microcrystalline Cellulose.
MDA	Malondialdehyde.
mRNA	Messenger Ribonucleic Acid.

MW	Molecular Weight.
NC	Nanocellulose.
OP	Oxygen Permeability.
PCA	Plate Count Agar.
PET	Polyethylene Terephthalate.
PHA	Polyhydroxyalkanoate.
PHB	Polyhydroxybutyrate.
PLA	Polylactic Acid.
POM	Polarized Optical Microscopy.
PVA	Polyvinyl Alcohol.
REO	Rosemary Essential Oil.
RF	Raw Fiber.
RH	Relative Humidity.
RTILs	Room Temperature Ionic Liquids.
SEM	Scanning Electron Microscopy.
SDGs	Sustainable Development Goals.
TAPPI	Technical Association of the Pulp and Paper Industry.
TBA	2-Thiobarbituric Acid.
TBARS	Thiobarbituric Acid Reactive Substances.
TCA	Trichloroacetic Acid.
TEM	Transmission Electron Microscopy.
TEP	1,1,3,3-Tetraethoxypropane.
Tg	Glass Transition Temperature.
TG	Thermogravimetric Curve.
TGA	Thermogravimetric Analysis.
Tm	Melting Point.
TMAM	Total Mesophilic Aerobic Microorganism.

TOCNFs	TEMPO-Oxidized Cellulose Nanofibers.
TPA	Total Pro-Oxidant Activity.
TPAM	Total Psychrotropic Aerobic Microorganism.
TPC	Total Phenolic Content.
TS	Tensile Strength.
TSA	Trypto-Casein Soy Agar.
TSB	Trypto-Casein Soy Broth.
TVB-N	Total Volatile Basic Nitrogen.
UN	United Nations.
UNL	Universidade Nova de Lisboa.
VIS	Visible Light.
VRBG	Violet Red Bile Glucose.
WCA	Water Contact Angle.
WVP	Water Vapor Permeability.
XRD	X-ray Diffraction.

1

INTRODUCTION

The excellent structural properties attributed to fossil-based plastics highlight them as an indispensable material that serves as a packaging foundation for several daily life products, securing the correct functioning of the global food system and associated value chains. However, their non-biodegradability and massive use have turned them into an acute universal dilemma that needs to be addressed. The packaging market is expected to grow following the increasing population trend in urban areas and the consequent demand for convenience foods. Unfortunately, this key sector will continue to generate millions of tons of plastic waste that will accumulate in ecosystems (Otoni et al., 2021; Sundqvist-Andberg and Åkerman, 2021). Furthermore, the continuous production of this fossil-based material is directly connected with the emission of greenhouse gases (GHG) into the atmosphere, contributing to accelerate global warming (Lau et al., 2020). The environmental problems associated with packaging become more accentuated due to the brief lifespan of single-use plastics, often discarded in inappropriate places outside the waste or recycling streams (Walker and Rothman, 2020). The majority of this non-reusable packaging is disposed of in landfills or incineration centers, with only a minor part being recovered through recycling. Inevitably, a large amount ends up reaching different aquatic ecosystems, which, through degradation processes, will be transformed into harmful micro or nanometer-size particles capable of infiltrating and contaminating the entire food chain (Rosenboom et al., 2022).

Societies must become more sustainable to prevent future environmental crises. In this sense, governments and civic institutions are responsible for adopting green policies to reduce the problems that fossil resources induce on the environment (García et al., 2016). Consumers also need to change their behavior in relation to plastic consumption, and the paramount attitude should be to follow the fundamental rule of the three R's (reduce, reuse and recycle)

(Emadian et al., 2017; Thakur et al., 2018). In 2019, European Union (EU) published the directive on single-use plastics to encourage the paradigm shift. Supported by the circular economy principles, this document proposed measures to drastically reduce the amount of plastic in products sold on the market (EU, 2019). However, the intention to eradicate plastic from food packaging is still controversial, as, over time, it can develop problems along the food chain, mainly in terms of food loss (Sundqvist-Andberg and Åkerman, 2021). Therefore, replacing non-biodegradable plastics with novel sustainable, functional alternatives made from renewable resources represents a significant opportunity to reduce the packaging's ecological footprint (Zhu et al., 2016).

The bio-based plastics/polymers, recurrently expressed in literature as bioplastics/biopolymers, have recently been appointed as one attractive solution to replace petroleum-based plastics. These are extracted from renewable resources found in nature in abundance at accessible prices. Moreover, these present superior biodegradation and composting rates and own reduced or non-toxicity (Pires et al., 2022a; Souza & Fernando, 2016). The first-generation bioplastics, like polylactic acid (PLA), are obtained from crop-based agricultural feedstocks, usually valuable in carbohydrates, like corn. Currently, these are in a stage of advanced technological maturity with a growing market expression, thus proving to represent a viable alternative to satisfy the future demands of the food packaging industry (Otoni et al., 2021). Notwithstanding bioplastics exhibiting beneficial features for the environment, like being biodegradable and renewable, this is not strictly synonymous with sustainability. Nowadays, the amount of arable land dedicated to growth feedstock for bioplastics only corresponds to 0.02 % of the global agricultural area, however, it follows a rising trend, which could step into ethical conflict with food cultivation and the use of drinkable water (Rosenboom et al., 2022; Sundqvist-Andberg and Åkerman, 2021). One solution may presuppose the upcycling of non-edible biomass from numerous agricultural and industrial activities, hitherto considered waste, to subsidize the production of novel second-generation biopolymers (Brigham, 2018; Karan et al., 2019; J.R.A. Pires et al., 2019b).

Chitin represents one primary constituent of the marine arthropods' exoskeleton, equally known as crustaceous. This bioresource can be widely extracted from the seafood industry waste, standing out as an economically competitive and commercially available by-product. Through chitin deacetylation, a cationic polysaccharide denominated as chitosan is originated (Flórez et al., 2022; Pires et al., 2018). This biocompatible and non-toxic polymer becomes soluble in slightly acidic environments (below its pKa ~ 6.3), formulating a viscous

solution that allows the development of films/coatings with intrinsic antimicrobial and antioxidant properties (Kumar et al., 2020). Therefore, chitosan is appraised as one of the most promising renewable materials to incorporate in active/intelligent food packaging by enriching food quality and safety, extending the food shelf-life (Irastorza et al., 2021; Souza et al., 2020b). In terms of functionality, the chitosan well-ordered matrix arrangement grants an effective barrier to oxygen. In contrast, like many other polysaccharides, these possess a hydrophilic nature resulting in unfavorable water vapor barrier properties, constituting a disadvantage in conserving perishable food products (Pires et al., 2021). To match the excellent mechanical, barrier, and thermal performance of non-biodegradable plastics, transforming the innovative biobased-packaging concept into objective reality, it is essential to optimize the chitosan properties. Among the strategies adopted to strengthen the chitosan (Ch) film composition, the introduction of nanofillers is one of the most prominent, creating a so-called bionanocomposite (Haghighi et al., 2020).

Lignocellulosic fibers are the most plentiful and renewable yet under-utilized bioresource in nature, being available in biomass from agricultural (straw, bark, shells, leaves, bagasse), forestry (hardwood and softwood), energy crops, and food-related industries. The amount of biomass generated annually is so substantial that even if the most part is employed for animal feed, organic fertilizer, or reused for bioenergy, the quantity considered waste remains quite accentuated (Koçar and Civa, 2013; Lee et al., 2014; Ravindran and Jaiswal, 2016). Cellulose is an inexhaustive source of raw materials that can be isolated from these lignocellulosic residues and posteriorly transformed, giving rise to a remarkable nanometer-scale biopolymer with highly ordered regions (Thomas et al., 2018). Nanocellulose is an organic filler that can be used to reinforce bio-based films (Corsello et al., 2017; Pires et al., 2022b; Salari et al., 2018; Yadav et al., 2020). Their surface is abundant in hydroxyl groups, allowing the chemical crosslinking with other polymers, like chitosan. Among its distinctive properties, these reinforcement agents own a high aspect ratio and significant levels of crystallinity. Therefore, an increase in the film´s functional properties is expected, even at low concentrations (Ahankari et al., 2021). Additionally, the cellulosic fillers offer fewer public health risks and are more eco-friendly than inorganic fillers since they are biodegradable, non-toxic, and extracted from several low-cost renewable lignocellulosic sources (Pires et al., 2019a). Accordingly, it is the right moment to upgrade the current technology/know-how to unlock unprecedented opportunities for biorefineries, favoring the conversion of agro-industrial waste into modern high-value bioproducts (Lee et al., 2014). In fact, besides the traditional bioenergetic purpose, taking

advantage of all crop parts that are not harvested increases biorefinery productivity and stimulates the achievement of some Sustainable Development Goals (SDGs) established for 2030 by the United Nations (UN) (UN, 2015). This purpose could be a relevant contribution to combat two critical ecological problems, the biomass overload in landfills and the dependency on fossil fuels (Souza & Fernando, 2016).

The introduction of essential oils (EO) or natural extracts in bio-based films is a novel strategy to be studied to increase the packaging antioxidant and antimicrobial activities and reduce the application of synthetic additives while increasing the food shelf life (Souza et al., 2017). The EO incorporation on the bionanocomposite instead of direct application on the food has as its core objective the controlled release to improve the stability of the active compounds and to prevent excessive oil absorption by the food that could cause harmful toxicological effects for the consumer. This technique also intends to avoid the transference of extreme odors and tastes that can negatively affect the food's organoleptic properties (Pateiro et al., 2021; Sharma et al., 2021). To our knowledge, little is known about the combined effect of CNCs as reinforcement and as encapsulation agents of natural antioxidant essential oils and the associated effect as active packaging to perishable food matrices. Therefore, the development of an active chitosan/nanocellulose bionanocomposite incorporated with essential oils is justified since it is a sustainable, convenient product that tends to add reliability and quality to the food while maintaining its safety and acceptable appearance for the consumer.

For the reasons presented, the specific objectives defined for this doctoral thesis are:

- Extract cellulose from lignocellulosic residues, optimizing the alkaline pre-treatment parameters and adapting an alternative fiber bleaching methodology to the use of chlorine;

- Convert the cellulose into nanocrystalline cellulose and evaluate its physical and chemical properties;

- Develop chitosan/nanocellulose (Ch + CNCs) bionanocomposites in the form of films and study the interaction between the biopolymer matrix and nanofiller, evaluating the relation structure/properties to determine the best reinforcement percentage;

- Evaluate the produced bionanocomposites structural, mechanical, thermal, barrier, and optical properties, as well as their morphology;

- Incorporate an essential oil into the bionanocomposites to increase its activity. Study the bionanocomposites, with and without EO, antioxidant and antimicrobial effectiveness in contact with fresh poultry meat, to extend the food shelf life.

Subsequently, this doctoral thesis contains one chapter dedicated to the thesis state of the art and one chapter detailing the methodology. Additionally, the thesis is complemented by three chapters of results and discussion, namely: (a) Chapter 4 – Isolation and characterization of nanocellulose extracted from energy crops; (b) Chapter 5 - Nanocellulose from energy crops as reinforcement agents in chitosan films; (c) Chapter 6 - Chitosan/nanocellulose bionanocomposite loaded with salvia essential oil as active packaging. During the development of this thesis, three state-of-the-art articles have already been published (Pires et al., 2019; Pires et al., 2022a, 2021). A research article corresponding to Chapter 4 has also been published (Pires et al., 2022b)and the articles related to Chapters 5 and 6 are in the process of being submitted for publication.

The stages projected for the development of this doctoral thesis are aligned with Sustainable Development with the United Nations Sustainable Development Goals (Agenda 2030) (UN, 2015): Goal 2. End hunger, achieve food security and improve nutrition and promote sustainable agriculture; Goal 12. Ensure sustainable consumption and production patterns; Goal 15. Protect, restore, and promote the sustainable use of terrestrial ecosystems, sustainably manage forests, combat desertification, halt and reverse land degradation and halt the loss of biodiversity.

2

STATE OF ART

2.1 From Biomass to Nanocellulose

2.1.1 Energy Crops: Advantages and Challenges

The interest in energy crops has increased globally due to their abundance, diversity, fast-growing, high yields, contribution to reducing CO_2 emissions, low cost, and potential to be grown productively on low-quality soils. Hence, these crops comprise a significant potential to meet the future worldwide energetic needs in a sustainable way (Fernando et al., 2018; Koçar and Civa, 2013). Introducing energy crops in non-arable fields represents a potential carbon-neutral, clean, and eco-friendly renewable alternative to traditional energy sources. Moreover, enables the growth and development of the agricultural and rural economies (Pandey et al., 2016; López-Bellido et al., 2014).

Different final products could be achieved depending on the crop species. Therefore, due to its polyvalence, it is not easy to divide the crops by categories (Koçar and Civa, 2013). Sims et al., (2006) proposed that energy crops should be divided into five categories: oil crops, cereals, starch and sugar crops, cellulose crops, and solid/dedicated energy crops (e.g., switchgrass (*Panicum virgatum* L.)). Although many crops may be used for energy purposes, that does not mean that all of them possess the requirements to be classified as suitable for bioenergy. To help distinguish these crops, Dubois, (2011) suggested a set of five criteria that crops should present to be able to produce biofuels sustainably: (i) Crops with rapid growth; (ii) High yield of usable biomass or seeds (maximum production of dry matter per hectare); (iii) Avoid competition with food crops; (iv) Ability to grow on poor soils and severe conditions; (v) High resistance for pests, diseases, and predators. Moreover, other characteristics are relevant to define an ideal energy crop, like low production cost, low energy input, low

nutrient requirement, and biomass should have low amounts of contaminants (Rahman et al., 2014). Miscanthus (*Miscanthus × giganteus* Greef et Deuter) (Clifton-Brown et al., 2004), jatropha (*Jatropha curcas* L.) (Makkar and Becker, 2009), giant reed (*Arundo donax* L.) (Mariani et al., 2010), cardoon (*Cynara cardunculus* L.) (Angelini et al., 2009), switchgrass(Gomes et al., 2022), kenaf (*Hibiscus cannabinus* L.) (Alexopoulou et al., 2013), and sorghum (*Sorghum bicolor* L. Moench) (Barbanti et al., 2006) are examples of feedstocks that showed promising results as energy crops.

Although large-scale energy crop plantations grant an excellent opportunity to reduce the dependence on non-renewable energy and materials, some inherent challenges deserve to be highlighted and optimized (Rahman et al., 2014). The growing demand for biomass will naturally increase the competition with food crops for available land, nutrient resources, and other inputs, threatening food security (Pandey et al., 2016; Fernando et al., 2018; López-Bellido et al., 2014). Furthermore, the effects of increasing biofuel production through the production of energy crops can drive undesired environmental and social impacts. If sustainability criteria are not followed properly, that could originate loss of habitats, dispersal of invasive species, potential shortages in the supply of fresh water, and pollution (López-Bellido et al., 2014). Additionally, energy crops like other agricultural and forestry crops, generate waste. These residues are mostly reused, by incorporating them into soils as a way to sustain the organic matter and prevent erosion, as a bed or feed to livestock, or as energy vectors (e.g., pellets) (García et al., 2016). Due to the vast amounts generated, lignocellulosic biomass reuse is not yet being properly leveraged. In fact, these biomass wastes from energy crops must be seen as raw materials with technological and economic potential. The cellulose extraction and subsequent CNCs production provide a viable solution, which goals to cut the amount of waste generated by the industry and simultaneously contribute to reducing the associated environmental impact (J.R.A. Pires et al., 2019b).

2.1.2 Lignocellulosic Biomass Structure

The lignocellulosic fiber is a complex biomaterial, mainly composed of three biopolymers: polymeric carbohydrates cellulose, hemicellulose, and aromatic polymeric lignin. In addition, other substances like ash, pectin, proteins, and extracts are fiber components. The quantity of each one varies according to factors like biomass origin or external conditions.

Therefore, it is crucial to perform a fiber characterization to plan the correct approach for CNCs extraction (Kim, 2018).

Cellulose is the most important, abundant, and renewable organic substance prevailing in the ecosystem, with an estimated annual production surpassing 7.5×10^{10} Mt. Furthermore, it is the most substantial component of lignocellulosic fibers, with variable content typically between 35–50 wt% (Brandt et al., 2013; Brinchi et al., 2013). Chemically, it is a high molecular weight homopolysaccharide with the empirical formula $(C_6H_{10}O_5)_n$ consisting of a linear chain of several hundred to many thousands of units of β (1–4) linked D-glucose, where every unit is corkscrewed 180° concerning its neighbors, thereby forming a cellobiose disaccharide repeating unit (figure 2.1) (Chen, 2014). The number of glucosidic units or average degree of polymerization ($\overline{DP}$) determines the cellulose properties. Cellulose has the highest $\overline{DP}$ among the biopolymers constituting lignocellulosic fibers, which can vary over a wide range of values, reaching up to 20,000 units or higher, depending on the cellulose source (Jonoobi et al., 2015; Klemm et al., 2018).

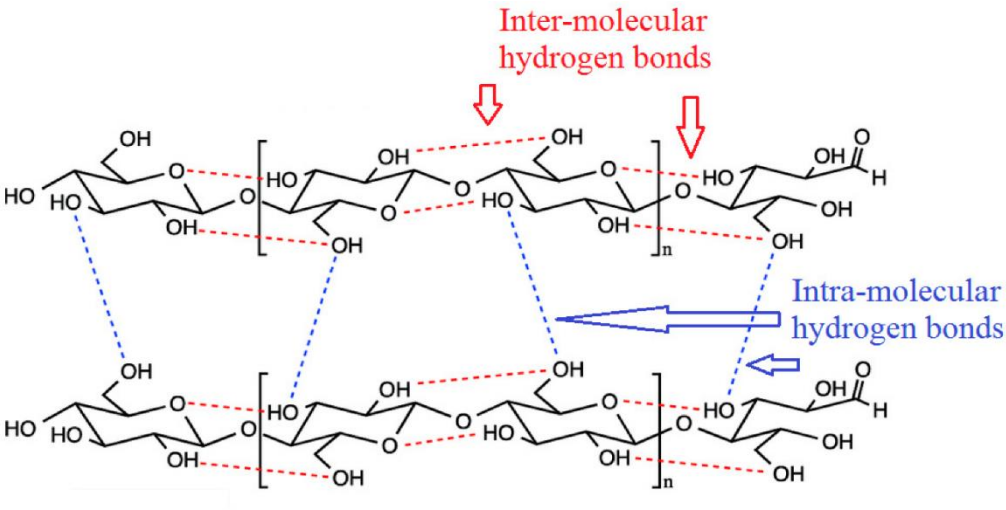

Figure 2.1— Cellulose structures. Adapted from Baghaei & Skrifvars, (2020).

The three free hydroxyl groups (−OH) located at C-2, C-3, and C-6 atoms per glucosidic unit can form hydrogen bonds with their nearest neighbors, fulfilling a significant role in crystalline packing (Brinchi et al., 2013; Khalil et al., 2014). These bonds influence the solubility and the physical properties of cellulose. Additionally, the hydrogen bond between cellulose chains makes it highly stable but poorly soluble in water and difficult to dissolve with common

organic solvents. Regardless of being a carbohydrate, it is not digested by the human body (Nascimento et al., 2018).

Cellulose from different plant sources can have different levels of purity, as well as varying levels of other components, thus, affecting the supramolecular structure of the cellulose, and leading to differences in the physical and chemical properties of the material. Similarly, the methods used for cellulose isolation can also affect its supramolecular structure. Different techniques can lead to changes in the degree of crystallinity and the size, and shape of the cellulose fibers. These differences can have significant implications for its processing and utilization, affecting its suitability for different applications and its performance in various industrial and commercial processes. As a result, understanding the factors that influence the supramolecular structure of cellulose is important for optimizing its use and developing new applications (Holtzapple, 2003; Yahya et al., 2015).

The differences are mainly due to the biosynthesis conditions, specific enzymatic terminal complexes, and chemical and physical configurations derived from the extraction procedures(J.R.A. Pires et al., 2019a). In nature, it typically appears in the native state as a crystalline form called "cellulose I". Besides the first type, three other cellulose configurations can be isolated through different pre-treatments, polymorphs II, III, and IV (Ravindran and Jaiswal, 2016). Due to the inter- and intramolecular hydrogen bonds cellulose molecules are organized into hierarchical structures that include microfibrils, conferring high levels of strength and stiffness per unit of weight, interspersed with less ordered domains called amorphous regions (Jonoobi et al., 2015). In its turn, the microfibrils arranged themselves in fibrils which sequentially make up the plant cell wall. This arrangement aids in the plant structure stabilization and suggests cellulose is a biomaterial with high strength and other superior mechanical properties (Brigham, 2018).

Depending on the direction, different forces rule the monoclinic crystalline unit aggregation, as stated in figure 2.2. In cellulose, the primary forces that govern the aggregation of the monoclinic crystal unit cells are hydrogen bonding, covalent bonding, and van der Waals forces. These intermolecular forces determine the arrangement of the cellulose chains in the crystal lattice and contribute to the stability of the crystal structure. Additionally, the orientation and packing of the cellulose chains also play a role in the overall crystal structure and its physical properties. Hydrogen bonds are medium-strength interactions (15 $kcal \cdot mol^{-1}$) and are located in the "a" direction in the cellulose structure. These occur between the hydrogen atom of one hydroxyl group in one glucose unit and an oxygen or nitrogen atom in another glucose

unit. The covalent bonds are the glycosidic linkages between the glucose monomers that follow the "b" direction, providing the strong foundation (50 kcal·mol^{-1}) for the structure of cellulose and making it one of the strongest (tensile strength of cellulose fibers can reach up to 1500 MPa) natural polymers. These linkages are formed between the hydroxyl group (-OH) of one glucose molecule and the anomeric carbon of the next glucose molecule, forming a long chain of repeating glucose units. In the "c" direction, weak Van der Waals forces hold the structure (8 kcal·mol^{-1}). These forces contribute to the formation of hydrogen bonds and intermolecular interactions, helping to maintain the organized structure of cellulose fibers. Continuous cellulose fiber is about four to five times stronger than steel with an identical cross-section (Holtzapple, 2003).

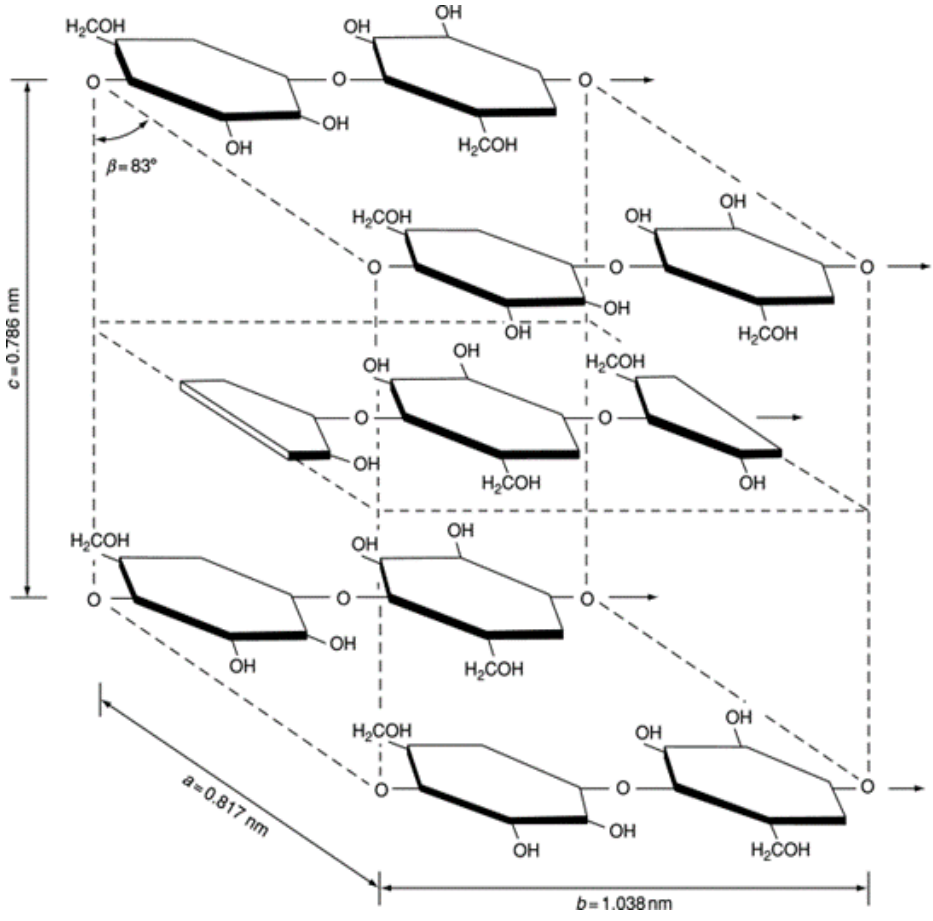

Figure 2.2 — Parallel cellulose I unit cell. Adapted from Holtzapple, (2003).

Hemicellulose represents another component of plant fiber, accounting for about 25 wt%. Compared to cellulose, it has a much more complex structure, being defined as a

heterogeneous carbohydrate assembled by short linear or branched chains of polysaccharide molecules like pentoses (e.g., xylose and arabinose), hexoses (e.g., mannose, glucose, and galactose), and sugar acids (Brandt et al., 2013; Ravindran and Jaiswal, 2016). Moreover, hemicelluloses may have diverse types of side chains bonded to the backbone chain, which imparts them a more complex frame. This molecule is also more susceptible to hydrolyses due to the low values of $\overline{DP}$ and crystallinity compared to cellulose chains. As consequence, hemicelluloses can undergo a chemical reaction in dilute alkali at temperatures above about 180°C generating viscous dark brown "black liquors" (Chen, 2014).

Lignin is the most recalcitrant element of the plant cell wall, making up 10–25 wt% of plant biomass. This heteropolymer imparts strength to the plant cell wall, providing structural support, impermeability, and resistance against microbial attack and oxidative stress (Hendriks and Zeeman, 2009). It is a complex amorphous, aromatic, and water-insoluble polyphenolic polymer with a three-dimensional network composed of two aromatic amino acids, tyrosine, and phenylalanine. These are converted to three different phenylpropene subunits, coniferyl alcohol, sinapyl alcohol, and with a minor content of p-coumaryl alcohol, linked to each other by irregular coupling of carbon-carbon, ester, and ether linkages (Velmurugan and Incharoensakdi, 2018). Although lignin has a relatively simple basic structure composed of three main monomeric units, the relative proportions of these units can vary significantly across different plant families and species (Chen, 2014).

Lignin, cellulose, and hemicellulose are not just individual units in a plant cell wall. These are intimately connected, lignin and hemicellulose are considered the essential 'glue' that maintains the polymers of the cell walls bonded. Different types and proportions of lignin and polysaccharides present in biomass lead to the formation of lignin–carbohydrate complexes (LCC) with a wide diversity of compositions and structures. The nature and number of LCC linkages and lignin substructures affect the yield of pulping, hydrolysis, and biomass digestibility. Cell walls in the biomass structure mainly consist of cellulose, hemicellulose, and lignin in a 4:3:3 ratio. This ratio differs from sources like hardwood, softwood, and herbs (Chen, 2014). Hydrogen bonding is the most significant linkage between cellulose, hemicellulose, and lignin. In addition, there are chemical bonds between galactose and arabinose residues on the side chains of hemicellulose molecules and lignin (Kim, 2018).

2.1.3 Recalcitrance and Pre-treatments

Recalcitrance, the plant cell's resistance to deconstruction, constitutes a barrier in the separation of highly crystalline cellulose from the complex polymeric matrix in which is embedded. Consequently, the lignin and hemicellulose content directly affect fiber degradation (Lee et al., 2014; Ravindran and Jaiswal, 2016). Further, the difficulty in accurately achieving cellulose isolation is directly related to other biomass aspects like crystallinity, the degree of polymerization, acetyl groups, plant protein-enzyme interaction, and the accessible surface to enzymatic degradation (Singh et al., 2015).

Pre-treatments are essential techniques to overcome the recalcitrance, promoting structural and compositional changes in the biomass. An appropriate pre-treatment is projected to (i) diminish crystallinity and degree of polymerization; (ii) increase porosity, inner surface, and reactivity; (iii) break the hydrogen bonds between cellulose and non-cellulosic compounds, increasing the accessibility to a cellulose-rich fraction. This fractionation naturally makes the cellulose more available for the following reactions, improving the depolymerization yield of the chain into nanocellulose (Kargarzadeh et al., 2017; Khalil et al., 2014; Ravindran and Jaiswal, 2016; Singh et al., 2015). Pre-treatments are typically categorized as physical, chemical, biological, or combined (table 2.1). In addition, these are subdivided into three particular classes in terms of pH: (i) acidic, (ii) alkaline, and (iii) neutral (Yahya et al., 2015).

The different pre-treatments are subject to variations in pH, temperature, types of catalyst, and reaction time, among others. These variables affect the pre-treatment severity and the biomass final composition (Pires et al., 2019b). If the process is unaligned, it could result in an imperfect separation of cellulose or over-degradation, leading to the formation of by-products (e.g., the polysaccharide converted to sugars) (Yahya et al., 2015). Therefore, to consider the cellulose separation effective, the pre-treatment should avoid the lignocellulosic components rupture or loss, minimize the energy input for cost-effectiveness, and generate minimum hazardous and toxic wastes. Farther, the choice should ponder based on ease of operation and the balance between various costs, including operating, capital, and biomass expenses (Lee et al., 2014; Singh et al., 2015).

Table 2.1 — Different pre-treatments applied to overcome biomass recalcitrance.

Category	Pre-treatment	References
Physical	Ultrafine Grinding	(Rambabu et al., 2016)
	Ball Milling	(Phanthong et al., 2016)
	High-intensity Ultrasonication	(Szymanska-Chargot et al., 2018)
	Centrifugal Grinding	(Liu et al., 2018)
Chemical	Alkaline	(Collazo-Bigliardi et al., 2018)
	Diluted Acid	(Souza et al., 2019a)
	Acid-Acetone	(Wang et al., 2019)
	Ionic Liquids	(Grabka-Zasadzinska et al., 2019)
	Organosolv	(Ferreira et al., 2018)
	Metal Chlorides	(Kamireddy et al., 2013)
	Deep Eutectic Solvents	(Sirviö et al., 2015)
	Carboxymethylation	(Naderi et al., 2014)
	Acetylation	(Trifol et al., 2015)
	Phosphorylation	(Noguchi et al., 2017)
	(TEMPO)-mediated Oxidation	(Isogai and Zhou, 2019)
Combined	Steam Explosion	(Zhang et al., 2017)
	Liquid Hot Water	(Ko et al., 2015)
	Wet Oxidation	(Morone et al., 2017)
	Ammonia Fiber Expansion (AFEX)	(Abdul et al., 2016)
	Super Critical CO_2	(Albarelli et al., 2016)
	Plasma	(Vizireanu et al., 2018)
Biological	Microbial Consortium	(Yuan et al., 2016)
	Fungal Species	(Mishra et al., 2017)
	Enzymatic	(Long et al., 2017)

The almost complete biomass delignification and hydrolysis of hemicellulose are possible by adopting traditional chemical operations under mild conditions (processes catalyzed by acids or alkalis, sulfites, and sulfates). These processes are considered the most efficient pre-treatments in terms of economic expense, even so, the associated formation of toxic by-products can raise some environmental concerns. Among the solvents most widely used in alkaline pre-treatment, sodium hydroxide (NaOH) emphasizes due to its delignification ability to achieve good biomass digestibility, increased reaction rate, high ethanol production, and non-generation of inhibitory material (Singh et al., 2015). Additionally, green techniques like

ionic liquids (ILs) are being studied to bring more sustainability to the chemical process (André et al., 2013; Yoo et al., 2017). Ionic liquids (ILs) are thermally stable organic salts, typically composed of an asymmetric cation (organic) and a counterpart anion (organic or inorganic), which have been investigated as a viable substitute for conventional volatile organic solvents due to their interesting physico-chemical properties (Espinoza-Acosta et al., 2014). Ionic liquids can remain in the liquid state at temperatures usually below 100 °C (substantially lower than normal salts, like NaCl), and if the melting temperatures are below room temperature, they are called as room temperature ionic liquids (RTILs) (Gupta and Jiang, 2015). Furthermore, ILs offers a great variety of physicochemical properties among which the most iconic are high polarity, great thermal stability (even above 300 °C), high conductivity (both electric and thermal), large electrochemical potential window (−4 to 4 V), high solvent power, negligible volatility and non-flammability, low energy requirement, and possibility to be recovered and reused. Considering how cost-intensive pre-treatments can be, these key properties are crucial and open the possibility to implement nanocellulose production in biorefineries (André et al., 2013; Gupta and Jiang, 2015; Ravindran and Jaiswal, 2016). Curiously, ILs are frequently called "designer solvents" due to large possible combinations of selected cations and anions, which will determine the tunable properties of ILs (Mora-Pale et al., 2011).

Other approaches are widely explored by the scientific community, presenting advantages and disadvantages. Physical pre-treatments are applied to increase the accessible surface area and pore size and decrease the cellulose crystallinity. However, it still shows lower yields in biomass deconstruction and is dependent on high energy consumption. Steam explosion (also called auto-hydrolysis) is one of the most extensively studied and promising methods for physicochemical conversion of the lignocellulosic feedstock and is seen as the best alternative to the traditional physical pre-treatments. Compared to the conventional mechanical procedures, steam explosion demands a 70 % lower energy consumption to get the same particle size of the substrate. Besides, this method has other advantages like reduced environmental impact, lower energy requirement, and little to no chemical usage. During the process, materials are treated in a vapor phase at a high-temperature range of 160–260 °C under steam pressure between 1 and 3.5 MPa for a few seconds to a few minutes in the saturated steam (Kargarzadeh et al., 2017; Kim, 2018). The compressed steam causes an explosive biomass decomposition when it is rapidly decompressed due to the flash evaporation of water which exerts a high force that causes the LCC physical breakdown (Ravindran and Jaiswal, 2016).

The steam stimulates structural changes including hemicellulose hydrolysis by organic acids created during the process, as well as the lignin degradation which helps to increase accessibility to cellulose. Cost-effective pre-treatment technologies like steam explosion are fundamental to the successful operation of future bio-refineries, converting biomass into a spectrum of fuel molecules and industrial chemicals (Zhang et al., 2017).

Biological pre-treatments reveal good potential due to low energy requirements and nonchemical use, even though these continue to be expensive and time-consuming, which makes them less suitable for industrial applications (Mishra et al., 2017; Rambabu et al., 2016). The method is based on the alteration or degradation of the lignocellulose cell wall structure by hydrolytic enzymes (e.g., hydrolases) and ligninolytic enzymes that depolymerize lignin. Relatively to the traditional pre-treatments, this strategy offers certain advantages since it is conducted under mild conditions, with low energy demands, and without the toxic compounds released (Alexandropoulou et al., 2017; Sharma et al., 2019). Nonetheless, the method is time-consuming (it takes at least one to a few weeks) and should be fulfilled in sterile conditions, thus is difficult to apply in large-scale operations. A good strain and culture choice optimization are fundamental to making the process more efficient, diminishing consumption and carbohydrate loss (Sindhu et al., 2016). Combining biological pre-treatment with another pre-treatment might help minimize the operation time. Additionally, the synergistic action of the microbial consortium with various bacteria and fungi has proved to be a strategic route to the effective biodegradation of lignocellulosic biomass. Some advantages of using microbial consortium include increased adaptability, higher productivity, upper enzymatic saccharification efficiency, control of pH during sugar utilization and increased substrate utilization (Sharma et al., 2019; Shirkavand et al., 2017; Song et al., 2013; Wang et al., 2012; Yu et al., 2009; Yuan et al., 2016).

After the pre-treatment, a bleaching process is performed as a complement. Traditional methods for obtaining cellulosic fibers demand the application of chlorine-based compounds as bleaching agents. These substances sustain a profound impact on human health and are not environment friendly. Thereby, chlorine-free bleaching with hydrogen peroxide (H_2O_2) should be applied alternatively. The reactivity attributed to H_2O_2 results in the generation of reactive species of superoxide radicals (O_2^-), which are in charge of lignin aromatic rings oxidation and parts of carboxylic acids from hemicellulose. Upon the bleaching completion, about a third of the hemicellulose will fractionate, while the lignin will practically disappear. In this

sense, the bleaching treatment removes chromophore groups, generating a whiter fiber with greater cellulose purity (Hafemann et al., 2019).

2.1.4 From Microcellulose to Nanocellulose

Cellulose is the most available natural biopolymer, however, it has been only recently that has gained notoriety as a nanoscaled material. Due to its nanometric size, nanocellulose (NC) has advantageous properties which include special morphology and geometrical dimensions, crystallinity, high specific surface area, rheological properties, liquid crystalline behavior, alignment and orientation, mechanical reinforcement, barrier properties, surface chemical reactivity, biocompatibility, biodegradability, and absence of toxicity. In comparison with microcrystalline cellulose (MCCs) nanocellulose present, higher structural characteristics, like high mechanical strength, and can be easily surface modified through different strategies (Lin and Dufresne, 2014). Exhibiting these important properties, nanocellulose has revealed a large potential for various applications and new added-value products, like additives to composites, polymer and paper reinforcement, emulsions, barrier films and water treatment, oxygen barrier in food packaging, electronics, cosmetics, pharmaceuticals, and biomedical devices (Lin and Dufresne, 2014; Yahya et al., 2015). Furthermore, depending on the source from which the cellulose is obtained, the pre-treatment and the conversion methods chosen, it is possible to model the NC properties for a specific application, opening a wide range of possibilities (García et al., 2016). The attention that nanocellulose is receiving is not only clear in academic articles, but it is also expressed by the raised number of patents that are published annually. These patents exploit various methods to obtain NC showing their viability to be incorporated into industrial processes (Córdova and Afewerki, 2016; Fan, 2016; Graveson and English, 2015; Laborie and Abushammala, 2018; Yoo and Youngblood, 2019).

The cellulose transformation into nanocellulose is performed in two steps. The first, as explained previously, pass through the raw material pre-treatment to obtain more "pure" cellulosic fibers. In the second step the fibers are converted into one of two main species of nanosized cellulosic materials: cellulose nanocrystals/nanowhiskers (CNCs/CNWs) or cellulose nanofibers (CNFs) (figure 2.3). In addition to these two types, we should also regard bacterial nanocellulose (BNCs) produced biotechnologically by bacteria (Klemm et al., 2018).

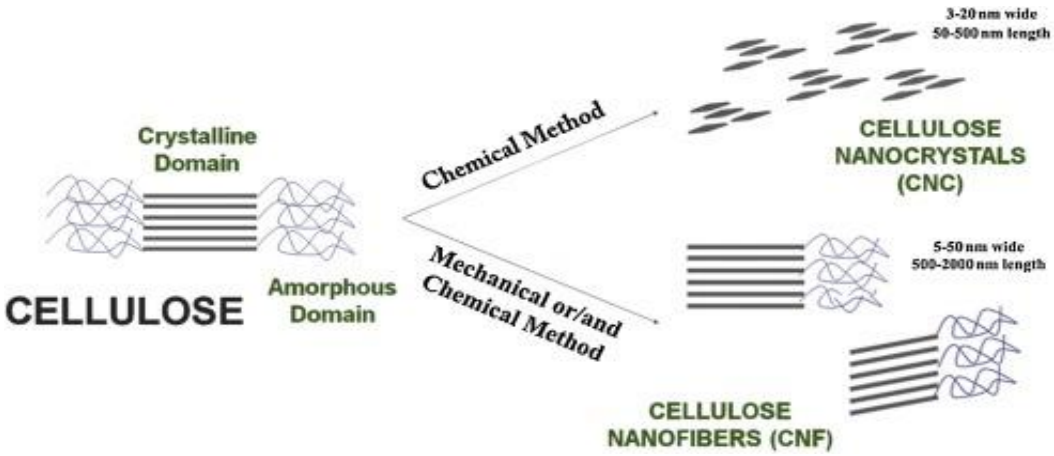

Figure 2.3 — Schematic figure of cellulose nanocrystals (CNCs) and cellulose nanofibers (CNFs) production methods. Adapted from Pires, Souza, and Fernando (2019).

2.1.4.1 Cellulose Nanocrystals

In the last decade, a considerable number of excellent review articles on CNCs have been published (Brinchi et al., 2013; Langerwall et al., 2014; Malucelli et al., 2017; Peng et al., 2011), and the publication of research works are increasing year after year, reflecting the scientific interest in this nanomaterial. Moreover, new International Organization for Standardization (ISO), Technical Association of the Pulp and Paper Industry (TAPPI), and Canadian Standards Association (CSA) Standards on CNCs are being developed and published, highlighting the potential of this nanomaterial in the technological market. The CNCs own spotlighted intrinsic characteristics that distinguish them from the other nanocellulose configurations, like their high crystallinity, strength, amphiphilic nature, chemical purity, optical properties, ability to be redispersed from dried powder, and perhaps above all, the fact that they can be uniformly and reproducibly produced (Klemm et al., 2018).

The most conventional and effective technique to produce CNCs is through acid hydrolysis. During the hydrolysis procedure, the amorphous zones of cellulose are preferentially digested because they are more sensitive to acidic attacks, contrarily to the crystalline regions that are more compact and resistant (García et al., 2016; Kargarzadeh et al., 2017). At the end of the reaction, rod-shaped cellulose nanocrystals with variable geometrical dimensions in the range of 3–20 nm wide and 50–500 nm in length, high aspect ratio, and large surface area (~ 400 m^2/g) are achieved (figure 2.4).

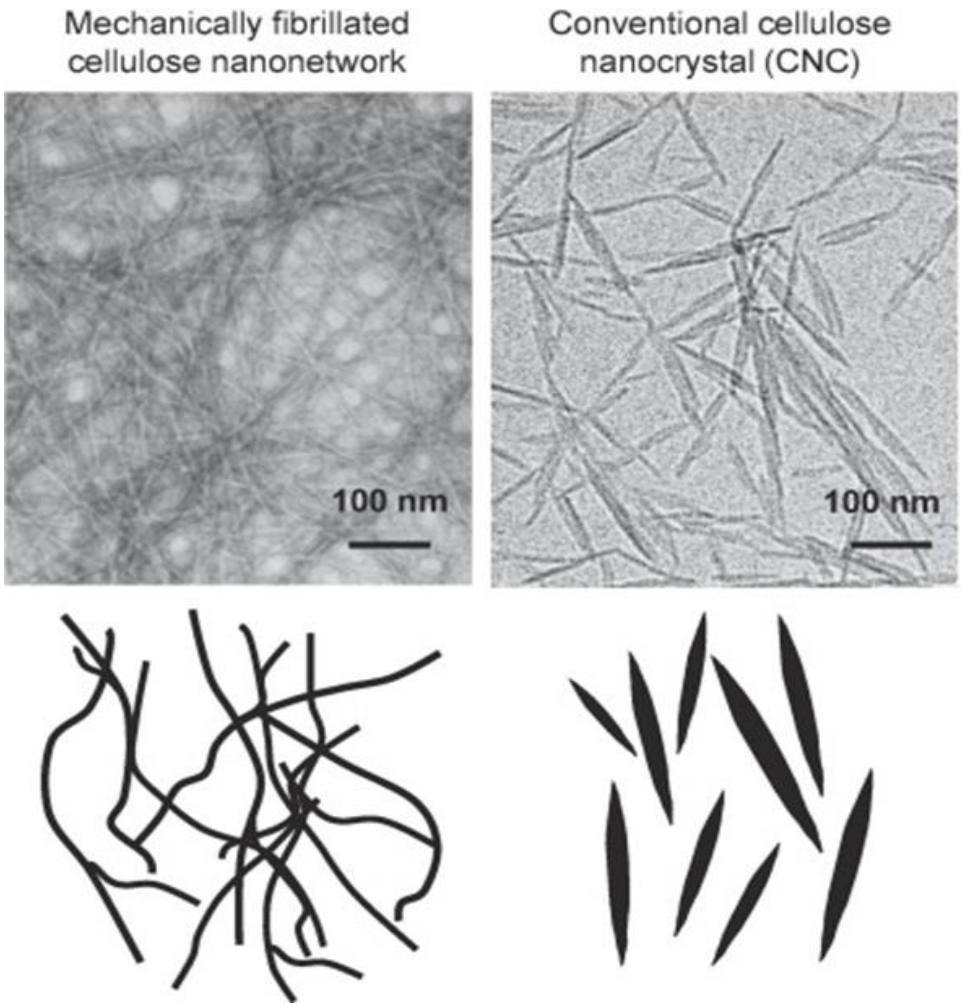

Figure 2.4 — Differences among morphologies of mechanically CNFs nanonetworks, and acid-hydrolyzed CNCs. Adapted from Isogai and Zhou (2019).

The operation consists of a strong and highly concentrated mineral acid hydrolysis of the cellulosic material (Brinchi et al., 2013; Miao and Hamad, 2013). Sulfuric is the most used acid as the hydrolyzing agent because the reaction with the surface hydroxyl groups via an esterification process allows the grafting of anionic sulfate ester groups. These negatively charged groups will develop a negative electrostatic layer that covers the nanocrystals, encouraging their dispersion in water. However, this can compromise the nanoparticles thermostability (Vilarinho et al., 2018). Other methodologies are applied as an alternative to hydrolysis with sulfuric acid, like oxidation or hydrolysis with other types of acids (hydrochloric, hydrobromic, citric, phosphoric, oxalic, and maleic acid) (Klemm et al., 2018). The dimensions, crystallinity, thermal stability, and surface charge of CNCs are highly dependent on various factors, like the cellulose source, type and concentration of acid, reaction time, and

temperature, accordingly, these parameters need to be carefully selected (J.R.A. Pires et al., 2019a). The hydrolysis is ended with a rapid dilution of the acid to stop the reaction, followed by acid removal with centrifugation and/or extensive dialysis against distilled water (Brinchi et al., 2013). Mechanical processes, like ultrasonication, are usually applied following acid hydrolysis to obtain a homogeneous CNCs suspension, preventing nanoparticle aggregation. Additionally, ultrasonication should be executed in an ice bath not to let the desulfation on the CNCs surface occur. In the end, a drying process is performed to reduce the cost of material packaging and transportation, facilitating the employment of CNCs in industrial applications. Freeze-drying is one of the most expensive methods at the moment. Nevertheless, this process shows more potential because it allows fast freezing and water removal, minor affecting the nanocellulose structure compared with other traditional drying methods (Malucelli et al., 2017).

Environmentally and economically speaking, cellulose nanocrystals production by acid hydrolysis is not correctly feasible since it produces effluents that require treatment, increasing processing costs (Lee et al., 2014). In response to this problem, Kontturi et al., (2016) proposed a new strategy for CNCs production. The nanocrystals were produced through rapid degradation and simultaneous crystallization by exposing the fibers to hydrochloric acid vapor. Due to the absence of texture changes in the sample and the lack of mass transfer in the substrate, it is possible to monitor the changes in crystallinity. In addition, it is a method that presents high yields of production as well as reduced water consumption. Other new and more eco-friendly methods have been examined, like undertaking the whole process through enzymatic hydrolysis (Cui et al., 2016)or applying ionic liquids (Abushammala et al., 2015), yet it is necessary to overcome the economic constraints that these processes entail.

2.1.4.2 Cellulose Nanofibers

Cellulose nanofibers consist of a bundle of stretched, long, flexible, and entangled nanosized fibers with approximately 5–50 nm in width and 500–2000 nm in length (figure 2.4), but some works have shown lower CNFs dimensions, mainly when chemical methods like (TEMPO)-mediated oxidation are fulfilled (Isogai and Zhou, 2019; Khalil et al., 2014).

Contrarily to nanocrystals, nanofibers are composed of alternate crystalline and amorphous strings (García et al., 2016). Additionally, CNFs own a high aspect ratio and can form gels in water with shear-thinning and thixotropic behavior (Nechyporchuk et al., 2016). Ideally, these nanofibers are produced using intensive mechanical delamination of softwood

pulp, with or without the assistance of chemical and biological pre-treatments. Mechanical approaches to transforming pulps into nanofibers can be divided into refining and homogenizing, microfluidization, grinding, cryo-crushing, and high-intensity ultrasonication (J.R.A. Pires et al., 2019b). The several steps necessary to increase the degree of fibrillation that composes the mechanical disintegration of cellulose fibers is a process that requires high energy consumption, and this condition continues to be the main barrier to the successful introduction of CNFs in the industry (Kargarzadeh et al., 2017). Nonetheless, the pre-treatment methods appear to be one of the pre-requisites for the economically efficient production of CNFs. The introduction of different pre-treatments before the mechanical processes aimed to reduce energy consumption and to make the surface hydrophobic so that CNFs can be a more attractive material for commercial applications. Examples of those pre-treatments are preliminary 2,2,6,6-tetramethylpiperidine-1-oxyl radical (TEMPO)-mediated oxidation, carboxymethylation, periodate oxidation, phosphorylation, and mild acidic or enzymatic hydrolysis (Nechyporchuk et al., 2016; Noguchi et al., 2017).

The literature has highlighted the potentialities of (TEMPO)-mediated oxidation as a pre-treatment system in the conversion of CNFs (Chitbanyong et al., 2018; Gamelas et al., 2015; Isogai et al., 2011; Saito et al., 2007). This oxidation process transforms the C6-hydroxyls groups present on the surface of native cellulose into carboxylate groups, preserving the crystallinity of the original sample. This process promotes the nanofribillation and is considered a chemical route to increase the crystallinity and water dispersion of nanocellulose. Moreover, in comparison with other pre-treatments, TEMPO offer clear advantages, like high conversion yield, enhanced selectivity, a partial decrease of polysaccharides molecular weight during the process (if controlled), and low cost as a co-oxidant. The obtained TEMPO-oxidized cellulose nanofibrils possess excellent tensile, gas-barrier, and thermal properties (Chitbanyong et al., 2018). Other pre-treatments like periodate–chlorite oxidation, periodate-bisulfite sulfonation, carboxymethylation, and phosphorylation were used to insert negative charges onto the cellulose surface to fade the inter-fibril bonding (Errokh et al., 2018; Im et al., 2018; Liimatainen and Visanko, 2013). The introduction of repulsive charges by chemical pre-treatments, increases the fibrillation efficiency. Thereby, the extracted cellulose nanofiber fractions are more regular and have lower fibril diameter than native CNFs produced only by mechanical methods (Nechyporchuk et al., 2016).

2.1.5 Nanocellulose Applications

Since ancient times, plant fibers have been used mainly for energy, building materials, paper, textiles, and clothing. Nowadays, the production of advanced and innovative materials from renewable and abundant bio-resources is becoming an important area of research since it offers an unparalleled combination of high physical properties and environmental benefits producing a variety of high-added value products (Brinchi et al., 2013; Deepa et al., 2015).

The nanocellulose unique properties are already well studied and defined, which led to the next step, the industrial applications development. Many studies and reviews have been made over the past few years, making the number of applications for NC increasing steadily. The nanocellulose-based materials that stand out most are the hydrogels, aerogels or new composites when blending with organic polymeric matrixes, carbon nanotubes, graphene, or inorganic materials. These materials can be applied in various scientific areas and industries, like food packaging, flexible electronics, sensing and biosensing, energy harvesting, liquid crystals, biomedicine and cosmetics, catalysis, adsorption, separation, decontamination, filtration or even fire retardants (figure 2.5) (Klemm et al., 2018; Malucelli et al., 2017; Thomas et al., 2018). Furthermore, CNCs are also revealing interesting properties, which are pertinent for new optical materials and devices (Godinho et al., 2014). Some of the enumerated applications based on NC were recently granted with a patent (Li et al., 2017; Mao et al., 2016; Nelson et al., 2017; Rauchfuss et al., 2018). The nanocellulose production high cost, mainly due to high energy consumption and waste treatment during the preparation process, together with some structural limitations, are still a barrier to new applications in the market. However, the NC production from low-cost raw materials like lignocellulosic wastes from energy crops, may prove to be a future solution, but the extraction processes for these materials still need to be optimized.

Figure 2.5 — Nanocellulose main applications. Adapted from Pires, Souza, and Fernando (2019).

2.1.5.1 Nanocellulose in Bionanocomposites

The nanocellulose addition to polymer films may match the traditional food packaging characteristics, with the advantage of being biodegradable and more environmentally friendly. Recently, progress has been reached, but an efficient and economical way to use NC as a reinforcement in polymer composites, to be introduced into the packaging industry, is still lacking. As there is a growing demand for more green technologies that can replace the traditional ones, based on fossil resources, more efficient strategies need to be established to produce bionanocomposites with optimal characteristics, including the scale-up of those to the industrial level (figure 2.6) (Bharimalla et al., 2017; Vilarinho et al., 2018).

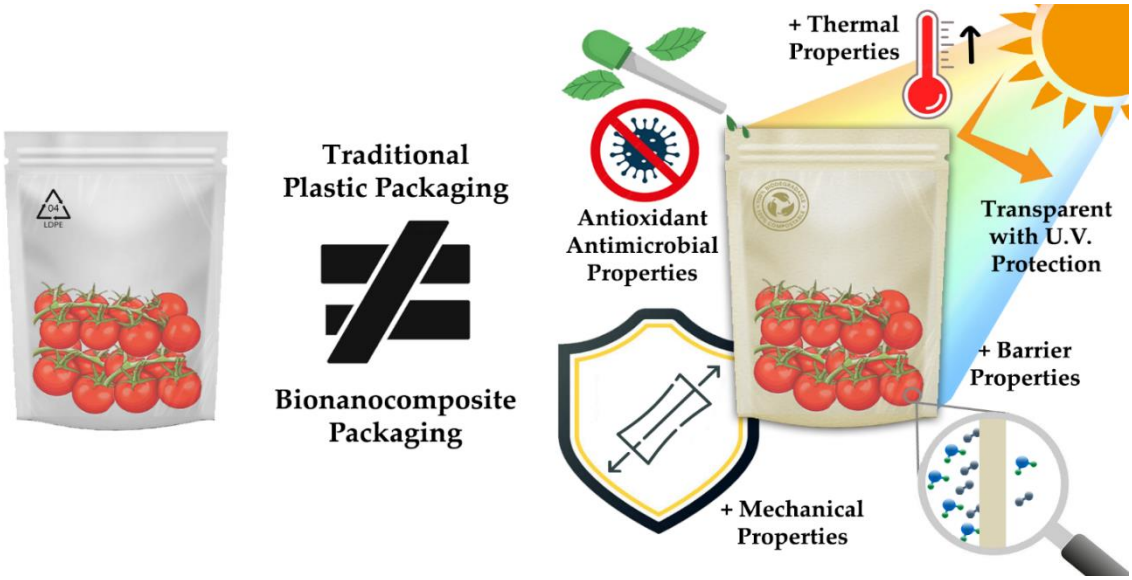

Figure 2.6 — Advantages of bionanocomposites compared to traditional petroleum-based packaging.

In most of the published articles (table 2.2), the authors seek to correlate and optimize the perfect amount of nanocellulose to be added to the bionanocomposite, maximizing the material's mechanical properties. The nanofiller ideal amount to be added is not consensual between the authors, varying according to the chosen polymer matrix. El Achaby et al., (2017) developed a new eco-friendly polyvinyl alcohol (PVA)/carboxymethyl cellulose (CMC) bionanocomposite filled with sugarcane bagasse CNCs. The authors found that the addition of 5 % (w/w) CNCs within a PVA/CMC increased the tensile modulus and strength by 141 % and 83 %, respectively, reduced the water vapor permeability by 87 %, and preserved the same transparency level of the film (transmittance of about 90 % in the visible region). In another study, Sukyai et al., (2018) investigated the effect of CNCs extracted from sugarcane bagasse residues on the properties of whey protein isolate-based films to determine their further utilization as a food packaging material. The results showed that the CNCs increased the hydrophilic nature of the film. In this case, the authors presumed that the bionanocomposite with 8 % (w/w) CNCs provided appropriate mechanical properties and barrier properties and can be applied as a food packaging material. Qian et al., (2018) produced CNCs from bamboo residues through acid hydrolysis and incorporated them into a polylactic acid (PLA) matrix in different contents aiming to know which optimal content of CNCs should be introduced in the PLA matrix. The authors observed that PLA/CNCs composites with 2.5 % (w/w) of

bamboo NC had a high level of transparency, high glass transition temperature, cold crystallinity, and tensile modulus. Additionally, it was verified that excessive CNCs contents lowered the tensile property.

Some constraints still need to be surpassed to have fully functionalized bionanocomposites, like the incompatibility between the CNCs and the hydrophobic polymer matrix, which leads to unfavorable mechanical effects (Yahya et al., 2015). Solutions such as adsorption of surfactant, chemical modification, physical treatment, and bacterial treatment on cellulose substrate decrease affinity and surface energy causing interface compatibility to increase. Moreover, the introduction of the electrostatic charge tends to stabilize the nanocellulose dispersion in the matrix through the surface negative charges. Suspensions of CNCs are frequently stabilized by negative surface charges from carboxyl or sulfate ester groups on their surface (Eyley & Thielemans, 2014; Yahya et al., 2015). The other constraint which needs to be overcome is the great number of chemicals used and water wasted during the process. It is fundamental to find favorable parameters of chemical and mechanical treatments to lower the consumption of reagents, assuring environmental sustainability, and diminish the prices of the product (Pires et al., 2019).

Table 2.2 — Mechanical properties of bionanocomposites reinforced with different NC types.

Raw Material	Type of NC	Matrix Material	% NC (w/w)	EM (MPa)	TS (MPa)	EAB %	References
Bamboo (*Phyllostachys edulis* (Carrière) J. Houz)	CNCs	Polylactic Acid	2.5	428	X	22	(Qian et al., 2018)
Coffee (*Coffea arabica* L.)	CNCs	Polylactic Acid	3	1419	60	6	(Sung et al., 2017)
Cotton (*Gossypium arboreum* L.)	CNCs	Chitosan	7	347	13	8	(Pereda et al., 2014)
Flax (*Linum usitatissimum* L.)	CNCs	Chitosan	20	52	7	35	(Mujtaba et al., 2017)
Hemp (*Cannabis sativa* L.)	CNCs	Polylactic Acid	3	1540	23	160	(Luzi et al., 2016)
Kenaf (*Hibiscus cannabinus* L.)	CNCs	Chitosan/Polyvinyl Pyrolidone	10	2190	40	51	(Poonguzhali et al., 2017)
Oat (*Avena sativa* L.)	CNCs	Whey Protein	5	100	4	11	(Qazanfarzadeh and Kadivar, 2016)
Rice (*Oryza sativa* L.)	CNCs	Polyvinyl Alcohol/Chitosan	5	1764	98	30	(Babu Perumal et al., 2018)
Sisal (*Agave sisalana* Perrine)	CNCs	Biopolyurethane	10	35	8	712	(Mondragon et al., 2018)
Sugarcane bagasse (*Saccharum officinarum* L.)	CNCs	Polyvinyl Alcohol/Carboxymethyl Cellulose	5	2747	119	10	(El Achaby et al., 2017)
	CNCs	Whey Protein	8	187	4	18	(Sukyai et al., 2018)
	CNCs	Starch	3	520	17	9	(Slavutsky and Bertuzzi, 2014)
Banana (*Musa x paradisiaca* L.)	CNFs	Starch	4	1048	11	21	(Maria Pelissari et al., 2017)
Cotton (*Gossypium arboreum* L.)	CNFs	Sodium Carboxymethyl Cellulose	5	1320	50	28	(Oun and Rhim, 2015)
Kenaf (*Hibiscus cannabinus* L.)	CNFs	Starch	10	141	38	27	(Babaee et al., 2015)
Rice (*Oryza sativa* L.)	CNFs	Starch	15	160	5	61	(Nasri-Nasrabadi et al., 2014)
Sugar Beet (*Beta vulgaris* L.)	CNFs	Polyvinyl Alcohol	2	1675	30	68	(Hietala et al., 2017)

** Nanocellulose (NC); Cellulose Nanofibers (CNFs); Cellulose Nanocrystals (CNCs); Elastic Modulus (EM); Tensile Strength (TS); Elongation at Break (EAB).*

2.1.5.2 Nanocellulose in Electronic Devices

It is not usual to fabricate electrical devices directly from nanocellulose because, technically, NC is not a good electrically conductor. However, conductivity is essential for some core components of an energy device. Thus, it is required to mix NC with another type of conductive material (e.g., conductive polymers, metallic particles, conductive carbon materials). These composite materials will take advantage of both materials, and therefore, the combination of NC properties and the new flexible and sustainable electronics will be able to meet the most demanding needs for energy applications (Du et al., 2017; Hoeng et al., 2016).

Bionanocomposites made in their majority of CNFs, also called nanopaper, demonstrated great potential as a substrate in printed electronics due to their flexibility, thermal stability, and biodegradability, pointing out the transparent nanocellulose substrates as a good alternative to the traditional plastic and glass substrates (Hu et al., 2013). In terms of applicability, the paper-based transistor can be used for low-cost microelectronics, characterized by being flexible and disposable, like biosensors or intelligent packaging (Kim et al., 2015). Besides, the smart paper could be also used for energy storage devices, like rechargeable lithium-ion batteries and supercapacitors, and are promising candidates for the fabrication of next-generation solar cell (Nair et al., 2016; Wang et al., 2015). The nanocellulose flexibility and lightness allow electronic devices to be incorporated into day-to-day consumer products, like sportswear, or military-grade material, thereby increasing its technological potential (Du et al., 2017). Moreover, applications have been developed for flexible energy storage devices as a result of the requirement to obtain sustainable solutions like miniaturization, flexibility, and thin, lightweight structures. The successful stress liberation from cellulose nanopaper, and also the ability to keep energy between polymer dielectric and cellulose nanopaper, fomented these advantageous properties. However, the performance of electronic components made from NC substrates still cannot compete with traditional electronics (Hoeng et al., 2016; Kim et al., 2015).

2.1.5.3 Nanocellulose in Biomedical Applications

The bionanocomposites evolution, with improvements in structure and properties, have increased the interest for their application in biomedical applications. The combination of multidisciplinary fields like engineering, chemistry, physics, biology, and life sciences has contributed to the research development of these nanostructured biomaterials for medical applications (Fernandes et al., 2013). New biomedical materials of nanocellulosic origin, from the

molecular level (cellular cultivation) to macroscopic biomaterials (e.g., drug delivery, substitute implants, tissue repair, regeneration), have emerged and have been highlighted due to the application of several innovative strategies that have overcome barriers that previously seemed difficult to surpass (Lin and Dufresne, 2014). The interest over the last years in the application of nanocellulose in the biomedicine area is attributed by their low toxicity, biocompatibility, good mechanical properties, high surface area-to-volume ratio and potential versatility in terms of chemical modification (Plackett et al., 2014). Regarding the nanocellulose toxicity, studies appoint to low values, but this is a theme that still generates discordance. The size, morphology and surface chemistry of nano-based materials directly affects the toxicity, so different made NC-based materials will conduct different toxic effects. More studies about NC toxicity are necessary since these nanomaterials have great potential to be applied in the biomedical field (Seabra et al., 2018).

When it comes to biological tissues, it is crucial to consider how important the biological properties of nanocelluloses are. Biocompatibility and right mechanical properties similar to natural tissue are essential to guarantee that nanocellulose-based biomaterials are able to supply a cell-friendly environment to boost cells attachment and proliferation as a special tissue bioscaffold. Nanocellulose have proven to be biocompatible, with almost no evidence of rejection by the human body *in vivo* trials, but in counterparts, the body cannot degrade them, which always implies some incompatibility. This incompatibility is a good characteristic when it is related to prosthetics (Lin and Dufresne, 2014). Most of the cellulose-based biological tissues lay on bacterial nanocellulose. The choice for this type of NC produced by microbial cells is mainly due to its similarity of size with collagen (100 nm), low cytotoxicity, high porosity, and superior biocompatibility, which facilitates the development of a structure for soft tissues, such as cartilage. Besides the soft tissues, these nanocellulose based scaffolds find various potential applications such as in the development of artificial ligament, as a component of bioink for 3D tissue printing, and wound dressing (Aljohani et al., 2018; Jorfi and Foster, 2015). Some wound healing applications brands made with bacterial nanocellulose, like XCell, Bioprocess, and Biofill, are already being commercialized, which demonstrate that they could become high-value products in the medical field.

The excellent functionality of nanocellulose as a binding matrix and controlled release of active drugs, both for topical or transdermal administration, is due to its high surface area-to-volume and its ease of chemical modification. Films, fibers, and gels display to be a great vehicle for the delivery of different pharmaceutical compounds, like anti-inflammatories, anti-

infectives, proteins, and steroids. The ease with which it releases hydrophobic and hydrophilic compounds makes these materials highly versatile with respect to drug delivery. Hereafter, it is expectable the emergence of commercial formulations that are capable to regulate the liberation rate and timeframe of different drugs (Fernandes et al., 2013; Plackett et al., 2014).

2.2 Bio-Based Polymers

The emergence of different plastics in daily products is related to the growth of life's quality since the 1950s, presenting new opportunities and more social benefits. It was effortless for plastics to grant the status of most handled material by distinct industries, demonstrating particular value in food and beverage packaging manufacturing, considering their exceptional intrinsic properties, versatility, reduced cost, and ease of processing (Mangaraj et al., 2018).

Despite all the appealing aspects undoubtedly connected to conventional plastic packaging, their non-renewable character, unsustainable use, and brief lifetime associated with their resistance to degradation caused a severe and realistic environmental problem, bringing out the responsibility to uncover new and better ways to improve the disposal systems (Fortunati et al., 2018). Especially in some countries, the lack of viable waste disposal alternatives to the clogged landfills boosts the accumulation of this non-degradable resource in water bodies, leaving a trail of pollution that can be seen from the shoreline to the ocean, causing potential health problems for the population worldwide (Pires et al., 2022a). In fact, it is currently possible to find a sizeable percentage of micro or nanometer-sized plastics in the marine fauna's diet, contaminating the food chain and endangering the health of all living animals who ingest this type of nourishment (Karan et al., 2019). Fortunately, new insights on waste recovery and management have increased inside the industry and the civil community, formalizing the stimulus to establish a sustainable and bio-based society (Fernando et al., 2015). Consumer awareness about the plastic problem allied with a healthier and sustainable lifestyle has inherently guided the replacement of traditional polymers for modern eco-friendly materials. Hereupon, it is essential to continue investing in scientific research and development of biodegradable and bio-based alternatives, and adopt new greener policies based on sustainable growth to reduce or even extinguish the negative footprint that petrochemical polymers induce in the environment (García et al., 2016; Lambert et al., 2017).

Bio-based plastics/polymers, recurrently expressed in literature as bioplastics or biopolymers, have recently been appointed as the logical candidates to replace conventional plastics

due to their renewability, high abundance, accessibility, low cost, reduced toxicity, and biodegradable character (Souza & Fernando, 2016). These consist of chain-like molecules of covalently bonded monomers, in which the difference for polymers resides exclusively in the prefix "bio", indicating their biological or renewable origin (Shankar and Rhim, 2018). If misunderstood, the "bioplastic" term could assume that all bio-based polymers are biodegradable and, in opposition, that every fossil-based polymer is non-biodegradable. Although this statement seems logical, it is not possible to say that it is correct for every situation because, during processing, some chemical changes take place (such as the addition of stabilizers, plasticizers, or fillers), which generate functional groups and copolymerizations that can limit the bioplastic degradability (Garrison et al., 2016). For this reason, it is essential to make an explicit distinction between the two classifications. Following the directions set by the American Society for Testing and Materials (ASTM), bio-based plastics are described as ''a plastic containing organic carbon of renewable origin like agricultural, plant, animal, fungi, microorganisms, marine, or forestry materials living in a natural environment in equilibrium with the atmosphere'' (ASTM International, 2016), while biodegradable plastic is ''a degradable plastic in which the degradation results from the action of naturally-occurring microorganisms such as bacteria, fungi, and algae'' (ASTM International, 2012). In favor of establishing a generic pattern, the European Bioplastics Association identifies bioplastics as a diverse family of materials, which can be either bio-based, biodegradable, or features both properties (figure 2.7) (European Bioplastics, 2016).

Convincing business owners to adapt their facilities and bet on new raw materials can represent a demanding task. Almost three decades after the beginning of this research area, bioplastics have only managed to enter a very small percentage of the market. To foster growth in these numbers, it is crucial that bioplastics could be considered a viable market option based on the right balance between environmental, economic, and social concerns (Mangaraj et al., 2018). In this context, biopolymers still must struggle with some key challenges, like sustainability, legislation, costs, downstream processing operations, and structural properties. Related to environmental sustainability, novel bio-based products must be intensively reviewed and optimized to mitigate the impact and reduce the waste associated with the end-of-life of single-use plastics. Therefore, before being addressed for commercial purposes, the product's full biodegradability must be ensured, and any harmful ecotoxicological effects arise from this degradation (Lambert et al., 2017). Another decisive aspect is the creation of grounding legislation since the implementation of new national and international standards to correctly

establish the concepts related to bioplastics will help in the sustainable progress of this rising industry. Additionally, it is prominent to create a competitive biopackaging market to overcome the traditional plastics low cost, by adopting abundant and inexpensive raw materials and optimizing processing techniques for efficient performance (Karan et al., 2019; Zhu et al., 2016). Compared to plastics, bioplastics present critical structural flaws, mainly in mechanical, thermal, and barrier properties coupled with processing struggles that diminish their industrial applicability (Shankar and Rhim, 2018). For biopolymer-based products to go from concept to reality, it is fundamental to strengthen its composition and modify and improve its properties. The insertion of homogeneously dispersed nanoparticles into the biopolymer matrix, with a high aspect ratio and high surface area, is considered a promising solution, creating a novel functional materials class named bionanocomposites (Fortunati et al., 2018).

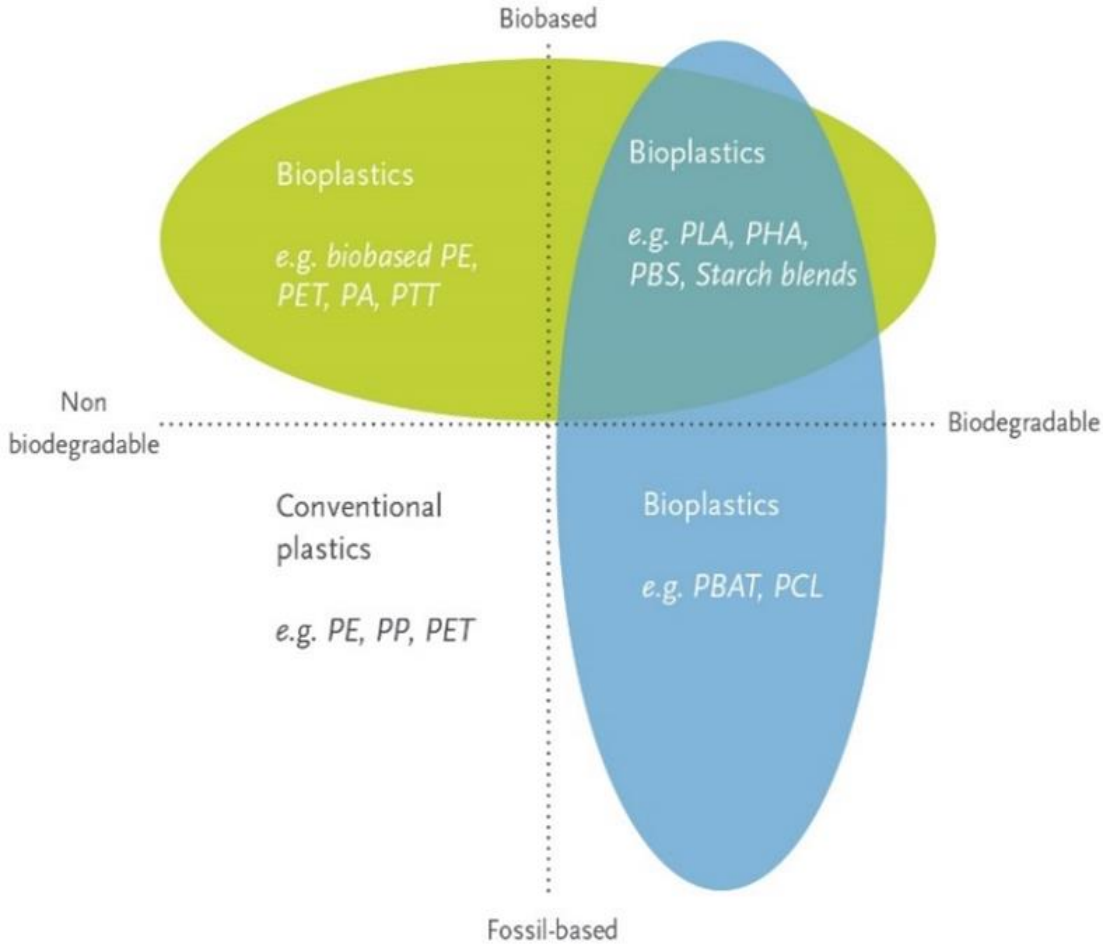

Figure 2.7 — Coordinate system of bioplastic. Adapted from European Bioplastics (2016).

2.2.1 Biodegradation Assessment

Biodegradability is, along with the renewable character, the key point of interest attributed to bioplastics when compared with traditional plastics. The biopolymers degradation process could occur by photooxidative mechanisms when exposed to sunlight or through the action of living organisms that secrete extracellular enzymes in the presence (aerobic degradation) or absence (anaerobic degradation) of oxygen. The organic chemical compounds will be converted into small molecular byproducts, like carbon dioxide, water, inorganic substances, methane, and biomass (figure 2.8). Besides, some of these materials can also be compostable, which indicates the decomposition process occurs in a compost facility at a rate consistent with familiar compostable materials (Fortunati et al., 2018; Souza and Fernando, 2016).

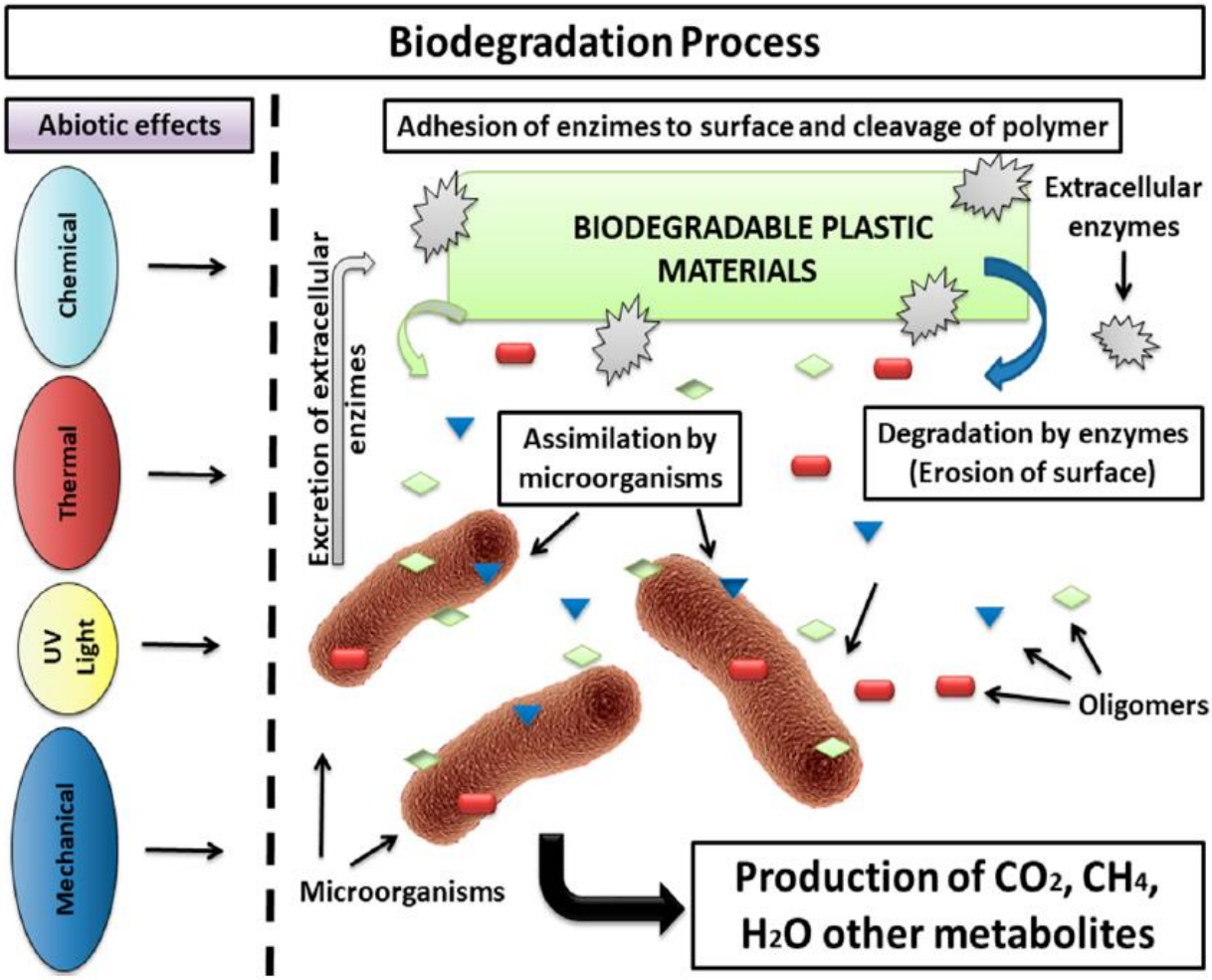

Figure 2.8 — Biodegradation process scheme. Adapted from (Souza, 2015).

Regardless of some of the European Union (EU) members having banned landfill applications, there are not yet sufficient alternatives to arouse a paradigm transition, wherein incineration is not an ecological option due to the emission of pollutant gases, in which about 2.8 kg of CO_2 is evolved in the combustion of 1 kg of plastic. Furthermore, recycling still faces difficulties in separating certain plastics from contaminants, remaining a low-yielding process that needs to be properly adjusted. Of all the plastic used in food packaging, about 9–10 % is recycled, and only half of that percentage survives more than one recycling cycle (Emadian et al., 2017; Shankar and Rhim, 2018). These remarkably low rates are associated with factors such as packaging composed by distinct layers of plastic material grades, contaminants present in the packaging (e.g., pigments, inks, and metals), unavailability of suitable waste sorting systems, and deficit of informative sorting and recycling labels (Sundqvist-Andberg and Åkerman, 2021). Following the recommendations published in the document "Use of Recycled Plastics in Food Packaging (Chemistry Considerations): Guidance for Industry" by the Food and Drug Administration (FDA), the recommended maximum level of a chemical contaminant present in recycled material, if there is a migration to food, should not exceed 1.5 micrograms/person/day (0.5 parts per billion (ppb) dietary concentration) (FDA, 2021). Composting is equally an alternative option to overcome the environmental impacts associated with plastics, but the resistance to microbial decomposition severely limits this approach (Lv et al., 2018; Salehpour et al., 2018). For example, common plastics found in food and beverage packaging, like polyethylene terephthalate (PET) and high-density polyethylene (HDPE), have an expected life span of 450 and 600 years, respectively (Qin et al., 2021).

Currently, there are no official guidelines to characterize the biodegradation profile of a bio-based polymer; consequently, it is difficult to guarantee that products made from them are labeled correctly. The research teams and certifying companies are compelled to base their results on individual standards used to evaluate conventional plastics. In addition, in many works presented in this review, the results were acquired through the application of ISO and ASTM standards and complemented with other data supported by extra laboratory methodologies. The discrepancy of approaches applied in each work is reflected on the different biodegradability rates identified for the same biopolymer. Therefore, it is urgent to create a policy framework that establishes specifications and validation criteria that fit as a foundation for new biodegradability standards adapted for each specific biopolymer and that can be applied in different environments (Pires et al., 2022a). Indeed, several procedures can be followed to evaluate the biodegradability of bio-based polymers, two of which are: (a) control of the

oxygen consumption or the carbon dioxide production; (b) via determination of mass loss (to evaluate disintegration of the plastic) (Miteluț et al., 2019). Yet, it is essential to study the degradation of the biopolymer at various levels. Analyzing the different compounds produced during the decomposition process chemically, and/or analyzing mass loss, and the visual, morphological, and thermal characterization, could provide hints on biodegradation mechanisms (Cano et al., 2016; Cinelli et al., 2019). Therefore, it is suggested that future standardized protocols to measure bio-base polymer degradation should also be rooted in complementing the standardization with the study of other parameters, namely through chemical analysis of the compounds liberated. A bioplastic solely represents a sustainable solution if it is fully biodegradable and if any adverse ecotoxicological effects arise from its degradation. To ensure this, it is fundamental characterization tests are executed not only at the laboratory scale but also in situ through ecotoxicological assessments. Additionally, the microbiota identification present in the ecosystems is also a key aspect to take into consideration in order to determine which taxonomic class produces the most adequate degradation enzymes to each biopolymer (Altun et al., 2020). This complementarity requires significant financial effort and is extremely difficult to implement for the majority of the research teams. It is therefore clear that much remains to be done, and legislators have a key role in establishing standards that help harmonize the biodegradability assays applicable to a biopolymer in order to secure the safety of these new products when distributed in the market (Harrison et al., 2018).

2.2.2 Polysaccharides for Edible Coatings and Films

Bio-based polymers are classified based on their origin into two broad groups, natural and synthetic (figure 2.9). The natural ones are extracted directly from biomass, like proteins (e.g., collagen or gelatin), polysaccharides (e.g., starch, cellulose, or chitin/chitosan), or lipids (e.g., waxes and free fatty acids) or could be produced by microbiological processes like polyhydroxyalkanoate (PHA) or polyhydroxybutyrate (PHB). Polylactic acid (PLA) and polyvinyl alcohol (PVA) represent some examples of synthetically produced biopolymers (Brigham, 2018; Shankar & Rhim, 2018; Youssef & El-Sayed, 2018).

Edible coatings and films are primary packaging systems made from food-grade edible ingredients safe for human consumption. These are idealized to substitute unnecessary non-degradable materials, posing a complementary barrier to secondary non-edible packaging needed for handling and hygienic purposes (Dehghani et al., 2018). The difference between

coatings and films relies on the physical state. Coatings are a liquid applied directly to food surface by spraying, dipping, and most recently through electro-spraying, whereas films are employed as a thin sheet in solid form, wrapping around the food ingredients or incorporated into multilayer food packaging as an inner layer (Yousuf et al., 2018). Both types are formed by having at least two groups of components, a biopolymeric matrix, and additives like plasticizers, cross-linkers, and nanoreinforcements. The natural biopolymers that are commonly used either independently or in combination as matrix precursors usually are divided into three distinct classes, lipids (e.g., fatty acids, waxes, acetyl glycerol), hydrocolloids (e.g., proteins, polysaccharides), and composites (Sharma et al., 2018).

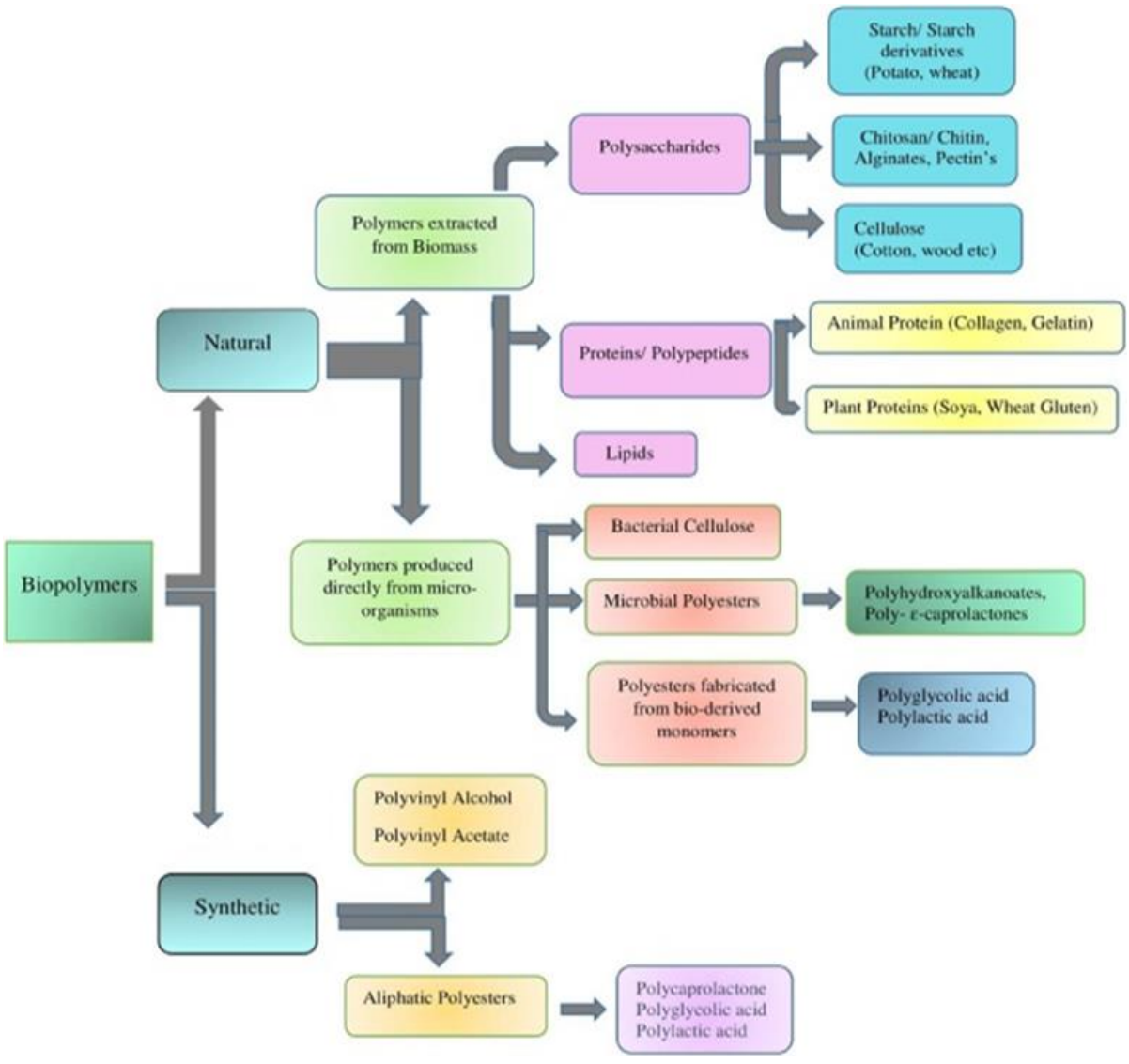

Figure 2.9 — Biopolymers broad classification. Adapted from Sharma et al. (2018).

Polysaccharides are widely produced by microorganisms, plants, and animals and play a fundamental role as structural units and energy resources in cells. This class of biopolymers is considered economically accessible since it can be extracted from renewable and abundant natural sources, often evaluated as waste or by-products. Further, the considerable number of hydroxyl and other polar groups in their structure provided numerous polysaccharides like cellulose, chitosan, starch, pectin, alginate, or carrageenan, with film-forming ability. This set of beneficial properties has encouraged food researchers and engineers to explore polysaccharides to develop new affordable biodegradable edible films and coatings (Chaichi et al., 2017; Fabra et al., 2018; Hubbe et al., 2017; Pires et al., 2018; Shojaee-Aliabadi et al., 2014; Talón et al., 2017). These novel layers support the thorny mission to behave similarly to traditional packaging, acting as selective barriers to oxygen uptake, moisture transfer, loss of flavor, and delaying lipid oxidation, thus, maintaining food safety and sensory quality (Souza et al., 2022). In this matter, due to the well-ordered hydrogen-bonded network configuration, polysaccharides reveal to be an effective barrier to gas transference, like O_2 and CO_2, preventing food dehydration, oxidative rancidity, and surface-browning. In contrast, they typically possess a hydrophilic nature resulting in poor water vapor and moisture barrier properties, which can be a problem in the perishable fresh-cut products preservation (Souza et al., 2017). Apart from their function as inert barriers, edible films and coatings can also carry natural functional ingredients (e.g., extracts, essential oils, nutrients). This grants additional activity to the packaging like antimicrobial, antioxidant, antibrowning, aromatic, sweetening, or coloring. The active package will interact with the food and/or the adjacent environment in a beneficial way, delaying food spoilage by absorbing or scavenging undesirable compounds that promote food degradation. The active compounds incorporation on the packaging instead of direct application on the food has as objective the controlled release to improve the active compounds stability and to prevent excessive oil absorption by the food that could cause harmful toxicological effects for the consumer. This innovative technology also intends to avoid the transference of excessive odors and tastes that can negatively affect the food's organoleptic properties (Pateiro et al., 2021; Sharma et al., 2021).

2.2.3 Chitosan

Chitin, a molecule derivative from glucose, is the second most plentiful natural polysaccharide found on our planet after cellulose and is majorly located in marine arthropods (more specifically in the exoskeleton of crustaceans) and many other invertebrates, like the cell

walls of some fungi and algae. When submitting chitin to a fully or partially N-deacetylation, the acetyl group (-C_2H_3O) from the amino group (-NH_2) at the C-2 position is removed, and a new bioactive polymer designated as chitosan arises (figure 2.10) (Souza et al., 2020a). Structurally, Ch is a linear cationic polysaccharide with variable molecular weight (MW), assembled by D-glucosamine and N-acetyl-d-glucosamine units bonded by β-1,4 glycosidic linkages, with one amino (NH_2) group and two hydroxyl (OH) groups in each repeating glycosidic units (Ali and Ahmed, 2018; Souza et al., 2021). The ratio of D-glucosamine units to the sum of D-glucosamine and N-acetyl-d-glucosamine units which constitute the Ch chain is defined as the degree of deacetylation (DD). Pure Ch is insoluble in water, alkaline solutions, and even in organic solvents, however, when the DD reaches about 50 % it becomes soluble in slightly acidic environments (below its pKa ~ 6.3). As a result, Ch forms a highly versatile viscous solution after being dissolved owing to the amino groups in the chain that protonate (-NH^{3+}), increasing intermolecular electric repulsions and resulting in a polycationic soluble polysaccharide, allowing it to activate reactive locations for a variety of new group attachments using mild reaction conditions (Pires et al., 2018).

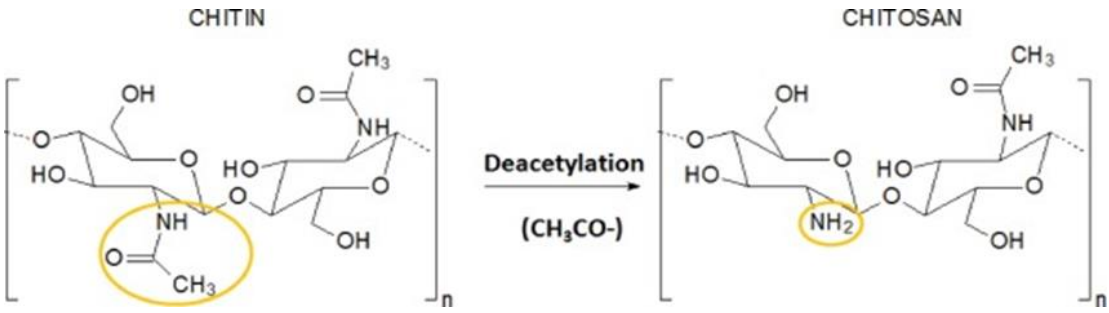

Figure 2.10 — Chemical structures of chitin and chitosan. Adapted from Ali and Ahmed (2018).

In the last years, films and coatings made of chitosan and derivatives have been extensively studied for fresh and processed foods conservation (Alves et al., 2018; Bhatnagar et al., 2021; Costa et al., 2021; Noshirvani et al., 2017), since they possess positive aspects inherently associated with polysaccharides previously described. Additionally, the combination of film-forming ability and antimicrobial/antioxidant activity unlocks the door to Ch active films and coatings in valuable scientific and technological markets like pharmaceutical, biomedical, and food applications (Kumar et al., 2020).

The characteristics presented by chitosan films could be very malleable depending on the ratio of several factors like the degree of deacetylation, the solution viscosity, drying temperature, the percentage of acid dissolution, and the type of composite if the films have other components. These parameters are responsible for physicochemical and biological properties fluctuations, including mechanical and barrier properties, thermal stability, and antimicrobial and antioxidant attributes. Therefore, it is crucial to carefully assess the film's properties, paying particular attention to the interactions between food and biopolymer (Elsabee and Abdou, 2013; Mangaraj et al., 2018). Moreover, one of the biggest concerns affecting consumers' judgment about new conservative formulations is whether it induces food toxicity. Accordingly, the low toxicity profile displayed by Ch is essential for the development of novel bioplastics to be applied directly to the food. Despite some *in vivo* essays already narrated that Ch purity coerces its toxicological profile, being safe in terms of inertness and weak or no toxicity unveiled, some allergenic concerns wait with expectation. Food and Drug Administration (FDA) already conferred some authorizations to chitosan products with the status of "Generally Recognized As Safe" (GRAS) (USFDA, 2013), authorizing its employment as dietary supplement. Even so, Ch ingestion is not recommended for people with shellfish allergy (Ma et al., 2017).

Regardless of being extensively studied and developed at the laboratory level, the transition to the industry has been a very demanding challenge for chitosan films. From the economic perspective, chitin is a reasonably cheap raw material once the crustacean exoskeleton is promptly and widely available as a by-product of the seafood processing industry. Consequently, it is presumable that Ch production on a large scale could be feasible. However, the observed poor mechanical properties and high-water vapor permeability rates require the combination of chitosan with other components. The formation of Ch composites depends on the inclusion of stringent chemical treatments, consequently increasing the final product manufacturing (Mujtaba et al., 2019). Novel technologies, like microwave technology combined with green solvents like deep eutectic solvents (DES) or ionic liquids (ILs), could help to outgrow the extraction time of chitin and make the production more environmentally friendly. Furthermore, the biological production of chitin and chitosan is considered an alternative process to ensure availability and reduce the allergenic issue (Souza et al., 2020b).

The most considerable losses in food are owing to microbiological contamination. Chitosan is a highly studied flexible biopolymer, and its antimicrobial activity is one of the primary reasons for the intensive number of scientific reviews year after year. This reality manifests itself through the countless cited publications proving that Ch successfully hinders the

growth of various microorganisms such as Gram-positive and Gram-negative bacteria, filamentous fungi, and yeast, assuring its worthwhile addition to packaging systems (Duan et al., 2019; Elsabee and Abdou, 2013; Hosseinnejad and Mahdi, 2016; Ma et al., 2017; Verlee et al., 2017). Moreover, distinctive studies proclaimed the Ch potential to act as a food preservative eradicating and/or inhibiting the spread of specific bacteria which are behind some foodborne illnesses like *Escherichia coli*, *Bacillus cereus*, *Salmonella typhimurium*, or *Staphylococcus aureus* (Fernandez-Saiz et al., 2010; Gomes et al., 2019; Paomephan et al., 2018; Vishu et al., 2007).

The mode of action responsible for the antimicrobial activity can be influenced by different microbial, environmental, and intrinsic factors (e.g., type of microorganism, molecular weight, and degree of deacetylation, among others) (figure 2.11). Therefore, it is hard to comprehend the precise mechanism in charge (Verlee et al., 2017).

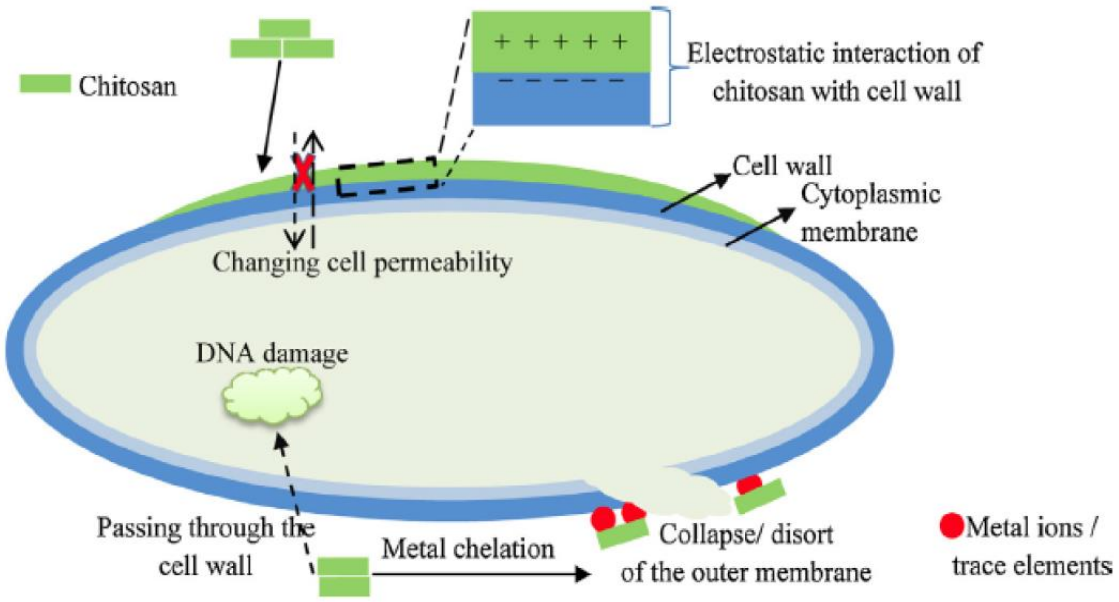

Figure 2.11 — Schematic representation of chitosan antimicrobial mechanisms. Adapted from (Hosseinnejad and Mahdi, 2016).

The broadly accepted hypothesis is the interaction between the positive polycationic nature of chitosan with negatively charged surface components of many microorganisms, causing modifications to the cell, leading to leakage of intracellular contents that ultimately outcome in cellular death. The number of protonated amino groups valent in chitosan increases with higher degrees of deacetylation which leverages the antimicrobial activity (Elsabee and

Abdou, 2013; Kumar et al., 2020). Moreover, Ch can act as a metal chelator, forming complexes with the metals circumjacent the bacteria, inhibiting various metabolic enzymes of microbial cells by blocking their active centers and consequently preventing the flow of essential nutrients (Gomes et al., 2019). The molecular weight is also a crucial aspect governing antimicrobial action. If the MW is high enough, Ch will cover the cell surface changing its permeability and blocking the intake of nutrients. On the other hand, if the MW is low, Ch could impregnate and link with the cell's DNA, culminating in interference with the synthesis of mRNA and proteins conducting to cell death (Muxika et al., 2017).

Food products are exposed to numerous ways of oxidative deterioration (Kumar et al., 2020). Food companies usually add synthetic substances with antioxidant properties as supplements to surpass this problem. Nevertheless, the consumer opinion concerning the application of these unnatural substances is not the best. This mistrust comes from the possibility of toxic compounds absorption and accumulation in body organs and tissues, which may be directly related to oncological problems (Anraku et al., 2018). Chitosan and derivatives offer a solution for food formulations because these possess an intrinsic antioxidant activity possibly related to free-radical scavenging ability and chelation of metal ions. Furthermore, an attractive strategy to improve the antioxidant activity of Ch films and coatings is incorporating natural ingredients extracted from plant polyphenols. The controlled liberation of these compounds from the Ch matrix is an efficient way to overcome some associated drawbacks that restrict the direct application of extracts and essential oils into food, like high cost, sensorial change, and potential toxicity (Souza et al., 2017; Yuan et al., 2016).

2.3 Chitosan/Cellulose Bionanocomposites

Gradually, several industries are changing, replacing traditional petroleum-based plastics with bio-based materials. However, the mechanical, thermal, and barrier properties are not yet at the same level as the materials currently used. One solution that could be an efficient way to enhance these properties is blending the polymer matrix with fillers (Dehnad et al., 2014; Shankar and Rhim, 2018). Bionanocomposites are mixtures of a biopolymer reinforced with small quantities of inorganic or organic micro/nanofillers with a particular size, geometry, and surface chemistry. The chosen polymers to serve as matrices are usually hydrocolloids, like proteins, starches, pectins, polysaccharides (e.g., chitosan), and synthetic biopolymers (Bharimalla et al., 2017).

Nanocellulose has been pointed out as a suitable biodegradable plant-based nanofiller for bionanocomposites due to its unique optical, rheological, chemical structure (abundant hydroxyl groups), and mechanical properties (high strength and high specific surface area) at low concentration (Chakrabarty and Teramoto, 2018; Chen et al., 2019; Xu et al., 2018). Additionally, it possesses fewer public health risks associated when compared to traditional nanofillers, like nanoclay, nanoaluminum oxide particles, silica, mica, and carbon blacks (Ng et al., 2017). In the literature, it is possible to find papers exposing the effects of NC incorporation in composites. Usually, the incorporated nanocellulose is produced from hydrolyzed microcrystalline cellulose, already prepared, and directly imported from specialized laboratories, making it difficult to know which raw source was used to extract the cellulose (Chaichi et al., 2017; Dehnad et al., 2014; Rong et al., 2017). The most significant nanocellulose effects on polymer matrices are associated with the tensile and barrier properties where both CNFs and CNCs present good reinforcement characteristics (tables 2.3 and 2.4).

2.3.1 Mechanical Reinforcement

Predominantly, chitosan matrixes reinforced with nanocellulose noted a growth in the tensile modulus and strength and a reverse decrease in the film elasticity. The nanofiller good dispersion in the Ch matrix, allied with the NC's higher crystallinity which confers strength and stiffness, is essential to justify this reinforcement ability (Pires et al., 2019b). In proper conditions, the reinforcement effect is also explained by the well-dispersed NC within the polymeric array through hydrogen bonds. Moreover, at low concentrations, NC demonstrates a considerable potential to develop percolating networks due to the high availability of free hydroxyl groups (Khan et al., 2012; Lan et al., 2021; Zhang et al., 2021b).

In order to build an improved mechanical network is necessary to take into account three fundamental characteristics, the nanofiller dispersion, the NC aspect ratio, and the force of interaction between filler and matrix (Dufresne, 2013). Bras et al., (2011) study proved that NC with a higher aspect ratio improves the film tensile strength, resulting in a percolation threshold decrease, allowing the reduction of the necessary filler content to achieve an effective reinforcing effect. Higher aspect ratio also contributes to nanoparticles with a higher specific surface area, which could promote an enriched connection between the Ch and NC, enabling a higher yield of stress transfer and restricting the polymer chain’s motion and flow (Ng et al., 2017). Moreover, the source and the methodology adopted in the cellulose isolation and

subsequent NC extraction affect its intrinsic characteristics, like crystallinity, which consequently will influence its mechanical reinforcement capacity (Talebi et al., 2021).

Based on the analyzed studies (table 2.3), a nanocellulose amount between 2-5 % is considered the most suitable percentage for mechanically reinforced Ch. Still, Azeredo et al., (2010), when evaluating the synergy between CNFs and glycerol added to chitosan films to improve its mechanical and barrier properties, verified that the optimum conditions were the addition of precisely 15 % CNFs and 18 % glycerol. Later, Gopi et al., (2019) studied the incorporation of CNFs extracted from turmeric residue into Ch films at four distinct levels (1–7 % (w/w Ch)). The tensile strength and young's modulus registered an increase for all concentrations, reaching the highest rise of 31 % and 18 %, respectively, for a 5 % CNFs amount. The interlinkage of CNFs by hydrogen bonding with Ch generated an ably reinforcing fibrillar network, which upgraded the mechanical properties considerably. In the same year, Jacob et al., (2019) and Kumar et al., (2019) used similar CNFs levels as reinforcement, with the cellulosic nanofibers extracted from ginger rhizomes and jute fiber, respectively. The results adopted the same trend of Gopi's work but with more significant improvement percentages. Of note, the superior strength and stiffness values obtained by Jacob's work, around 126 % and 89 %, reached with 5 % CNFs. The authors stated predominant and most intense intermolecular hydrogen bonds between the bionanocomposite components, data supported by the FTIR results exposed in the same study. Kumar's work also complemented, expressing that the CNF's inferior size and uniform distribution in the Ch matrix could signify a decrease of pours and failure spreading points. Furthermore, for both studies % EAB diminished with the NC incorporation, as expected.

The chitosan films reinforced with cellulose nanocrystals indicate similar mechanical behavior to the ones with the nanofibers. Khan et al., (2012)prepared chitosan-based biodegradable films reinforced with four different concentrations of nanocrystalline cellulose (1–10 % (w/w Ch)). The most noticeable mechanical improvement was attributed to bionanocomposites with 5 % CNCs, in which the TS improved by 25 % and the EM by 87 %. The explanation behind the favorable Ch/CNCs interactions could reside in the suitable interface between the anionic sulfate groups of CNCs and the cationic amine groups of Ch. Beyond this CNCs amount, a potential nanoparticles aggregation occurred that did not help to improve the mechanical properties. In opposition, the authors stated a slight decrease relative to elongation at break. This decrease suggested a strong interaction between filler and matrix, which narrowed the matrix mobility. In order to value agricultural waste, Xu et al., (2018) isolated CNCs from

rice straws and used them to develop high value bionanocomposites. The authors observed a constant increment in the tensile strength until the optimal CNCs value of 5 %. Again, it was verified that the filler's reinforcing capacity decreases for more than this percentual. In addition to the aggregation of nanoparticles, the authors attribute the weak interfacial compatibility between Ch/CNCs to the charge neutralization between –COO– and $–NH^{3+}$. On the other hand, the % EAB proportionally decreased with the CNCs content rise. Observing other studies presented in table 2.4 is possible to conclude that the ideal CNCs incorporation level to grasp the upper-interfacial compatibility should be around 2-5 %. This percentage allows optimal nanocellulose dispersion, robust hydrogen bonding, and electrostatic interactions between Ch and CNCs. Interestingly, the work of Mujtaba et al., (2017) has slightly deviated from the formerly exposed tendency. This research focused on the CNCs extraction from flax fibers, which were later used in higher percentages (5–30 % (w/w Ch)) to reinforce Ch films. The authors determined that TS and EM values increased with the CNCs addition, with the amount of 20 % revealing the optimal results.

2.3.2 Barrier Reinforcement

The observed trend exposed in table 2.4 indicates that WVP reduces with the incorporation of nanocellulose particles, up to a maximum of 10 % of nanofillers. Above this incorporated NC amount, the reinforcement of barrier properties is no longer efficient. Furthermore, this property appears to be independent of the NC type or source used. In the study of Corsello et al., (2017), bionanocomposites based on chitosan incorporated with CNCs at four increasing levels (1, 3, 5, and 10 % w/w Ch) showed a reduction in the WVP up to 38 % in comparison to pristine chitosan films. The authors verified a WVP minimum value for the Ch sample reinforced with 5 % CNCs. Comparatively, it was stated that increasing the amount of reinforcement did not increase the barrier property. The authors mainly attributed the WVP reduction to the presence of CNCs, which increased the tortuosity in the polymer matrix films, leading to slower water vapor diffusion processes. Other factors might account for the WVP reduction, like i) the increase in the polymer's crystallinity (acting as crystalline fillers that increase the distance for the molecules of water to pass through); ii) the improvement in the film uniformity, and iii) making the film tough enough to decrease the frequency of cracks or other defects that could lead to a high permeability (Ferrer et al., 2017). In contrast, excessive CNCs

destroyed the polymeric network structure of chitosan, allowing for the formation of gaps for water vapor molecules to pass through (Azeredo et al., 2010).

The oxygen permeability study is scarce, and few studies investigate it simultaneously with water vapor permeability. Zhang et al., (2021) proposed a novel bionanocomposite of chitosan reinforced with curcumin grafted TEMPO-oxidized cellulose nanofibers (TOCNFs) at 10 %, 17 %, 25 %, and 33 % (w/w Ch). Regarding WVP, similar behavior was reported, with a reduction in WVP with TOCNFs incorporation. On the other hand, the bionanocomposites OP increased with the nanoparticle incorporation, thus, the addition of TOCNFs had a more powerful destructive effect than improved crystallinity for the polymer network, and the hydrophobicity of TOCNFs was not sufficient to counterbalance this, contributing less to the oxygen barrier.

Table 2.3— Mechanical properties of chitosan films reinforced with nanocellulose compared to pristine chitosan films.

Formulation	Incorporation Method	Tensile Strength (Relatively to Control)	% Elongation at Break (Relatively to Control)	Elastic Modulus (Relatively to Control)	References
1% (w/v) Ch (DD of 88%)	Rotor–stator homogenizer (Ultra-Turrax)	1% CNCs: Increased ~ 9% 3% CNCs: Increased ~ 17% 5% CNCs: Increased ~ 25% 10% CNCs: Increased ~ 24%	1% CNCs: Decreased ~ 25% 3% CNCs: Decreased ~ 40% 5% CNCs: Decreased ~ 55% 10% CNCs: Decreased ~ 55%	1% CNCs: Increased ~ 43% 3% CNCs: Increased ~ 60% 5% CNCs: Increased ~ 87% 10% CNCs: Increased ~ 80%	(Khan et al., 2012)
2% (w/v) Ch (DD not specified)	Mechanical stirring and ultrasonic homogenizer	Ch+1% CNCs: Increased ~ 1% Ch+3% CNCs: Decreased ~ 3% Ch+5% CNCs: Increased ~ 18% Ch+10% CNCs: Increased ~ 8%	Ch+1% CNCs: Decreased ~ 33% Ch+3% CNCs: Decreased ~ 14% Ch+5% CNCs: Increased ~ 24% Ch+10% CNCs: Increased ~ 28%	Ch+1% CNCs: Increased ~ 13% Ch+3% CNCs: Increased ~ 47% Ch+5% CNCs: Increased ~ 32% Ch+10% CNCs: Increased ~ 2%	(Corsello et al., 2017)
1% (w/v) Ch (DD of 98%)	Mechanical stirring and Silent Crusher-Heidolph homogenizer	Ch+5% CNCs: Increased ~ 9% Ch+10% CNCs: Increased ~ 11% Ch+20% CNCs: Increased ~ 24% Ch+30% CNCs: Increased ~ 17%	5% CNCs: Increased ~ 22% 10% CNCs: Decreased ~ 2% 20% CNCs: Decreased ~ 5% 30% CNCs: Increased ~ 1%	Ch+1% CNCs: Increased ~ 7% Ch+3% CNCs: Increased ~ 22% Ch+5% CNCs: Increased ~ 140% Ch+10% CNCs: Increased ~ 86%	(Mujtaba et al., 2017)
4% (w/v) Ch (DD of 90%)	Mechanical stirring and ultrasonic homogenizer	1% CNCs: Increased ~ 5% 3% CNCs: Increased ~ 30% 5% CNCs: Increased ~ 71% 8% CNCs: Increased ~ 52% 10% CNCs: Increased ~ 46%	1% CNCs: Decreased ~ 15% 3% CNCs: Decreased ~ 20% 5% CNCs: Decreased ~ 20% 8% CNCs: Decreased ~ 35% 10% CNCs: Decreased ~ 40%	Not Performed	(Xu et al., 2018)
1% (w/v) Ch (DD of 90%)	Mechanical stirring and ultrasonic homogenizer	Ch+2% CNCs: Increased ~ 5% Ch+4% CNCs: Increased ~ 39% Ch+6% CNCs: Increased ~ 35% Ch+8% CNCs: Increased ~ 32%	Ch+2% CNCs: Decreased ~ 23% Ch+4% CNCs: Decreased ~ 55% Ch+6% CNCs: Decreased ~ 58% Ch+8% CNCs: Decreased ~ 59%	Ch+2%CNCs: Increased ~ 39% Ch+4%CNCs: Increased ~ 79% Ch+6%CNCs: Increased ~ 72% Ch+8% CNCs: Increased ~ 69%	(Yadav et al., 2020)
Not specified % (w/v) Ch (DD of 90%)	Mechanical stirring and ultrasonic homogenizer	Ch+1% CNFs: Increased ~ 10% Ch+3% CNFs: Increased ~ 22% Ch+5% CNFs: Increased ~ 31% Ch+7% CNFs: Increased ~ 25%	Ch+1% CNFs: Decreased ~ 8% Ch+3% CNFs: Decreased ~ 18% Ch+5% CNFs: Decreased ~ 28% Ch+7% CNFs: Decreased ~ 22%	Ch+1% CNFs: Increased ~ 7% Ch+3% CNFs: Increased ~ 14% Ch+5% CNFs: Increased ~ 18% Ch+7% CNFs: Increased ~ 14%	(Gopi et al., 2019)
1% (w/v) Ch (DD of 75–80%)	Mechanical stirring and ultrasonic homogenizer	Ch+1%CNFs: Increased ~ 31% Ch+3%CNFs: Increased ~ 87% Ch+5% CNFs: Increased ~ 126% Ch+7% CNFs: Increased ~ 92%	Ch+1% CNFs: Decreased ~ 10% Ch+3% CNFs: Decreased ~ 15% Ch+5% CNFs: Decreased ~ 19% Ch+7% CNFs: Decreased ~ 37%	Ch+1% CNFs: Increased ~ 20% Ch+3% CNFs: Increased ~ 43% Ch+5% CNFs: Increased ~ 89% Ch+7% CNFs: Increased ~ 51%	(Jacob et al., 2019)

** Chitosan (Ch); Cellulose Nanocrystals (CNCs); Cellulose Nanofibers (CNFs); Degree of Deacetylation (DD).*

Table 2.4— Barrier properties of chitosan films reinforced with nanocellulose compared to pristine chitosan films.

Formulation	Incorporation Method	Water Vapor Permeability (Percentage Relatively to Control)	Oxygen Permeability (Percentage Relatively to Control)	References
2% (w/v) Ch (DD not specified)	Mechanical stirring and ultrasonic homogenizer	Ch + 1% CNCs: Decreased 34% Ch + 3% CNCs: Decreased 16% Ch + 5% CNCs: Decreased 38% Ch + 10% CNCs: Decreased 25%	Not Performed	(Corsello et al., 2017)
1% (w/v) Ch (DD of 90%)	Mechanical stirring and ultrasonic homogenizer	Ch + 2% CNCs: Decreased 24% Ch + 4% CNCs: Decreased 29% Ch + 6% CNCs: Decreased 34% Ch + 8% CNCs: Decreased 37%	Not Performed	(Yadav et al., 2020)
3% (w/v) Ch (DD of 94%);	Mechanical stirring	Ch + 10% CNCs: Decreased 32% Ch + 20% CNCs: Decreased 28%	Not Performed	(Azeredo et al., 2010)
2% (w/v) Ch (DD not specified)	Mechanical stirring	Ch + 10% TOCNFs: Decreased 6% Ch + 17% TOCNFs: Increased 2% Ch + 25% TOCNFs: Decreased 4% Ch + 33% TOCNFs: Decreased 7%	Ch + 10% TOCNFs: Increased 13% Ch + 17% TOCNFs: Increased 16% Ch + 25% TOCNFs: Increased 3% Ch + 33% TOCNFs: Increased 62%	(Zhang et al., 2021b)
1% (w/v) Ch (DD of 75–85%)	Nanoparticles were dispersed with the aid of mechanical stirring	Ch + 2% BNCs: Decreased 9% Ch + 4% BNCs: Decreased 20% Ch + 6% BNCs: Decreased 27%	Not Performed	(Salari et al., 2018)

** Chitosan (Ch); Cellulose Nanocrystals (CNCs); Bacterial Nanocellulose (BNCs); Degree of Deacetylation (DD); TEMPO-Oxidized Cellulose Nanofibers (TOCNFs).*

3

MATERIALS AND METHODS

3.1 General Methodology

The doctoral thesis entitled "Development of Chitosan Bionanocomposites Reinforced with Nanocellulose Extracted from Energy Crops: Characterization and Application as Active Packaging" was developed in two research centers, MEtRiCS, and CENIMAT|i3N in partnership with the Departments of Chemistry and Material Science, located at NOVA School of Science and Technology (FCT/UNL), in Portugal. The experimental procedure was divided in three stages:

Stage (i) Stems from three selected low indirect land-use change (ILUC) crops (*Miscanthus × giganteus* Greef et Deuter, *Arundo donax* L., *Hibiscus cannabinus* L.) were washed, micronized, and characterized. After that, cellulose was isolated from the fibers and sequentially converted into cellulose nanocrystals by an alkaline pre-treatment, bleaching, and acid hydrolysis. The fibers were analyzed before and after the pre-treatment/bleaching steps to study the influence that these processes have on the cellulosic fiber purification before the transformation into nanocellulose. For such characterization, the fiber composition, yield, morphology (polarized optical microscopy (POM)), crystallinity (X-ray diffractometry (XRD)), thermal stability (differential scanning calorimetric (DSC) and thermal gravimetric analysis (TGA)), functional groups and chemical structures (Fourier-transform infrared spectroscopy (FTIR)) were performed. Additionally, the produced nanocelluloses were also characterized in terms of chemical structure, thermal stability, crystallinity using the same techniques. Additionally, the CNCs were subjected to a morphology analysis (atomic force microscopy (AFM)), and dispersion stability (Zeta potential).

Stage (ii) Chitosan bio-based films were reinforced with nanocellulose extracted from the three different biomasses obtained in Stage (i). The nanofillers were incorporated at three different percentages, and the bionanocomposites were characterized to evaluate the reinforcement interference in the biopolymer functional properties. For such evaluation, colorimetric, moisture, swelling, water-solubility, oxygen and water vapor permeability analyzes in conjunction with mechanical properties, FTIR, crystallinity (XRD), thermal stability (DSC/TGA) and scanning electron microscopy (SEM) were performed. Chitosan biofilms reinforced with commercial nanocellulose (extracted from cotton) at the same percentages were evaluated for comparison. The objective of this step is to evaluate whether there were differences in the bionanocomposites properties reinforced with CNCs extracted from different biomasses and choose the ideal amount to be introduced as reinforcement in chitosan biofilms;

Stage (iii) The best chitosan/nanocellulose bionanocomposites produced in Stage (ii) were evaluated as a primary packaging layer for a perishable product. This stage aimed to evaluate the capacity to extend the shelf-life of fresh poultry meat with an eco-friendly active film. This novel approach followed the circular economy concept, reusing biomass, to develop a new high added-value material to be used in the future as a fully biodegradable and active element in food packaging. Additionally, bionanocomposites incorporated with salvia essential oil (SEO) were also produced to study the cellulosic nanoreinforcement as an encapsulation agent of natural active compounds and the associated effect as active packaging to perishable food matrices. For such evaluation, "*in situ*" parameters, composed of physicochemical (pH, total volatile basic nitrogen (TVB-N) and moisture), lipid oxidation (TBARS index) and microbial growth (Total mesophilic aerobic microorganism (TMAM), total psychrotropic aerobic microorganism (TPAM), and *Enterobacteriaceae*) were studied. Additionally, "*in vitro*" evaluation was performed to study the bionanocomposites antioxidant activity (DPPH (2,2-Diphenyl-1-picrylhydrazyl) method) and the phenolic compounds migration (Folin-Ciocalteu method).

3.2 Materials

All chemical reagents used are of analytical purity and the water was purified using the Milli-Q system (Millipore, Bedford, MA, USA). Chitosan with a high molecular weight (31–37 kDa), 2,2-Diphenyl-1-picrylhydrazyl (DPPH), and 1,1,3,3-tetraethoxypropane (TEP) were acquired from Sigma-Aldrich (Steinheim, Germany). Trichloroacetic acid (TCA), 2-

thiobarbituric acid (TBA), Folin-Ciocalteu reagent, and anhydrous sodium carbonate (Na_2CO_3) were obtained from PanReac (Barcelona, Spain). Absolute ethanol (C_2H_5OH), glacial acetic acid (CH_3COOH), glycerol ($C_3H_8O_3$), sodium hydroxide (NaOH), hydrogen peroxide (H_2O_2), sulphuric acid 95-97 % (H_2SO_4), calcium nitrate ($Ca(NO_3)_2$), sodium bromide (NaBr), potassium acetate (CH_3COOK, 99 % purity), and Tween® 80 were purchased from Alfa Aesar (Kandel, Germany). The microbiological reagents "Violet Red Bile Glucose" (VRBG), "Trypto-Casein Soy Agar" (TSA), and "Trypto-Casein Soy Broth" (TSB) and "Plate Count Agar" (PCA) were purchased from Biokar (Allonne, France). Commercial Nanocellulose was kindly supplied by Nanocrystacell (Podcerkev, Slovenia). The food grade essential oil of sage (*Salvia officinalis* L.) produced by Biover (Nazareth, Belgium) was purchased in a local market. Giant reed, kenaf, and miscanthus biomass were harvested from pilot fields settled in Caparica, near Lisbon, in the Peninsula of Setúbal, Portugal. The kenaf and miscanthus biomass was collected in November 2018, while the giant reed biomass was gathered in January 2020. The reaped material was dried at 40ºC in a vacuum oven, cut into small pieces, and stored in darkness, in a dry place at room temperature until further use.

3.3 Cellulose Nanocrystals Production

The cellulose nanocrystals isolation **(Stage (i))** followed and adapted the procedures reported for various biomass sources. The experimental operation respected three subsequential stages, alkali pre-treatment, chlorine-free bleaching, and acid hydrolysis (Collazo-Bigliardi et al., 2018; Ferreira et al., 2018; Xu et al., 2018).

Initially, the raw fibers were grinded by a high-speed blade crusher (Hukoer, China) and sieved to a particle size of 60-80 mesh (150-200 μm) followed by a washing step with ethanol 20 % (v/v) at a fiber/solution ratio of 1:5. The alkali pre-treatment was fulfilled on the fiber powder with a 7 % (w/v) NaOH solution, with a fiber/solution ratio of 1:10. The system was maintained for 3 h at 70ºC under continuous mechanical stirring. The pre-treatment was performed one more time. In the next stage, the pre-treated fibers were bleached for 4 h at 60ºC in a solution composed of 4 % (w/v) NaOH and 24 % (v/v) H_2O_2 at a proportion of 1:1 (v/v), adopting a fiber/solution ratio of 1:20 (w/v). The fibers were mixed in the NaOH solution and the H_2O_2 was added by dripping. This treatment was done three times, and after the last bleaching, the fibers were washed with hot distilled water several times and dried in an oven (WTB binder, Germany) at 80ºC until registered a constant weight.

To obtain the CNCs from the bleached cellulosic fibers, these were hydrolyzed with 64 % (w/w) H_2SO_4 solution in fiber to acid ratio of 1:20 (w/v) for 45 min at 45ºC. To quench the reaction, ten times more ultrapure water (4ºC) was added. The resulted suspension was centrifuged with distilled water at 10.000 rpm at 0°C for 15 min to remove the excess H_2SO_4. Several centrifugations were done until the CNCs suspension reached a pH of 5, then these were neutralized with a few drops of 7 % (w/v) NaOH. In the end, the nanoparticles were homogenized under constant mechanical stirring for 15 min with ultraturrax (15.000 rpm) (IKA®T18, Germany), followed by 30 min in ultrasound bath (360 W) (Selecta, Spain). The homogenization process was repeated three times. The CNCs mixture was carefully dried in an oven at 50ºC until a gel is achieved, with 80–90 % of water. The gel was frozen until the beginning of the essays to secure that it is stored over time without degradation (Ditzel et al., 2017; Mohaiyiddin et al., 2018).

3.4 Bionanocomposites Preparation

For the **Stage (ii)**, the bionanocomposites were prepared according to (Souza et al., 2019b). Film-forming dispersion (FFD) was prepared by dissolving 1.5 % (w/v) of chitosan in 1 % (v/v) of a glacial acetic acid solution under vigorous mechanical stirring for 24 h at room temperature. After, glycerol, as a plasticizer, was added at the percentage of 30 % (w/w) of Ch in all treatments. This amount of glycerol added (corresponding to only 0.45 % w/v in the FFD) was chosen based on previous experiences with Ch bionanocomposites (e.g., (Souza et al., 2019b) work found this amount optimal for film formation, and to obtain improved barrier and mechanical properties). Moreover, as the amount of glycerol was constant in all the composite films, differences among them were determined by the effect of the extracted biomass-derived CNCs incorporated in the chitosan (that also has glycerol). To transform the bio-based films into bionanocomposites, the CNCs from the three different biomasses in the levels (1.5, 2, or 2.5 % (w/w) of Ch) were added to the FFD. The bionanocomposites were denominated as Ch + G (Chitosan/Giant Read CNCs), Ch + M (Chitosan/Miscanthus CNCs), and Ch + K (Chitosan/Kenaf CNCs). Thereafter, three agitation cycles of 5 min agitation with ultraturrax (15.000 rpm) pursued by 15 min degasification in an ultrasound bath (360 W) were performed. These three cycles were adopted to assure a suitable exfoliation and dispersion of the CNCs into the polymeric chain. The finished dispersion was then cast in glass molds (18 x 25 cm) and left to dry with the aid of a circulatory hot fan (30ºC room temperature) for approximately 24

h. When totally dried, the bionanocomposites were peeled and saved protected from light in a desiccator containing saturated calcium nitrate solution at 25ºC and 50 % relative humidity. Aiming to study the reinforcing impact of mixing CNCs, a Ch film without any amount of reinforcement and Ch film reinforced with commercial nanocellulose (Ch+CNCC) (at the same percentages) were produced for comparison. The formulation parameters for each bionanocomposite assembled on Stage (ii) can be consulted in table 3.1.

For packaging application **(Stage (iii))** were produced only bionanocomposites with the best reinforcement amount established in the previous stage. The bionanocomposites incorporated with sage essential oil were made using the same methodology, in which 1 % (v/v FFD) of SEO was added along with 0.45 % (w/v FFD) of glycerol and Tween® 80 at a level of 0.2 % (w/v SEO), to function as an emulsifier. Following that, the dispersion was submitted to 5 min agitation with ultraturrax (15.000 rpm) pursued by 15 min degasification in an ultrasound bath (360 W). To transform the bio-based FFD into bionanocomposites, 2.5 % of CNCs (w/w Ch), isolated from the three identified biomasses, was added. Thereafter, two more cycles of ultraturrax and ultrasound in the same conditions were done to guarantee a correct exfoliation and dispersion of all components into the polymeric chain. Aiming to study the encapsulation effect of CNCs on SEO, Ch films only with the addition of essential oil were assembled (Ch + SEO). Moreover, Ch films reinforced with CNCC and SEO (at the same percentages) were achieved for comparison. Supplementary pristine Ch films were produced to be used as a control for all samples. The formulation parameters for each bionanocomposite assembled on Stage (iii) can be consulted in table 3.2.

Table 3.1 – Formulation parameters for each bionanocomposite assembled on Stage (ii).

Specimen	Bionanocomposite Formulation Parameters					
	Chitosan (% w/v FFD)	**Glycerol (% w/w Ch)**	**Commercial CNCs (% w/w Ch)**	**CNCs Giant Reed (% w/w Ch)**	**CNCs Kenaf (% w/w Ch)**	**CNCs Miscanthus (% w/w Ch)**
Pristine Ch	1.5	30	0	0	0	0
Ch + 1.5% CNCC	1.5	30	1.5	0	0	0
Ch + 2% CNCC	1.5	30	2	0	0	0
Ch + 2.5% CNCC	1.5	30	2.5	0	0	0
Ch + 1.5% G	1.5	30	0	1.5	0	0
Ch + 2% G	1.5	30	0	2	0	0
Ch + 2.5% G	1.5	30	0	2.5	0	0
Ch + 1.5% K	1.5	30	0	0	1.5	0
Ch + 2% K	1.5	30	0	0	2	0
Ch + 2.5% K	1.5	30	0	0	2.5	0
Ch + 1.5% M	1.5	30	0	0	0	1.5
Ch + 2% M	1.5	30	0	0	0	2
Ch + 2.5% M	1.5	30	0	0	0	2.5

** Chitosan (Ch); Cellulose Nanocrystals (CNCs); Commercial Nanocellulose (CNCC); Giant Reed Nanocellulose (G); Kenaf Nanocellulose (K); Miscanthus Nanocellulose (M).*

Table 3.2— Formulation parameters for each bionanocomposite assembled on Stage (iii).

Specimen	Bionanocomposite Formulation Parameters							
	Chitosan (% w/v FFD)	**Glycerol (% w/w Ch)**	**Tween® 80 (% w/v SEO)**	**Commercial CNCs (% w/w Ch)**	**CNCs Giant Reed (% w/w Ch)**	**CNCs Kenaf (% w/w Ch)**	**CNCs Miscanthus (% w/w Ch)**	**Sage Essential Oil (% v/v FFD)**
Ch	1.5	30	0	0	0	0	0	0
Ch+CNCC	1.5	30	0	2.5	0	0	0	0
Ch+G	1.5	30	0	0	2.5	0	0	0
Ch+K	1.5	30	0	0	0	2.5	0	0
Ch+M	1.5	30	0	0	0	0	2.5	0
Ch+SEO	1.5	30	0.2	0	0	0	0	1
Ch+CNCC+SEO	1.5	30	0.2	2.5	0	0	0	1
Ch+G+SEO	1.5	30	0.2	0	2.5	0	0	1
Ch+K+SEO	1.5	30	0.2	0	0	2.5	0	1
Ch+M+SEO	1.5	30	0.2	0	0	0	2.5	1

** Chitosan (Ch); Cellulose Nanocrystals (CNCs) Commercial Nanocellulose (CNCC); Giant Reed Nanocellulose (G); Kenaf Nanocellulose (K); Miscanthus Nanocellulose (M); Salvia Essential Oil (SEO).*

3.5 Cellulose Material Characterization

3.5.1 Fiber Compositional Characterization

The main constituents (cellulose, hemicellulose, lignin, ash, total fiber) present in giant reed, kenaf, and miscanthus fiber will be quantified at two different stages, initial, and after alkaline pre-treatment/bleaching, following the Van Soest methodology (Soest, 1963).

3.5.2 Extraction Yield

The cellulose extraction (after pre-treatment and after bleaching) yield in percentage were calculated. Initial dry sample weight (M_i) and after process dry sample weight (M_f) were measured to calculate the yield, as exposed in the equation 1.

$$\boldsymbol{Yield}\ \% = \frac{\boldsymbol{M_f}}{\boldsymbol{M_i}} \times \mathbf{100} \quad (1)$$

3.5.3 Microaggregates Morphology: Polarized Optical Microscopy

The initial untreated fibers and the CNCs microaggregates obtained after the acid hydrolysis stage were observed under an Olympus BX51 polarized optical microscope (POM) (Tokyo, Japan) equipped with transmitted and reflected light. The samples were observed between cross and parallel polars connected to a SCHOTT KL2500 LCD cold light source. An equipped camera (Olympus DP73) along with Olympus Stream Basic 1.9 software was used for image capture. To perform a feasible identification, the initial fibers were dispersed in water while the microparticles were identified using the final suspensions after acid hydrolysis. Each sample was placed into individual rectangle hollow glass tubes (VitroTubes™, 50 × 4 mm^2, 0.4 mm path length). Five images of each sample were taken, and were treated using ImageJ software (Maryland, USA) to quantify the cellulose microaggregates identified in the measured region and consequently measure their average size. This software analyzes the POM images by identifying, counting the microaggregates and drawing an outline on them. Through a scale introduced in the software, the width and length were measured using the defined outlines.

3.5.4 Nanocellulose Morphology: Atomic Force Microscopy

Atomic force microscope topography of the chitosan film surface, where the CNCs were inserted at the percentage 2.5 wt%, was acquired with an Asylum Research MFP-3D Standalone system (Oxford Instruments, UK) operated in room conditions, in alternate contact mode, using commercially available silicon probes (Olympus AC160TS, f0 = 300 kHz, k = 26 N/m). Topographs were low-level plane fitted and exported to images using the Gwyddion software.

3.5.5 Zeta Potential

The nanocellulose´s zeta potential was calculated by measuring the droplets electrophoretic mobility using a capillary electrophoresis cell (Zetasizer nano ZS, Malvern Instruments Ltd., Malvern, United Kingdom). The suspensions were diluted to a concentration of 0.01 wt% with deionized water. Before the test, the diluted solutions were homogenized for 5 min at 15000 rpm using a high-speed homogenizer, and 15 min in the ultrasonic bath. Each sample were balanced for one minute inside the instrument before data were registered over at least 10 sequential readings. Then, the Smoluchowsky mathematical model was applied by the software to convert the electrophoretic mobility measurements into the zeta potential values. The procedure was performed in triplicate for each sample.

3.5.6 X-Ray Diffractometry

X-ray diffraction patterns of the raw fiber, bleached fiber, and CNCs were recorded using a diffractometer (PANalytical Xpert PRO MRD, United Kingdom) with copper radiation (CuK α, λ = 1.5418Å) at 40 KV, current of 30 mA. In this analysis, the samples were scanned at 2θ range of 5–60°, with a step size of 0.02°. Crystallinity index (CI) was calculated using the follow equation 2.

$$\boldsymbol{CI} = \left(\frac{\boldsymbol{I_{002}} - \boldsymbol{I_{am}}}{\boldsymbol{I_{002}}}\right) \times \mathbf{100} \quad (2)$$

Where I_{200} is the maximum intensity of the principal peak (002) lattice diffraction at 2θ = 22° for cellulose I, 2θ = 20° for cellulose II, I_{am} is the intensity of diffraction attributed to

amorphous cellulose at 2θ = 18° for cellulose I, and 2θ =16° for cellulose II (Naduparambath et al., 2018).

3.5.7 Infrared Absorption Spectroscopy with Fourier Transform

Fourier transform infrared (FT-IR) spectroscopy was used to detect possible changes in the functional groups existing in the fibers at different stages of extraction. FT-IR spectra of raw fiber, bleached fiber, and CNCs were recorded in the range of 4000–400 cm^{-1}, using infrared spectrophotometer model PerkinElmer spectrum Two (Perkin Elmer, USA) (Naduparambath et al., 2018).

3.5.8 Thermal Analysis

The thermal stability of the initial fiber, and CNCs were analyzed using differential scanning calorimetric (DSC) and gravimetric (TGA) analyses, using DSC equipment (DSC 204 F1 Phoenix®, Netzsch, Germany) and PerkinElmer STA 6000 "Simultaneous Thermal Analyzer" (Germany), respectively. Dried CNCs samples of approximately 10 mg were packed in an aluminum pan, sealed, and subjected to the heating cycle (20°C to 400°C) at a constant rate of 20°C $\cdot min^{-1}$ under a nitrogen atmosphere (flow 50 mL $\cdot min^{-1}$) (Woranuch and Yoksan, 2013).

In the thermogravimetric analysis, under a nitrogen atmosphere, about 10 mg of each dried sample was heated to 400ºC at a rate of 10°C/min and kept in isotherm for 3 min (Higueras et al., 2013). The decomposition temperatures of the compounds were measured from the first derivative of mass loss (%) (DTGA) "versus" temperature.

3.6 Bionanocomposites Characterization

3.6.1 Thickness and Mechanical Properties

Thickness is a key feature when it comes to packaging materials development, as it is directly related to other packaging properties, like mechanical and barrier properties. In this way, its determination is necessary and fundamental for the material characterization. A Mitutoyo digital micrometer (Mitutoyo, Kawasaki, Japan), with a 0.001 mm precision, was used to measure the thickness of the bionanocomposites in ten random points of each sample.

The mechanical properties were set according to ASTM D882-18 (ASTM International, 2018). Five strings of each sample (150 mm x 25 mm) were mounted in the tensile grips with a 0.5 kN load cell (Autograph Shimadzu, Sydney, Australia), with a 50 mm initial gauge length and stretched at a crosshead speed of 50 mm/min until breakage (figure 3.1).

The uniaxial mechanical tests were performed and the values of Young's modulus also known as elastic modulus (EM), tensile strength (TS), and percentage of elongation at break (EAB) were calculated.

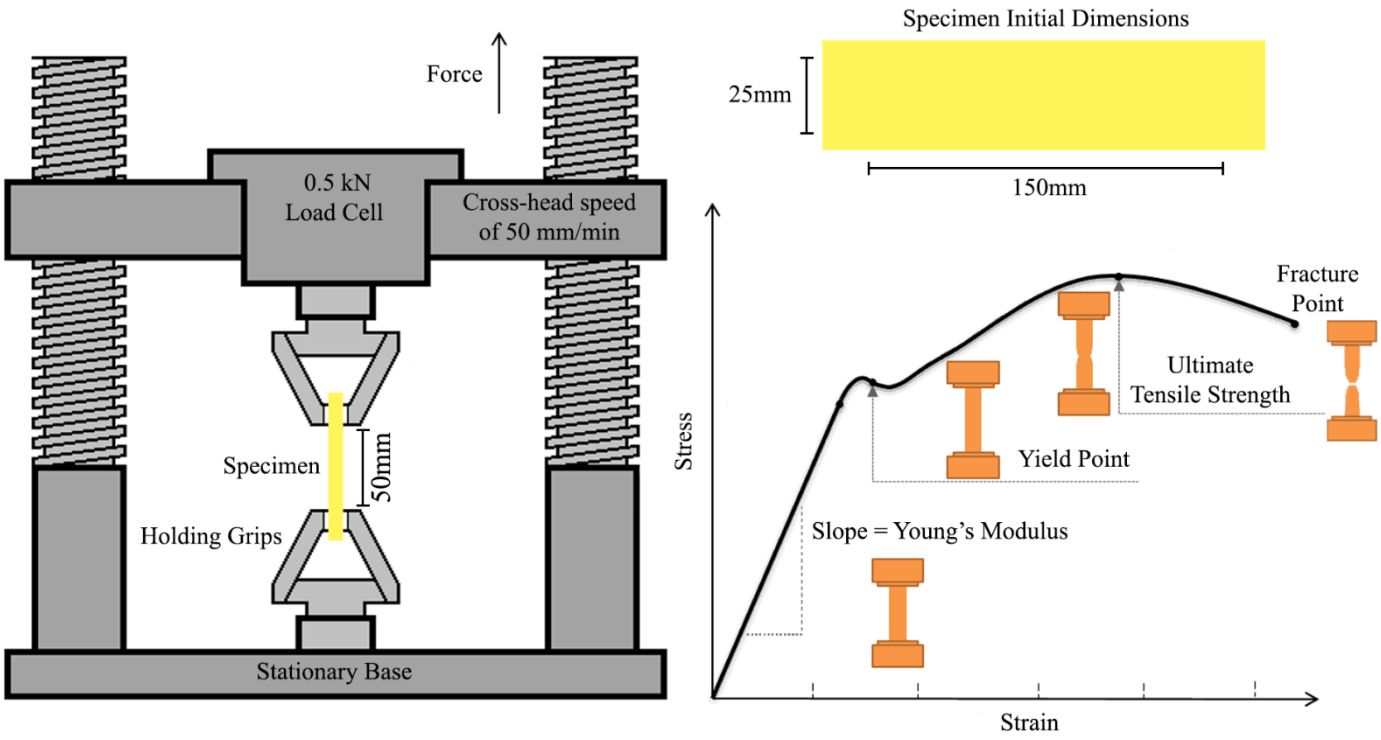

Figure 3.1 — Mechanical test apparatus and example of a traditional stress/strain curve for a ductile material.

3.6.2 Morphological Characterization

The morphological characterization was done following the work of Souza et al., (2019b). Basically, to analyze the bionanocomposite morphology, scanning electron microscopy (SEM) micrographs of the film's surface and cross-section. The images were acquired from a Zeiss instrument (Model DSM 962, Oberkochen, Germany) under vacuum, accelerated at 3 kV. The samples were set with a double adhesive coated carbon tape on aluminum stubs and covered with gold-palladium using a sputter coater. Cross-section images were carried out in samples previously submitted to fractions after contact with liquid nitrogen.

3.6.3 Optical Properties

The bionanocomposite optical properties were determined following the work of (Souza et al., 2019b). The color of each specimen was observed through the colorimeter CR410 (Minolta Co., Tokyo, Japan) with a 10 mm diameter window and D65 illuminant/10° observer, which exposes the CIE-L*a*b* coordinates (L* indicates black (0) to white (100); a* indicates red (+) to green (-) and b* indicates yellow (+) to blue (-)) useful to calculate the optical parameters chroma (c*) and Hue angle (hue). The measurements were taken on a white background pattern and the equations used were the following:

$$c^* = (a^{*2} + b^{*2})^{1/2} \tag{3}$$

$$hue = \arctan\left(\frac{b^*}{a^*}\right) X \frac{180}{\pi}, \ for\ a^* > 0\ and\ b^* > 0 \tag{4}$$

$$hue = \arctan\left(\frac{b^*}{a^*}\right) X \frac{180}{\pi} + 180, \ for\ a^* < 0 \tag{5}$$

$$hue = \arctan\left(\frac{b^*}{a^*}\right) X \frac{180}{\pi} + 360, \ for\ a^* > 0\ and\ b^* < 0 \tag{6}$$

Likewise, the light absorption at 600 nm per mm of film thickness, which measure the light being absorbed due to the constituents of the films, were registered by direct absorbance reading of rectangular simples at 600 nm using a UV-vis spectrophotometer (Model Spekol 1500, Analytikjena, Germany) and calculated according to the equation (7).

$$Abs600/mm = \frac{absorbance\ 600\ nm}{sample\ thickness\ (mm)} \tag{7}$$

Ultimately, the light transmittance was acquired from spectrum scans of each specimen (wavelengths between 190 to 900 nm) employing a UV-vis spectrophotometer. Air was used as a reference and the outcome expressed as a percentage of transmittance.

3.6.4 Solubility and Swelling Degree

In the first place, film specimens were cut into a rectangle (2 x 2 cm) and weighted (precision 0.0001 g) in an analytical balance (Mettler Toledo AB204, Switzerland), obtaining the initial weight (M1); then the samples were placed to dry at 70ºC for 24 h in a conventional oven, and weighted to get the initial dry mass (M2). Later, to enable the swelling process, the films were placed in Petri dishes containing 30 mL of Milli-Q water and stored for 24 h at room temperature (25 ± 2ºC). After this contact period, the specimens were superficially dried with filter paper and weighted (M3) again. Finally, the reminiscent of each film was dried in oven at 70ºC for 24 h to determine the final dry mass (M4). Two measurements from each film sample were taken, and the parameters calculated according to equations (8) and (9) (Souza et al., 2021).

$$\%Solubility\ \left(\frac{g}{100\ g}\ of\ film\right) = \frac{(M2-M4)}{M2}\ X\ 100 \quad (8)$$

$$\%Swelling\ degree\ \left(\frac{g}{100\ g}\ of\ film\right) = \frac{(M3-M2)}{M2}\ X\ 100 \quad (9)$$

3.6.5 Water Contact Angle

The sample hydrophilic character was assessed from water drop contact angles on the film's upper surfaces, using the sessile drop technique. This feature denominated water contact angle (WCA) was measured using a goniometer (KSV Instruments Ltd., CAM 100, Finland) with the software KSV CAM 100. The experiments were performed at room temperature (25 ± 2ºC / RH ~ 52 %) over the course of 5 s after a water drop was placed on the upper surface of the film. For each film type, at least five measurements at a different position on the surface of the films were performed.

3.6.6 Water Vapor Permeability

Water vapor permeability (WVP) was determined using a gravimetric method at 30ºC as described by Ferreira et al., (2016). Briefly, the samples were sealed on the top of 45 mm diameter glass cells containing 8 mL of saturated NaCl solution (relative humidity (RH) = 76.9 %), then, these cells were placed inside a desiccator containing saturated potassium acetate

solution (RH = 22.5 %) and equipped with a fan to promote air circulation and keep a constant driving force. The temperature and relative humidity were monitored with a thermohygrometer (Vaisala, Finland). The water permeated through the film and absorbed by the desiccant was determined from the weight loss of the permeation cell (measured every 1 h during 10 h), and WVP calculated following equation (10).

$$WVP = \frac{N_W X \delta}{\Delta P_{w.eff}} \quad (10)$$

Where N_W (mol/m².s) is the water vapor flux, δ (m) is the film thickness and $\Delta P_{w.eff}$ (Pa) is the effective driving force. Results are the average ± standard deviation of the three replicates analyzed.

3.6.7 Oxygen Permeability

Oxygen permeability (OP) was measured according to (Souza et al., 2021). Before testing, the films were stored in an equilibrated environment at 30ºC and RH of 55 % ± 5 % (desiccator containing saturated sodium bromide solution). Briefly, the film specimen was positioned in a cell between two identical stainless-steel chambers, one of the chambers (feed) was filled with 0.7 bar pure oxygen (99.999 % purity) (Praxair, Spain) and the oxygen permeability was measured by the pressure change in both chambers over time, monitored using two pressure transducers (Jumo, Model 404327, Germany). To guarantee a constant temperature, the system was kept inside a thermostatic water bath at 30ºC (Julabo, Model EH, Germany) (figure 3.2). The permeability was calculated using equation (11):

$$\frac{1}{\beta} ln \frac{\Delta p_0}{\Delta p} = P \frac{t}{\delta} \quad (11)$$

$$\beta = A(\frac{1}{Vf} + \frac{1}{Vp}) \quad (12)$$

Where Δp (mbar) is the pressure difference between the feed and permeate compartment, P (mol.m/m².s.Pa) is the gas permeability, t (s) is the time, δ (m) is the film thickness and β is the geometric parameter of the cell. This parameter was calculated using equation (12), where V_f and V_p are the volumes of the feed and permeate compartments, respectively, and A is the film area resulting in a value of 116.2 m^{-1}.

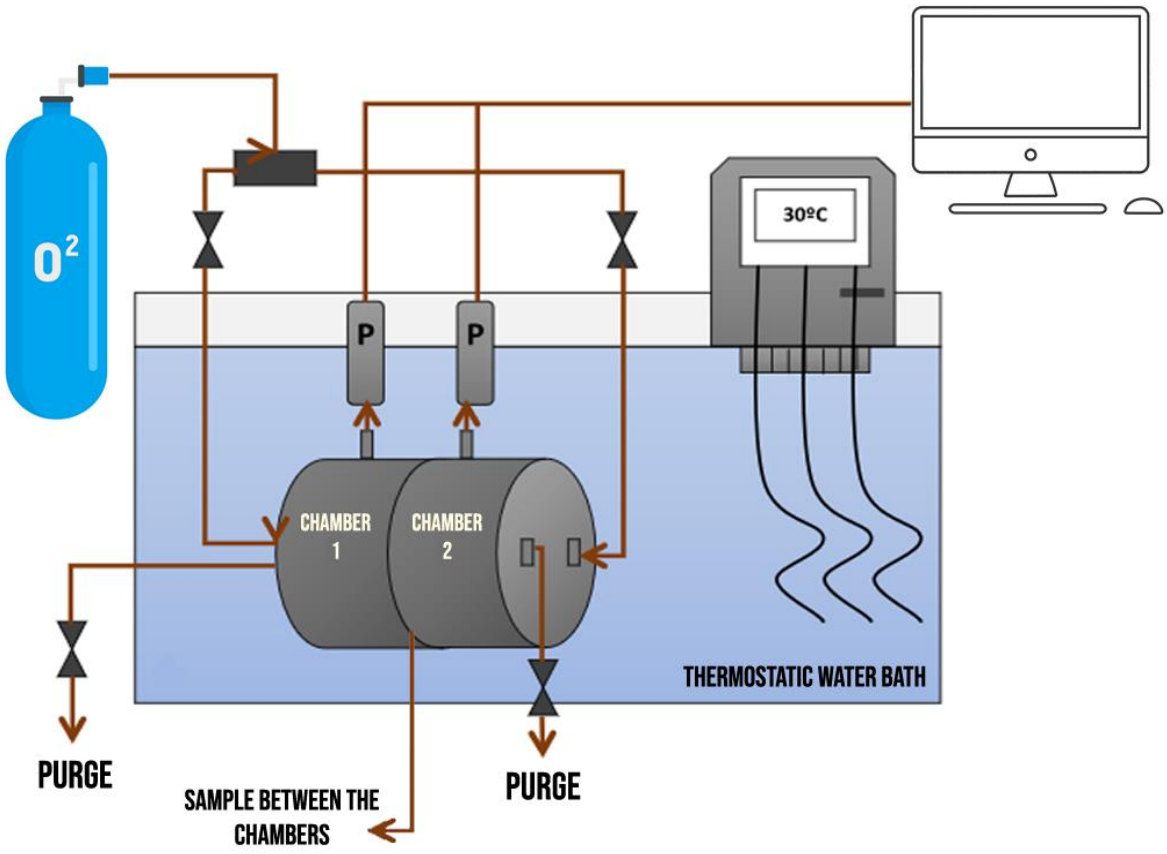

Figure 3.2 — Oxygen permeability test apparatus.

3.6.8 Infrared Absorption Spectroscopy with Fourier Transform

This analysis relies on the chemical bonds present in the sample that have specific vibrational frequencies. Therefore, the frequency of radiation absorption in the infrared is particular for each type of bond, enabling the identification of interactions between the polymeric matrix and the compounds incorporated in the bionanocomposites (Barbosa, 2007). Using this technique, it was expected to identify the interactions between the functional groups presents in the polymer chains and in the nanocellulose particles.

The spectra were obtained using infrared spectrophotometer model PerkinElmer spectrum Two (Perkin Elmer, USA). Infrared absorption spectroscopy with Fourier transform (FT-IR) in "Attenuated total reflectance" (ATR) with 32 sweeps and 1 cm^{-1} resolution in the 4000 cm^{-1} to 500 cm^{-1} wavelength range was used.

3.6.9 X-Ray Diffractometry

Through the X-ray diffraction technique, it was possible to verify the level of exfoliation of nanocellulose between chitosan polymer chains. The improvement of the mechanical, barrier, and thermal properties are closely related to the exfoliation degree of the nanofiller, and this determination is essential to explain the behavior of bionanocomposites.

The samples were analyzed in a diffractometer (PANalytical Xpert PRO MRD, United Kingdom) with copper radiation (CuKα, λ = 1.5418 Å) at 40 KV, current of 40 mA, under 2θ angle ranging from 10° to 40° with a step interval of 0.02°. The specimens were mounted on silicon wafers in order to guarantee flatness and inserted in the diffractometer.

3.6.10 Thermal Analysis

The bionanocomposites thermal properties were analyzed using differential scanning calorimetric (DSC) and gravimetric (TGA) analyses, using DSC equipment (DSC 204 F1 Phoenix®, Netzsch, Germany) and PerkinElmer STA 6000 "Simultaneous Thermal Analyzer" (Germany), respectively. The glass transition temperature (Tg) of the films was determined in DSC. Film samples of approximately 10 mg were packed in an aluminum pan, sealed, and subjected to the heating cycle (20°C to 400°C) at a constant rate of 20°C $\cdot min^{-1}$ under a nitrogen atmosphere (flow 50 mL $\cdot min^{-1}$) (Woranuch and Yoksan, 2013).

In the thermogravimetric analysis, under a nitrogen atmosphere, about 10 mg of each film were heated to 400ºC at a rate of 10°C/min and kept in isotherm for 3 min (Higueras et al., 2013). The decomposition temperatures of the compounds were measured from the first derivative of mass loss (%) (DTGA) "versus" temperature.

3.7 Bionanocomposite Application as Active Packaging - "*In Situ*" Characterization

3.7.1 Fresh Poultry Meat Preparation

Fresh poultry meat was purchased from the local market with the longest possible shelf life. For each treatment, performed in triplicate, the meat was minced and divided into 4 samples (one for each evaluating time) of 30 g, encompassing a total of 12 samples. An additional unwrapped sample was used as a control. Then, each specimen was wrapped on the respective bionanocomposite (5×15 cm) and conditioned inside sterile plastic boxes, under refrigeration (5°C ± 2°C) (figure 3.3). Each treatment was collected and evaluated at 3, 6, 9, and 12 days of storage. At the initial time (0 days of storage) only the unwrapped meat was characterized.

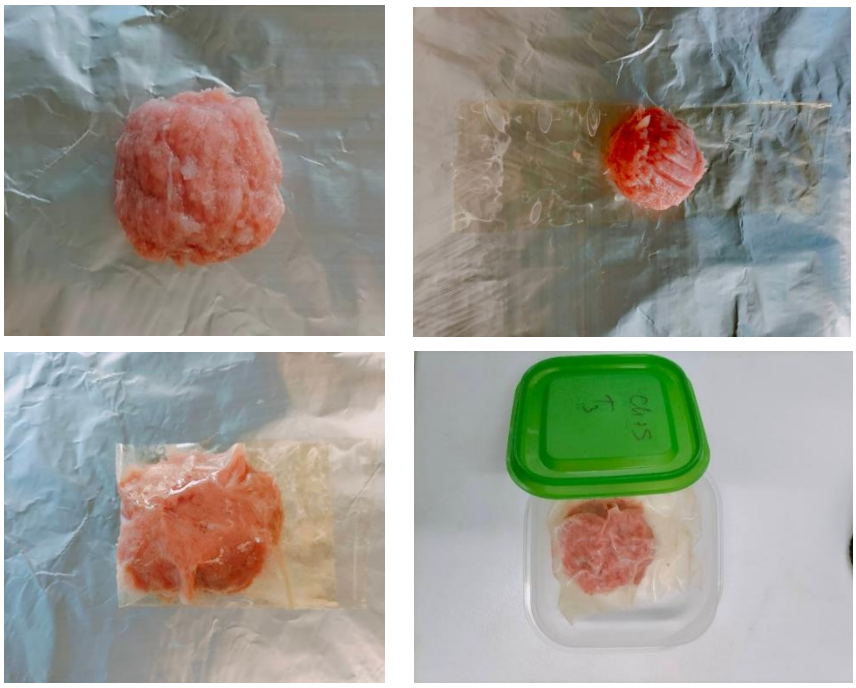

Figure 3.3 — Assembly of the "*in situ*" tests.

3.7.2 Physicochemical Characterization

The physicochemical characterization consisted of pH, total volatile basic nitrogen (TVB-N) and moisture laboratorial tests according to the AOAC method (Association of Official Analytical Chemists) (AOAC, 2016).

Instrumental color was measured on the meat surface through the setting of the CIE-L*a*b* (International Commission on Illumination) coordinates, using a CR 410 colorimeter with D65 light source, and visual angle of 10°. The color measurements will be performed 3 times at 3 different points of the sample, for average purposes, on a standardized white background. Hue angle (hue) will be evaluated according to equations 4-6.

3.7.3 Lipid Oxidation (TBARS Index)

The oxidative state of the samples was evaluated by the determination of the thiobarbituric acid reactive substances (TBARS) values, according to (Rosmini et al., 1996). For each treatment, 10 g of poultry meat was mixed with 20 ml of TCA 7.5 % (w/v) and agitated for half an hour in a shaker water bath (Tuttnauer, Israel). The supernatants were filtered, and 5 mL of the filtrate blended with 5 mL of TBA 0.02 M in test tubes. The tubes were heated at 95°C for 30 min in a water bath (Memmert, Germany). After being cooled to room temperature, the samples absorbance was observed using an UV/VIS spectrophotometer (Model Spekol 1500, Analytikjena, Germany) at 530 nm. The quantification of malonaldehyde (MDA), used to determine the TBARS index, was calculated from calibration curves made with known concentrations of MDA (from TEP solution). Results were expressed as mg of MDA/kg of sample.

3.7.4 Microbiological Growth

Total mesophilic aerobic microorganism (TMAM), total psychrotropic aerobic microorganism (TPAM), and *Enterobacteriaceae* quantification were determined to estimate the microbiological quality of the wrapped samples, according to ISO 4833-1:2013 (ISO, 2013), ISO 17410:2019 (ISO, 2019), and ISO 21528-2:2017 (ISO, 2017). TMAM and TPAM counts were observed in PCA after incubation at 30°C for 72 h or 7°C for 168 h, respectively. *Enterobacteriaceae* counts were stated in violet red bile glucose (VRBG) agar after incubation at 30°C for 24 h. Results were expressed as log CFU (colony forming units)/g of meat.

3.8 Bionanocomposites Antioxidant Activity - "*In Vitro*" Study

3.8.1 Antioxidants Diffusion Assessment

The "*in vitro*" quantification of antioxidant compounds migration from the bionanocomposites over time was performed using a diffusion test (Dicastillo et al., 2011). It was chosen two solutions of 50 % (dairy products) and 95 % ethanol (fatty foods) as a simulator media, at 40°C ± 2°C for 10 days. These food simulators were chosen since the packaging's main objective is to delay the oxidative process in food matrices, in this way, this is considered most susceptible to such spoilage processes.

Periodically, the total phenolic compounds concentration in the simulant medium were determined by the Folin-Ciocalteu method (Singleton et al., 1999). Briefly, 1 mL of the simulant medium were added to 3 mL of water and 0.25 ml of the Folin-Ciocalteu reagent. After 3 min, 0.75 mL of sodium carbonate (5 % w/v) was added, and the mixture was incubated for 60 min in the dark and at room temperature (20°C ± 5°C). The phenolic compounds quantification was performed using a UV/VIS spectrophotometer by reading the absorbance at a wavelength of 760 nm. A gallic acid calibration line (0-200 mg/L) was used to calculate the results, which were expressed in mg gallic acid equivalent (mg GAE/L).

3.8.2 Antioxidant Activity

From the aliquots collected under the test conditions described in item 3.8.1, the "*in vitro*" antioxidant activity was determined by the DPPH radical capture assay (2,2-diphenyl-1-picrylhydrazyl) according to the methodology described by Dicastillo et al., (2011).

In 3 ml of 60 μM ethanolic DPPH solution, an aliquot of 1 mL of the simulant medium was added. The mixture was kept protected from light and at room temperature (20 °C ± 5 °C) for 20 minutes. Quantification was performed using a UV/VIS spectrophotometer at a wavelength of 517 nm by reading the absorbance. The inhibition percentage (%) was calculated using equation 14. As a control, 1 ml of 95 % ethanol was used.

$$Inhibition\ (\%) = \frac{\text{Abscontrol} - \text{Abssample}}{\text{Abscontrol}} \times 100 \qquad (14)$$

In addition, based on the Fick's second law described in equation 15 and using initial migration data, the diffusion coefficient (D) of phenolic compounds was calculated from the plot of $M_{F,t}/M_{P,0}$ versus $t^{0.5}$ (Chung et al., 2002).

$$\frac{M_{F,t}}{M_{P,0}} = \frac{2}{\delta}\left(\frac{Dt}{\pi}\right)^{0.5} \quad (15)$$

where $M_{F,t}$ (mg GAE) is the TPC in the food simulant at time t, $M_{P,0}$ (mg GAE) is the initial TPC in the film, D (cm^2/s) is the diffusion coefficient of TPC and δ (m) is the film thickness.

3.8.3 Antimicrobial activity – Colony-forming unit counting method

In order to complement the study of antimicrobial activity, the method of counting colony-forming units (Nouri et al., 2017) for Gram-negative (*Salmonella enterica* subsp. *enterica* serovar Choleraesuis ATCC® 10708TM) and Gram-positive (*Bacillus cereus* ATCC® 11778TM) foodborne bacteria was carried out for the bionanocomposites developed. Initially, 0.2 g of each film was immersed in 4 mL of TSB nutrient medium containing approximately 106 CFU/mL of the bacteria under test. Then, the system was maintained at 37 °C (*S*. Choleraesuis) or 30 °C (*B. cereus*) for 24 h with continuous agitation (150 rotations per minute (r.p.m.)) using an incubator with agitation (Innova model, New Brunswick Scientific, U.S). Tubes without the films were used as a control. After incubation, 100 µL of serial dilutions were inoculated by spreading on TSA plates, which were subsequently incubated at the respective optimal growth temperature of each evaluated bacterium for 16-24 h. The number of colony-forming units was manually counted, and the antimicrobial activity was expressed as the number of log reductions (CFU)/mL, calculated according to equation 16.

$$Log\ reductions = Log\ B - Log\ A \quad (16)$$

Where B and A correspond to the counts of viable bacteria (CFU/mL) in the control treatment and in the treatments evaluated after 24 h of incubation, respectively.

3.9 Statistical Analysis

All experiments were conducted in a completely randomized design with three replications. Statistical analysis of the obtained data was performed using a one-way analysis of variance using IBM SPSS Statistics version 23 (IBM, USA), and differences between mean values were processed by Tukey's test. Significance was set at $p < 0.05$.

4

RESULTS AND DISCUSSION
ISOLATION AND CHARACTERIZATION OF NANOCELLULOSE EXTRACTED FROM ENERGY CROPS

The first stage of this doctoral thesis had as its core objective to evaluate the potential for cellulose extraction from three different lignocellulosic biomasses. The choice fell on the energy crops, giant reed, kenaf, and miscanthus, as these are used as feedstocks to produce low ILUC biofuels, avoiding displacement of food and feed crops through improved agricultural practices or through the cultivation of areas not previously used for crop production. In addition, these species are easily adapted to different climatic conditions with high productivity, low demand for nutrient inputs, have a high carbon dioxide sequestration rate, and offer protection against soil erosion. Besides, in many areas of the planet, these are considered invasive species that are often cut down and left unattended without any profitable request (Abreu et al., 2022; ICCT, 2018). The energy crops residues can be used to extract cellulose, which can be depolymerized giving rise to an extraordinary nanometer-scale bio-based material. Combining the bioenergetic purpose with bioproducts increases the capacity to use the crop, consequently increasing the biorefinery profitability (J.R.A. Pires et al., 2019b).

After the fiber's characterization, a methodology was applied consisting of an alkaline pre-treatment and chlorine-free bleaching, with the aim of isolating the cellulose with the highest degree of purity possible. The obtained celluloses were then submitted to acid hydrolysis to be converted into nanocellulose. Once the aim of producing these nanoparticles is to be used as reinforcing agents to chitosan films, the obtained CNCs were characterized in terms of mechanical, barrier, and thermal properties were evaluated. In addition, it was studied their morphological characterization, dispersion stability, and crystallinity.

4.1 Fiber Compositional Characterization and Extraction Yields

The chemical composition of giant reed, kenaf, and miscanthus was determined in the original raw fibers and after the bleaching stage, with the data being summarized in table 4.1. The yields (%) obtained after the two alkaline pre-treatments and after three bleaching treatments are exposed in table 4.2. As complementary visual information, figure 4.1. shows the path taken by the three fibers from the beginning to the isolation of the respective CNCs.

Table 4.1 — Fiber composition before and after the pre-treatment/bleaching.

		Giant Reed	**Kenaf**	**Miscanthus**
Untreated Fibers	Hemicellulose (%)	24.8±1.0	25.1±1.0	28.7±2.1
	Cellulose (%)	39.2±1.1	52.7±1.1	41.3±0.4
	Lignin (%)	27.5±0.5	12.0±1.0	21.3±1.8
	Total Fiber (%)	91.5±0.4	89.8±0.3	91.3±0.7
	Ash (%)	1.9±0.3	1.7±0.8	2.4±1.4
After Alkali and Bleaching Treatment	Hemicellulose (%)	3.6±0.3	3.7±0.8	3.2±0.8
	Cellulose (%)	90.0±1.6	90.2±1.3	87.2±2.0
	Lignin (%)	1.4±0.1	0.9±0.3	3.6±0.8
	Total Fiber (%)	95.0±1.4	94.8±2.8	94.0±0.4
	Ash (%)	0.8±0.4	1.7±0.8	1.2±0.2

Table 4.2 — Pre-treatment and Bleaching yield (%) for each biomass.

		Treatment Yield (%)	**Mass Loss (%)**
Giant Reed	Pre-Treatment	46.7±1.2	53.3±1.2
	Bleaching	71.3±0.7	28.7±0.7
Kenaf	Pre-Treatment	62.9±1.2	37.1±1.2
	Bleaching	60.8±2.2	39.2±2.2
Miscanthus	Pre-Treatment	56.3±0.8	43.7±0.8
	Bleaching	73.0±1.0	27.0±1.0

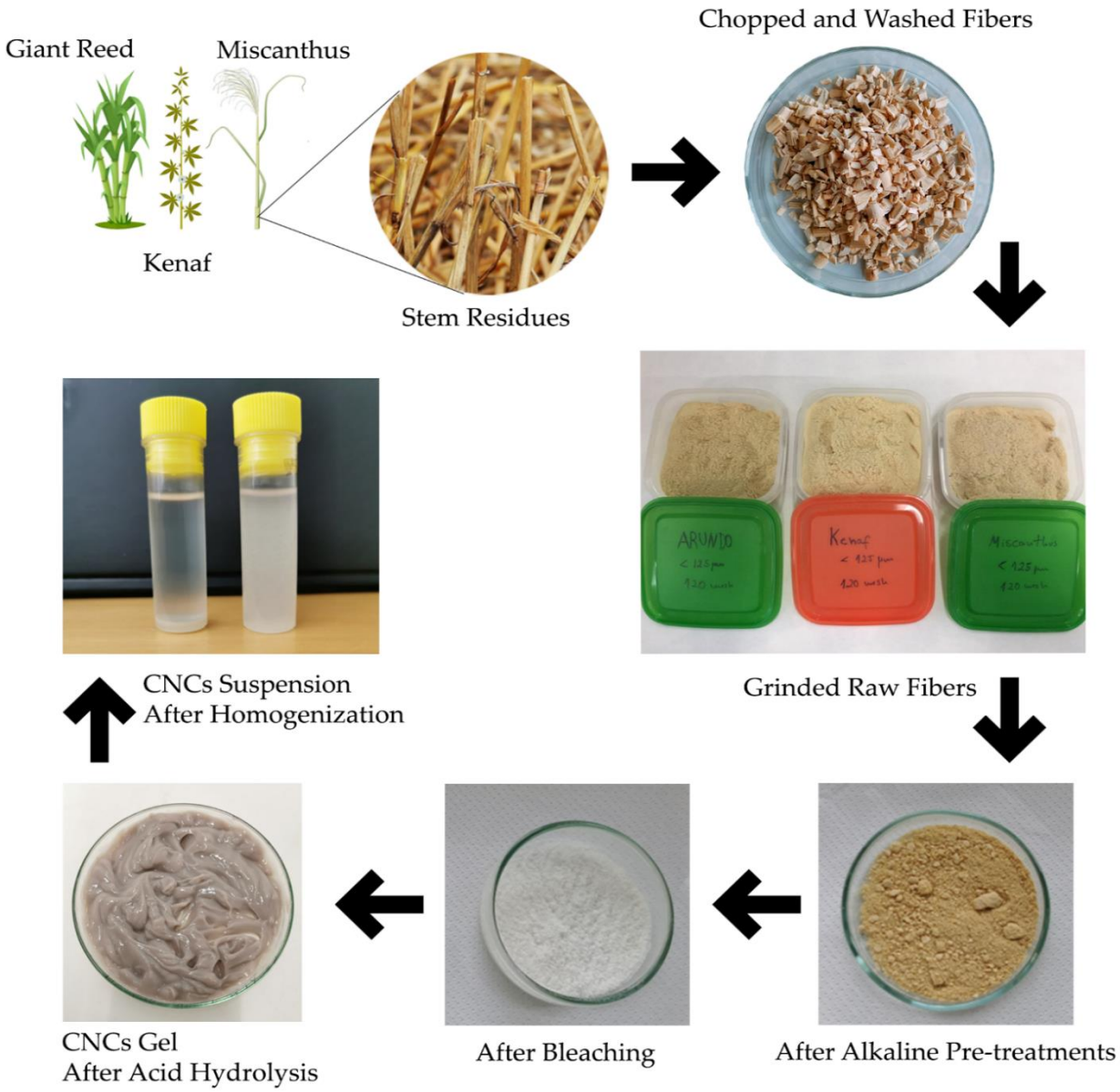

Figure 4.1 — Sample path from raw material to nanocellulose.

The raw kenaf fiber presented the highest cellulose content, 52.7 wt%, followed by miscanthus with 41.3 wt%, and giant reed with 39.2 wt%. Analogously, kenaf fibers have the lowest lignin content, with only 12 wt%, while giant reed fibers were the ones that presented the highest lignin level, 27.5 wt%. Therefore, lignin contents for the three different crops can be considered to be at satisfactory levels for nanocellulose extraction (<30 %). In practice, this lignin amount could mean that these fibers require pre-treatments with milder pulping conditions (lower temperatures and chemical charges) than those extracted from soft- and

hardwoods. It also may indicate the potential of these lignocellulosic materials to experience bleaching treatments effortlessly and with fewer chemicals (Trache et al., 2020; Ververis et al., 2004). Regarding hemicellulose, the values obtained were similar between samples, with miscanthus reaching the highest quantity, 28.7 wt%. The three analyzed biomasses presented appreciable values of cellulose demonstrating to have the potential for nanocellulose extraction, however, the kenaf fibers are the ones that indicate a higher potential since they contain a lower value of lignin and consequently lower recalcitrance level. Even within the same species, the fiber composition can vary, considering several factors, like the climate and geographic conditions of the region where the crops are produced. However, the results presented in this work are in agreement with others found in the literature (Bernstein and Moholkar, 2020; Lv et al., 2021; Suranjoy et al., 2020; Tsalagkas et al., 2021; Yang et al., 2020).

Upon the alkali pre-treatment and bleaching, the cellulose content continuously rises as expected, reaching values around 90 wt% of the total fiber. In result, the combination of alkaline pre-treatment and bleaching process demonstrated to be efficient in removing hemicellulose and lignin, decreasing them to residual values below 5 %. It was verified that, despite the different initial compositions, the treatments applied had the same effect on the three samples. The alkali pre-treatment efficiently removed hemicellulose, which is explained by the cleavage of the ester-linked substances (Kallel et al., 2016). To promote the remaining lignin degradation, a bleaching treatment was applied composed of a mixture of sodium hydroxide and hydrogen peroxide. The oxidation of the lignin aromatic rings and hemicellulose carboxylic acids is mainly due to the superoxide radicals (O_2^-), a highly reactive compound. In this sense, bleaching enables the removal of the chromophore groups from the fiber, generating a whiter fiber with a higher cellulose purity (Hafemann et al., 2019).

Regarding the treatments yields (%) associated with each cellulose isolation step, it was observed that the most significant mass loss, mainly related to the degradation of hemicellulose, occurred with the alkaline pre-treatment. The degraded components were majority soluble in the black liquor, which presented a darker color when compared to the bleaching liquor, as can be observed in figure 4.2. Giant reed fibers registered the highest mass loss, around 53.3 ± 1.2 wt% for alkaline pre-treatment, and 28.7 ± 0.7 wt% for bleaching, which was expected since this specimen owned the initial highest amount of non-cellulosic components. The sample amount after the treatments applied for cellulose isolation is smaller than the amount of cellulose present in the initial fibers, indicating that some cellulose degradation may occurred during the process. In future work, it will be necessary to review the parameters adopted in

each step and adapt them to try to improve the yield of cellulose extraction. Additionally, to optimize the cellulose extraction process so that it can be considered environmentally correct, it must be taken into account that the residual liquors generated have to be reused or recovered. Even though black liquor is frequently used for heat and power generation, the separation and upgrading of the compounds present in the liquors can significantly enrich the process economics. Consequently, extracting lignin or hemicellulose from these by-products can be considered a key issue in the successful development of biorefineries (Pola et al., 2022).

Figure 4.2 — The three residual liquors generation during the cellulose isolation.

4.2 Nanocellulose and Microaggregates Morphology

Initially, the fibers were ground until being able to pass through a sieve with a mesh size of less than 150 µm. Observing images A1 to C1, shown in figure 4.3, it is possible to observe that the kenaf fibers are the ones that have a smaller initial size, despite all the ground fibers having been sieved through a filter with the same mesh size. The same figure shows the microaggregates of CNCs formed after the acid hydrolysis step (images A2 to C2). As can be seen, the aggregation power of nanocelluloses is very relevant, so the correct CNCs dispersion in the aqueous medium is one of the most paramount challenges to be overcome. Although nanocellulose disperses in water relatively easily, the hydrogen bonds between the hydroxyl

groups of the nanoparticles limited the dispersion stability to a certain extent (Chu et al., 2020). One of the causes of the formation of microaggregates (MCCs) was the employment of an ultrasonic bath with a lower frequency for the correct dispersion of the CNCs in the homogenization process. The process must then be optimized, and the application of an ultrasound probe with frequencies above 20 kHz has been reported as an effective method (Foster et al., 2018; Kininge and Gogate, 2022; Singh et al., 2014; Velmurugan and Muthukumar, 2012). In the same figure, the graphs adjacent to the images of the MCCs indicate the average aspect ratio of the microaggregates for each sample obtained. Analyzing, it was found that the kenaf sample had the lowest average aspect ratio, with 1.3 μm, as had happened for the size of the initial fibers. Comparatively, giant reed and miscanthus recorded average aspect ratios around 4.4 μm and 6.2 μm, respectively. In short, the results indicate that a correlation may have been established between the size of the fibers before the delignification steps and the size of the MCCs after the acid hydrolysis step.

Knowing the CNCs aspect ratio is important because, like crystallinity, it has a direct influence on the physical properties of the films in which it will function as mechanical reinforcement. As it is recognized, for greater stress transfer from film matrix to reinforcing material, a minimum aspect ratio is necessary (Babaei-Ghazvini and Acharya, 2022; Mujtaba et al., 2017). The cellulose nanoparticles produced from each fiber was inserted into a chitosan film in order to try to determine its size, shape, and aspect ratio. This is a method that requires the nanoparticles to be very well dispersed in the substrate. If this does not happen, the contrast between the individual nanocrystals is always not evident, hence, the identification of isolated nanocrystals becomes a challenging, or almost impossible task (Foster et al., 2018). Figure 4.4 exposes the topographic surface image of different chitosan films loaded with 2.5 % CNCs. For all samples, it was possible to identify the nanocellulose crystals represented with a rod-shaped structure randomly dispersed throughout the polymer matrix. Along with this, it was possible to observe that some aggregation phenomenon characteristic of CNCs occurred during the drying process. As CNCs occupied interstitial spaces in the polymer matrix, it was very difficult to identify individual nanoparticles, however, through the scale marks present in the figure, it was possible to determine that the nanoparticles have a length and diameter in the nanometer size range. Hereupon, it was not possible to access and measure the average length and diameter to calculate the aspect ratio of the nanoparticle. The use of another substrate, with smaller amounts of sample, coupled with better CNCs dispersion techniques can also help to make it possible to individually identify cellulose nanocrystals.

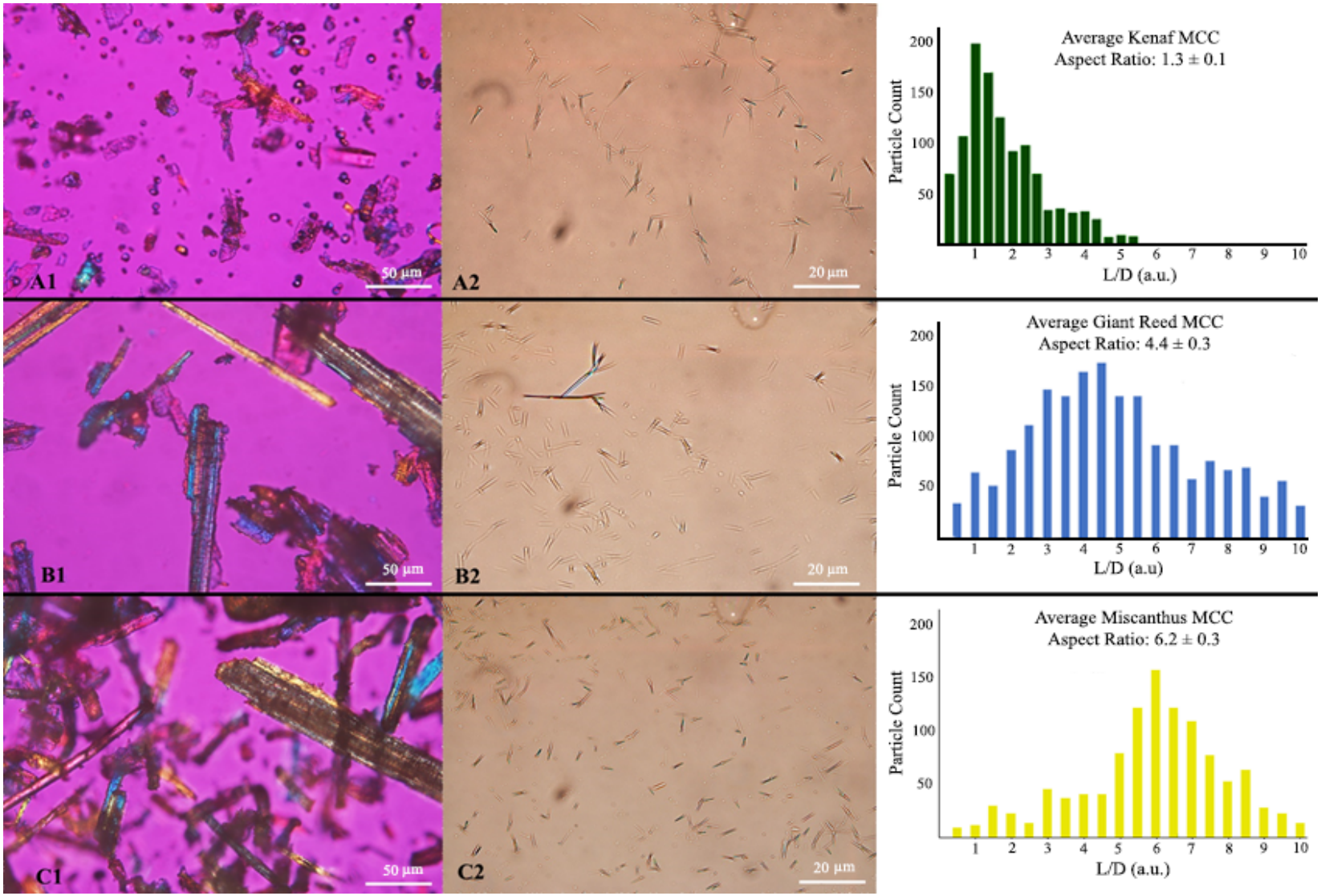

Figure 4.3 — Polarized optical microscopy from (A1-C1) untreated fibers; (A2-C2) CNCs microaggregates. Average microparticle length analysis after the acid hydrolysis stage. *Cellulose Nanocrystals (CNCs); Microcrystalline Cellulose (MCC).*

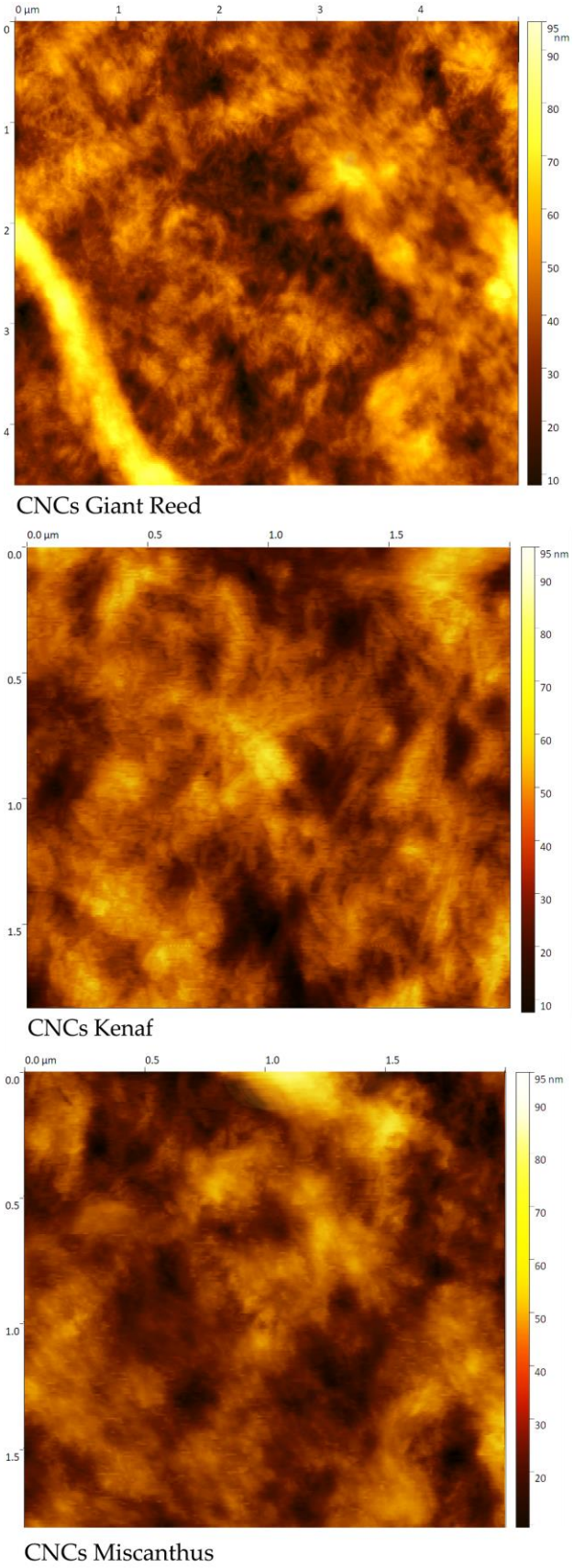

Figure 4.4 — Atomic force microscopy image of CNCs from three different fibers. *Cellulose Nanocrystals (CNCs).*

4.3 Zeta Potential

The evaluation of the zeta potential parameter is important to analyze the colloidal dispersion stability of CNCs, thus reflecting their agglomeration process (Ioelovich, 2017). Particles with similar electrical charges tend to repel each other according to the Coulomb force, affecting the CNCs agglomeration and consequently defining their dispersion stability in an aqueous suspension (Yang et al., 2017). Notwithstanding the fact that nanocellulose can be dispersed in water, the hydrogen bonding between hydroxyl groups limits the dispersion stability to some extent. In this work, to aid the nanocellulose dispersion, high-pressure homogenization and ultrasonic bath were applied to weaken the hydrogen bonding (Chu et al., 2020). The zeta potential values obtained for each nanocellulose can be seen in table 4.3.

Table 4.3 — Crystallinity index (%) and zeta potential (mV) for the different biomasses throughout the nanocellulose extraction process.

Sample	**Cristallinity Index (%)**	**Zeta Potential (mV)**
Giant Reed Raw Fiber	49	-
Giant Reed Bleached Fiber	69	-
Giant Reed Nanocellulose	73	-27.9 ± 0.5
Kenaf Raw Fiber	27	-
Kenaf Bleached Fiber	63	-
Kenaf Nanocellulose	76	-23.9 ± 0.4
Miscanthus Raw Fiber	53	-
Miscanthus Bleached Fiber	74	-
Miscanthus Nanocellulose	78	-21.1 ± 0.6

One of the most determining factors in the dispersion stability of nanocellulose is its surface charge density. Through the traditional acid hydrolysis process with sulfuric acid, CNCs with sulfate groups incorporated via esterification are obtained, which significantly increases the negative charge density on the nanoparticle's surface, thus making it possible to achieve stable aqueous suspensions with few aggregates. Generally, the absolute value of less

than 15 mV represents the agglomeration onset, in which weak electrostatic repulsion was not enough to offset the effect of hydrogen bonding. To consider a nanocellulose dispersion stable in water, the absolute value of zeta potential should be higher than 30 mV (Chu et al., 2020; Yang et al., 2017). The giant reed CNCs showed the highest dispersion stability, with a zeta potential of -27.9 ± 0.5, very close to the accepted value for the suspension to be considerably stable. On the other hand, the CNCs obtained from miscanthus fibers were the ones that showed the greatest instability, with a zeta potential of -21.1 ± 0.6 (Table 4.3).

Two different phenomena may have been responsible for the less negative zeta potential, higher than -30 mV, presented by the different CNCs. The first reason was the application of a drying process to form the CNCs gel. The drying process was applied taking into consideration the future ease and cost reduction associated with the storage and transport of nanocellulose if this methodology is applied at an industrial level. Another reason was that by keeping the CNCs in an aqueous suspension these are more susceptible to degradation by microorganisms. Unfortunately, as the drying process takes place and the moisture evaporates, the distance between two CNCs particles shortens, and interfibrillar hydrogen bonds will be developed between them, leading to the aggregation of these nanoparticles (Xu et al., 2022).

The stability of colloidal suspensions can be affected by adding salts, which modifies the electrostatic contribution to the interparticle interactions. The inclusion of electrolytes, for example, salts diluted in polar solvents such as water, filters the colloid's surface charge diminishing the repulsive barrier in the interaction potential, and destabilization takes place when the interparticle forces become attractive (Phan-Xuan et al., 2016; Xu et al., 2020). Therefore, another phenomenon that could have affected the zeta potential of CNCs was the addition of sodium hydroxide to neutralize the samples. As studied by Zhong et al., (2012) increasing the concentration of inorganic cation ions (Na^+) led to a loss of dispersion stability with the increase of nanocellulose aggregation. Moreover, the work of Boluk et al., (2011) also observed that the presence of inorganic salts lowers the absolute value of zeta potential of CNCs particles, due to the adsorption of Na^+ counter-ions.

4.4 Cristallinity Analysis

The mechanical and thermal properties of products made or reinforced with nanocellulose are linked to the crystallinity index, therefore the investigation of this parameter is essential. The XRD patterns for each lignocellulosic fiber at different stages of treatment (raw fiber,

bleached fiber, and nanocellulose) are exposed in figure 4.5, and the respective crystallinity index is presented in table 4.3.

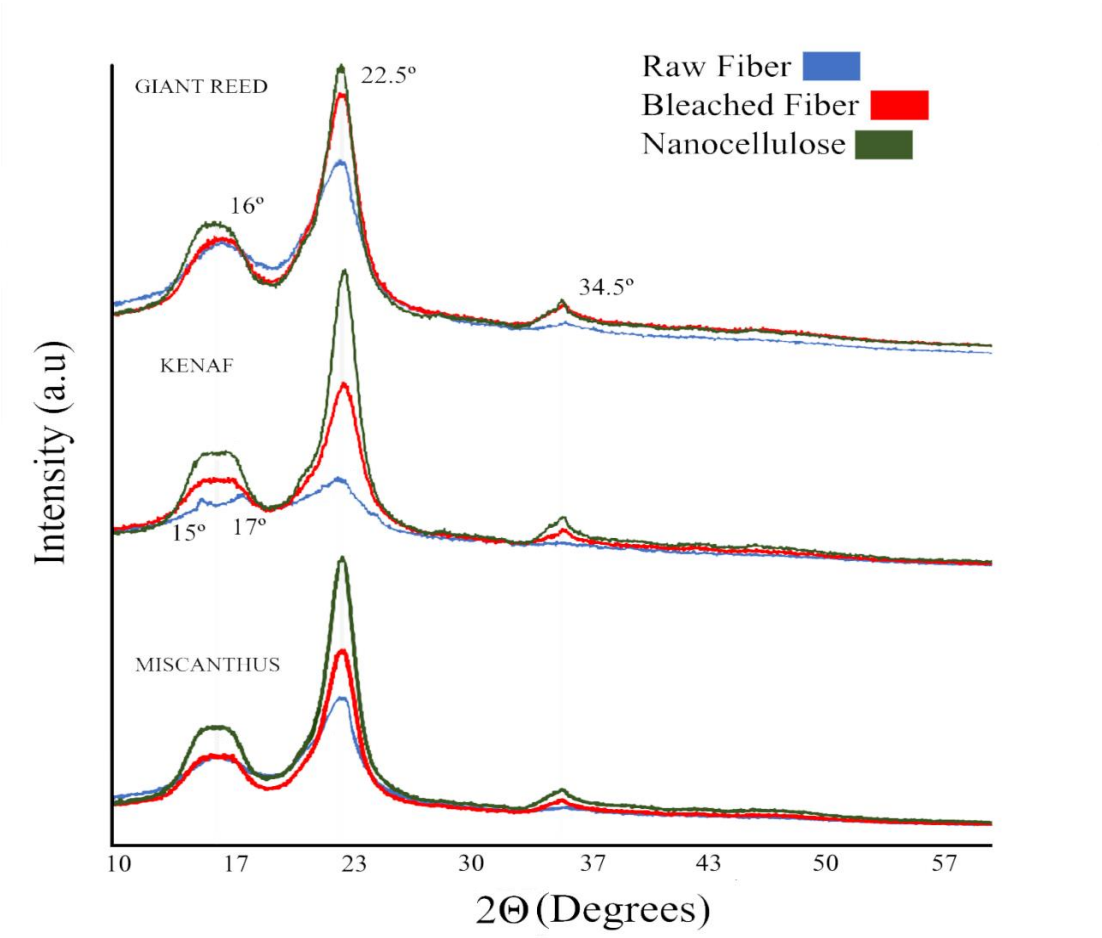

Figure 4.5 — XRD patterns of raw fiber, bleached fiber and nanocellulose isolated from the three different biomass sources.

As displayed, it was possible to state that the untreated fibers have similar XRD diffractograms, typical of semi-crystalline materials, with characteristic peaks at 2Θ = 16°, 22.5°, and 34.5°. The three identified diffraction peaks correspond to the (110), (002), and (004) crystallographic planes of the cellulose I lattice, respectively, as indicated by the International Centre for Diffraction Data (ICDD). Although, the kenaf fibers presented a slight difference, with two distinct peaks at 2Θ = 15° and 17°, assigned to the (10 (-1)), (101) crystallographic planes. It could be stated that cellulose was configurated as cellulose I, and not cellulose II because there is no doublet in the prominent peak situated at 22.5° (Beroual et al., 2021; Ilyas et al., 2018; Kian et al., 2018).

It was possible to observe that as the fiber treatment steps advance, the crystalline peak $2\Theta = 22.5^{o}$ becomes progressively tight and sharper. The lignocellulosic fiber's degree of crystallinity is directly related to the sharpness of the diffraction peak. Therefore, the growth in the peak intensity for nanocellulose samples compared with the untreated and bleached fibers is an indicator that sample crystallinity increased throughout the process (Ilyas et al., 2018; Karimi et al., 2014; Tarchoun et al., 2019). This observation was confirmed by the results achieved for the crystallinity index (CI) data.

The crystallinity index is calculated to represent the material crystallinity, expressed as the crystalline compound mass ratio in the total dry sample based on the crystallographic two-phase model (Daicho et al., 2018). The CI obtained for the untreated fibers was remarkably lower than those achieved for treated fibers and CNCs, with giant reed and miscanthus raw fibers recording similar initial values, around 50 %, and the kenaf raw fibers presenting lower CI, 27 %. Cellulose owns a crystalline structure in opposition to hemicellulose and lignin, which are amorphous in nature (Islam et al., 2018). Thus, it was expected that the kenaf fibers would have a similar or higher CI than the other two since its compositional characterization showed that it is the sample with the highest initial cellulose content. Similar studies in which the crystallinity index of kenaf stems was evaluated show that this parameter should be around 40-60 % (Jonoobi et al., 2011; Karimi et al., 2014; Öztürk et al., 2010).

Although the kenaf fibers presented CI percentual values lower than those of the other two fibers, after the bleaching step this difference was almost not noticed, with crystallinity values reaching marks between 63-74 %. These results acknowledged that the non-cellulosic amorphous molecules were removed as intended by the applied alkali and consecutive bleaching methodology. Therefore, eliminating the majority of lignin, hemicelluloses, and other small components, leads to an increase in the intra- and intermolecular hydrogen bonding by the hydroxyl groups, growing the fiber crystalline regions. The cellulosic chains line up together closely in an orderly system, having their free movement restricted by the hydrogen bonds. Farther, the bleaching treatment had an accelerated effect on the cleavage of the cellulose molecular chains within the amorphous regions, hence, increasing the crystallinity of the bleached fibers (Wang et al., 2019).

The step of converting cellulose into nanocellulose through acid hydrolysis with sulfuric acid was also demonstrated to increase the crystallinity of the samples, although this increment was not as significant as in the previous step. Overall, the three CNCs had similar CI values, between 70-80 %. During the hydrolysis process, the hydrolytic cleavage of glycosidic

bonds takes place, preferably in the amorphous zones of the cellulose, which are more accessible to the hydronium ions. This will potentiate the release of individual crystallites at the same time that the growth and realignment of single crystals occur, thus increasing the crystallinity of the cellulose nanoparticles (Wang et al., 2019). It is important to consider that the crystallinity index of cellulosic materials differs depending on the measurement technique and analytical processing. Therefore, this index should be applied for comparison purposes, as it only offers a qualitative or semi-quantitative appraisal (Daicho et al., 2018). Comparing with similar lignocellulosic raw materials and using resembling extraction methodologies, it was verified that the crystallinity index of the CNCs obtained in this work are in the same range as the following works, 77 % for miscanthus stalks (Vasylieva et al., 2020), 78 % for hemp stalks (Kassab et al., 2020), 71 % for kenaf bast fibers (Bhatnagar et al., 2021), 75 % for kenaf core wood (Chan et al., 2013), 78 % for corncob (Silvério et al., 2013), 75 % for rice straw (Thakur et al., 2020).

The superior CNCs crystallinity will expand its implementation range and could be considered an encouraging reinforcement for bionanocomposite materials due to the significant young's modulus of the crystalline region along the longitudinal direction.

4.5 Chemical Analysis - FT-IR

The chemical structure of the three lignocellulosic fibers were analyzed using FT-IR spectroscopy. The FT-IR spectrum of the raw fibers, bleached cellulosic fibers, and nanocellulose obtained from giant reed, kenaf, and miscanthus, respectively, are presented in figure 4.6. The table 4.4 resumes the FT-IR spectral characteristic peaks assignments.

In general, the obtained FT-IR spectrums were similar between the three studied samples, with no significant differences being identified between them. In the FT-IR spectrum associated with raw fibers was identified the presence of characteristic peaks associated with hemicellulose and lignin (1245, 1430, 1605, 1505, 1735 cm^{-1}). The peak at 1245 cm^{-1} is related to the axial asymmetric stretch of C-O bond in ether, ester, and phenol groups of lignin and hemicellulose. The small peak at 1430 cm^{-1}, associated with the functional group CH_3, was still visible after the acid hydrolysis, which could be associated with the small quantities of insoluble lignin, recognized by the slight yellow-brown color sedimentation in nanocellulose solution. The absorption bands at 1605 and 1505 cm^{-1} are associated with C=C in plane symmetrical stretching vibration of aromatic ring present in lignin. The band at 1735 cm^{-1} is linked to

C=O bonds of the acetyl and uronic ester group of hemicellulose, or the ester linkage of carboxyl groups of ferulic and p-coumaric acids of lignin (Beroual et al., 2021; Faradilla et al., 2016; Mandal and Chakrabarty, 2011; Martínez-Sanz et al., 2018; Mohaiyiddin et al., 2016; Morán et al., 2008). These bands associated with non-cellulosic compounds are visible in the initial fibers spectrum but progressively disappear after the application of the alkaline pre-treatment and subsequent bleaching, disappearing almost completely, or in some cases completely, in the spectrum associated with the respective nanocelluloses. These observations proved that the applied isolation methodology efficiently separated the cellulose from the non-cellulosic components as intended, being possible to obtain CNCs with highest cellulose purity degree.

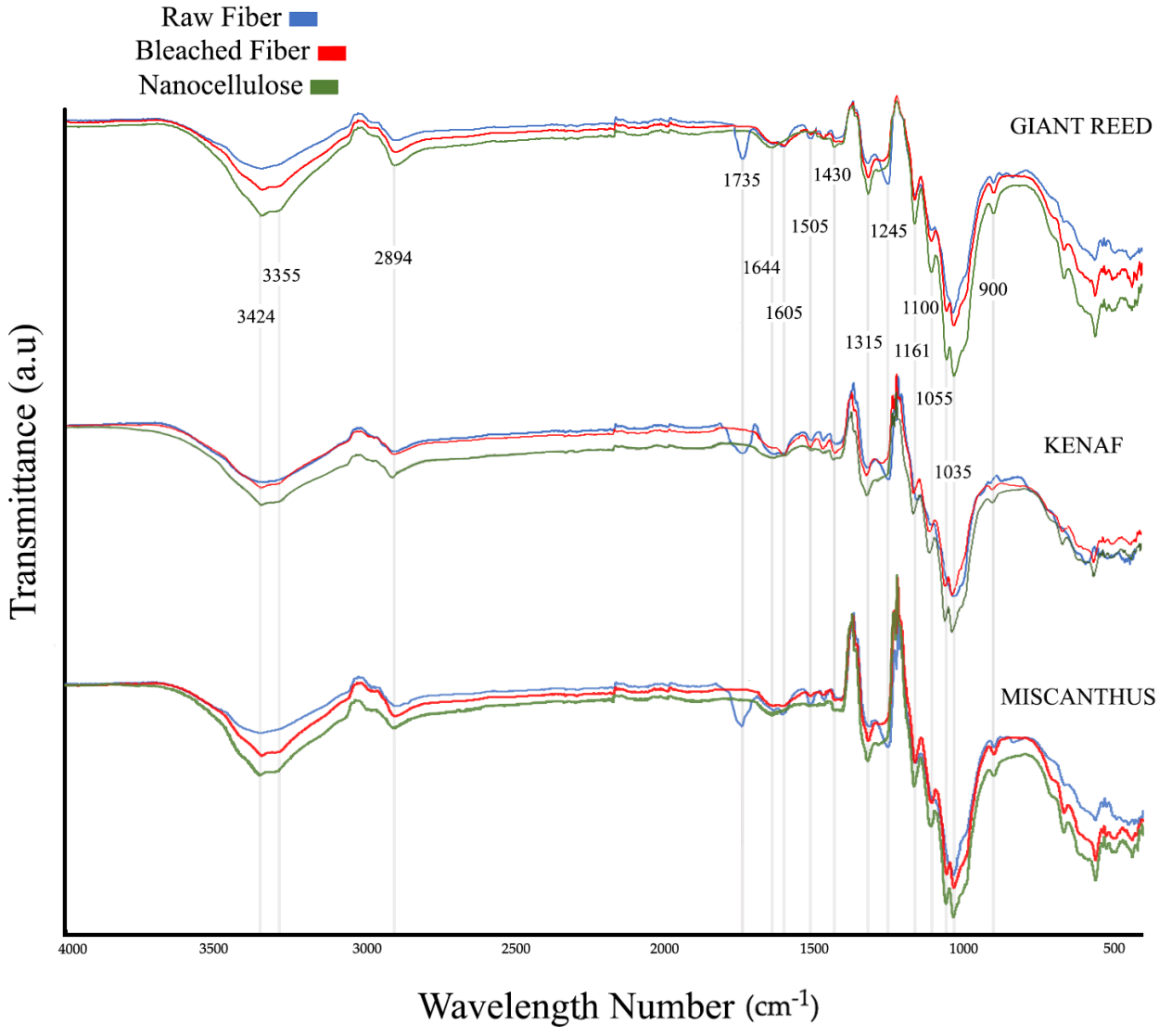

Figure 4.6 — FT-IR spectra of raw fiber, bleached fiber and nanocellulose isolated from the three different biomass sources.

The lignocellulosic fiber's FT-IR spectrum for all stages has exposed a broad band associated with cellulose in the region 3500–3200 cm^{-1} related to the free O–H stretching vibration of the hydroxyl groups. The presence of a much broader peak in this zone for the CNCs spectrum is due to increased water absorption as a result of the removal of the amorphous cellulose. Additionally, it was verified a characteristic peak at 2894 cm^{-1} linked to the C–H stretching vibrations in methyl (CH_3) and methylene (CH_2) functional groups of cellulose (Al-Dulaimi and Wanrosli, 2017; Mandal and Chakrabarty, 2011; Onkarappa et al., 2020). The peaks at 1644 cm^{-1} were assigned to the C=C stretching band and identified the bending vibrations of O–H groups in the absorbed water (George et al., 2022).

In addition to the peaks already identified, there was an increase in the intensity of some bands after the application of chemical treatments. Three other bands (1100, 1315, 1430 cm^{-1}), related to the cellulose crystalline content, registered an intensity increment after the purification treatments (Martínez-Sanz et al., 2018). Moreover, it was observed an augmentation in the peaks at 1161, 1055, 1035 and 900 cm^{-1}, for the CNCs spectrum. These correspond to the β-glycosidic bond stretch, C–O–C pyranose ring skeletal stretch, and β-glycosidic linkages between glucose units in cellulose (Beroual et al., 2021; Mandal and Chakrabarty, 2011). The FT-IR of the produced nanocelluloses showed that the characteristics peaks were similar to the bleached fibers spectrum. This observation predicts that the use of hydrogen peroxide in the bleaching process does not produce any oxidizing effect on the cellulose (Dien et al., 2019).

Table 4.4 — FT-IR spectral characteristic peaks assignments.

Wave Number (cm^{-1})	Appearance	Functional Group	Component
3500–3200	RF, BF, CNCs	O–H stretching vibration	Cellulose
2894	RF, BF, CNCs	C–H stretching vibration	Cellulose
1735	RF	C=O stretching vibration	Hemicellulose, Lignin
1644	RF, BF, CNCs	O–H bending	Absorbed Water
1605, 1505	RF, BF	C=C symmetrical stretching vibration of aromatic ring	Lignin
1430	RF, BF, CNCs	$-CH_3$ and $-CH_2$ scissoring vibrations	Lignin and Cellulose
1315	RF, BF, CNCs	C-C and C–O skeletal vibrations	Cellulose
1245	RF	C–O asymmetric stretching	Hemicellulose, Lignin
1161	RF, BF, CNCs	C–C ring stretching vibrations	Cellulose
1100-1035	RF, BF, CNCs	C–O–C pyranose ring stretching vibration	Cellulose
900	RF, BF, CNCs	β-glycosidic linkages between glucose units	Cellulose

** Raw fiber (RF); Bleached Fiber (BF); Cellulose Nanocrystals (CNCs).*

4.6 Thermal Properties

The determination of the CNCs thermal properties is essential to establish their compatibility as nanoreinforcement in bionanocomposites since the thermoplastic processing temperature generally surpasses 200ºC (Ilyas et al., 2018). The CNCs thermal stability is determined by several factors, like the biomass source, the methodology applied to isolate the nanocellulose, the sulfate content, and the crystallinity of nanocellulose, representing a deep impact on the thermal properties (Gan et al., 2020). The thermogravimetric curve (TG) and its derivative curve (DTG) for the three raw lignocellulosic fibers and respective isolated cellulose nanocrystals are exposed in figure 4.7. Additionally, table 4.5 shows the comparison of percentage weight loss and main degradation temperatures, between the different raw fibers and corresponding CNCs.

Conducting a careful analysis of the TGA thermographs, it was observed that all samples, whether raw fiber or nanocellulose, registered two characteristic degradation steps with associated weight loss (%) until 400°C is reached. The first stage of thermal degradation corresponded to an exceedingly small weight loss when compared to the total and was registered

below 100ºC. At this stage, weight loss was around 2-3 %. This phenomenon is associated with the evaporation of intermolecular hydrogen-bonded water and low molecular weight compounds present in these samples. The second thermal degradation occurrence represents a more significant weight loss, between 60-70 %, contributing significantly to the total weight variation, and was observed between 250-400ºC, ascribed to the pyrolysis of the cellulosic material, comprehending assorted steps like dehydration, depolymerization, and decomposition of glycosidic units (Babicka et al., 2022; Ilyas et al., 2018). Moreover, the thermal degradation of raw fibers displayed several peaks in the DTG curves between 200-300ºC, indicating the presence of different components, like hemicellulose and lignin, which decompose at different temperatures. The same peaks disappeared almost completely in the CNCs curve, indicating the removal of these non-cellulosic substances. As mentioned in the literature, the hemicellulose depolymerization usually occurs between 180-350ºC, while lignin degrades slowly and possesses superior thermal stability, due to its high molecular weight and heavily cross-linked structure, with degradation temperatures between 250-700ºC (Poletto et al., 2012; Santmartí and Lee, 2018; Yang et al., 2006).

Overall, the CNCs samples showed slightly higher weight losses, around 5-10 %, than raw fibers. Relatively to thermal stability, the giant reed and kenaf CNCs presented similar behavior, superior to the miscanthus CNCs. In detail, the giant reed raw fiber sample started to degrade to a considerable degree at a $T_{10\%}$ (temperature at which the sample lost 10 % of its initial weight) of 290ºC, reaching a maximum thermal decomposition peak at 368ºC, recorded by the DTG curve. Comparatively, giant reed CNCs recorded a slightly lower degradation temperature range, with a $T_{10\%}$ of 285ºC and a maximum degradation peak of 365ºC. The miscanthus samples registered a behavior between raw fibers and CNCs similar to that of the giant reed, however, the range of degradation temperatures was much lower, about 20-40ºC lower. The slightly lower thermal stability presented by the CNCs could be related to a combination of two effects, the nanocellulose high surface area of the crystals which represents more exposure of the surface to heat, and the effect of acid hydrolysis promoting the replacement of hydroxyl groups with sulfate groups on the CNCs surface, which have catalytic effect by reducing the activation energy of cellulose chain degradation (Bano and Negi, 2017; Rashid and Dutta, 2020).

The raw fibers from kenaf began to decompose significantly at lower temperatures, recording the lowest $T_{10\%}$ among the three initial samples, at a temperature of 256ºC. Analogously, the maximum degradation peak temperature for this fiber, detected in the DTG, was

also the lowest, at 320ºC. This could be due to the lowest crystallinity index presented by the kenaf fiber. As observed by other works, the crystalline structures are more resistant to higher temperatures than those with less compact and amorphous compositions (Poletto et al., 2012). Moreover, the lowest $T_{10\%}$ could be associated with the lowest amount of lignin, which also explains the higher temperatures to decompose the giant reed raw fiber. Therefore, the cellulose and lignin are bound as a robust lignin–cellulose complex more thermally stable than pure cellulose. Contrary to what was observed for the other two fibers, the kenaf CNCs showed higher thermal stability than the untreated fibers, with a $T_{10\%}$ of 293ºC and a maximum peak temperature of 370ºC, much higher than that presented by the miscanthus CNCs and equivalent to giant reed's CNCs. This can be explained by the increase in crystallinity between the initial kenaf fibers and the CNCs, also observed in the respective XRD patterns.

Raw fibers and nanocellulose thermal stability analysis were complemented by differential scanning calorimetry, which is an analysis required to evaluate the energy requirement for the thermal degradation of organic and inorganic substances. The DSC diagrams, represented in figure 4.8, followed the trend presented in the TGA and DTG curves. The DSC data related to the endothermic zones can be consulted in table 4.6. All analyzed samples presented two zones of distinct endothermic changes for the studied temperature range. Among the three lignocellulosic fibers, it was possible to verify that the diagrams differ slightly, which is natural because the nature of the endothermic curves is related to the compositional structure of each sample. The first endothermic curve started at temperatures below 100°C and had a reduced expression since the samples were dried before being analyzed. In concordance with the thermogravimetric analysis, this curve is related to the loss of moisture and volatile compounds due to evaporation. In this step, it was found that the T_{onset} and T_{peak} were higher for the raw fibers than for the CNCs, and the T_{offset} was similar between them. Therefore, the small amount of moisture adsorbed by the nanocellulose surface evaporates more easily at lower temperatures. This is because untreated fibers still have several hydrophilic components, like hemicellulose and lignin, capable to retain moisture for higher temperatures. Furthermore, with acid hydrolysis, a sulfated surface was generated on the nanocellulose, acting as a dehydrating catalyst, consequently reducing the affinity for moisture absorption (Mandal and Chakrabarty, 2011).

The second endothermic peak is related to the different stages of cellulose decomposition, normally established between 300ºC and 400ºC, a temperature at which the cellulose is practically completely pyrolyzed (Kim et al., 2016). Moreover, small endothermic curve was

detectable in raw fibers between 200-250ºC, being practically invisible in CNCs curves. These curves could be related with the energy absorbed by the sample for the decomposition of non-cellulosic components, like hemicellulose. The beginning of the second endothermic curve was registered at temperatures above 250ºC for raw fibers and CNCs of giant reed and kenaf. However, the miscanthus samples started this step at significantly lower temperatures, 180ºC for the raw fibers and 240ºC for the CNCs. Complementing the TGA analysis, it was possible to verify that the cellulose present in the miscanthus samples was the one that degraded at lower temperatures. These results are not in agreement with the results collected from the compositional analysis and the crystallinity index of the miscanthus raw fibers and CNCs. More studies must be conducted to understand what the factors were, in addition to those already mentioned, that led to the lower thermal stability of this sample.

To conclude this topic, the main observations to be drawn from the evaluation of thermal properties are that nanocelluloses lose slightly more weight than raw fibers and started to decompose at slightly lower temperatures. It was also verified that the nanocelluloses presented considerable thermal stability, with peak temperatures for the decomposition of the cellulose above 300ºC. However, the miscanthus sample showed significantly lower results than the kenaf and giant reed CNCs that had similar behaviors.

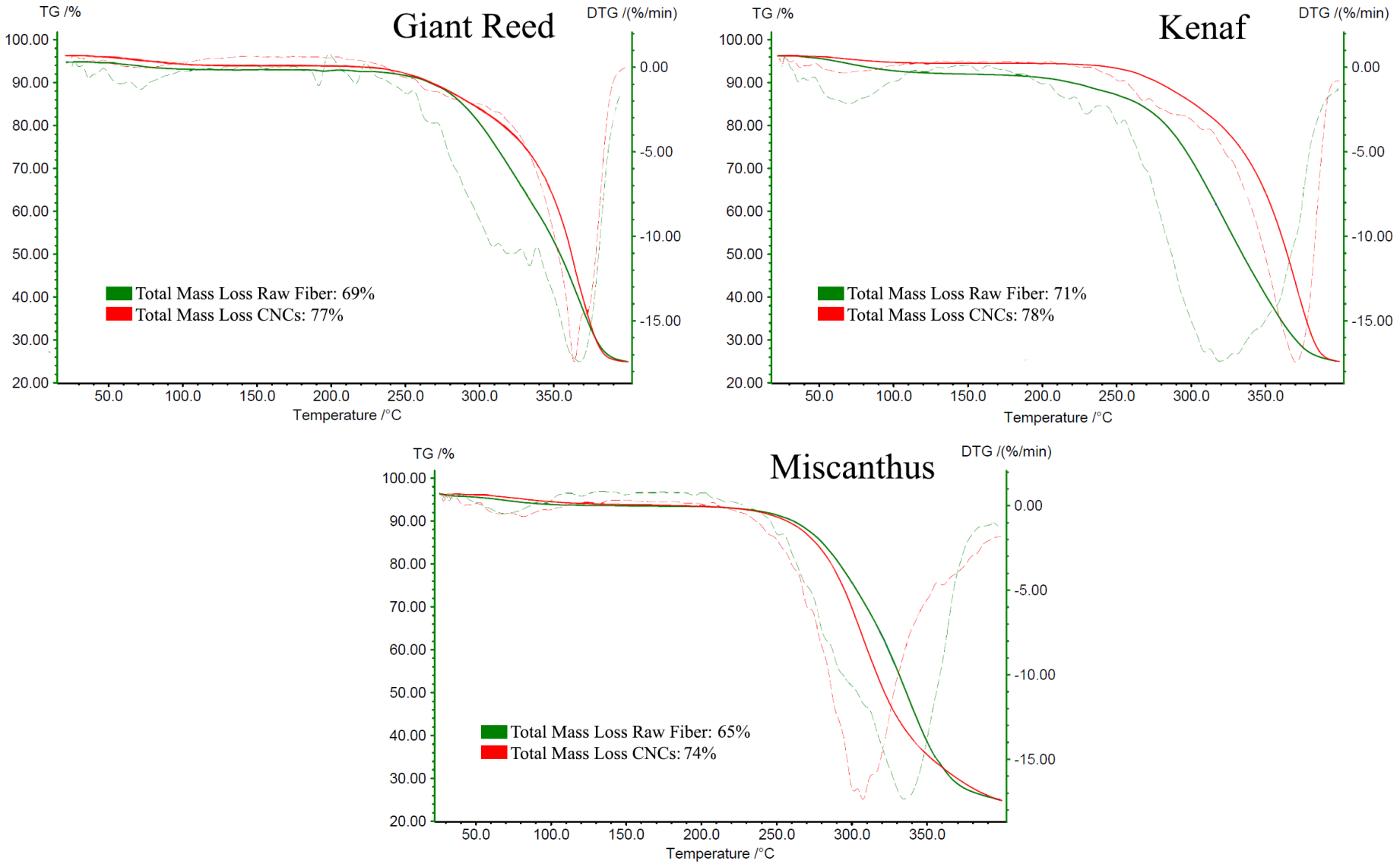

Figure 4.7 — TGA and DTG curves of raw fiber and nanocellulose isolated from the three different biomass sources. *Cellulose Nanocrystals* (CNCs).

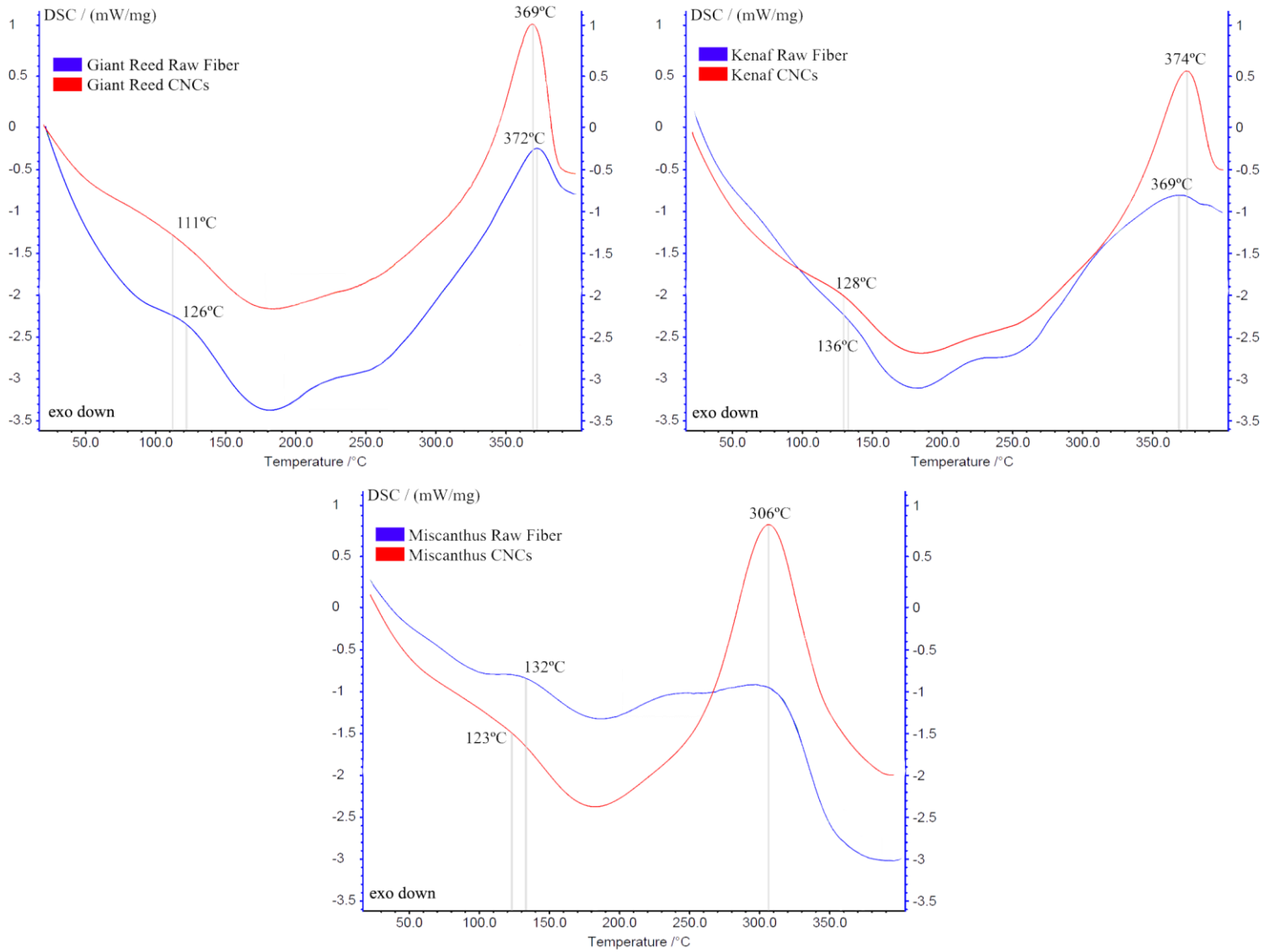

Figure 4.8 — DSC curves of raw fiber and nanocellulose isolated from the three different biomass sources. *Cellulose Nanocrystals* (CNCs).

Table 4.5 — TGA and DTG data of raw fiber and nanocellulose isolated from the three different biomass sources.

	TGA Data			DTG Data							
Sample	**$T_{10\%}$ (°C)**	**$T_{50\%}$ (°C)**	**Total Weigth Loss (%)**	**$Tpeak_1$ (°C)**	**$Tpeak_2$ (°C)**	**$Tpeak_3$ (°C)**	**$Tpeak_4$ (°C)**	**$Tpeak_5$ (°C)**	**$Tpeak_6$ (°C)**	**$Tpeak_7$ (°C)**	**Tmax (°C)**
Giant Reed Raw Fiber	290	362	69	190	215	250	265	308	317	330	368
Giant Reed Nanocellulose	285	362	77	260	310	-	-	-	-	-	365
Kenaf Raw Fiber	256	340	71	160	200	215	230	250	308	-	320
Kenaf Nanocellulose	293	364	78	270	310	-	-	-	-	-	370
Miscanthus Raw Fiber	278	346	65	180	255	270	290	310	-	-	335
Miscanthus Nanocellulose	270	323	74	245	270	300	-	-	-	-	318

Table 4.6 — DSC data of raw fiber and nanocellulose isolated from the three different biomass sources.

	DSC Data					
	1st Endothermic Zone			**2st Endothermic Zone**		
Sample	**T_{onset} (°C)**	**T_{peak} (°C)**	**T_{offset} (°C)**	**T_{onset} (°C)**	**T_{peak} (°C)**	**T_{offset} (°C)**
Giant Reed Raw Fiber	84	126	165	270	372	390
Giant Reed Nanocellulose	51	111	162	280	369	387
Kenaf Raw Fiber	95	136	165	250	369	-
Kenaf Nanocellulose	70	128	167	310	374	395
Miscanthus Raw Fiber	97	132	163	185	306	352
Miscanthus Nanocellulose	55	123	165	240	306	360

4.7 Chapter Conclusions

In this chapter, nanocrystalline cellulose was isolated from three lignocellulosic biomasses, giant reed, kenaf, and miscanthus, applying a pre-treatment methodology composed by delignification and bleaching processes, followed by acid hydrolysis. The samples were properly characterized from the beginning of the experiment to the CNCs. The three fibers showed initial high cellulose values and less than 30 wt% of lignin, indicating that are suitable to produce nanocellulose, applying milder pulping conditions for pre-treatment and bleaching. Kenaf fibers were the ones that showed the highest potential for nanocellulose extraction, by showing the higher cellulose and a lower lignin content. However, through the results obtained in this work, it was possible to verify that the application of a combined alkaline pre-treatment with bleaching was capable to decrease the amount of non-cellulosic components equally for each fiber, reaching an almost pure fiber with high cellulosic content (90 %). These results were supported by the information from the FT-IR spectrum where was observed a progressive disappearance of the characteristic bands of these elements.

Regarding the individual characteristics of the raw fibers, it was found that after grinding the kenaf sample had the smallest particle size, and the same trend was observed in the aspect ratio of the cellulose microaggregates analyzed by polarized microscopy. Although individualized AFM images of the nanocellulose crystals were not obtained so that it would be possible to determine their size, it was possible to observe that all CNCs presented a characteristic rod-like shaped appearance. The evaluation of the zeta potential indicated that the CNCs were negatively charged and presented acceptable dispersion stability indexes above the absolute value of 15 mV, yet there were steps in the CNCs extraction process that reduced the potential for better stability values. The crystallinity index of the initial and final samples, calculated after analyzing the XRD diffractograms, indicated that there was a progressive increase in crystallinity throughout the entire process. This increase was more significant in the kenaf sample since it was also the sample with the lowest initial CI (%), in opposition to what was estimated due to the highest amount of cellulose. The thermal analyzes demonstrated that the obtained CNCs have high thermal stability, with maximum peaks of cellulose degradation above 300ºC, demonstrating its possible applicability with mechanical reinforcement in thermoplastics. It was also possible to observe that lower decomposition temperatures were necessary for the miscanthus CNCs, indicating that something happened in this sample to have

affected this parameter since the morphological, compositional, and crystallinity characteristics of this sample did not show significant differences from the others.

In conclusion, the fibers of the three chosen lignocellulosic biomasses showed potential for cellulose isolation followed by transformation into nanocellulose. However, due to the properties studied, the kenaf and giant reed fibers showed a higher potential than the miscanthus fibers, mainly in terms of thermal stability. Moreover, for future works, the applied methodology should still be subject to optimizations to improve the CNCs properties.

5

RESULTS AND DISCUSSION
NANOCELLULOSE FROM ENERGY CROPS AS REINFORCEMENT AGENTS IN FILMS

This chapter corresponds to stage 2 of the doctoral thesis and the main objective was defined as the production of functional chitosan bioplastics reinforced with different nanocelluloses extracted from the three lignocellulosic biomasses, testing three incorporation concentrations (1.5, 2, and 2.5 %). It was decided to use the three nanocelluloses because it was observed in the previous chapter that all showed potential to be used as nanoreinforcements, despite the properties of the CNCs of giant reed and kenaf having shown a slightly higher potential.

For each bionanocomposite was carried out an extensive characterization of the functional properties with the aim of comparing them with each other, with a pristine chitosan film, and with a control in which commercial nanocellulose (extracted from cotton) was used as reinforcement. This characterization also had the objective of defining the best percentage of CNCs to be used, verifying whether it fits with the values observed in the literature.

5.1 Bionanocomposites Characterization

5.1.1 Mechanical Properties

The material's mechanical properties are generally assessed through the tensile test. For the execution of this test, a string sample from the material, with a known cross-sectional area and length, was clamped to tension grips. Then, a load force, which increases progressively over time at a defined speed, was applied along the sample's longitudinal axis. The stress-strain curve was then constructed, and the mechanical parameters, tensile strength (TS), elastic modulus (EM), and elongation at break (EAB), were calculated (Wahba, 2020). Before the performance of mechanical tests, the bionanocomposites were characterized in terms of thickness and density (table 5.1). As predicted, it was observed that samples loaded with CNCs

presented a slight but significant increment ($p < 0.05$) in these features, since it added a new solid component to the matrix.

Table 5.1 — Mechanical properties for Ch bionanocomposites with different CNCs concentrations (0, 1.5, 2, 2.5 wt%).

Specimen	Thickness (μm)	Volume (cm^3)	Density (g/cm^3)	Tensile Strength (MPa)	Elastic Modulus (MPa)	Elongation at Break (%)
Pristine Ch	40.3 ± 1.1^{c}	0.15 ± 0.03^{b}	1.30 ± 0.09^{c}	34.6 ± 3.7^{cd}	1415.4 ± 94.0^{e}	27.9 ± 1.6^{a}
Ch + 1.5 % CNCC	56.1 ± 0.4^{b}	0.21 ± 0.01^{a}	1.32 ± 0.05^{bc}	34.0 ± 0.3^{d}	1636.0 ± 76.5^{cd}	21.6 ± 0.4^{b}
Ch + 2 % CNCC	55.8 ± 0.6^{b}	0.21 ± 0.01^{a}	1.31 ± 0.03^{bc}	43.8 ± 0.5^{b}	2221.8 ± 141.2^{a}	16.7 ± 2.6^{c}
Ch + 2.5 % CNCC	58.2 ± 0.8^{a}	0.22 ± 0.02^{a}	1.42 ± 0.01^{ab}	37.2 ± 2.3^{c}	2035.3 ± 107.3^{ab}	10.9 ± 2.2^{de}
Ch + 1.5 % G	52.9 ± 0.9^{b}	0.20 ± 0.01^{a}	1.31 ± 0.06^{bc}	40.8 ± 4.4^{bc}	2022.0 ± 92.1^{ab}	8.9 ± 1.7^{de}
Ch + 2 % G	53.6 ± 0.3^{b}	0.20 ± 0.01^{a}	1.46 ± 0.08^{a}	42.2 ± 4.5^{b}	1983.5 ± 34.1^{b}	9.8 ± 1.2^{de}
Ch + 2.5 % G	54.2 ± 0.2^{b}	0.20 ± 0.01^{a}	1.46 ± 0.04^{a}	47.5 ± 1.5^{a}	2216.0 ± 83.9^{a}	7.0 ± 2.2^{e}
Ch + 1.5 % M	54.9 ± 1.7^{b}	0.21 ± 0.02^{a}	1.30 ± 0.03^{c}	31.2 ± 1.9^{e}	1258.3 ± 104.2^{e}	10.7 ± 2.6^{de}
Ch + 2 % M	56.0 ± 0.4^{b}	0.21 ± 0.01^{a}	1.32 ± 0.07^{bc}	33.2 ± 1.0^{d}	1541.8 ± 19.4^{d}	9.3 ± 2.0^{de}
Ch + 2.5 % M	57.7 ± 1.4^{ab}	0.22 ± 0.02^{a}	1.34 ± 0.08^{bc}	37.9 ± 0.2^{c}	1745.3 ± 68.5^{c}	6.6 ± 1.9^{e}
Ch + 1.5 % K	54.6 ± 0.8^{b}	0.20 ± 0.01^{a}	1.36 ± 0.05^{bc}	36.5 ± 0.7^{c}	1964.9 ± 32.1^{b}	11.7 ± 1.5^{d}
Ch + 2 % K	55.3 ± 0.9^{b}	0.21 ± 0.01^{a}	1.39 ± 0.06^{b}	39.0 ± 1.4^{c}	2053.6 ± 51.8^{ab}	9.5 ± 0.7^{de}
Ch + 2.5 % K	56.7 ± 1.1^{ab}	0.21 ± 0.02^{a}	1.43 ± 0.03^{ab}	43.2 ± 1.9^{b}	2125.7 ± 43.9^{ab}	7.1 ± 1.5^{e}

** Chitosan (Ch); Commercial Nanocellulose (CNCC); Giant Reed Nanocellulose (G); Kenaf Nanocellulose (K); Miscanthus Nanocellulose (M). Values are expressed as mean ± SD. Different letters in the same column correspond to samples statistically different.*

The stress-strain curves revealed that the pristine chitosan film had 34.6 ± 3.7 MPa for TS, 1415.4 ± 94.0 MPa for EM, and 27.9 ± 1.6 % for EAB. The nanofillers proved to be effective as a reinforcement agent since the bionanocomposite strength and stiffness were improved, while the ductility decreased. The Ch bionanocomposite loaded with 2.5 % giant reed CNCs registered the highest TS value, 47.5 ± 1.5 MPa (more 37 % than control). This value proved to be significantly higher ($p < 0.05$) than the TS achieved by the CNCs derived from kenaf and miscanthus. Compared with commercial CNCs, the highest value recorded for this parameter

was reached for a concentration of 2 %, 43.8 ± 0.5 MPa. For the above concentration, the TS value dropped to 37.2 ± 2.3 MPa. For the Elastic Modulus parameter, the highest value obtained corresponded to the Ch + 2 % CNCC sample, with 2221.8 ± 141.2 MPa (more 57 % than the control). Once again, this value was higher for 2 % than 2.5 %. Moreover, the EM value of the bionanocomposite with commercial nanocellulose did not show significant differences ($p > 0.05$) for the samples with CNCs of giant reed and kenaf. Although the sample with miscanthus CNCs had shown an improvement in mechanical properties when compared with the control sample, it presented values for TS and EM much lower than those achieved by the other samples.

The bionanocomposite strength and stiffness decrease for amounts of commercial CNCs above 2 %, was possibly due to the fact that the number of nanoparticles exceeded the acceptable limit for the matrix and therefore agglomerates were formed, which began to deteriorate the mechanical properties. Comparatively, bionanocomposites with CNCs extracted from the lignocellulosic biomass demonstrated a mechanical upgrade proportional to the amount added, being achieved a maximum for the 2.5 % load, hence, not predicting the occurrence of the same phenomenon below this amount. The results revealed a similar trend as indicated in other works which verified that introducing nanocellulose concentrations of up to 3 % raised the film's strength and stiffness (Mao et al., 2019; Xu et al., 2018). Khan et al., (2012) and Xu et al., (2018) observed that at CNCs concentrations above 5 % the TS and EM decreased, which was attributed to the existence of nanocellulose aggregates that promoted fracture points in the bionanocomposite.

The nanocellulose's reinforcing effect on mechanical properties can be explained through different factors. Intrinsically, these particles possess a considerable aspect ratio, opening a route to more uniform stress distribution, and allowing a superior stress transfer through the matrix/reinforce interface. Moreover, these own a huge specific surface area that grants the filler enhanced mechanical properties even at low concentrations (Khan et al., 2012; Mujtaba et al., 2017; Talebi et al., 2021). By filling the spare space amidst the polymer chains, the suitable electrostatic interaction between the CNCs anionic sulfate groups and Ch cationic amine groups generated a strong interface between them. Additionally, if it is granted a correct homogeneous dispersion, the chance to develop percolating networks with the free hydroxyl groups into the biopolymer matrix will increase. This ability could be responsible for the creation of more enduring intermolecular and intramolecular bonds (Costa et al., 2021; J.R.A. Pires et al., 2019a; Salari et al., 2018).

The EAB describes the material's capacity to support shape modifications without fracture development. Contrary to the increase presented by the TS and EM, it was noticed that the CNCs introduction made the bionanocomposites less elastic, thus, for greater filler concentrations, the ductility shown to be lower. The lowest EAB percentage was achieved with a 2.5 % amount without a statistical difference ($p > 0.05$) between samples, an approximated 75 % reduction when compared with the control sample. These results are in agreement with Salari et al., (2018), which justifies the EAB reduction with the presence of nanoparticles that fabricated a dense layout with increased continuities within the polysaccharide network. However, Mujtaba et al., (2017) and Talebi et al., (2021) observed opposite results. In these studies, with more significant reinforce amounts, higher values for EAB were registered. In Mao et al., (2019) study, two different phenomena occurred that can help to explain this disparity. The authors have prepared two Ch/CNCs bionanocomposites by two different methodologies, in which one system displayed cellulose nanoparticles more dispersed than the other. For the equivalent amount, the membrane with the better particle dispersion showed superior EAB values when compared with the pristine Ch, and the membrane with lower particle dispersion acquired inferior EAB values compared with the control. Accordingly, a righteous reinforce dispersion could be an indication of better stress transfer between polymer matrix and nanofillers, thus, reaching higher values of elasticity.

To conclude, it is predictable that the increase in film's strength and stiffness is due to the good interaction among CNCs anionic sulfate groups and Ch cationic amine groups, and the decrease of elasticity owns to the cellulose nanoparticles that are not very well dispersed and oriented, diminishing the stress transfer between the matrix and the filler leading to more compacted structures. It is also important to point that the origin and the methodology used to isolate cellulose and successive hydrolysis influence the nanoparticle´s intrinsic characteristics as the crystallinity, which controls their mechanical reinforcement capacity. Further, Ch/CNCs bionanocomposite unique formulation can elucidate the differences detected in the literature (Pires et al., 2021). Achieving a completely homogeneous dispersion represents a challenging task that needs to be optimized. Naturally, the nanoparticles tend to agglomerate due to the high specific surface area and surface energy. Therefore, when these are in powder form, unrepairable phenomena of agglomeration, reorganization, and co-crystallization take place. The use of an ultrasound probe capable of generating high frequencies in the suspension of CNCs before their introduction into the biopolymeric matrix, can originate more

homogeneous bionanocomposites and thus be able to achieve better mechanical properties (Kargarzadeh et al., 2017).

5.1.2 Morphological Characterization

Morphological characterization was performed by scanning electron microscopy technique to the Ch films cross-sections with CNCs, in the amount of 2.5 %. As presented by figure 5.1, it was possible to observe that the chitosan film possesses a homogeneous surface. Reinforced bionanocomposites showed a rougher surface with some appearance of micro cracks, without being possible to note significant differences between samples. Additionally, it was possible to observe the formation of some aggregates at the bottom of the films, probably due to the effect of gravity during the drying process, which pushes the nanoreinforcements to the bottom of the bionanocomposite.

In order to better understand the effect of nanoparticles on the bionanocomposites, SEM images (figure 5.2) were taken with a large zoom at the bottom of the films, where it was possible to observe the existence of a higher concentration of nanoparticles. Image A corresponds to Ch film with commercial CNCs. It was observed a homogeneous fillers dispersion through the matrix, with a smooth and nonporous surface and without cracks, indicating that this bionanocomposite was dense and compact. In contrast, for the remaining bionanocomposites, the nanocellulose introduction led to an increase in roughness and the appearance of some cracks, which could pledge the bionanocomposite properties. However, these observations do not seem to have had a direct influence on the mechanical properties, since the bionanocomposites with the giant reed, kenaf, and miscanthus CNCs showed mechanical reinforcement values equal to or higher than those obtained with the commercial CNCs.

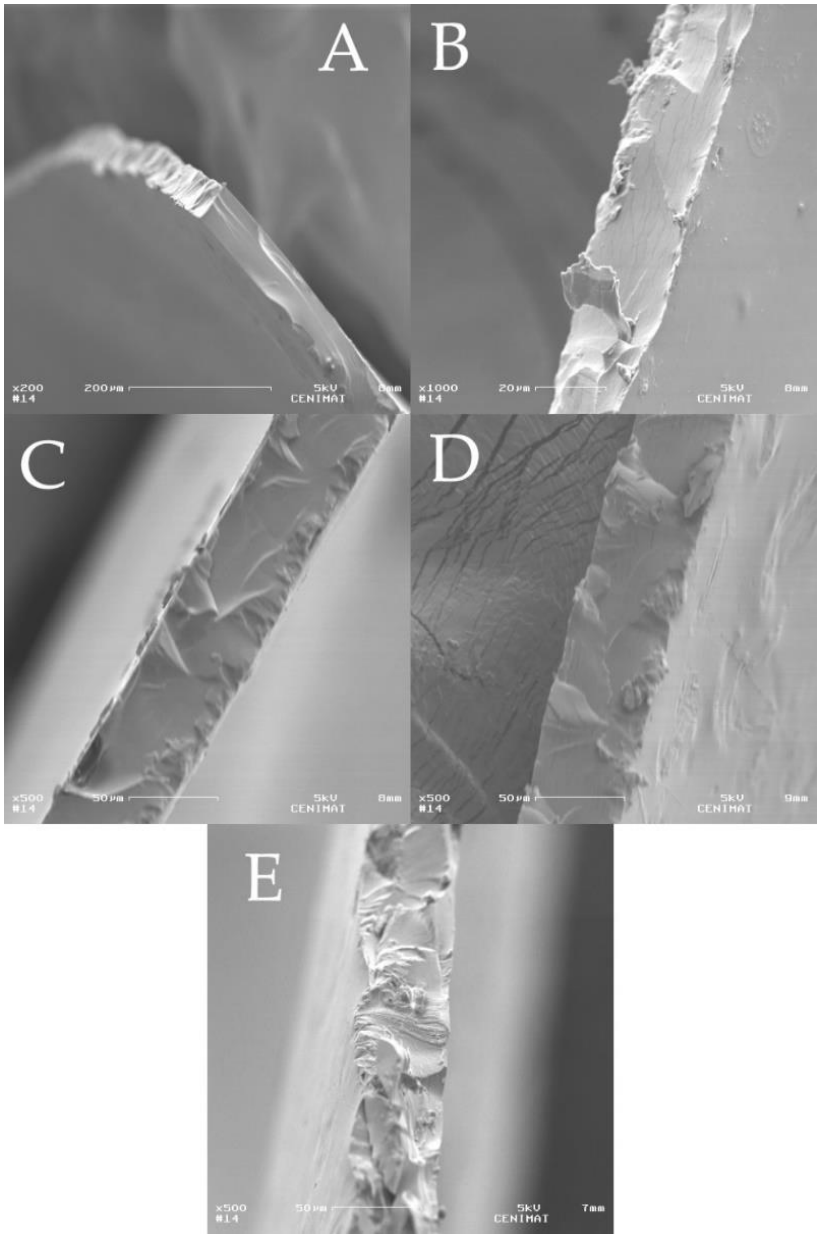

Figure 5.1 — Scanning electron microscopy (SEM) of cross section of (A) Ch; (B) Ch + 2.5 % CNCC; (C) Ch + 2.5 % CNCs Giant Reed; (D) Ch + 2.5 % CNCs Miscanthus: (E) Ch + 2.5 % CNCs Kenaf. *Chitosan (Ch); Nanocrystalline Cellulose (CNCs); Commercial Nanocellulose (CNCC).*

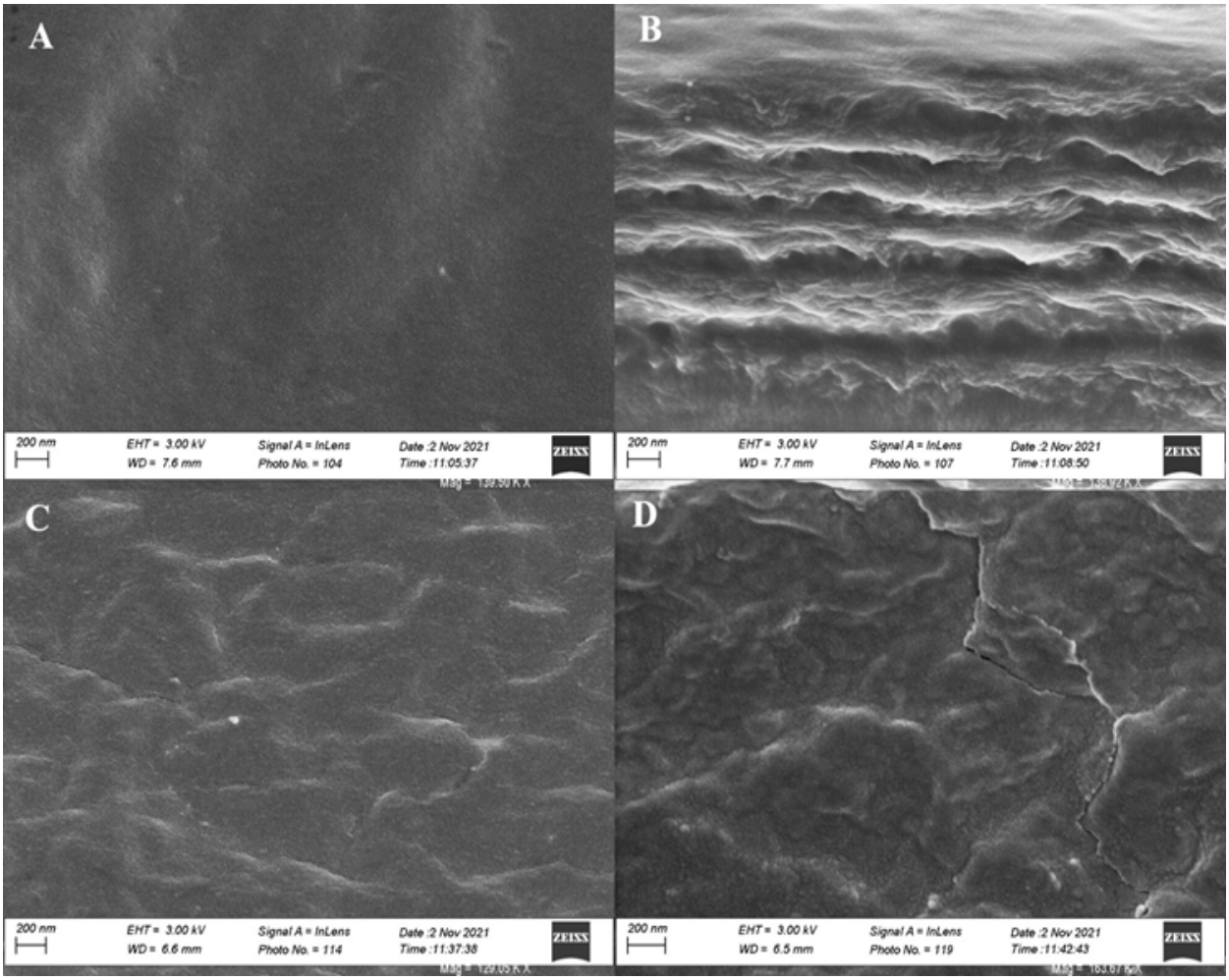

Figure 5.2 — Zoom SEM of the cross section lower part of (A) Ch + 2.5% CNCs Commercial; (B) Ch + 2.5 % CNCs Giant Reed; (C) Ch + 2.5 % CNCs Kenaf; (D) Ch + 2.5 % CNCs Miscanthus. *Chitosan (Ch); Nanocrystalline Cellulose (CNCs).*

It should additionally be noted that the spherical particles observed in image D, referring to miscanthus, have a more considerable size when compared with those observed in image C, referring to kenaf. In image B, corresponding to the bionanocomposite with particles extracted from giant reed, a phenomenon of wrinkles formation was observed. The appearance of wrinkles is usually the outcome of an inhomogeneous deformation, provoked by stress and shrinking, in surface layers with distinct mechanical properties, providing different surface reliefs concerning the stress directions (Izawa et al., 2021). A hypothesis for this spontaneous phenomenon can be attributed to a concentration gradient promoted by different deposition of the nanoparticles between the top and the bottom of the film, which can occur during the drying process. This gradient leads to different mechanical properties, between the film's top and the bottom, occurring the formation of micro wrinkles. Although this behavior has been

reported for another biomatrix (Rizzieri et al., 2006), there is not enough information to help explain this phenomenon in chitosan films. One of the few reports found in the literature that addresses this topic is the work of the Japanese team (Izawa et al., 2021). The author's prepared chitosan films with induced surfaced wrinkles by regulating the drying stress on oriented substrates, conducting a novel controlled surface wrinkling system using a drying process.

5.1.3 Optical Properties

The bionanocomposite optical properties analysis is crucial when it is intended to incorporate them into a packaging system. These layers may interfere with consumer acceptance since they can filter and alter the product's appearance inside the packaging (Souza et al., 2019b). The Ch film and bionanocomposites, even with the highest CNCs reinforcement levels, displayed a high degree of transparency and a slightly yellowish color, as depicted in figure 5.3. The optical properties results are presented in table 5.2.

It was observed that the introduction of CNCs in different amounts was not enough to significantly change ($p > 0.05$) the bionanocomposite's hue. Considering the luminosity parameter (L*), there was a significant decrease ($p < 0.05$) for an amount equal to or greater than 1.5 % in the case of commercial CNCs and 2.5 % for CNCs extracted from the three biomasses. Regarding the chroma value, also defined as the color intensity or saturation, it was noted that there were no significant changes ($p > 0.05$) between the Ch control film and the Ch/CNCs bionanocomposites. The measurement of light absorption by the bionanocomposite at 600 nm (visible light) per mm of thickness, or opacity, revealed that Ch/CNCs bionanocomposites absorbed more light than the pristine Ch film. Indeed, it was clearly identified that the opacity values rise was proportional to the reinforcement content, having been achieved the maximum for the 2.5 % CNCs load with no significant difference ($p > 0.05$) for the 2 %.

Figure 5.3 - Ch film and Ch bionanocomposites with 2.5 % CNC optical configuration. *Chitosan (Ch); Commercial Nanocellulose (CNCC); Giant Reed Nanocellulose (G); Kenaf Nanocellulose (K); Miscanthus Nanocellulose (M).*

Table 5.2 — Optical properties of obtained bionanocomposites with different CNCs concentrations (0, 1.5, 2, 2.5 wt%).

Specimen	Luminosity (L*)	Hue Angle	Chroma	Opacity (mm^{-1})
Pristine Ch	92.3 ± 0.2^{a}	98.5 ± 0.1^{a}	7.5 ± 0.5^{a}	1.0 ± 0.1^{c}
Ch + 1.5 % CNCC	91.2 ± 0.3^{b}	98.8 ± 0.4^{a}	8.1 ± 0.1^{a}	1.3 ± 0.1^{bc}
Ch + 2 % CNCC	91.6 ± 0.1^{b}	97.5 ± 0.3^{a}	8.0 ± 0.1^{a}	1.7 ± 0.4^{ab}
Ch + 2.5 % CNCC	91.5 ± 0.3^{b}	97.9 ± 0.3^{a}	7.8 ± 0.5^{a}	1.5 ± 0.2^{ab}
Ch + 1.5 % G	92.0 ± 0.1^{ab}	98.5 ± 0.7^{a}	7.6 ± 0.1^{a}	1.2 ± 0.1^{bc}
Ch + 2 % G	91.9 ± 0.5^{ab}	97.6 ± 0.1^{a}	7.9 ± 0.1^{a}	1.5 ± 0.3^{ab}
Ch + 2.5 % G	91.4 ± 0.1^{b}	98.2 ± 0.2^{a}	8.2 ± 0.3^{a}	1.8 ± 0.3^{a}
Ch + 1.5 % M	92.1 ± 0.1^{ab}	98.6 ± 0.2^{a}	7.4 ± 0.2^{a}	1.0 ± 0.0^{c}
Ch + 2 % M	92.2 ± 0.0^{a}	98.2 ± 0.1^{a}	7.4 ± 0.2^{a}	1.1 ± 0.2^{bc}
Ch + 2.5 % M	91.4 ± 0.0^{b}	98.1 ± 0.2^{a}	8.2 ± 0.2^{a}	1.4 ± 0.0^{ab}
Ch + 1.5 % K	92.1 ± 0.2^{a}	98.4 ± 0.1^{a}	7.7 ± 0.4^{a}	1.3 ± 0.1^{bc}
Ch + 2 % K	92.0 ± 0.1^{ab}	98.0 ± 0.2^{a}	7.6 ± 0.1^{a}	1.6 ± 0.1^{ab}
Ch + 2.5 % K	91.7 ± 0.3^{b}	97.7 ± 0.3^{a}	8.0 ± 0.2^{a}	1.8 ± 0.4^{a}

** Chitosan (Ch); Commercial Nanocellulose (CNCC); Giant Reed Nanocellulose (G); Kenaf Nanocellulose (K); Miscanthus Nanocellulose (M). Values are expressed as mean ± SD. Different letters in the same column correspond to samples statistically different.*

The presence of ultraviolet light could be an accelerator of oxidation processes, therefore, if the bionanocomposite can confer protection against this external phenomenon, it could be recognized as an advantage for food packaging (Salari et al., 2018). Accordingly, the UV light transmittance scanning spectra was evaluated for bionanocomposites with 2.5 % CNCs and then compared with the control samples (with wavelengths between 200 and 400 nm) as stated in figure 5.4. In general, it was found that the produced bionanocomposites had a better performance in this parameter in relation to the control film, this effect can be attributed to the introduction of CNCs. For short-wave UV (till 220 nm) more than 90 % of the light was absorbed by all specimens. From this point on, it was possible to observe the CNCs influenced the bionanocomposite transmittance. For medium-wave UV (near 300 nm) the control Ch film blocked nearly 60 % of this light, while 70-90 % for bionanocomposites. At least, for long-wave

UV (400 nm), usually denominated as black light, almost 20-25 % of the light was absorbed for control and Ch/CNCs from kenaf, increasing a little to Ch/CNCs from giant reed and miscanthus, and increasing substantially to 60 % with Ch/CNCC. These results can be explained by the CNCs incorporation in the polymeric matrix, causing light diffusion or lower light transmittance rates.

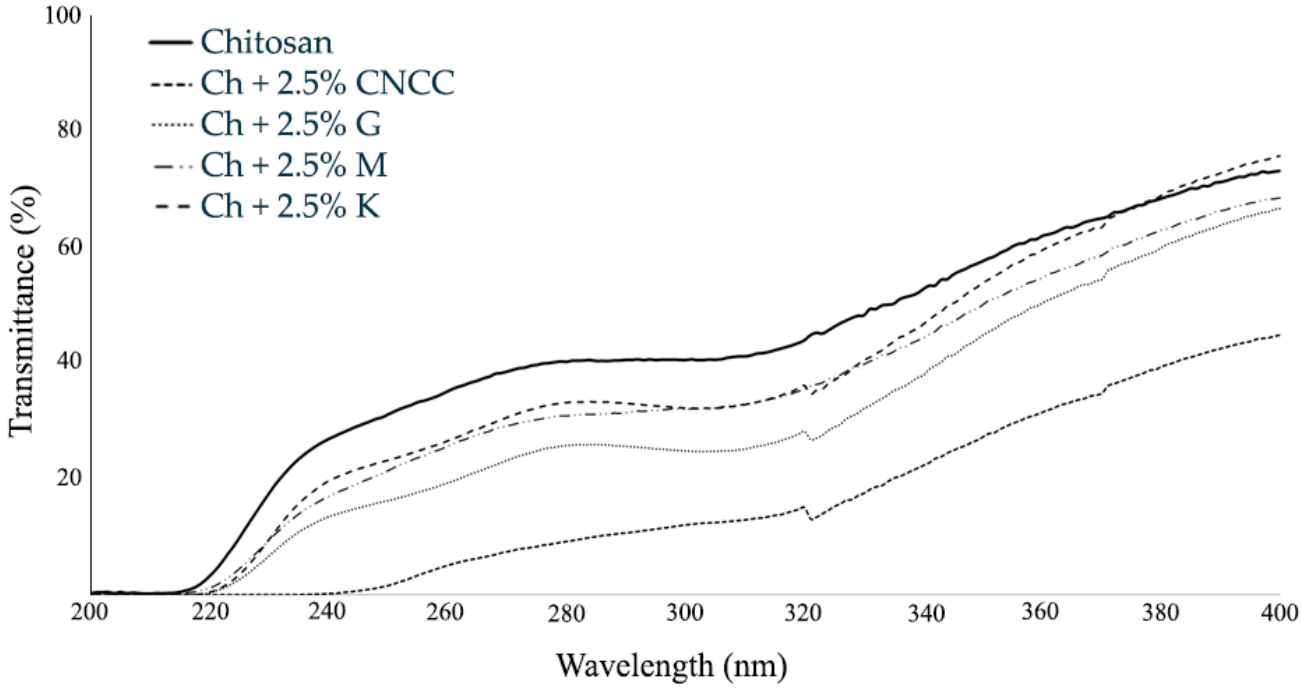

Figure 5.4 — Ultraviolet light transmittance (%) scanning spectra for Ch film and Ch bionanocomposites with 2.5% CNCs. *Chitosan (Ch); Commercial Nanocellulose (CNCC); Giant Reed Nanocellulose (G); Kenaf Nanocellulose (K); Miscanthus Nanocellulose (M).*

5.1.4 Wettability Properties

The wettability properties knowledge is indispensable to perceive the bionanocomposite behavior when in contact with food matrices with high water content. It also gives the possibility to understand the resistance to degradation under those conditions if the material is discarded in a marine environment (Souza et al., 2018). Table 5.3 illustrates the action of the different reinforcing agents on the bionanocomposite water uptake.

Introducing nanofillers to the polymeric matrix had a direct effect on the sample's wettability properties, decreasing the swelling capacity and solubility, and increasing the contact angle, thus transforming the bionanocomposites more hydrophobic. The laboratory test to

evaluate the swelling and solubility rates was designed to run for 24 h, because, using previous work, a balance in saturation levels was observed at the end of this time (Corsello et al., 2017; Xu et al., 2018). Regarding the first two mentioned properties, they registered similar behaviors. When the CNCs percentage is 1.5 %, no marked reductions ($p > 0.05$) were noted, however, for Ch + CNCC, there was even a slight increase. For concentrations of 2 % CNCs, a more pronounced decrease was verified, and for CNCs amounts of 2.5 %, the water uptake was statistically different ($p < 0.05$) from those obtained by the Ch control film. The most considerable reduction observed was attributed to bionanocomposite with 2.5 % commercial CNCs, minus 26 % and 24 %, for swelling and solubility, respectively. Comparatively, the lignocellulosic CNCs did not exhibit as expressive reductions as the CNCC, however, these also proved to be statistically different ($p < 0.05$) from the pristine Ch. The bionanocomposite swelling ability is strictly dependent on the film matrix and the filler's characteristic, like crystallinity. Analyzing the obtained results, it was possible to assume that a good hydrogen bonding and electrostatic association occurred between the cellulose nanoparticles and chitosan molecules, reducing the number of free -OH groups, thereby creating a less porous network with fewer paths where water molecules can infiltrate (Mao et al., 2019; Yadav et al., 2020). These results are in line with those presented by (Talebi et al., 2021), who also stated that the free amino groups, responsible for the chitosan hydrophilic nature, may have decreased with the nanocellulose introduction.

The contact angle evaluates the relative amounts of adhesive (liquid-to-solid) and cohesive (liquid-to-liquid) forces operating on a liquid and is classified over the scale of $0° \leq \theta \leq 180°$. The WCA measurements obtained for pristine Ch and different bionanocomposites with 2.5% CNCs can be stated in figure 5.5. When a drop of water falls over the bionanocomposite, it will propagate on the surface based on the intermolecular interactions between the film and the water (Souza al., 2019). As illustrated in table 5.3, the Ch film WCA was 78.4 ± 2.1º. For the majority of samples, it was visible that a minimum CNCs concentration was enough to register a significant increase ($p < 0.05$) in the bionanocomposite hydrophobicity. This behavior increased proportionally as the nanoparticles amount in the bionanocomposite rises, with a maximum being achieved for the 2.5 % amount. The sample "Ch + 2.5 % G" recorded the most considerable increase ($p < 0.05$) compared with the control, about 18 %, thus being considered the most hydrophobic specimen. It should also be remarkably noted that the nanocellulose obtained from lignocellulosic biomass presented similar or better contact angle results

compared with the commercial one, thus demonstrating its full potential. It is then possible to conclude that the bionanocomposites become more hydrophobic, due to the blocking of functional groups that would interact with the water, which is correlated with a decrease in swelling and solubility parameters (Slavutsky and Bertuzzi, 2014).

Table 5.3 — Wettability properties for Ch bionanocomposites with different CNCs concentrations (0, 1.5, 2, 2.5 wt%).

Sample	Swelling (%)	Solubility (%)	Contact Angle (Degrees)
Pristine Ch	174.9 ± 1.5^{b}	23.0 ± 1.2^{bc}	78.4 ± 2.1^{f}
Ch + 1.5 % CNCC	203.0 ± 17.5^{a}	21.2 ± 0.8^{cd}	84.3 ± 2.6^{cde}
Ch + 2 % CNCC	154.1 ± 5.9^{cd}	21.0 ± 1.2^{cd}	87.6 ± 0.8^{bc}
Ch + 2.5 % CNCC	130.1 ± 3.1^{e}	17.6 ± 0.7^{e}	89.9 ± 1.3^{ab}
Ch + 1.5 % G	169.1 ± 15.9^{bc}	22.4 ± 1.3^{bc}	86.4 ± 3.1^{bcd}
Ch + 2 % G	158.5 ± 9.5^{cd}	21.8 ± 2.3^{bc}	88.5 ± 1.1^{bc}
Ch + 2.5 % G	157.8 ± 1.9^{c}	21.5 ± 0.6^{cd}	92.3 ± 1.6^{a}
Ch + 1.5 % K	160.6 ± 11.1^{bc}	25.8 ± 0.5^{a}	82.1 ± 2.5^{def}
Ch + 2 % K	149.7 ± 2.0^{cd}	20.4 ± 0.1^{d}	85.8 ± 2.7^{cde}
Ch + 2.5 % K	145.0 ± 2.1^{d}	18.5 ± 1.0^{de}	89.3 ± 1.4^{abc}
Ch + 1.5 % M	171.6 ± 2.4^{b}	23.2 ± 0.3^{b}	83.7 ± 1.1^{de}
Ch + 2 % M	168.7 ± 7.9^{bc}	21.6 ± 0.9^{cd}	87.2 ± 0.9^{c}
Ch + 2.5 % M	159.3 ± 4.5^{c}	20.4 ± 0.4^{d}	90.3 ± 3.4^{abc}

** Chitosan (Ch); Commercial Nanocellulose (CNCC); Giant Reed Nanocellulose (G); Kenaf Nanocellulose (K); Miscanthus Nanocellulose (M). Values are expressed as mean ± SD. Different letters in the same column correspond to samples statistically different.*

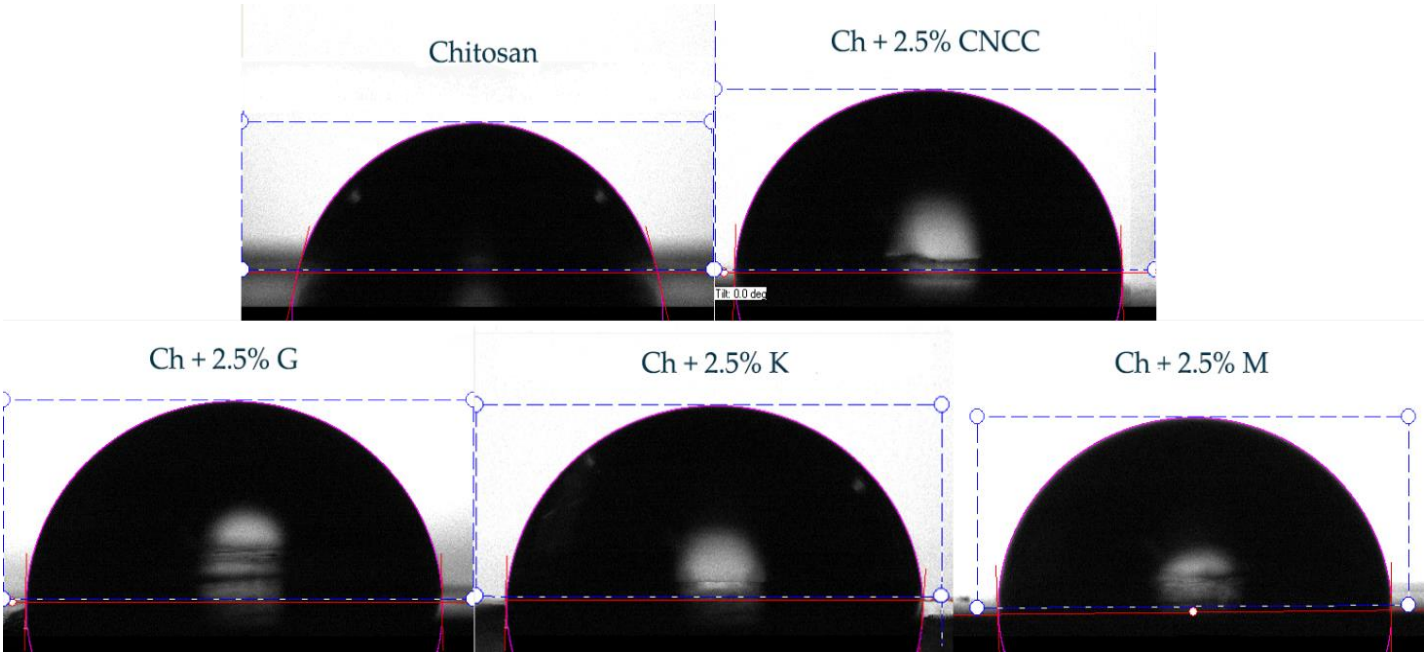

Figure 5.5 — Water contact angle measurements for Ch film and Ch bionanocomposites with 2.5 % CNCs concentration. *Chitosan (Ch); Commercial Nanocellulose (CNCC); Giant Reed Nanocellulose (G); Kenaf Nanocellulose (K); Miscanthus Nanocellulose (M).*

5.1.5 Barrier Properties

The capacity to prevent moisture and oxygen transfer between the inside of the packaging and the surrounding atmosphere is one of the most desirable features attributed to biodegradable films, thus, water vapor and oxygen permeability should remain as low as possible. To improve that ability, the biopolymer barrier properties can be remarkably changed by the inclusion of organic or inorganic nanoparticles with a high aspect ratio that modifies the gas molecules diffusion pathway (Pires et al., 2021). Before the results presentation and discussion, it is necessary to clarify that the bionanocomposites' barrier properties depend on a vast variety of factors intrinsic to its composition, like the biopolymer chemical structure, polarity, degree of crystallinity, density, and molecular weight, as well as the presence of other plasticizers or crosslinkers. The complex combination of these factors will determine the bionanocomposites affinity for the different gas molecules (Zhang et al., 2021b). As the bionanocomposites formulation was the same except for CNCs origin and quantity, it was attributed that the differences obtained should fall only on the nanofiller reinforcing influence.

The results for water vapor and oxygen permeability followed a similar tendency introduced in the previous sub-chapter for swelling and solubility indexes and are presented in

table 5.4. The two investigated variables demonstrated that bionanocomposites permeability followed a descendent trend when CNCs were incorporated, and this decrease was more accentuated as the reinforcement amount increased. This tendency is in accordance with related works found in the literature (Azeredo et al., 2010; Corsello et al., 2017; Salari et al., 2018; Yadav et al., 2020; Zhang et al., 2021b).

The commercial nanocellulose revealed no significant differences ($p > 0.05$) between 2 % and 2.5 % amounts in both parameters, achieving a maximum reduction of 11 % and 38 %, for WVP and OP respectively. In the case of CNCs from lignocellulosic biomasses, the most considerable permeability values decrease was attained for the 2.5 % level. The sample Ch + 2.5 % G held a reduction of 40 % and 54 %, while Ch + 2.5 % K got a decrease of 27 % and 46 %, and Ch + 2.5 % M drew a lowering of 30 % and 57 %, toward WVP and OP sequentially. The explanation that supports our data could reside in the addition of nanofillers with a high aspect ratio that increases the bionanocomposites crystallinity (acting as crystalline fillers that increase the distance for the molecules of water to pass through, i.e., a more tortuous path) (Pires et al., 2021). Furthermore, well scattered and arranged cellulosic CNCs inside the Ch matrix, could enhance the interactions between the polymeric chains, which will decrease the free space and slow the molecular chain mobility. Then, the gas particles were obliged to discover new, long, and harder trajectories to surround these particles, making it difficult the gas diffusion through the film (García et al., 2020).

When compared with other similar studies, the reductions presented by the bionanocomposites appear to be rather promising, as the CNCs amount introduced into Ch films was quite small. Similarly, Corsello et al., (2017) created Ch/CNCs bionanocomposites but employed higher nanoparticles levels (1, 3, 5, and 10 % w/w Ch). Comparatively to the control film, a 38 % reduction was the best rate that the authors achieved, correspondent to the amount of 5 % CNC added. When the nanocellulose percentage increased to 10 %, the WVP decreased to 25 %. The presence of CNCs, which added more tortuous paths inside the biopolymeric matrix was the explanation utilized to describe the lower water vapor diffusion processes. This trend happened until a critical nanoparticle content, after which a constant or a modest increase of permeability was detected, which was also verified in the work of (Costa et al., 2021)for CNCs concentrations over 25 %. Excessive nanofiller content could disrupt some particular points of the biopolymeric network generating the formation of gaps in which the water vapor molecules will pass through (Pires et al., 2021).

There is not certain that a decrease in the WVP will always happen with nanocellulose addition, as demonstrated by the work carried out by Mujtaba et al., (2017). The authors added different CNCs concentrations, extracted from flax fibers, on Ch films, verifying that for the 10 % CNCs the WVP value increased by 39 % relative to the control. The reason for this growth can own to several factors, like the CNCs hydrophilicity that extended the film hydrophilicity or the fact that CNCs linked to places that were formerly used by Ch to bind to water molecules. According to the Mujtaba's work, the most substantial factor affecting the WVP may be the nanocellulose crystallinity, enhancing the adsorption percentage in a negative or positive way. When CNCs crystallinity is small, there are not enough crystalline zones to capture water molecules, increasing the diffusion through the amorphous parts, in the contrary, for higher crystalline rates, the permeability is restricted since the crystalline parts are able to trap the water molecules (Mujtaba et al., 2017).

Studies considering an OP evaluation for Ch/CNCs formulations are still scarce in the literature, some of them do it simultaneously with WVP, as the works of Zhang et al., (2021) and Costa et al., (2021). In the first one, the authors proposed a novel Ch film reinforced with curcumin grafted TEMPO-oxidized cellulose nanofibers (10 %, 17 %, 25 %, and 33 wt%). In the second one, the authors evaluated the potential of Ch/CNCs (5, 10, 25, and 50 wt%) films to be applied as active pads for meat packages. Although both indicated works applied CNC percentages in similar ranges, they obtained contradictory results. For Zhang et al., (2021) the bionanocomposites OP increased with the incorporation of the nanoparticle complex. Costa et al., (2021) work, in concordance with our results, showed a reduction of OP values with the CNCs incorporation, confirming the nanocellulose effectiveness to decrease the film affinity for the oxygen molecules. Moreover, in the work of Lavric et al., (2021), it was verified that the best OP result between 25 different formulations (based on BNCs, CNCs, CNFs, Ch, or alginate) was for specimens reinforced with 3 % CNCs, decreasing 45 % or 38 % when compared to the control, for alginate and chitosan as biopolymeric matrix respectively.

Overall, the ability of nanocellulose additives to preserve the structure and function of Ch films in a humid environment was convincingly demonstrated. The WVP and OP analysis also exposed that nanocellulose characteristics, mainly its crystallinity rate, and the percentual amount included in the bionanocomposite, are essential to ascertain an effective reinforcement of the bionanocomposites final barrier properties.

Table 5.4 – Water Vapor Permeability (WVP) and Oxygen Permeability (OP) coefficients for Ch bionanocomposites with different CNCs concentrations (0, 1.5, 2, 2.5 wt%).

Sample	Water Vapor Permeability (10^{-11} mol/m·s·Pa)	Oxygen Permeability (10^{-16} mol/m·s·Pa)
Pristine Ch	1.49 ± 0.29^{b}	1.36 ± 0.10^{a}
Ch + 1.5 % CNCC	1.92 ± 0.10^{a}	1.21 ± 0.12^{ab}
Ch + 2 % CNCC	1.65 ± 0.06^{ab}	0.72 ± 0.01^{d}
Ch + 2.5 % CNCC	1.33 ± 0.18^{bc}	0.84 ± 0.05^{cd}
Ch + 1.5 % G	1.56 ± 0.07^{ab}	1.02 ± 0.08^{bc}
Ch + 2 % G	1.35 ± 0.08^{bc}	0.71 ± 0.20^{cde}
Ch + 2.5 % G	0.90 ± 0.05^{d}	0.63 ± 0.13^{de}
Ch + 1.5 % M	1.66 ± 0.11^{ab}	1.06 ± 0.01^{b}
Ch + 2 % M	1.48 ± 0.08^{b}	1.02 ± 0.01^{c}
Ch + 2.5 % M	1.05 ± 0.07^{cd}	0.58 ± 0.01^{e}
Ch + 1.5 % K	1.63 ± 0.05^{ab}	1.10 ± 0.01^{b}
Ch + 2 % K	1.42 ± 0.06^{b}	0.98 ± 0.05^{c}
Ch + 2.5 % K	1.09 ± 0.13^{cd}	0.74 ± 0.10^{cd}

** Chitosan (Ch); Commercial Nanocellulose (CNCC); Giant Reed Nanocellulose (G); Kenaf Nanocellulose (K); Miscanthus Nanocellulose (M). Values are expressed as mean ± SD. Different letters in the same column correspond to samples statistically different.*

5.1.6 Thermal Properties

The effect of cellulose nanocrystals on the thermal properties of chitosan films was studied by relying on TGA curves, and DSC thermograms (figures 5.6 and 5.7), since it is a determinative evaluation to explore the thermal decomposition of polymeric materials. For this assay, only the bionanocomposites with the 2.5 % CNCs level were analyzed and compared, since this percentage proved to be the most effective in optimizing the mechanical and barrier properties.

Pointing out to the final of each TGA curve, at 400ºC, it was stated that the bionanocomposites absolute mass loss was around 60 %, except for the sample "Ch + 2.5 % M" which reached 65 %. In comparison, the chitosan film presented a mass loss of 74.6 %, being possible

to demonstrate that nanocellulosic fillers had a positive thermal reinforcing effect. Both mass loss percentages are in concordance with the ones presented by Mujtaba et al., (2017). It can be stated through figure 5.6 that bionanocomposites mass loss occurred mainly in three steps. The first mass loss step appears around 50–135°C which cause can be attributed to the volatile molecule's evaporation, like the physically adsorbed and strongly hydrogen-bonded water, and residual acetic acid (Costa et al., 2021). The respectively endothermic broadband is positioned in a region between 81-91°C. A second minor endotherm (in the range of 130–145 °C) appears in the sample "Ch + 2.5 % K", probably due to water molecules retained by the plasticizer glycerol as it is hydrophilic in nature (Akyuz et al., 2018). The second step of noteworthy mass loss fluctuated between 130ºC to 270°C and may be associated with glycerol degradation and chitosan chain depolymerization through de decay of amine groups and cleavage of glycosidic linkages via dehydration and deamination. The exothermic peak relative to the decomposition temperature is perceived to be around 265-270°C. The biopolymer degradation due to thermal split of Ch backbone, with -CH_2OH degradation, started at 290ºC, where is verified the third mass loss, and was permanent to 400ºC (Celebi and Kurt, 2015). A late slight endothermic peak, around 340-370ºC, appeared in the bionanocomposites with CNCs from lignocellulosic biomasses, which can be related with the particle decomposition probably due to pyrolysis as reported by some literature sources (Elias et al., 2017; Ismail et al., 2019). This peak is not very pronounced as the amount of nanocellulose introduced was not very high either.

Comparing the three major degradation temperatures (T10, T50, and Tmax), some differences can be observed, as exposed in table 5.5. The thermal degradation patterns of the Ch/CNCC and Ch/CNCs from giant reed can be considered almost identical, but these two samples showed a shift to a higher degradation temperature than Ch/CNCs from kenaf and miscanthus. These results demonstrated the same trend already shown by the mechanical and barrier results, in which the nanocellulose from giant reed fibers possess more similarities with the commercial nanocellulose and, consequently, better results than the ones produced through kenaf or miscanthus fibers.

Glass transition temperature (Tg) and melting point (Tm) are two significant parameters used for plastic identification. The Tg value represents the temperature at occurs a change from hard to soft in amorphous polymers. The concentration of crystalline regions in amorphous (semicrystalline) polymers affects the polymer rigidity, thereby when the nanoparticles are introduced into the film it is intended to increase the crystallinity and consequently upgrade the thermal properties (Pacáková and Virt, 2005). Tm represents the temperature at

which an ordered crystalline solid becomes a disordered melt and is also a barometer of atomic bonding strength establishing a relationship with the mechanical properties. The general tendency is that a higher melting temperature supposes a higher modulus and vice versa (Salamon, 2014). In this work, the Tg and Tm range were similar for all specimens, was estimated to be between 50-100ºC and 250-270°C, respectively.

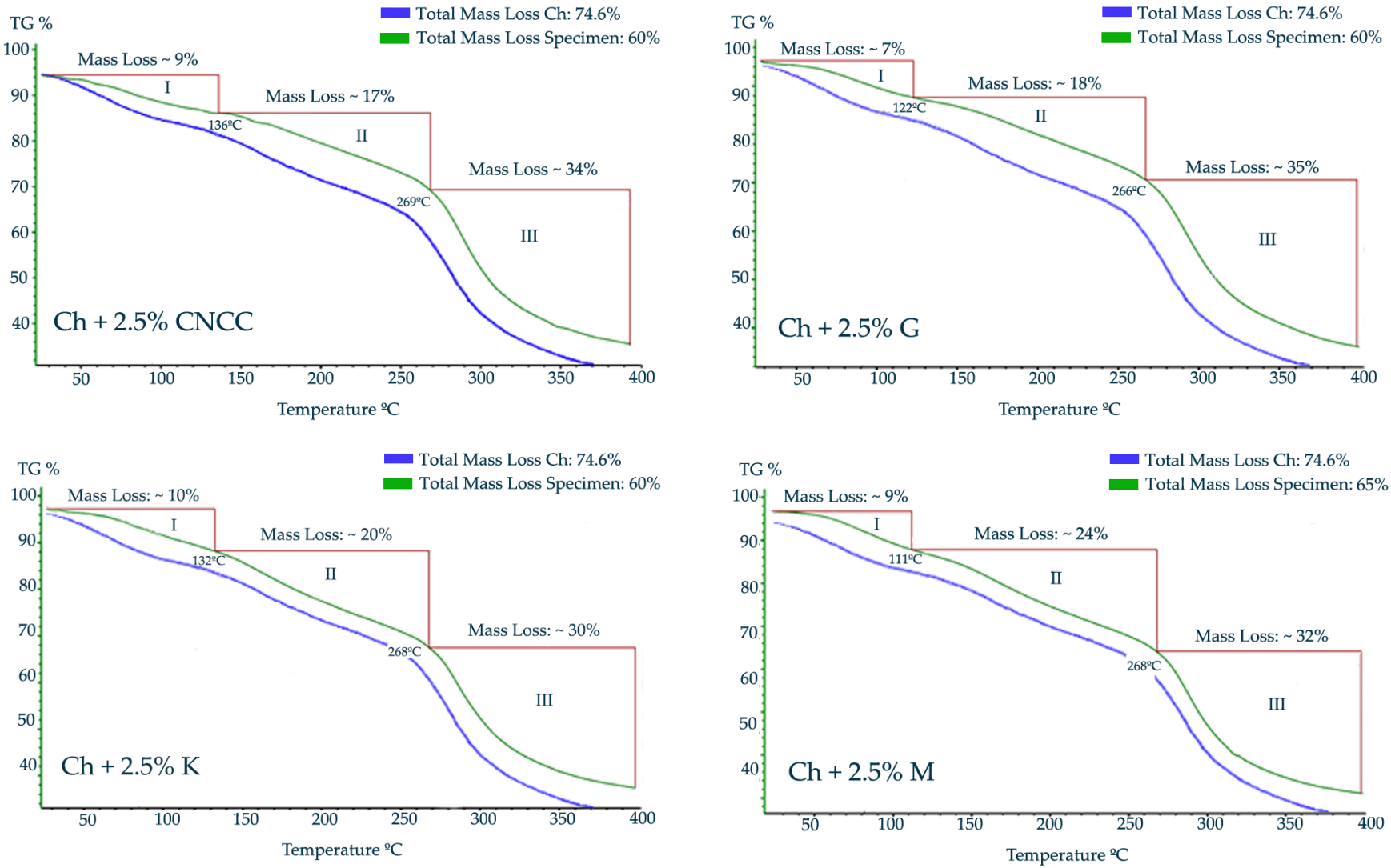

Figure 5.6 — TGA curves for Ch film and Ch bionanocomposites with 2.5 % CNCs concentration. *Chitosan (Ch); Commercial Nanocellulose (CNCC); Giant Reed Nanocellulose (G); Kenaf Nanocellulose (K); Miscanthus Nanocellulose (M).*

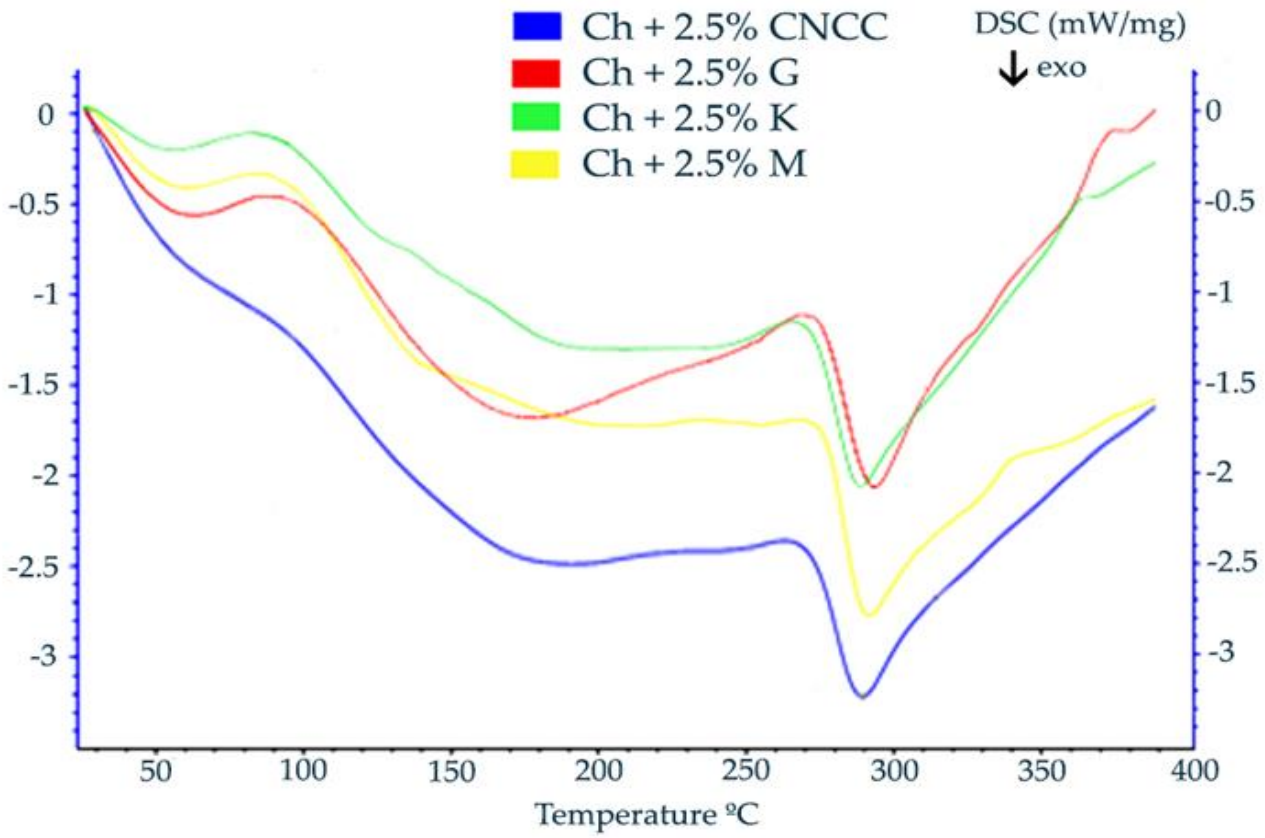

Figure 5.7 — DSC thermograms for Ch bionanocomposites with 2.5 % CNCs concentration. *Chitosan (Ch); Commercial Nanocellulose (CNCC); Giant Reed Nanocellulose (G); Kenaf Nanocellulose (K); Miscanthus Nanocellulose (M).*

Table 5.5 — Major thermal degradation temperature of bionanocomposites.

Sample	**T_{10} (ºC)**	**T_{50} (ºC)**	**T_{max} (ºC)**
Ch + 2.5 % CNCC	155	334	289
Ch + 2.5 % G	161	337	291
Ch + 2.5 % K	142	313	290
Ch + 2.5 % M	122	301	290

** Chitosan (Ch); Commercial Nanocellulose (CNCC); Giant Reed Nanocellulose (G); Kenaf Nanocellulose (K); Miscanthus Nanocellulose (M).*

5.1.7 Chemical Analysis - FT-IR

The chemical analysis to evaluate the structural relation established between chitosan and nanocellulose was performed with FT-IR in ATR mode. This technique is widely used to

identify the materials´ chemical composition as well as the intermolecular bonds. Among the range of applications of this analytical method, the ability to study the interactions between the different components present in composite materials stands out. Figure 5.8 displays the different spectra obtained for the Ch film and for the Ch bionanocomposites reinforced with 2.5 % CNCs.

The bionanocomposites spectra showed to be remarkably similar to the one presented by the Ch control film, with only minor modifications. Since the chemical composition of cellulose and chitosan is practically identical and the CNCs amount introduced was small, the obtained result was expected. Moreover, it could be an indicator that the particles attached well with the polymer matrix attributed to strong interactions via hydrogen bonds between the functional groups of the composite components. The FTIR spectra showed that there were two leading absorptions regions in spectra, a low-wavelength section from 600 to 1700 cm^{-1} and a high-wavelength zone from 2800 to 3500 cm^{-1}. The chitosan characteristic absorption bands were identified in all spectra: at 3355 cm^{-1} (O-H stretching vibration); 3275 cm^{-1} (-NH asymmetric stretching); 2921-2885 cm^{-1} (C-H of the methyl group -$NHCOCH_3$ symmetric and asymmetric vibrations); 1631 cm^{-1} (C=O stretching (Amide I)); 1547 cm^{-1} (N-H bending (Amide II)); 1377-1407 cm^{-1} (-CH_2 bending); 1319 cm^{-1} (skeletal vibration involving the stretching of the C-N bond (Amide III)). The last bands correspond to saccharide structure: 1251 cm^{-1} (C-N stretching), 1150 cm^{-1} (asymmetric stretching of the C–O–C bridges), and 926-1033 cm^{-1} (C-O stretching at C-3 position) (Costa et al., 2021; Khan et al., 2012; Xu et al., 2018). In the bionanocomposites spectrum, the differences for the control were practically non-existent, however, it appears that the peak at 1377 cm^{-1} disappears, and two very subtle peaks appeared at the wavelengths of 1220 cm^{-1} and 1360 cm^{-1}. Following the observations of Morais et al., (2013) these peaks could be related to the presence of sulfonates present in the nanocellulose, generated during the hydrolysis step. Messa & Faez, (2020) also identified the appearance of a new band at 1202 cm^{-1} and related that peak with the S=O stretching vibrations, due to the sulfate groups on nanocellulose as a consequence of sulfuric acid hydrolysis.

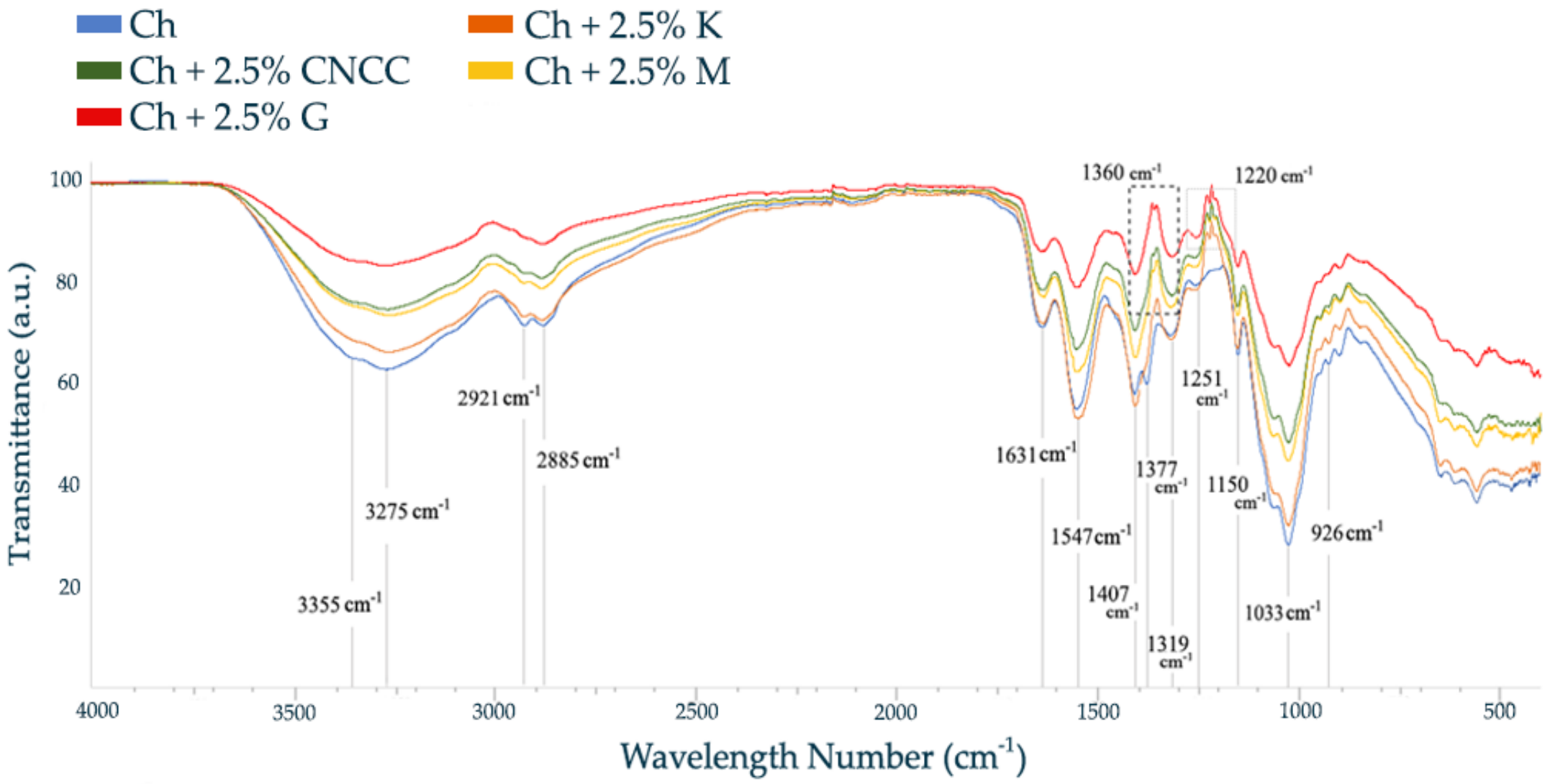

Figure 5.8 — FT-IR spectra of Ch film and for Ch bionanocomposites with 2.5% CNCs concentration. *Chitosan (Ch); Commercial Nanocellulose (CNCC); Giant Reed Nanocellulose (G); Kenaf Nanocellulose (K); Miscanthus Nanocellulose (M).*

5.1.8 Cristallinity Analysis

The application of the X-ray diffraction technique aims to examine the level of nanoparticles exfoliation between the polymer chains of chitosan. The improvement of the mechanical, barrier, and thermal properties are narrowly connected to the degree of exfoliation, such a fundamental determination (Yadav et al., 2020).

The pristine Ch sample and the films reinforced with 2.5 % CNCs diffractograms are presented in figure 5.9. The Ch control film presented two characteristic diffraction peaks at 2 Θ = 11.4°, 18.0°, and a shallow peak between 20º-22.5º. The first peak corresponds to a crystalline structure and the last one to the amorphous structure associated with the semi-crystalline chitosan nature. Accessing the literature, it is possible to identify that chitosan powder has a characteristic broad peak close to 2Θ = 20º, related to the amorphous state The lowering of this peak in the Ch film may be a sign that the original crystalline form of Ch was destroyed after mixing it with acetic acid (Mao et al., 2019; Patel et al., 2021; Wardhono et al., 2019).

Although the peaks continue to be visible, with the CNCs introduction in the polymer matrix, a decrease in the Ch characteristic peaks was observed. A slight increase in peak intensity was also observed at 2Θ = 22.5°, mainly for the film with 2.5 % commercial CNCs, indicating the successful blending of CNCs and Ch. This peak is directly related to the crystallographic plane (200) present in crystalline cellulose I. The fact that it is possible to observe peaks referring to the two compounds that form the bionanocomposite is an indication of some preservation of the crystal structure of both. However, the gradual decrease mainly in the crystalline peak at 2Θ = 11.4° in 2.5 % CNCs embedded films may assume that the nanoparticles slightly restricted the film crystallinity.

The incorporation of fillers modified the chitosan crystalline composition resulting in bionanocomposites with a higher crystalline index than the control sample film. The highest crystallinity index was registered by the film with 2.5 % CNCC, with 31.7 %, and the lowest by the Ch control sample with 20.6 %, as expected. Between the CNCs samples was not verified significant differences in this index with values being around 23-25 %.

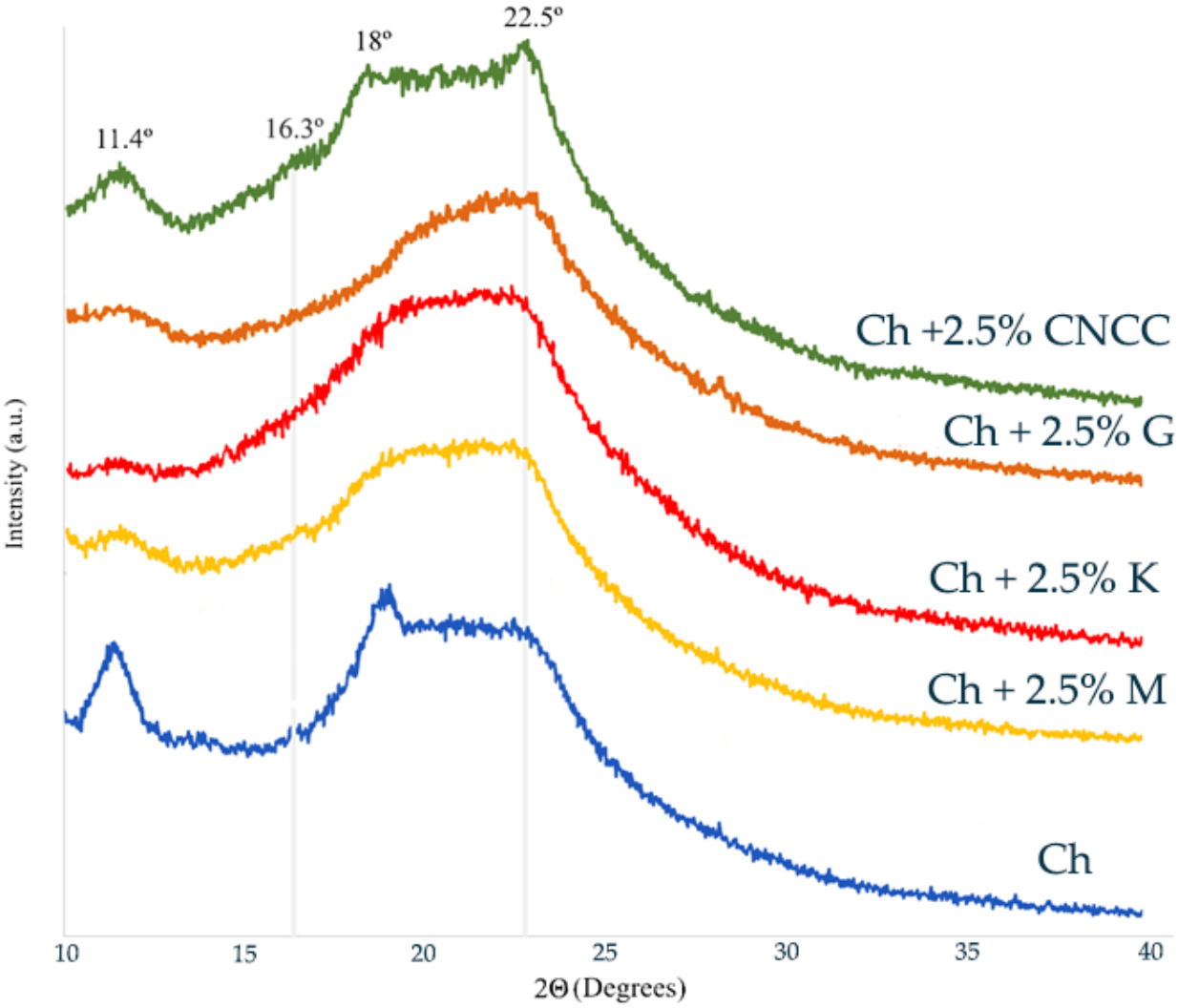

Figure 5.9 — XRD patterns of Ch film and for Ch bionanocomposites with 2.5% CNCs concentration. *Chitosan (Ch); Commercial Nanocellulose (CNCC); Giant Reed Nanocellulose (G); Kenaf Nanocellulose (K); Miscanthus Nanocellulose (M).*

5.2 Chapter Conclusions

The purpose of this chapter was to produce and characterize chitosan bionanocomposites reinforced with the different nanocelluloses extracted in chapter 4. The nanocelluloses were introduced in three different concentrations (1.5, 2 and 2.5 %), and the bionanocomposites properties were evaluated.

The Ch/CNCs bionanocomposites were successfully produced, and it was observed that the introduction of nanofillers was effective in mechanically reinforcing the chitosan films,

increasing strength and stiffness values, and decreasing ductility (p<0.05). For this parameter, the amount of CNCs that generated better results was 2.5 %. The sample with giant reed CNCs showed the best reinforcement values, comparable to commercial CNCs at 2 %. Regarding the optical properties, it was verified that the produced bionanocomposites presented a high degree of transparency and a slightly yellowish color. The introduction of nanoparticles in different amounts was not enough to significantly change the original color, opacity, and saturation of the chitosan film (p>0.05). However, the introduction of 2.5 % CNCs played a crucial role in increasing the ultraviolet light barrier. Introducing nanofillers to the polymeric matrix had a direct effect on the sample's wettability properties, decreasing the swelling capacity and solubility, and increasing the contact angle, consequently transforming the bionanocomposites more hydrophobic. Barrier properties followed a similar trend, with the introduction of CNCs being shown to be beneficial in decreasing oxygen and water vapor permeability. Once again it was observed that for the maximum values of CNCs introduced, 2.5 %, the permeability registered the lowest values. In addition to the mechanical and barrier properties, the thermal properties of bionanocomposites with 2.5 % CNCs were also evaluated. There was a lower percentage of mass loss for the bionanocomposites than for the unreinforced control sample, thus showing the positive effect that the nanoparticles had on the thermal stability of the film. The suitable interaction between the chitosan biopolymer matrix and the nanocellulose mechanical reinforcement was demonstrated by crystallinity and chemical composition analyses. The increase in the bionanocomposite crystallinity due to the introduction of nanoreinforcements was essential to improve its properties.

In general, it can be concluded that it was possible to improve the mechanical, barrier, and thermal properties of a chitosan film by introducing nanocrystalline cellulose extracted from lignocellulosic biomass. In this work, the CNCs obtained from giant reed fibers showed the best potential for applicability and were the ones that presented more similarity to the commercial CNCs already in the market. Additionally, the incorporation of 2.5 % CNCs in the film formulation presented the best results, as such it was chosen as the most indicated to be applied in chapter 6.

6

RESULTS AND DISCUSSION CHITOSAN/NANOCELLULOSE BIONANOCOMPOSITE LOADED WITH SALVIA ESSENTIAL OIL AS ACTIVE PACKAGING

This chapter corresponds to stage 3 of the doctoral thesis and aimed to assess the capacity of the bionanocomposites produced in the previous stage, with the best percentage of nanocellulose (2.5 %), to protect and extend the shelf life of perishable food. Consequently, this work aimed to understand the future viability of bionanocomposites to be introduced as an active layer of food packaging.

In addition to the bionanocomposites established in the previous chapter, novel formulations were evaluated, introducing sage essential oil before being reinforced with nanocellulose. This complement aimed to increase the active properties of bionanocomposites as well as to study the ability of nanocellulose to interact with the essential oil.

To conduct this study, samples of fresh poultry meat were wrapped in different bionanocomposite formulations, and their physical-chemical properties and microbiological growth were evaluated at different times during refrigerated storage. Additionally, an "*in vitro*" study were performed to evaluate the migration of phenolic compounds from bionanocomposites to the simulate medias and their respective antioxidant activity.

6.1 "*In Situ*" Meat Characterization

6.1.1 Microbiological Growth

The antimicrobial activity represents an essential property to be evaluated during the development of novel active packaging applications, especially for perishable foods. Fresh meat constitutes a wealthy source of nutrients (like sugars, amino acids, and vitamins), having a pH close to five and high levels of water activity, essential characteristics for microbiological

development, thus, distinguishing itself as an ideal substrate for the rapid proliferation of numerous types of microorganisms. Individually, poultry meat is considered a highly perishable food product, known to have elevated initial rates of microbiological contamination, deteriorating above tolerable levels after four days post-slaughter under typical refrigerated storage conditions (Pelissari et al., 2017; Samapundo et al., 2019).

In this work, based on the microorganism's survivability at different temperatures, the microbiological growth assessment over storage time was established by the total mesophilic aerobic microorganisms (TMAM) quantification, bearable to temperature ranges 10ºC – 40ºC. Moreover, since the poultry meat was stored under refrigeration, the total psychrotrophic aerobic microorganism (TPAM), that can grow at temperature ranges of 2ºC – 7ºC, was also evaluated. Complementary, the analysis of *Enterobacteriaceae* was equally performed. The quantification of this group of Gram-negative bacteria is a valuable indicator of food quality and safety, since among this vast family many are dangerous pathogens for human health, like *Salmonella*, *Shigella*, or *Escherichia coli* (Halkman and Halkman, 2014).

At the end of the experiment, it was observed that all treatments suffered an inevitable deterioration process, registered by the significant increase ($p < 0.05$) of microbial colonies in the three individual indicators (Table 6.1). As expected, the unwrapped meat reported the highest and fastest microbial contamination, recording on the first evaluation date a count of 2.11 ± 0.21 log CFU/g for TMAM and 2.31 ± 0.49 log CFU/g for TPAM. These numbers increased steadily until the last day to 9.81 ± 0.37 log CFU/g and 9.58 ± 0.01 log CFU/g, respectively. Regarding *Enterobacteriaceae*, the same sample recorded an initial value of 2.26 ± 0.12 log CFU/g and 9.41 ± 0.32 log CFU/g on the twelfth day. These values were slightly lower when compared with the other two parameters, which was expected since this indicator focuses on a more restricted group of bacteria.

Compared to the control, all packaged samples showed significantly lower contamination levels ($p < 0.05$), approximately 2 log CFU/g less for TMAM and TPAM, and 2-3 log CFU/g for *Enterobacteriaceae*, confirming that the produced bionanocomposites hold an antimicrobial activity capable of delaying microbial propagation. These positive results should be mainly attributed to the recognized Ch antimicrobial property. The responsible mechanism behind this intrinsic activity, most commonly accepted by the scientific community, is ascribed to the electrostatic interactions between the positively charged amine groups of the polymer and the negatively charged microorganism cell surface, resulting in cell death by permeabilization and emptying of intracellular material from the cytoplasm into the extracellular space (Souza et al., 2019c). High-molecular weight chitosan, like the one used in this work, generally has difficulty penetrating the cell membrane, so its antimicrobial effect may also be related to selective metal chelation, inhibiting various metabolic enzymes of microbial cells by blocking

their active centers, or forming an impermeable layer on microbial surface, blocking the entry of nutrients into the cell (Kumar et al., 2020).

Regarding the samples wrapped in reinforced chitosan films, it was observed that the introduction of commercial CNCs resulted in less contamination in the first six days compared to the Ch pure film, even so, this difference was not found to be significant ($p > 0.05$). However, CNCs reinforced bionanocomposites extracted from lignocellulosic cultures proved to be more effective, as they significantly delayed ($p < 0.05$) the contamination of mesophilic and psychrotrophic microorganisms in the first three days. From then until day nine, the results continued to be better than those of the protected control sample, although significant differences were no longer detected ($p > 0.05$). The decrease in microbiological contamination rates is due, to a certain extent, to the increase in the film's oxygen barrier enhanced by the incorporation of nanocellulose, as observed in our previous work (Pires et al., 2022b). The oxygen barrier is essential in food packaging, as the existence of this gas favors the growth of aerobic microorganisms, contributing to spoiling fresh products and consequent loss of their nutritional qualities (Ahankari et al., 2021). Reinforcements like CNCs have the ability to form hydrogen bonds with other biopolymers, forming a compact network with smaller pore sizes. Thus, the oxygen molecules are forced to cross a longer diffusion path, making it more difficult for them to reach the surface of the meat (Pires et al., 2021). The results also indicated that the incorporated reinforcement agents did not provide a noticeable expression in the antimicrobial property of the bionanocomposite as expected, which may be correlated to the fact that cellulose by itself and without any functionalization does not hold intrinsic antimicrobial mechanisms that allow it to grant broader activity (Norrrahim et al., 2021). As demonstrated in Jannatyha et al., (2020) work, CMC films reinforced with different concentrations of nanocellulose (0.1, 0.5, and 1 %) did not show any inhibition zone against *P. aeruginosa*, *S. enteritidis*, *E. coli*, *B. cereus*, *S. aureus*. On the contrary, the same study proved that the combination of CMC with nanochitosan showed inhibitory action against all strains. In addition to the null antimicrobial activity of cellulose, these results may also indicate there was an adequate interaction between the fillers and chitosan, in which the number of free amino groups to react with the cell membrane of the microorganism decreased (Souza et al., 2020a). This idea is supported by the outcomes presented in our previous work (Pires et al., 2022b), in which the physical properties of bionanocomposites were evaluated. Through XRD patterns it was possible to determine that the introduction of commercial CNCs and lignocellulosic biomass CNCs resulted in successfully exfoliated bionanocomposites.

It is possible to find studies demonstrating that the direct application of sage, either in essential oil or in extract, caused an antimicrobial effect on meat, therefore indicating the feasibility of using it as a natural additive to replace synthetic preservatives. This activity could

be explained by the fact that sage represents a valuable source of phenolic acids, monoterpenes, and diterpenes (Branislav et al., 2018; Cegielka et al., 2019; Pateiro et al., 2021). Currently, only the work of Ehsani et al., (2020) applied chitosan/sage essential oil films in a food matrix (fish burgers), verifying that the addition of SEO significantly improved the film's antimicrobial activity. In contradiction, in our work was found that the incorporation of SEO in the Ch films (at a concentration of 1 % v/v FFD) did not improve significant differences ($p > 0.05$) in the antimicrobial activity, thus assuming that the delay of microbiological contamination in the packed samples is mainly attributed to the intrinsic antimicrobial property of chitosan combined with its high oxygen barrier property. For the same percentage of oil added to the films, similar results were obtained for different essential oils, like rosemary, ginger (Pires et al., 2018), thyme, and basil (Bonilla et al., 2014). As reported in the work of Sánchez-González et al., (2011) the growth of pathogens can be influenced by the type of polymer matrix where the essential oil is distributed. One hypothesis is that chitosan could have been bonded with phenolic compounds or other active substances, like terpenes, present in the essential oil and thus limiting not only the release of these molecules to the meat but also decrease the free chitosan amino groups that would react with the cell membrane (Matei et al., 2020; Qin and Li, 2020). In a similar study, Sedlaříková et al., (2017) combined two essential oils, oregano, and marjoram, with chitosan-based solutions. Through SEM images the authors found that the combination of chitosan/marjoram resulted in a much more compact structure than that of chitosan/oregano, which resulted in limited antimicrobial activity against the microorganisms assessed. The authors attributed the more compact structure to the better compatibility between chitosan and the hydrophilic compound terpinene-4-ol (present in marjoram) while the major component identified in oregano essential oil was a more hydrophobic compound, carvacrol, thus forming a less compact structure.

Following the guidelines of the European Commission (EC) expressed in document Commission Regulation (EC) No 2073/2005 of 15 November 2005 on microbiological criteria for foodstuffs (EU, 2005), foods must not contain microorganisms or their toxins or metabolites in amounts that pose an unacceptable risk to human health, in which the count of aerobic colonies in uncooked minced meat must not exceed 6.70 log CFU/g of meat. Additionally, when this value of microbiological contamination is exceeded, it is possible to notice unpleasant odors derived from biogenic amines, like putrescine and cadaverine, which will irreversibly change the flavor of the meat (Marmion et al., 2021). Observing the results, it is possible to verify that this limit was exceeded by the unwrapped meat on day three. Comparatively, the same limit was surpassed for almost all wrapped treatments on day nine, being possible to verify that packing the meat with the novel bio-based films allowed the poultry meat microbiological conservation period to be extended by at least six extra days. Moreover, within the

protected specimens, those that were packed in Ch films reinforced with CNCs demonstrated a slower microbiological growth, without significant differences ($p > 0.05$) observed regarding the other samples.

Table 6.1 — Fresh poultry meat microbiological evaluation over the storage time.

Parameters	Storage Days	Samples										
		Unwrapped	**Ch**	**Ch+CNCC**	**Ch+G**	**Ch+K**	**Ch+M**	**Ch+SEO**	**Ch+CNCC+SEO**	**Ch+G+SEO**	**Ch+K+SEO**	**Ch+M+SEO**
TMAM (Log CFU/g meat)	**0**	2.11±0.21^{cA}	2.11±0.21^{cA}	2.11±0.21^{dA}	2.11±0.21^{dA}	2.11±0.21^{dA}	2.11±0.21^{dA}	2.11±0.21^{cA}	2.11±0.21^{cA}	2.11±0.21^{dA}	2.11±0.21^{cA}	2.11±0.21^{cA}
	3	7.26±0.08^{bA}	5.35±0.33^{bB}	4.28±0.21^{cBC}	3.53±0.33^{cC}	3.70±0.20^{cC}	3.88±0.13^{cC}	5.93±0.62^{bAB}	4.88±0.28^{bBC}	3.85±0.20^{cC}	4.00±0.49^{bC}	4.34±0.33^{bBC}
	6	8.91±0.11^{aA}	6.26±0.32^{bB}	5.47±0.25^{bB}	5.11±0.11^{bB}	5.30±0.17^{bB}	5.51±0.36^{bB}	5.97±0.10^{bB}	6.50±0.17^{aB}	5.51±0.15^{bB}	5.90±0.76^{aB}	5.16±0.39^{bB}
	9	9.74±0.36^{aA}	7.02±0.06^{aB}	7.06±0.26^{aB}	6.34±0.34^{aB}	6.43±0.36^{aB}	6.88±0.28^{aB}	7.30±0.18^{aB}	6.98±0.73^{aB}	6.61±0.25^{abB}	6.57±0.29^{aB}	6.70±0.13^{aB}
	12	9.81±0.37^{aA}	7.11±0.11^{aB}	7.70±0.34^{aB}	7.04±0.26^{aB}	7.10±0.21^{aB}	7.02±0.15^{aB}	7.52±0.29^{aB}	7.66±0.42^{aB}	7.23±0.18^{aB}	6.92±0.31^{aB}	6.88±0.17^{aB}
TPAM (Log CFU/g meat)	**0**	2.31±0.49^{cA}	2.31±0.49^{cA}	2.31±0.49^{dA}	2.31±0.49^{dA}	2.31±0.49^{dA}	2.31±0.49^{dA}	2.31±0.49^{cA}	2.31±0.49^{cA}	2.31±0.49^{dA}	2.31±0.49^{dA}	2.31±0.49^{dA}
	3	7.29±0.06^{bA}	5.53±0.26^{bB}	3.74±0.34^{cC}	3.61±0.20^{cC}	3.35±0.17^{cC}	3.70±0.49^{cC}	5.97±0.55^{bAB}	4.35±0.41^{bBC}	3.01±0.04^{cC}	3.04±0.56^{cC}	3.64±0.46^{cC}
	6	9.16±0.19^{aA}	6.51±0.39^{abB}	5.44±0.05^{bB}	5.43±0.04^{bB}	5.66±0.11^{bB}	5.34±0.20^{bB}	6.09±0.50^{bB}	6.91±0.53^{aB}	5.91±0.21^{bB}	5.97±0.60^{bB}	5.56±0.21^{bB}
	9	9.24±0.47^{aA}	6.81±0.40^{aB}	6.75±0.70^{aB}	6.26±0.25^{abB}	6.17±0.10^{baB}	6.30±0.11^{abB}	7.39±0.03^{aB}	7.62±0.43^{aB}	6.63±0.05^{aB}	6.43±0.08^{aB}	6.48±0.11^{aB}
	12	9.58±0.01^{aA}	7.23±0.18^{aB}	6.97±0.29^{aB}	7.47±0.37^{aB}	7.53±0.51^{aB}	7.28±0.46^{aB}	7.81±0.41^{aB}	7.70±0.59^{aB}	6.73±0.10^{aB}	6.80±0.21^{aB}	6.73±0.10^{aB}
***Enterobac-teriaceae* (Log CFU/g meat)**	**0**	2.26±0.12^{dA}	2.26±0.12^{bA}	2.26±0.12^{cA}	2.26±0.12^{cA}	2.26±0.12^{cA}	2.26±0.12^{cA}	2.26±0.12^{cA}	2.26±0.12^{cA}	2.26±0.12^{cA}	2.26±0.12^{cA}	2.26±0.12^{cA}
	3	6.06±0.17^{cA}	3.45±0.71^{bB}	2.52±0.21^{cB}	2.64±0.08^{cB}	2.74±0.10^{cB}	2.58±0.17^{cB}	3.11±0.21^{cB}	3.14±0.12^{bcB}	2.36±0.12^{cB}	2.58±0.55^{cB}	2.88±0.10^{bcB}
	6	7.00±0.06^{bA}	5.49±0.09^{aB}	4.14±0.43^{bBC}	3.61±0.33^{bC}	3.35±0.25^{bC}	3.53±0.18^{bC}	5.11±0.21^{bB}	4.36±0.08^{bBC}	3.65±0.03^{bC}	3.65±0.44^{bC}	3.27±0.10^{bC}
	9	8.89±0.13^{aA}	5.71±0.21^{aC}	6.17±0.37^{aBC}	5.56±0.49^{aC}	5.97±0.20^{aC}	5.51±0.06^{aC}	5.56±0.10^{abC}	6.48±0.14^{aB}	5.86±0.17^{aC}	5.87±0.03^{aC}	5.67±0.06^{aC}
	12	9.41±0.32^{aA}	6.11±0.21^{aB}	6.92±0.24^{aB}	6.46±0.32^{aB}	6.53±0.04^{aB}	6.16±0.26^{aB}	6.30±0.49^{aB}	7.18±0.47^{aB}	6.13±0.04^{aB}	6.29±0.15^{aB}	6.11±0.06^{aB}

** Total Mesophilic Aerobic Microorganisms (TMAM); Total Psychrotrophic Aerobic Microorganisms (TPAM); Chitosan (Ch); Commercial Nanocellulose (CNCC); Giant Reed Nanocellulose (G); Kenaf Nanocellulose (K); Miscanthus Nanocellulose (M); Sage Essential Oil (SEO). a-e: Different letters indicate significant differences between lines ($p < 0.05$). A-D: Different letters indicate significant differences between columns ($p < 0.05$).*

6.1.2 Physicochemical Characterization

6.1.2.1 Meat Color

The visual perception of the fresh meat product is the first evaluation parameter available to the consumer at the purchase time. Therefore, color plays a significant role in the acceptance of the meat to be purchased, with the bright red/pink tone arousing more desire in the consumer by being associated with a higher level of freshness. This property is dependent on factors like the chemical form and myoglobin concentration, the morphology of the muscle structure, and its ability to absorb or scatter incident light (Robertson, 2013).

Fresh poultry meat presented an initial hue angle of $45^{o} \pm 1^{o}$ (Table 6.2), which is in the red range. For the unwrapped sample, the hue was maintained ($p > 0.05$) during the first six days. From that day until the end, the meat showed a significant change in its tonality ($p < 0.05$), increasing to $56^{o} \pm 2^{o}$, meaning that as time passes and deterioration increases, the unwrapped meat color tends to approach a yellowish hue (Figure 6.1). During meat storage, atmospheric oxygen diffuses into the meat, which is initially beneficial as the O_2 favors the formation of oxymyoglobin (the reduced pigment state of myoglobin (Fe^{2+}) in which O_2 occupies the ligand position), responsible for the bright red color. However, after a few days of exposure to oxygen, oxidation processes occur, modifying this chemical form to metmyoglobin (the oxidized pigment state of myoglobin (Fe^{3+})), giving rise to discolored and undesirable meat, darker and more brownish (Cardoso et al., 2016; Singh et al., 2011).

Regarding the luminosity parameter, the unpackaged meat became darker ($p < 0.05$) right after day three, a value that remained equal until day nine. From that day until the end of the experiment, the L* value increased significantly ($p < 0.05$) due to the protein denaturation of the meat, leading to a reduction in the water holding capacity. The extent of light scattering, influenced by the muscle structural attributes, is directly proportional to the degree of protein denaturation. As the storage time proceed, structural changes occur in the muscle, like proteins denaturation or aggregation, myofibrillar or fiber shrinkage, and osmolarity of the sarcoplasm extracellular space. These changes lead to an increase in the drip, which will influence the amount of light reflected from the meat surface. It is possible to observe in Figure 6.1 some of this drip accumulated on the meat´s surface. Accordingly, the refractive index of the medium (sarcoplasm and extracellular space) will modify and an increase in lightness is perceived (Hughes et al., 2014; Mir et al., 2017).

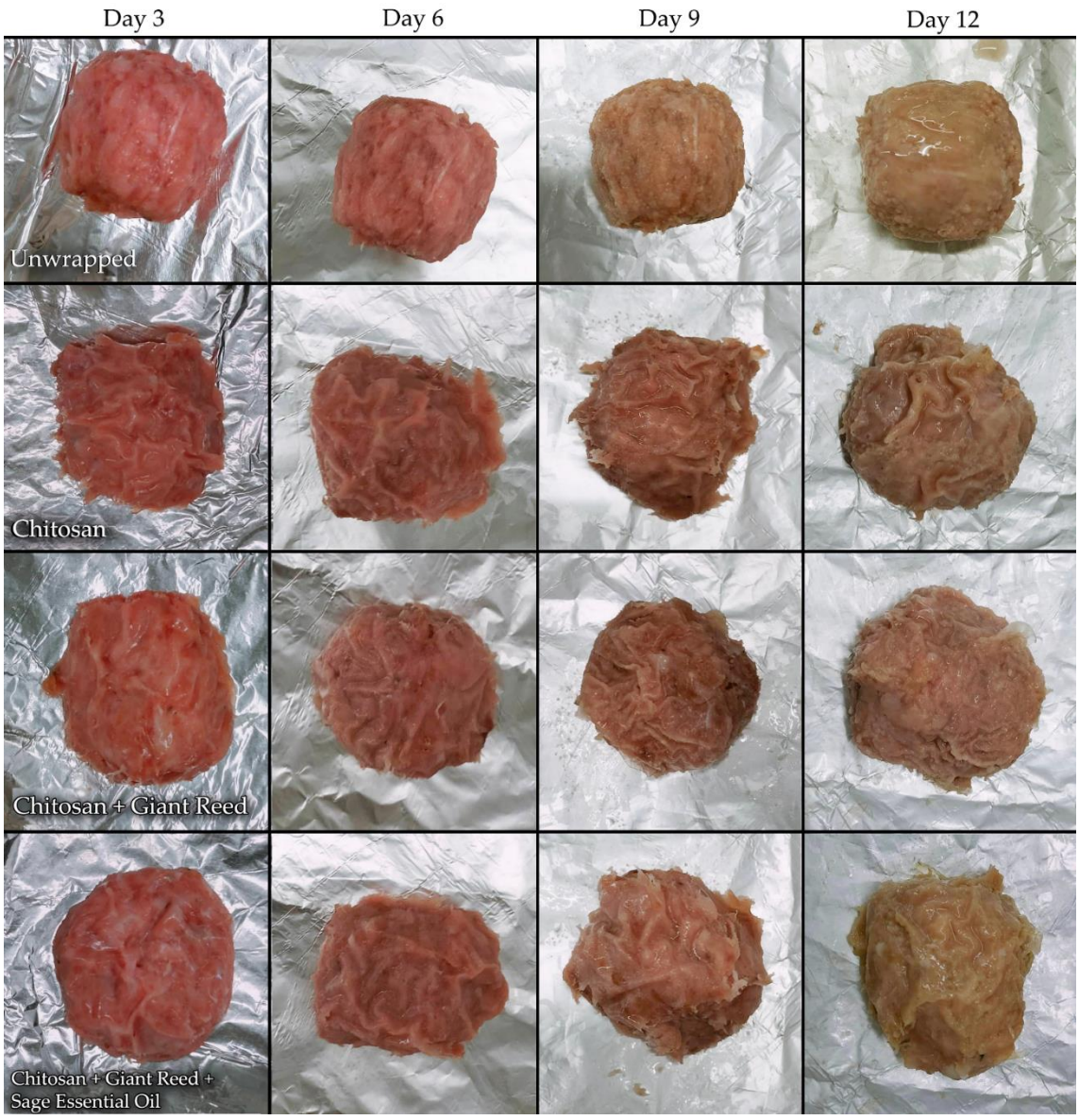

Figure 6.1 — Meat color over the analyzed assay times for the samples with the most significant differences.

The sample wrapped with the Ch film maintained the hue angle intact for nine days ($p > 0.05$), more three than the unwrapped one. The consistent behavior was also observed for bionanocomposites incorporated with nanocellulosic reinforcements, however on the last assessment day, hue angle values were slightly lower ($p > 0.05$) than those presented by the control trials, being even significantly different ($p < 0.05$) for the sample wrapped in the Ch+CNCC, consequently suggesting that a more efficient color protection has occurred. The biomass source of the incorporated CNCs did not affect the outcomes for this parameter ($p >$

0.05). The mechanism responsible for the preservation of meat color by chitosan has not yet been fully identified, nevertheless, it was prospective that the chitosan would help to maintain the meat color for a long time as this biopolymer demonstrates the intrinsic chelating ability to scavenge the iron (Fe^{3+}) present in the meat, contributing to retard the oxidative process catalyzed by this metal. As exposed in the early work of (Knorr, 1991), chitosan absorbed Fe^{3+} at a rate of 17.6 mg per gram in 30 min. The fact that bionanocomposites displayed more satisfactory results in meat color retention than Ch films without reinforcement may be related to the increase in the oxygen barrier with the incorporation of nanocellulose, as demonstrated in our previous work, thus reducing the oxygen exchange between the outside and inside of the package, limiting the gas interactions with iron presented in myoglobin (Pires et al., 2022b).

Regarding the L* parameter, all packaged samples showed a significant reduction ($p > 0.05$) in the first three days, as was observed for the unpacked specimen. Contrary to the control, for treatments without SEO, this variable remained unchanged until the end. This result may indicate that the meat did not undergo such severe degradation processes, maintaining its water retention capacity, or that the water released by meat over time has been absorbed by the bionanocomposite, not being able to interfere with the luminosity parameter.

The incorporation of sage essential oil directly influenced on the meat's hue angle as shown by the data and exposed in figure 6.1. In the beginning, the values increased significantly ($p < 0.05$) in opposition to the other samples, which may indicate that some oil (which present a yellowish color) has migrated from the film surface to the meat, affecting the color perception. In the work of Ünal et al., (2014), minced beef samples were homogenized with different essential oils at 2 % (w/w), including sage, and the hue angle was evaluated. The authors observed that, among the evaluated oils, sage and oregano were the ones that most altered the meat tonality. A similar effect was also monitored in our previous work with ginger essential oil (Souza et al., 2018a). Although the results were not significant ($p > 0.05$), the chitosan bionanocomposites in which reinforcement particles were added after SEO proved to be more effective in maintaining the hue angle in the first six days, which may indicate an encapsulating effect on the essential oil. From that day on, bionanocomposites, due to their hydrophilic character, began degrading, going from a film to a gel, thus releasing the essential oil into the meat surface, which significantly increased the final values of the hue angle. The bionanocomposite deterioration phenomenon also affected the L* parameter, with a significant increase ($p < 0.05$) in meat lightness observed on the last evaluation day.

To conclude, the developed bionanocomposites demonstrated potential as preservative agents for poultry meat color, improving the visual qualities of this type of fresh food over longer shelf life. However, the incorporation of essential oils in bionanocomposites can directly interfere with the color of the food if this substance is not properly encapsulated within the biopolymer matrix, thus migrating to the surface of the meat.

6.1.2.2 Moisture

Moisture represents a crucial feature of the meat's sensory aspects, influencing quality attributes like tenderness, juiciness, and processing. In addition, it is significant in meat's shelf life since higher moisture values increase the probability of microbial growth. This parameter is equally relevant from an economic point of view since water contributes to the meat weight, therefore, influencing the product price. Moisture content depends on livestock species, typically ranging from 41 % to 76 %. In addition, the water-holding capacity is different for each species, with poultry meat possessing one of the lowest retaining rates (Dave and Ghaly, 2011; Warner, 2017).

At the beginning of the experiment, the moisture content of the meat was settled at 74.7 ± 0.3 % (Table 6.2). The unpacked meat showed a gentle increment ($p > 0.05$) in water content over the storage time, recording an increase of 4 % on the twelfth day. Contrarily, all the packed samples evidenced a prompt decrease in moisture on the third evaluation day without significant changes ($p > 0.05$) until the end of the experiment. The fact that there was no variability in the moisture between this period can be explained by the barrier created by the bionanocomposites, hindering the transport of water vapor between the meat and the environment, preventing moisture gain or loss (Souza et al., 2022). On average, there was a considerable reduction ($p < 0.05$) of this variable, between 4-10 %, with any significant differences ($p > 0.05$) stated among specimens. These results may be explained by the chitosan film hydrophilic character that has absorbed water from the meat surface, as previously noticed in other works with chitosan bionanocomposites packaging fresh poultry (Pires et al., 2018; Souza et al., 2020). The results recorded in this parameter agree with the data obtained in the microbiological evaluation, as the samples packaged with lower moisture levels over time were able to preserve the microbial contamination for a longer period.

Table 6.2 — Meat's color and moisture parameters over the storage time.

Parameters	Storage Days	Samples										
		Unwrapped	Ch	Ch+CNCC	Ch+G	Ch+K	Ch+M	Ch+SEO	Ch+CNCC+SEO	Ch+G+SEO	Ch+K+SEO	Ch+M+SEO
Hue angle (Degrees)	0	45±1^{cA}	45±1^{bA}	45±1^{bA}	45±1^{cA}	45±1^{cA}	45±1^{bA}	45±1^{cA}	45±1^{cA}	45±1^{cA}	45±1^{cA}	45±1^{cA}
	3	43±2^{cB}	48±2^{bAB}	50±3^{aAB}	49±1^{bAB}	48±1^{bAB}	46±1^{bAB}	52±0^{bA}	44±1^{cB}	50±1^{bAB}	49±2^{bAB}	48±2^{bAB}
	6	45±0^{cB}	46±2^{bAB}	46±0^{bAB}	48±1^{bAB}	48±2^{bAB}	47±2^{bAB}	52±1^{bA}	49±3^{bAB}	51±2^{bA}	49±2^{bAB}	49±1^{bAB}
	9	50±1^{bAB}	48±1^{bAB}	45±0^{bC}	47±0^{bB}	46±0^{bB}	45±1^{bBC}	50±0^{bAB}	52±1^{bAB}	53±2^{bA}	51±1^{bAB}	49±1^{bAB}
	12	56±2^{aB}	55±1^{aB}	50±1^{aC}	53±1^{aBC}	51±2^{aBC}	52±2^{aBC}	56±2^{aB}	68±3^{aA}	69±4^{aA}	66±7^{aAB}	71±1^{aA}
Lightness (L*)	0	54±1^{aA}	54±1^{aA}	54±1^{aA}	54±1^{aA}	54±1^{aA}	54±1^{aA}	54±1^{aA}	54±1^{aA}	54±1^{aA}	54±1^{aA}	54±1^{aA}
	3	47±1^{bB}	45±1b^{BC}	47±0^{bB}	46±1^{bB}	47±0^{bB}	47±1^{bB}	45±0^{cC}	47±0^{bB}	50±0^{bA}	50±1^{bA}	49±1^{bAB}
	6	46±0^{bB}	44±0^{bC}	47±0^{bB}	46±1^{bB}	46±1^{bB}	47±1^{bB}	46±0^{bB}	49±1^{bAB}	50±1^{bA}	49±1^{bAB}	48±1^{bAB}
	9	48±1^{bB}	49±1^{bBC}	47±1^{bBC}	46±1^{bBC}	47±0^{bB}	48±1^{bB}	44±1^{bcC}	49±0^{bA}	49±1^{bAB}	50±0^{bA}	49±0^{bAB}
	12	52±2^{aAB}	48±2^{bB}	49±1^{bB}	49±2^{bB}	48±2^{bB}	49±2^{bB}	47±1^{bB}	56±2^{aA}	56±2^{aA}	55±2^{aA}	57±1^{aA}
Moisture (%)	0	74.7±0.3^{aA}	74.7±0.3^{aA}	74.7±0.3^{aA}	74.7±0.3^{aA}	74.7±0.3^{aA}	74.7±0.3^{aA}	74.7±0.3^{aA}	74.7±0.3^{aA}	74.7±0.3^{aA}	74.7±0.3^{aA}	74.7±0.3^{aA}
	3	76.2±2.6^{aA}	69.4±0.1^{bAB}	69.6±0.6^{bAB}	70.2±1.1^{bAB}	71.1±2.6^{bAB}	70.8±2.1^{bAB}	65.8±2.0^{bcB}	68.4±4.1^{bAB}	65.8±1.0^{cB}	66.8±2.1^{bcB}	67.7±1.3^{bAB}
	6	74.7±0.1^{aA}	65.5±2.9^{cB}	66.6±0.2^{cB}	68.4±1.3^{bAB}	69.4±0.4^{bAB}	70.3±2.0^{bAB}	65.2±0.3^{cB}	69.9±2.8^{bAB}	70.6±0.9^{bAB}	65.8±1.0^{cB}	68.8±3.3^{bAB}
	9	76.6±0.4^{aA}	69.7±1.0^{bB}	68.7±0.6^{bB}	70.5±0.2^{bB}	69.8±0.6^{bB}	69.1±1.2^{bB}	69.4±0.8^{bB}	69.4±0.6^{bB}	69.2±1.3^{bcB}	69.7±1.3^{bB}	72.4±5.9^{bB}
	12	77.3±0.1^{aA}	67.9±0.1^{bcB}	67.8±1.0^{bB}	69.4±0.8^{bB}	70.3±1.5^{bB}	71.5±2.1^{bB}	68.9±1.9^{bB}	69.0±0.4^{bB}	66.9±0.6^{cB}	68.7±0.4^{bB}	69.5±0.8^{bB}

** Chitosan (Ch); Commercial Nanocellulose (CNCC); Giant Reed Nanocellulose (G); Kenaf Nanocellulose (K); Miscanthus Nanocellulose (M); Sage Essential Oil (SEO). a-e: Different letters indicate significant differences between lines ($p < 0.05$). A-D: Different letters indicate significant differences between columns ($p < 0.05$).*

6.1.2.3 pH and Total Titratable Acidity

Under regular conditions, the pH of poultry living muscle should be close to neutral values, decreasing to values between 5.6 and 6.4 after the animal's death. The tissue acidification is an outcome of postmortem glycolysis. Once all oxygen is consumed in the muscle, glycogen along with phosphate compounds are mobilized to maintain adenosine triphosphate (ATP), accumulating lactate and ultimately H^+ ions due to the lack of an effective elimination mechanism. Therefore, pH is determined by the quantity of glycogen present in the muscle preceding slaughter and the rate of glycogen conversion into lactic acid subsequent to slaughter. The decrease in pH has a direct influence on the fresh meat quality attributes like tenderness, water-holding capacity, color, juiciness, and shelf life (Chauhan et al., 2019; Matarneh et al., 2017; Mir et al., 2017).

On the initial storage day, the meat registered a pH value of 6.0 ± 0.0 (Table 6.3). The unwrapped meat pH underwent the first significant increase ($p < 0.05$) at six days of testing, following a rising trend until the last day, where it lodged the highest pH value among all samples, 7.3 ± 0.2. The significant increase in pH after six days is an indication that from this date onwards the unwrapped meat is in an advanced state of decomposition, being in concordance with the microbiological results (above 7 log CFU/g). Since poultry meat is classified as high perishable food and owns a relatively high initial pH, it is promptly supporting the growth of microorganisms when stored under refrigeration or room conditions (Robertson, 2013). During storage, the occurrence of meat degradation processes results in an increase in alkaline compounds like ammonia, amines, or sulfides, consequently raising the pH. This phenomenon directly influences the speed of biochemical processes, generating more favorable conditions for the growth of the microbial population (Bekhit et al., 2021).

As reported in previous parameters, the developed bionanocomposites proved to be suitable for extending the meat shelf-life. The pH evaluation also supported that analysis, as it was shown that the packaged samples kept the meat's pH equal for longer. The pH of the media is a crucial parameter to activate the antimicrobial capacity of Ch, demonstrating more efficiency at pH values below 6.5. The manifestation of this phenomenon is predicted to be due to the large amount of positively charged amine groups $–NH^{3+}$ that bind to negatively charged membrane constituents from pathogenic bacteria (El-Hack et al., 2020). In comparison with the unwrapped treatment, all protected specimens presented significantly lower pH values ($p < 0.05$) from the sixth day onwards. Although not being a significant result ($p > 0.05$), a

slight decrease in pH was observed in the meat packaged with the pristine Ch film, probably because chitosan owns an acidic character since it was dissolved in an aqueous solution of acetic acid (Pires et al., 2018). In opposition, this small acidification was not observed for samples wrapped in bionanocomposites, which may reflect the suitable interlinkage between the reinforcement nanoparticles and the polymer that can decrease the number of Ch amino groups able to react in the membrane of microorganisms (Souza et al., 2020b). The pH of samples packed in Ch film without SEO remained unchanged ($p > 0.05$) during the first nine days. However, it was noticed that the pH starts significantly increasing ($p < 0.05$) on the last evaluation day, demonstrating that the meat degradation becomes too substantial to be contradicted by the chitosan antimicrobial properties. Furthermore, the introduction of SEO in the bionanocomposites caused the meat samples to have the lowest pH ($p < 0.05$) from day six onwards. For these samples, after an initial slight decrease ($p > 0.05$), the pH value remained unchanged until the end of the trial. Although these samples showed a lower pH, it was not verified that it had a direct influence on microbiological contamination rates. These results are in agreement with those presented by our previous works, in which poultry meat wrapped in Ch combined with other natural preservatives, like rosemary essential oil (REO) and ginger essential oil (GEO) (Pires et al., 2018; Souza et al., 2019c).

The total titratable acidity measures the total acid concentration in a food. In addition to pH, is another interrelated concept in food analysis in determining the acidity of a sample. Nevertheless, the methodology of these two analytical parameters is different, providing particular insights into food quality (Tyl and Sadler, 2017). As observed in table 6.3, the acid concentration of the control meat decreased significantly ($p < 0.05$) over time, following the tendency observed for the pH, already explained. For the meat samples wrapped in the bionanocomposites, only was observed and an initial significant decrease ($p < 0.05$) for the first evaluation day. From day three to the end of the experiment, no significant changes ($p > 0.05$) were observed in this parameter.

6.1.2.4 Total Volatile Basic Nitrogen

Total volatile basic nitrogen (TVB-N) represents the volatile substances, like amines and ammonia, resulting from the degradation of proteins and other nitrogen-containing compounds. In the course of the postmortem state of meat, there is a progressive denaturation of muscle proteins due to changes in muscle structure resulting from biochemical processes that occur during meat ripening, in which energy resources (glycogen, ATP, CK) are degraded

(Grashorn, 2010). As it is commonly associated with spoilage mechanisms, like proteolytic enzyme exudation and microorganisms' growth, the quantification of these compounds is considered an important physicochemical indicator of meat freshness. Above certain levels, some of the amines could practice a negative influence on the meat product, changing its color and flavor, and may exhibit toxicity, being poisonous by inhalation, ingestion, or skin absorption (Bekhit et al., 2021).

The TVB-N values were evaluated at three different times and can be consulted in Table 6.3. All treatments showed a significant increase ($p < 0.05$) between the initial and the last assessment day. The unwrapped meat had an initial value of 14.1 ± 1.0 mg/100 g of meat, and exhibited the highest result in the end, with 87.8 ± 15.4 mg/100 g of meat, reporting to be the most deteriorated sample. The meat protected with the bionanocomposites presented significantly lower values ($p < 0.05$), less than 33-52 % compared to the unpacked specimen. Therefore, these proved to hold the evolution of the TVB-N, maintaining the meat in an acceptable fresh-ness status through the refrigeration storage time. Other works have reported similar effects (Cheng et al., 2021; Mehrabi et al., 2021; Zhang et al., 2019), in which the chitosan's antimicrobial activity is the most plausible justification for delaying the TVB-N progress. Indeed, the formation of compounds categorized as TVB-N follows the meat deterioration process, being established a correlation with the results obtained in the pH and microbiological growth assays. After the animal dead, contamination by microorganisms on the meat's surface increases, depleting the main energy sources, consequently causing a gradual shift from glycogen-dependent microbes to protein-degrading types of bacteria. The degradation of proteins into low molecular weight compounds, such as amino acids, increases the pH, creating a favorable environment to potentiate an even greater proliferation of microorganisms and endogenous enzymes able to decompose alkaline ammonia compounds (Bekhit et al., 2021).

The samples wrapped in Ch films reinforced with CNCs showed significantly lower results ($p < 0.05$) when compared with the ones protected by the pristine Ch film, less than 13-19 %. Costa et al., (2021) also proved that chicken meat in contact with Ch/CNCs membranes had lower TVB-N values when compared to meat in contact with a Ch or commercial membrane, thus being more effective in delaying meat deterioration in the end of fourteen storage days. Analogously, a significant decrease ($p < 0.05$) was observed in meat samples wrapped in films with SEO. It should be highlighted that the treatment Ch+SEO presented the lowest TVB-N value at the end of twelve days, 42.1 ± 5.4 mg/100 g of meat. Although not a significant result ($p > 0.05$), the treatments in which CNCs was combined with SEO had slightly higher

values than the sample in which the SEO acted isolated, which might indicate a slight entrapment of the essential oil by the cellulosic nanoparticles. The beneficial effect in the TVB-N obtained after the introduction of SEO in Ch films is in agreement with the results of similar works in which sage, in the form of essential oil (Çoban et al., 2016) or extract (Mehdizadeh et al., 2019), was added directly to fish products.

Table 6.3 — Meat's pH, titratable acidity, and total volatile basic nitrogen over the storage time.

Parameters	Storage Days	Samples										
		Unwrapped	Ch	Ch+CNCC	Ch+G	Ch+K	Ch+M	Ch+SEO	Ch+CNCC+SEO	Ch+G+SEO	Ch+K+SEO	Ch+M+SEO
pH	0	6.0±0.0^{cA}	6.0±0.0^{bA}	6.0±0.0^{bA}	6.0±0.0^{bA}	6.0±0.0^{bA}	6.0±0.0^{bA}	6.0±0.0^{aA}	6.0±0.0^{aA}	6.0±0.0^{aA}	6.0±0.0aA	6.0±0.0^{aA}
	3	5.9±0.1^{cA}	5.9±0.0^{bA}	6.1±0.1^{bA}	6.0±0.0^{bA}	5.9±0.1^{bA}	6.0±0.0^{bA}	5.8±0.0^{aA}	5.7±0.1^{aA}	5.6±0.1^{aA}	5.5±0.0aA	5.8±0.0^{aA}
	6	6.7±0.0^{bA}	5.9±0.1^{bB}	6.3±0.0^{bAB}	6.1±0.0^{bB}	6.0±0.0^{bB}	6.1±0.0^{bB}	5.8±0.0^{aBC}	5.6±0.0^{aC}	5.5±0.0^{aC}	5.4±0.2aC	5.5±0.1^{aC}
	9	7.0±0.1^{abA}	5.8±0.1^{bBC}	6.3±0.0^{bB}	6.3±0.0^{bB}	6.1±0.0^{bB}	6.0±0.1^{bB}	5.6±0.1^{aC}	5.6±0.1^{aC}	5.6±0.0^{aC}	5.5±0.2aC	5.5±0.0^{aC}
	12	7.3±0.2^{aA}	6.3±0.0^{aB}	6.6±0.1^{aB}	6.7±0.1^{aB}	6.5±0.0^{aB}	6.4±0.1^{aB}	5.8±0.1^{aC}	5.7±0.0^{aC}	5.6±0.1^{aC}	5.5±0.1aC	5.7±0.2^{aC}
Titratable acidity (% Oleic acid equivalent)	0	1.5±0.2^{aA}	1.5±0.2^{aA}	1.5±0.2^{aA}	1.5±0.2^{aA}	1.5±0.2^{aA}	1.5±0.2^{aA}	1.5±0.2^{aA}	1.5±0.2^{aA}	1.5±0.2^{aA}	1.5±0.2^{aA}	1.5±0.2^{aA}
	3	1.0±0.2^{bA}	1.0±0.2^{bA}	1.2±0.2^{bA}	1.1±0.0^{bA}	1.0±0.1^{bA}	1.1±0.0^{bA}	1.1±0.1^{bA}	1.0±0.0^{bA}	1.0±0.2^{bA}	1.0±0.1^{bA}	1.0±0.0^{bA}
	6	0.9±0.0^{bA}	1.1±0.4^{bA}	1.1±0.2^{bA}	0.9±0.1^{bA}	1.0±0.0^{bA}	1.0±0.1^{bA}	0.9±0.2^{bA}	1.1±0.1^{bA}	1.0±0.0^{bA}	1.0±0.0^{bA}	1.2±0.1^{bA}
	9	0.4±0.0^{cB}	0.8±0.2^{bA}	0.9±0.0^{bA}	0.8±0.1^{bA}	0.9±0.2^{bA}	1.0±0.1^{bA}	1.0±0.1^{bA}	1.2±0.1^{bA}	1.0±0.2^{bA}	1.1±0.2^{bA}	1.1±0.2^{bA}
	12	0.6±0.3^{cB}	0.9±0.0^{bA}	0.8±0.1^{bAB}	0.9±0.1^{bAB}	0.7±0.2^{bAB}	0.8±0.1^{bAB}	1.0±0.1^{bA}	1.0±0.1^{bA}	1.0±0.0^{bA}	1.0±0.2^{bA}	1.0±0.0^{bA}
TVB-N (mg/kg meat)	0	14.1±1.0^{cA}	14.1±1.0^{cA}	14.1±1.0^{cA}	14.1±1.0^{cA}	14.1±1.0^{cA}	14.1±1.0^{bA}	14.1±1.0^{bA}	14.1±1.0^{bA}	14.1±1.0^{bA}	14.1±1.0^{bA}	14.1±1.0^{bA}
	6	60.6±0.3^{bA}	38.0±1.9^{bB}	41.3±1.1^{bB}	42.4±1.5^{bB}	40.9±2.3^{bB}	43.6±3.8^{aB}	38.7±6.7^{aB}	44.4±3.1^{aB}	37.6±3.5^{aB}	40.2±1.8^{aB}	38.4±3.2^{aB}
	12	87.8±15.4^{aA}	59.7±2.8^{aB}	52.1±3.1^{aC}	50.7±3.6^{aC}	49.2±6.7^{aC}	48.5±5.6^{aC}	42.1±5.4^{aC}	43.8±3.6^{aC}	44.9±5.2^{aC}	47.6±2.5^{aC}	47.2±3.4^{aC}

** Chitosan (Ch); Commercial Nanocellulose (CNCC); Giant Reed Nanocellulose (G); Kenaf Nanocellulose (K); Miscanthus Nanocellulose (M); Sage Essential Oil (SEO). a-e: Different letters indicate significant differences between lines ($p < 0.05$). A-D: Different letters indicate significant differences between columns ($p < 0.05$).*

6.1.2.5 Lipid Oxidation (TBARS Index)

Poultry meat possesses high concentrations of unsaturated fat that is highly susceptible to lipid oxidation. Lipid oxidation is one of the principal causes of food spoilage, being responsible for the alteration of significant sensory attributes (like odor development, rancidity, and meat discoloration), in most cases associated with rejection or loss of value of food products by consumers. Consequently, increasing attention has been allocated to developing biomaterials with film-forming capacity in conjunction with antioxidant properties to improve food safety and shelf life (Wan et al., 2013).

The increase in TBARS values is linked to lipid oxidation products (mainly aldehydes) accumulation, in which higher TBARS values are associated with unacceptable off-flavors/odors in meat products. Therefore, in this study, malondialdehyde, one of the major hydroperoxides decomposition products of polyunsaturated fatty acids, formed from the oxidation of fatty acid was calculated as the value of thiobarbituric acid reactive substances (Cheng et al., 2021). It was noted that the initial TBARS values were approximately 0.03 mg MDA/kg of meat, followed by an increasing tendency for all samples over time (Figure 6.2). As expected, the unpackaged meat reached the highest average value of 0.32 mg MDA/kg of meat at the end of the 12 days of testing, while the samples protected by the chitosan film and respective Ch bionanocomposites maintained significant lower ($p < 0.05$) MDA levels for all evaluation times, thus delaying the meat degradation by lipid oxidation mechanisms.

During the 12 testing days, there were no significant differences ($p > 0.05$) between the sample packed in the Ch film compared to the CNC-reinforced bionanocomposites. Furthermore, the meat wrapped in the Ch films had slightly lower MDA concentration values at each evaluation time. The protection effect associated to chitosan may be attributed to the good oxygen barrier and the chelator ability of this biopolymer to donate electrons and stabilize free radicals, acting as antioxidants. The -OH radical has the most active reaction to oxygen between several species, thus, it can readily react with active hydrogen atoms available in chitosan biomolecules, constituting a more stable compound. The incorporation of CNCs in the polymeric matrix and their good binding with Ch decreased reactive sites and consequently caused a decrease in the film's antioxidant activity (Contini et al., 2021). It was also stated that no observable differences ($p > 0.05$) occurred between bionanocomposites reinforced with the different nanocelluloses extracted from lignocellulosic crops. Moreover, these samples

reported similar MDA concentrations as the specimen wrapped in the bionanocomposite with commercial CNCs.

Several reports found in the literature stated that the introduction of small amounts of essential oils into chitosan films has the ability to significantly delay or inhibit the oxidation of oxidizable substrates and may act at different levels in an oxidative sequence (Contini et al., 2021; Mehdizadeh and Langroodi, 2019). The EO's antioxidative properties have been commonly related to their phenolic content, which acts as hydrogen donators and radical scavengers (Ehsani et al., 2019). The results present in this work showed that SEO incorporation in the Ch film significantly ($p < 0.05$) increased the meat´s MDA values soon after day 3, compared to the control sample wrapped in Ch. This result could indicate a possible pro-oxidant effect associated to SEO. These results do not agree with those presented by (Ferreira et al., 2022), in which *Salvia officinalis* L. powder was added to salmon hamburgers. The results of this study showed that *Salvia officinalis* L. at three different concentrations (0.5, 1, and 1.5 %) was able to stop the oxidation process of the hamburgers, presenting a good antioxidant and antimicrobial potential. In another study, sage essential oil and sage extract obtained from sage (*Salvia officinalis* L.) herbal dust (food industry by-product) were directly applied to fresh pork sausages (Branislav et al., 2018). Once again, it was verified that the addition of these two active compounds significantly ($p < 0.05$) reduced the TBARS values. The study developed by (Kenar et al., 2010) supports our results, which evaluated the effects of rosemary and sage tea extracts on the sensory, chemical, and microbiological changes of vacuum-packed and refrigerated sardine (*Sardina pilchardus*) fillets. In this work, the sample treated with sage tea showed significantly higher MDA values when compared to the control, indicating the pro-oxidant effect of sage tea on fish muscle.

As can be seen, there is an ambiguity in results, and it is difficult to predict whether SEO has an anti- or pro-oxidant profile. In the work presented by (Akyüz et al., 2017), a novel protein-based solid-biosensor for determining the pro-oxidant activity of phenolic compounds was developed and extracts (testing different dilutions) of sage, green tea, mint, and marjoram plants were studied as real samples to test total pro-oxidant activity (TPA). It was observed that sage presented the highest TPA values for the 1:5 dilution (v/v). The authors justified that it is quite difficult to make a general assessment of the anti- or pro-oxidant behavior of polyphenols since the ability of polyphenols to behave under *in vitro* and *in vivo* systems depends on different factors like the polyphenol concentration and structure, the free radical source, and the molecules present in substrate to be protected.

Additionally, contrary to the results presented by Ch + SEO bionanocomposites, samples packed in Ch + CNCs + SEO bionanocomposites showed the lowest MDA values ($p < 0.05$) among all samples studied, between days 3 and 6. These results may be due to the incorporation of components into the biopolymer matrix, increasing the barrier capacity to gases, like oxygen. It was verified once again that the CNCs introduction had an essential oil retention effect and therefore the results for these samples were lower than those presented by the Ch + SEO.

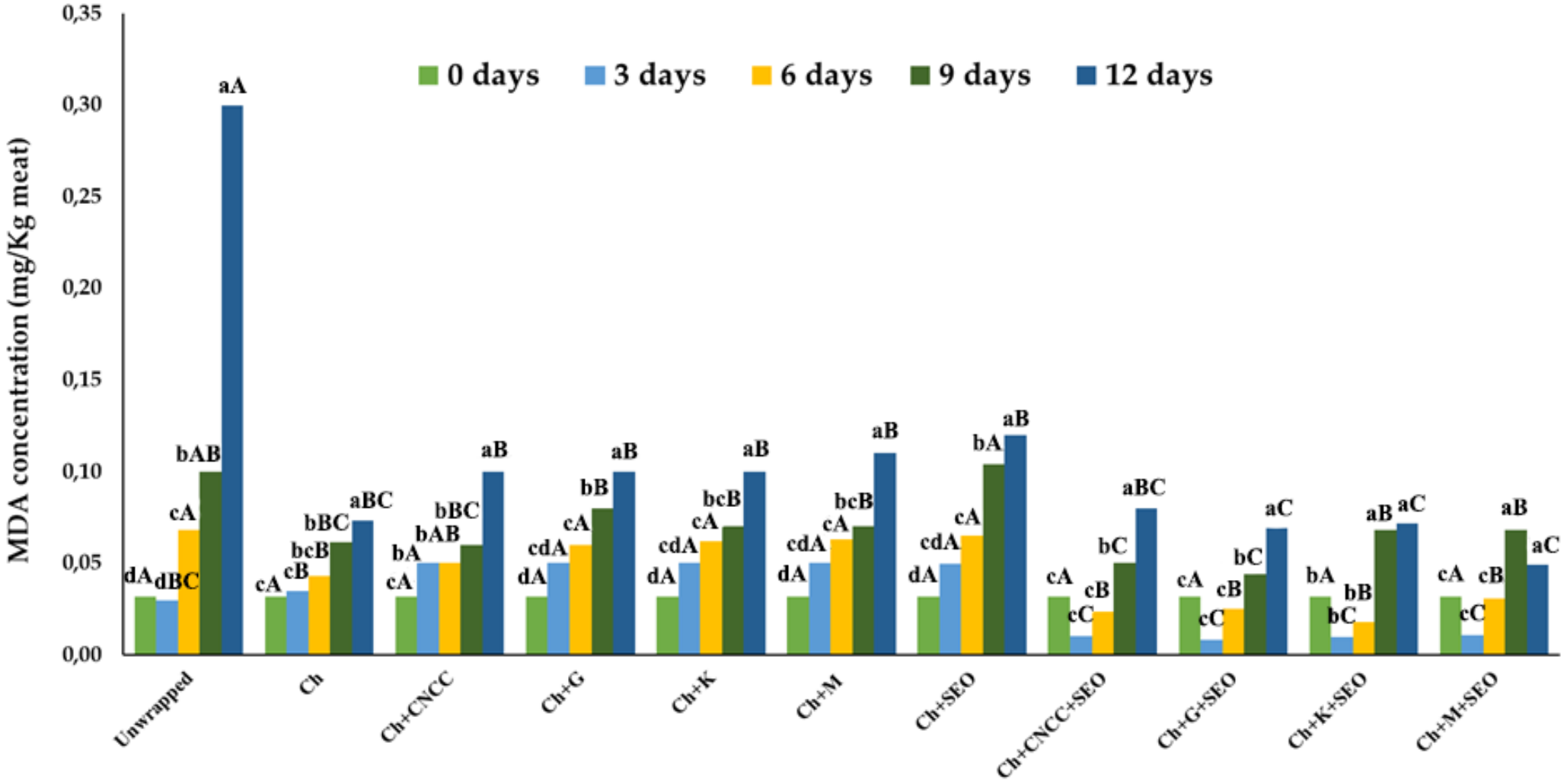

Figure 6.2 — TBARS index of the meat over the storage time. *Chitosan (Ch); Commercial Nanocellulose (CNCC); Giant Reed Nanocellulose (G); Kenaf Nanocellulose (K); Miscanthus Nanocellulose (M); Sage Essential Oil (SEO). a-e: Different letters indicate significant differences between days ($p < 0.05$). A-D: Different letters indicate significant differences between samples ($p < 0.05$).*

6.2 "*In vitro*" Bionanocomposite Study

6.2.1 Specific Migration of Antioxidant Compounds

The introduction of novel materials in food packaging requires careful monitoring of the bioactive compound migration present in its formulation. Understanding the migration profile of these substances is crucial to predict the packaging behavior when in direct contact with the food. Additionally, with this test is possible to analyze the magnitude order of phenolic compounds released, essential to understanding the substance´s antioxidant activity and the possible danger these may yield to the final consumer, as well as their potential to modify the food's nutritional and organoleptic properties. Therefore, it is fundamental to balance the active agents release from the packaging, promoting a better and prolonged preservation of the food, with the non-occurrence of potentially toxic side effects in the product that may affect the human health (Souza et al., 2019b; Zhang, Ismail, et al., 2021).

Food is made up of a complex diversity of substances, making it difficult to accurately evaluate their migration. As an alternative, to make this determination, it is usual to resort to food-simulating agents, duly regulated by competent authorities, e.g., European Food Safety Authority (EFSA), Food and Drug Administration (FDA), to mention a few. Several factors influence the migration severity when the package contacts the food, like time, temperature, compound structure and concentration, type of polymeric matrix, and food's physical-chemical characteristics. The main objective of applying bionanocomposites in fresh poultry meat was to hinder the progression of deterioration processes, like lipid oxidation, thus justifying the choice of the two-simulating media (Ribeiro-Santos et al., 2017). Therefore, in this work, the release of sage essential oil from chitosan-based bionanocomposites into a food simulant for dairy products (ethanol 50 %), and fatty acid products (ethanol 95 %) was studied as a function of time. The migration profile was not contemplated for other hydrophilic simulants, like water, and ethanol 10 % (for alcoholic products), since in previous works it was verified a partial degradation of the bionanocomposites between 24-48 hours (data not shown). Moreover, the conditions chosen for this assay (evaluation time (10 days) and temperature (40ºC)) were intended to simulate an extreme conservation scenario. The total phenolic compound migration profile for the two simulants is presented in Figures 6.3 and 6.4. The diffusion coefficient, according to Fick's second law, and the rate of release of the phenolic compounds, were

calculated to determine the rate and amount of release of these compounds for each sample and simulating medium, are exposed in Table 6.4.

The migration profile of phenolic compounds was similar for both simulating media, showing a pattern of "exponential growth to a maximum". As an aid to decoding the TPC migration pattern, logarithmic trend lines were drawn. In this way, it was verified that the TPC migration profile reached an equilibrium after the maximum point being reached. However, the amount released as well as the speed at which the compounds diffused to the outside was not the same for both cases. Lower diffusion coefficients were obtained for ethanol 50 %, indicating a more gradual release. Moreover, the samples showed a higher release rate of phenolic compounds for ethanol 50 % (between 71-85 % of the total incorporated) than for ethanol 95 % (between 54-75 % of the total incorporated), with the maximum release peak occurring after 168 h and 48 h, respectively.

The exponential TPC release verified in the first hours can be explained by the non-adsorbed SEO present in the bionanocomposite surface, which rapidly migrated to the outside (Montero et al., 2021). After reaching the maximum, a dispersion of points was observed characterized by a slight decrease followed by a final growth. The decrease could be related to the lack of stability of the phenolic compounds. Despite the high applicability potential, the agri-food industry often struggles with the instability of these bioactive substances. Polyphenols have unsaturated bonds and a high antioxidant capacity, which makes them sensitive to a large number of factors, including temperature and long-term storage time, which are related to this work (Esparza et al., 2020). Determining the exact point where the degradation of these compounds began is difficult to set with accuracy, since at the point of maximum migration it may already be occurring. However, the decrease observed after 48 h for ethanol 95 %, and 168 h for ethanol 50 %, may indicate that from that time on, the amount of TPC degraded is greater than the amount released (Souza et al., 2019b). In the last evaluation time, an increase in TPC was observed in ethanol 95 %, which is due to the beginning of the bionanocomposites decomposition, also verified in the last evaluation time (12 days) when the samples were in contact with the fresh poultry meat. The migration profile from the samples to ethanol 95 % was similar to that exposed in the work of (Souza et al., 2018b).

The higher total phenolic compounds amount observed for ethanol 50 %, throughout all evaluation times, could be related to different factors. A similar result was recorded in the work of (Zhang et al., 2020), although the migration profile of phenolic compounds from banana peels extract was only evaluated after 4 h. According to the authors, the TPC values were

significantly higher for more hydrophilic media, like pure water and ethanol 50 %, due to the hydrophilicity of the Ch film, thus, for superior solubility of the film, higher release of phenolic compounds. As stated by Buonocore et al., (2003), the release of an active compound from a polymeric network occurs in several steps. When diffusing from the simulating solution to the polymeric matrix, the water molecules weaken and change the structure of the network, allowing the phenolic compound diffusion, until thermodynamic equilibrium is reached. However, other works stated opposite results. In the work of (Sánchez-González et al., 2011a), the highest limonene, a major component of bergamot oil, released from Ch was verified in all films for ethanol 95 % aqueous solutions. For higher ethanol concentrations, the polarity of the solvent decreased, and consequently, the chemical affinity and solubility of limonene increased, justified the authors. In another similar work, the migration profile of ginger (GEO) and rosemary (REO) essential oils from Ch films were compared to different simulant media. The results showed differences in the two samples, with REO having a greater affinity for ethanol 10 %, while GEO had higher release amounts for ethanol 95 %. The authors justified the results by stating that the components present in GEO were more lipophilic than those in REO, which on the other hand were more hydrophilic (Souza et al., 2019b). It can thus be seen that the chosen polymer matrix, as well as the composition of the essential oil and the food matrix where the bionanocomposite will be applied, are important factors in determining the migration profile of total phenolic compounds over a period.

Continuing to review the work of Souza et al., (2019), the authors verified that the main components of GEO (Zingiberene and α-Curcumene) have a more complex structure with a higher molecular weight than the components of REO (camphor and eucalyptol), causing a reduction in the intermolecular friction with the polymer (higher plasticizing effect) that contributed to the active compounds release, especially in the more hydrophobic simulant (ethanol 95 %). In our work, the study of the chemical composition of the essential oil of sage (*Salvia officinalis* L.) was not carried out, however, resorting to the literature, it was found that there was a consensus that the most predominant compounds in this oil are the oxygenated monoterpenes, like camphor and α-thujone (Abbasi et al., 2021; Cuceu et al., 2015). The fact that the sage chemical composition is more similar to rosemary than to ginger, since both belonging to the same botanical family and genus (*Lamiaceae*, Salvia), may help to justify why there was a greater affinity for more hydrophilic media. However, both camphor and α-thujone are practically insoluble in water and easily soluble in alcohol and many organic solvents, contradicting our results (O'Neil, 2013; Yalkowsky et al., 2010). Consequently, analyzing all the factors,

the most plausible justification for understanding the migration profile of the phenolic compounds from SEO obtained to the two simulated media lies in the hydrophilic profile and the wettability properties of the chitosan bionanocomposites, in which the swelling and solubility of them govern the higher substance release for more hydrophilic systems. In future work, a complete characterization of the properties of bionanocomposites loaded with SEO, an analysis of the chemical composition of the essential oil, as well as a specific migration analysis for the largest compounds detected, are fundamental to better understanding this phenomenon.

Analyzing Figures 6.3 and 6.4, it was verified that the release of phenolic compounds was more limited in the bionanocomposites incorporated with nanocellulose compared to the "Ch + SEO" film. In comparison, the release rate from the bionanocomposites was shown to be inferior between 15-20 % (Table 6.4). Among the added nanoreinforcements, no significant differences were verified ($p > 0.05$), however, the commercial nanocellulose bionanocomposite showed a slightly higher encapsulation capacity. The lower release of essential oil to the simulating media from the reinforced bionanocomposites was in agreement with the results from other studies in which nanoparticles were added to reinforce chitosan films (Lan et al., 2021; Surendhiran et al., 2022). The compact network formed between the nanocellulose, and the chitosan trapped the essential oil, hindering its diffusion from the interior to the surface of the bionanocomposite. Moreover, it was verified in our previous work that the addition of nanocellulose decreases the swelling and solubility of the chitosan film, making it more hydrophobic (Pires et al., 2022b). This factor determines that the polymeric matrix structure is more resistant to modifications and therefore fewer gaps are created when in contact with water, impairing the diffusion of oil to the outside.

Table 6.4 — Diffusion kinetics of phenolic compounds.

	Diffusion Coefficient (cm^2/s)		**Maximum Diffusion / Total Incorporated**	
Sample	**Ethanol 50 %**	**Ethanol 95 %**	**Ethanol 50 %**	**Ethanol 95 %**
Ch + SEO	$4,4 \times 10^{-11}$	$8,9 \times 10^{-11}$	0,85	0,75
Ch + CNCC + SEO	$4,0 \times 10^{-11}$	$3,7 \times 10^{-11}$	0,71	0,54
Ch + G + SEO	$4,2 \times 10^{-11}$	$3,8 \times 10^{-11}$	0,73	0,57
Ch + K + SEO	$4,3 \times 10^{-11}$	$4,8 \times 10^{-11}$	0,73	0,60
Ch + M + SEO	$4,6 \times 10^{-11}$	$5,6 \times 10^{-11}$	0,76	0,60

** Chitosan (Ch); Commercial Nanocellulose (CNCC); Giant Reed Nanocellulose (G); Kenaf Nanocellulose (K); Miscanthus Nanocellulose (M); Sage Essential Oil (SEO).*

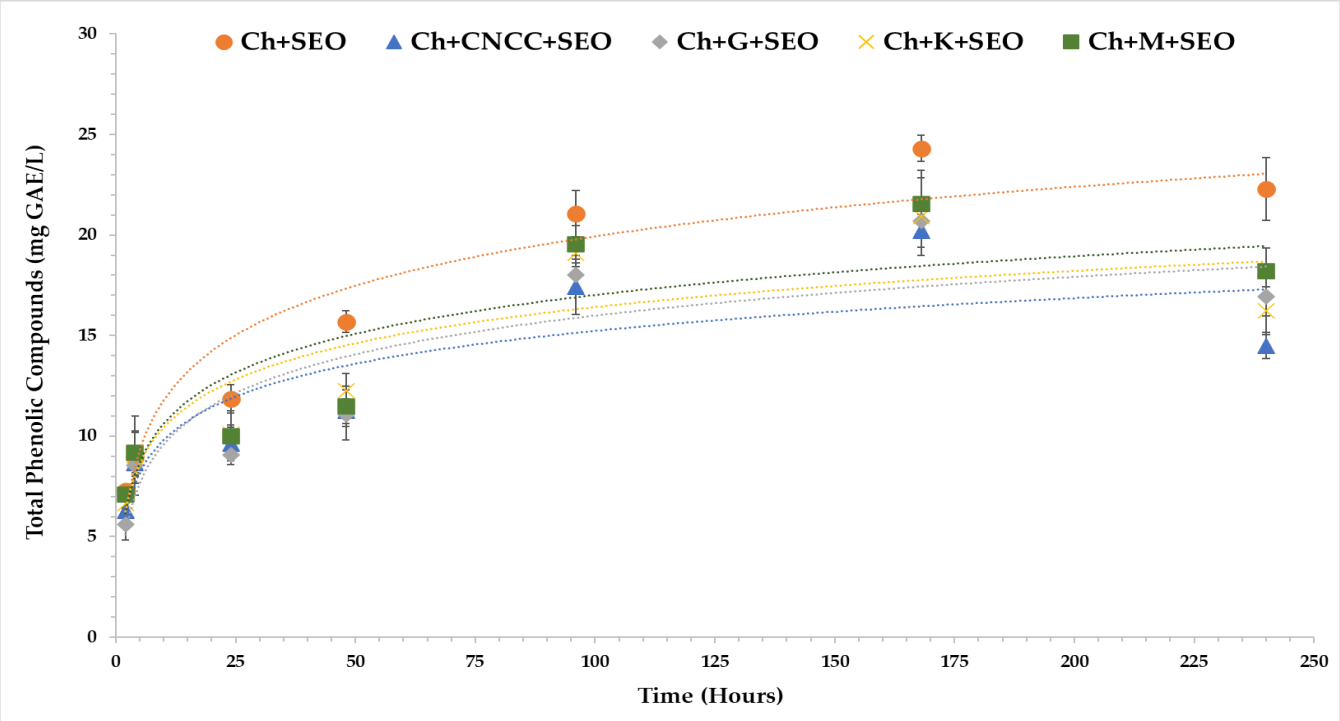

Figure 6.3 — Total phenolic migration profile for the simulant ethanol 50 %. *Chitosan (Ch); Commercial Nanocellulose (CNCC); Giant Reed Nanocellulose (G); Kenaf Nanocellulose (K); Miscanthus Nanocellulose (M); Sage Essential Oil (SEO).*

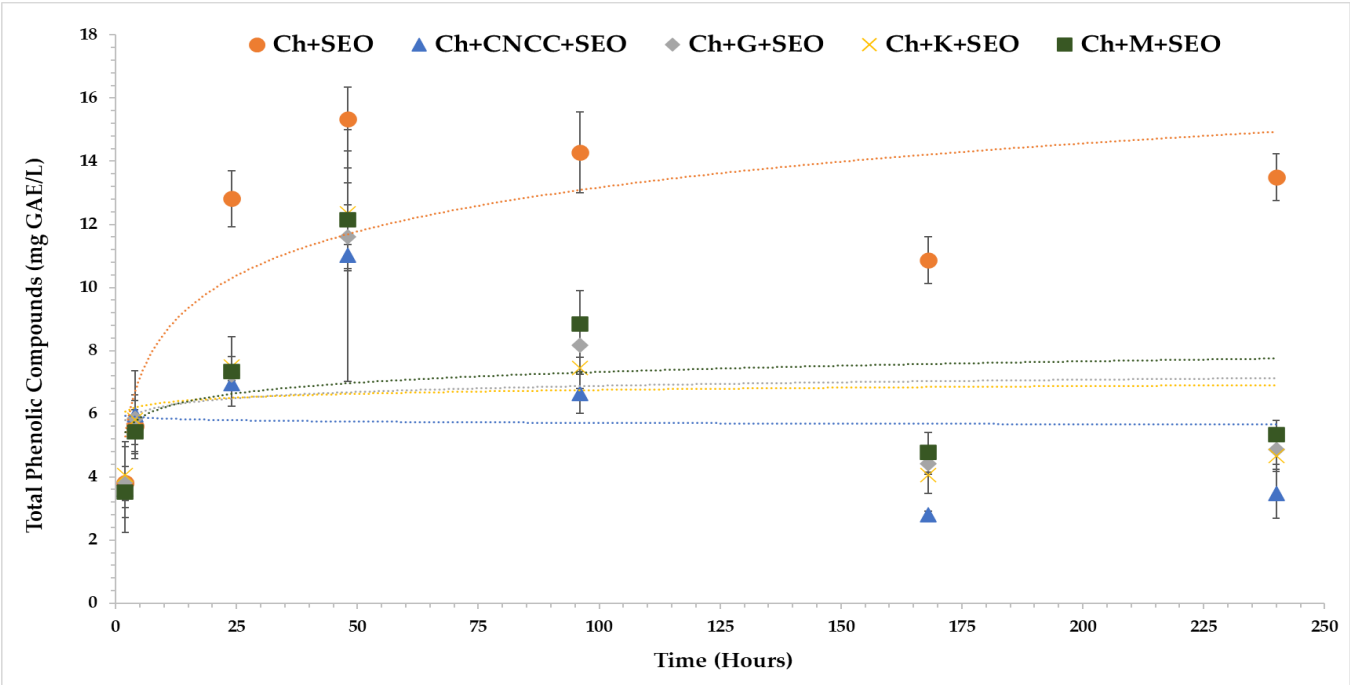

Figure 6.4 — Total phenolic migration profile for the simulant ethanol 95 %. *Chitosan (Ch); Commercial Nanocellulose (CNCC); Giant Reed Nanocellulose (G); Kenaf Nanocellulose (K); Miscanthus Nanocellulose (M); Sage Essential Oil (SEO).*

6.2.2 Antioxidant Activity

The antioxidant activity of the compounds that migrated from the bionanocomposite to the simulating media was evaluated using the radical scavenging method (DPPH). The study was conducted at the same time as the migration of phenolic compounds and the results are expressed in the percentage of inhibition of the DPPH radical, as can be seen in Figures 6.5 and 6.6. DPPH is a free radical with hydrogen acceptor capacity characterized by its deep violet color. By reacting with this stable molecule, antioxidants deliver an electron or hydrogen atom, thereby reducing DPPH. The resultant colorless or pale-yellow substance is easily monitored with a spectrophotometer, in which the decolorization is stoichiometric with respect to the number of electrons taken up. Therefore, this methodology was chosen since it is reliable, simple, and inexpensive to estimate the compound's ability to act as free radical scavengers or hydrogen donors and to evaluate their antioxidant activity (Kedare and Singh, 2011).

Observing the results, it was stated that there was a higher percentage of DPPH radical inhibition in the simulating media ethanol 50 %, for all evaluation times. These values may be due to the greater number of phenolic compounds released into this simulant, as observed in the previous assay. For both media, it was observed that the antioxidant activity results adopted an increased tendency over the first 24 h, followed by a decrease until a new rise with a peak of activity at 168 h. The recorded antioxidant activity profile was similar to that of TPC for ethanol 95 %, however, it did not follow the longer gradual release observed in ethanol 50 %. This may indicate a relevant degradation of the phenolic compounds released after this time, thus decreasing their antioxidant activity. The peak of activity recorded at 168 h was to a great extent due to the beginning of the bionanocomposites degradation process, which granted a greater release of phenolic compounds. Additionally, the antioxidant activity for both media was lower for the nanocellulose-reinforced bionanocomposites than for the "Ch + SEO" film, justified by the lower release of phenolic compounds.

Inhibition values never exceeded 5 % for both analyzed media, corresponding to a slight antioxidant activity. These values proved to be below those obtained for rosemary and ginger (Souza et al., 2019b). In the literature, it is possible to verify that sage essential oil demonstrated good DPPH scavenging activity, being commonly associated with a compound with good antioxidant activity. In fact, two different works, when comparing *Rosmarinus officinalis* L. and *Salvia officinalis* L. essential oils, attributed the greater neutralization of the DPPH radical to sage, since the percentage of inhibition of 50 % was achieved for considerably lower

oil concentrations (Bozin et al., 2007; Viuda-Martos et al., 2009). Therefore, it was expected that by using sage essential oil in chitosan bionanocomposites it would be possible to enhance their antioxidant capacity. However, the results obtained showed that, although there was a release of total phenolic compounds to the simulating media, these did not demonstrate a marked ability to inhibit the DPPH radical. Moreover, these observations may help to explain why no significant improvement in lipid oxidation results was observed in meat wrapped in bionanocomposites incorporated with SEO.

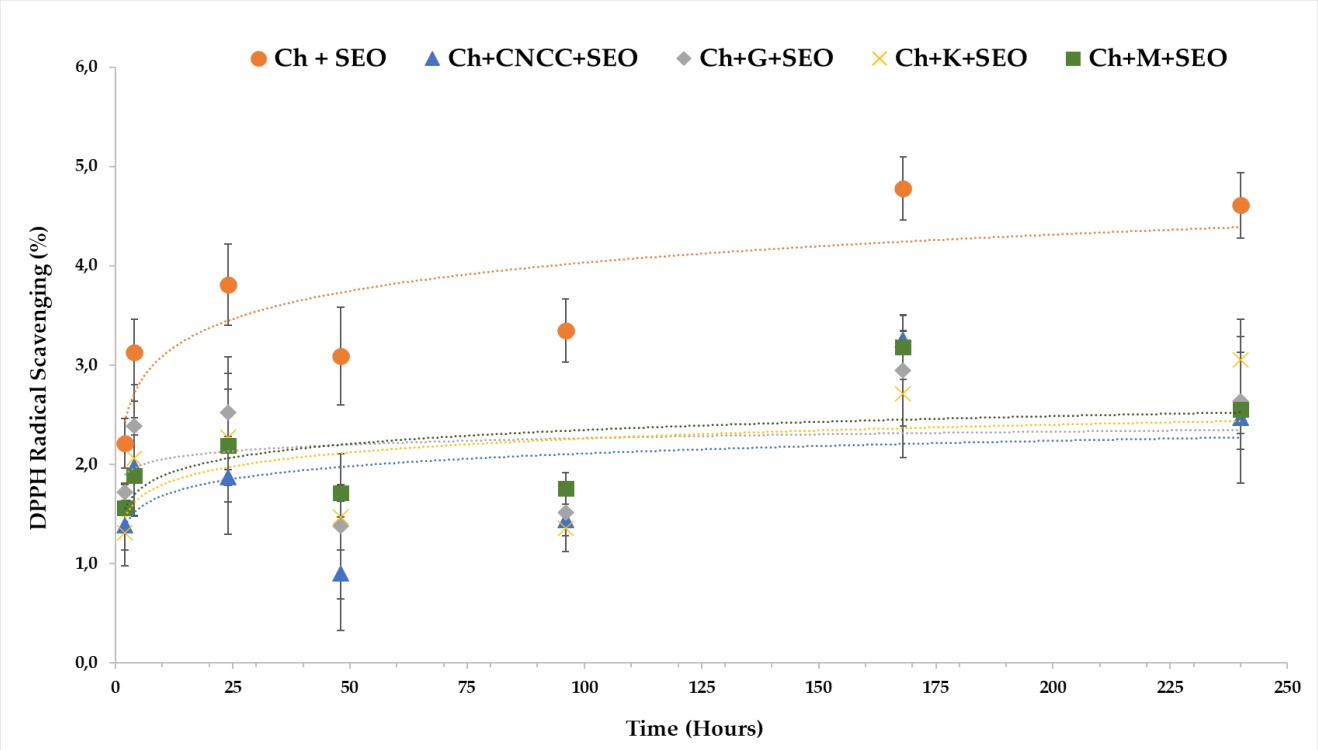

Figure 6.6 — DPPH radical Scavenging (%) profile for the simulant ethanol 50 %. *Chitosan (Ch); Commercial Nanocellulose (CNCC); Giant Reed Nanocellulose (G); Kenaf Nanocellulose (K); Miscanthus Nanocellulose (M); Sage Essential Oil (SEO).*

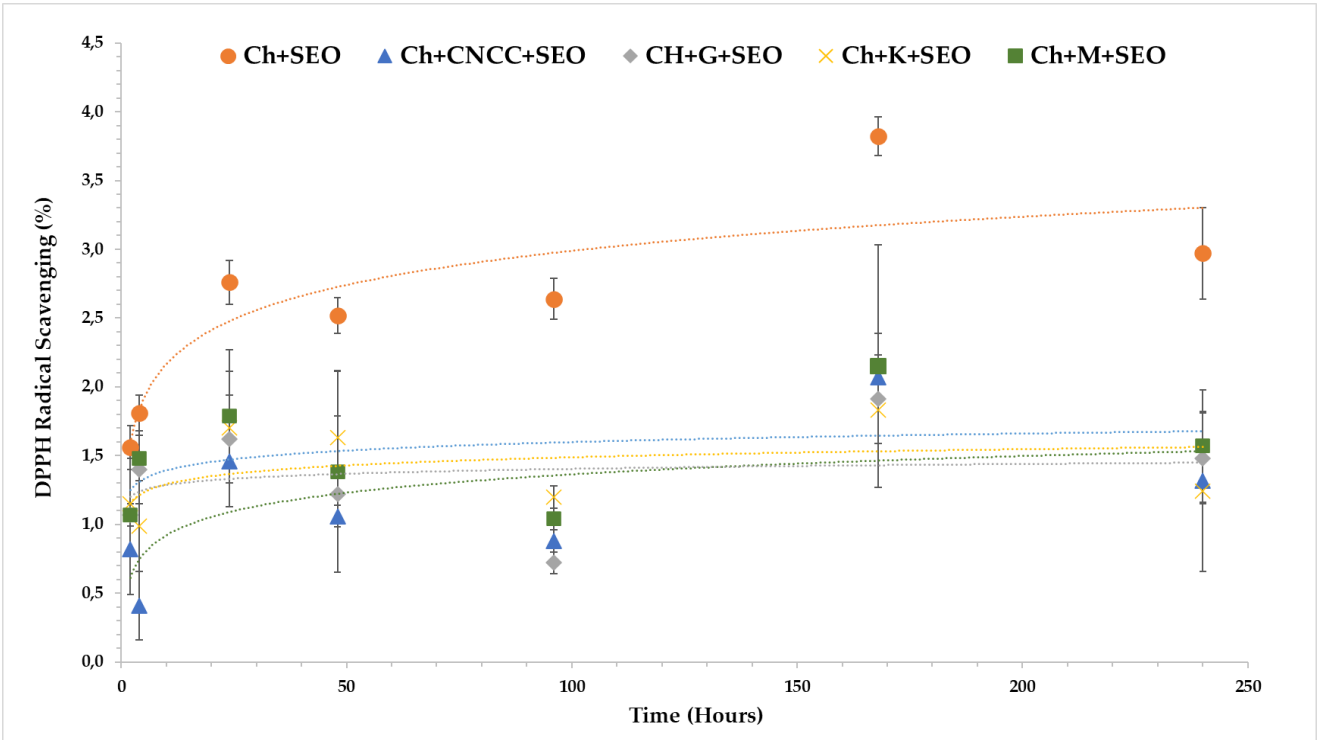

Figure 6.5— DPPH radical Scavenging (%) profile for the simulant ethanol 95 %. *Chitosan (Ch); Commercial Nanocellulose (CNCC); Giant Reed Nanocellulose (G); Kenaf Nanocellulose (K); Miscanthus Nanocellulose (M); Sage Essential Oil (SEO).*

6.2.3 Antimicrobial activity – Colony-forming Unit Counting Method

The results presented in Table 6.5 shows that the analyzed bionanocomposites had an elevated antimicrobial activity against both Gram-positive and Gram-negative foodborne bacteria. In this table, the results obtained for the remaining films reinforced with CNCs were not included, since no significant differences between them were observed ($p > 0.05$).

Table 6.5 – "*In vitro*" antimicrobial activity of bionanocomposites - colony-forming unit counting method.

	Bacillus cereus		*Salmonella* Choleraesuis	
Sample	Log CFU/mL	Logarithmic reduction	Log CFU/mL	Logarithmic reduction
Control	9.2 ± 0.4		9.7 ± 0.2[a]	
Ch	< 1	>8.2 ± 0.4	3.7 ± 0.3[c]	6.0 ± 0.3[a]
Ch+SEO	< 1	>8.2 ± 0.4	4.5 ± 0.1[b]	5.1 ± 0.1[b]
Ch+CNCC+SEO	< 1	>8.2 ± 0.4	4.0 ± 0.3[c]	5.7 ± 0.3[a]

a-b: Different letters indicate significant differences between lines ($p < 0.05$).

Colony Forming Units (CFU).

It was stated that all samples tested were more efficient against Gram-positive bacteria (*B. cereus*) with an almost total reduction superior to ~8.2 log, after 24 h incubation time. Comparatively, for the Gram-negative bacteria (S. *Choleraesuis*) the maximum reduction registered was for the pristine chitosan film, ~6.0 log. The incorporation of nanocellulose did not statistically interfere ($p > 0.05$) with the antibacterial activity detected, which is in line with the results verified in chapter 6.1.1. However, the addition of SEO to Ch's film slightly but statistically decreased ($p < 0.05$) the antimicrobial capacity against S. *Choleraesuis*. It can therefore be assumed that the chitosan intrinsic antimicrobial activity is the factor most responsible for the reduction in microbiological viable counts. These results agree with the results obtained in the evaluation of microbiological growth in packaged meat samples. These results are in agreement with the work of (Souza et al., 2019b).

Chitosan has been shown to have antimicrobial properties against a wide range of microorganisms, including both Gram-positive and Gram-negative bacteria (Nouri et al., 2017). There are various factors that can impact the efficiency of chitosan against distinct bacterial species. These may include the degree of deacetylation and the molecular weight of the

chitosan, as well as the specific environmental conditions in which the bacteria are grown. Moreover, particular bacterial strains could have different susceptibilities to chitosan, and the emergence of chitosan resistance is a possibility that should be taken into account (Kou et al., 2022). Gram-negative bacteria are typically more resistant to antimicrobial agents due to the presence of an outer membrane that serves as a permeability barrier, limiting the access into the bacterial cell of antimicrobial agents. However, chitosan has been shown to exhibit significant antimicrobial activity against gram-negative bacteria due to the cationic nature of chitosan, which allows it to interact with the negatively charged bacterial outer membrane and penetrate the cell wall, leading to disruption of the cytoplasmic membrane and cell death. On the other hand, Gram-positive bacteria lack the outer membrane but possess a thicker layer of peptidoglycan that binds non-covalently with chitosan through teichoic acids. This interaction can also lead to the disruption of the bacterial cell wall and subsequent cell death (El-Hack et al., 2020; Ke et al., 2021).

In general, the wide-ranging ability of chitosan to prevent the growth of both gram-negative and gram-positive bacteria makes it a promising option for use as an antimicrobial agent in various areas, such as preserving food, healing wounds, and coating medical devices. Nonetheless, additional investigations are necessary to comprehend the underlying mechanisms of chitosan's antimicrobial activity and to refine its effectiveness against diverse types and strains of bacteria.

6.3 Chapter Conclusions

This study demonstrated that although there was a logical degradation in the meat's properties over the 12 days of evaluation, there was a significant delay in the food degradation processes when preserved in the diverse bionanocomposites. Through the different microbiological parameters studied, it was verified that the packaged samples presented lower contamination values by about 2-3 logs. The delay of microbiological contamination in these samples showed that the protected meat is acceptable for human consumption for a longer useful time. The good antimicrobial activity shown was supported by the "*in vitro*" assays in which the films were able not only to inhibit the growth of both Gram-positive and Gram-negative bacteria, but also to significantly reduce the initial bacterial contamination. Furthermore, the positive results obtained in evaluating the physicochemical parameters of meat freshness, like pH, total titratable acidity, color, humidity, total volatile basic nitrogen, and lipid oxidation, help justify the fresh poultry meat shelf-life extension.

Regarding the addition of nanocellulose, several observations were recorded. First, the nanocellulose extracted from lignocellulosic biomass had a similar performance to the commercial nanocellulose, effectively increasing the barrier properties of the bionanocomposites, preventing gas exchanges between the outside and inside of the package and consequently improving food conservation. However, the excellent bond between the nanocellulose and the polymer matrix could cause a decrease in the active properties as there was a reduction in the chitosan free active groups.

The addition of sage essential oil in the bionanocomposites brought relevant changes to the samples, which is important to highlight. In positive terms, these bionanocomposites slightly lowered the pH of the sample, which allowed for lower results for TVB-N. However, this phenomenon did not result in significant improvements in microbiological control. Negatively, the oil directly interfered with meat color from the first day of evaluation and showed a slight pro-oxidant activity. However, these aspects were mitigated by introducing nanocellulose, proving that this nanoreinforcement had an encapsulating effect, promoting a more controlled release of the oil into the food.

The "*in vitro*" migration assay proved that SEO had a greater affinity for the ethanol 50 %, demonstrating a more significant and controlled migration of phenolic compounds to the dairy food simulant than the food simulant media of fatty foods, ethanol 90 %. This diffusion pattern can be justified by the Ch film's intrinsic properties, which started to degrade sooner for systems with higher water content, thus causing superior essential oil amounts to migrate. Accordingly, a higher percentage of DPPH radical inhibition was registered for ethanol 50 %. However, the inhibition values never exceeded 5 % for both media, which can be correlated

with a slight antioxidant activity. Moreover, this assay showed that CNCs incorporated into the film after the essential oil demonstrated an encapsulating effect, delaying the SEO migration. This phenomenon was observed by reducing the meat's hue changing and on the prooxidant activity recorded in the TBARS assay.

In conclusion, through this scientific work, it was possible to observe that it is possible to extend the shelf life of a perishable food, like fresh poultry meat, by packaging it in a bionanocomposite made from renewable and biodegradable material, capable of replacing in the future packaging layers made from fossil-based polymers. However, the hydrophilicity associated with chitosan, improved with the introduction of nanocellulose, hinders its applicability in foods with high water content. Therefore, for now, these materials should focus on preserving dried foods. Consequently, optimizations will still have to be made for this type of material to be produced efficiently at the industry level, with greater applicability.

7

FINAL CONSIDERATIONS AND FUTURE PERSPECTIVES

The objectives proposed for this doctoral thesis were successfully achieved. The conducted work was divided into three stages with the final objective of producing a biodegradable and functional bionanocomposite with active properties, which would demonstrate potential to replace fossil-based plastics in food packaging.

Presently, nanocellulose is a high-added-value product with applications in diverse technological fields, and its primary raw material for extraction is cotton. As such, in the first stage, three different energy crops (*Miscanthus × giganteus* Greef et Deuter, *Arundo donax* L., and *Hibiscus cannabinus* L.) were selected as a source to extract cellulose to add value to lignocellulosic biomass with the potential to be used in the biorefinery context. Later, the isolated cellulose was converted into crystalline nanocellulose. These lignocellulosic biomasses were chosen due to their low ILUC profile, highlighting them as potential feedstocks for biofuel and bioproducts. To isolate cellulose from the non-cellulosic compounds, present in the fiber, and posteriorly convert it into nanocellulose, a protocol consisting of three steps, alkaline pre-treatment, bleaching, and acid hydrolysis, was established. From the morphological characterization of the initial biomass, it was observed that the three fibers have an acceptable quantity of cellulose, above 40%, and lignin amount below 30 %, demonstrating the potential of these fibers to be treated with milder pulping conditions. The application of the chosen methodology to isolate cellulose had the expected outcome, obtaining almost pure white fibers with cellulose contents above 90% and remarkably low amounts of lignin and hemicellulose. The elimination of non-cellulosic components was also recorded in the FT-IR spectra, with a pronounced reduction or even elimination of their characteristic bands. Although the three fibers were equally micronized to pass through a sieve with the same mesh size, analyzing their morphology shown that kenaf fibers were the ones that presented a smaller initial size. After acid hydrolysis, the CNCs presented a superior aggregation capacity, demonstrating that the dispersion method was insufficient and urges to be optimized. In addition, the methodology employed to neutralize the CNCs, with a pH increase aided by sodium hydroxide, was not the most suitable for their effective dispersion, as observed by the zeta potential analysis. The CNCs aggregation made it arduous to observe and accurately determine its aspect ratio

through AFM, yet it was possible to notice through the images that nanoparticles presented a rod-like shape, characteristic of crystalline nanocellulose. Regarding the crystallinity of the samples, it was observed that as the non-cellulosic components were eliminated, the crystallinity index increased, reaching values close to 80 % after the application of acid hydrolysis. The slight increase in the crystallinity after this step also indicated that there was a removal of the cellulose amorphous parts. Thermal analyzes conducted by TGA and DSC determined that CNCs lost more mass and started the degradative process earlier than the initial fibers. However, they demonstrated superior thermal stability, reaching peaks of thermal decomposition at higher temperatures.

The properties studied in stage 1 demonstrated that nanocelluloses obtained from the three biomasses shown potential to be introduced as mechanical reinforcement in chitosan biofilms. Despite slight differences, none of the samples significantly outperformed in any property. As such, it was decided to proceed with the study of the applicability of nanocellulose using the three samples produced in this stage. The similarity shown between samples, highlights the possibility of mixing these fibers at the beginning of the extraction process for future work, thus increasing the profitability of nanocellulose production. From a future perspective, it is also essential to find applicability to give value for the liquors resulting from each step, since these are rich in sugars and phenolic compounds derived from hemicellulose and lignin. The use of these liquors for lignin extraction and conversion to nanolignin, as well as their use as a substrate to feed systems with algae or for the production of biogas are suggestive ideas. Furthermore, studying the replacement of the reagents used in the methodology applied in this thesis by chemically greener reagents, like ionic liquids and deep eutectic solvents, would be interesting to increase the sustainability of the process. In the context of industry, the costs associated with the nanocellulose production can be considered substantial for the associated yield, so it is essential to balance the entire process with more efficient methodologies that manage to reduce the times, temperatures, and costs of reagents. The use of technological complements, like ultrasounds or microwaves, could be an alternative to be explored.

The application of biopolymers from polysaccharides in bioplastics by the industry is still in a preliminary phase, broadly due to their properties that are not yet comparable with traditional plastics of fossil origin. As such, it is essential to find a solution that helps to enhance this type of bioproduct without affecting its biodegradability. The introduction of compatible nanoreinforcements of natural origin and biodegradable in the biopolymer matrix is presented as a viable solution. In the second stage of this doctoral thesis, different formulations of bionanocomposites composed of chitosan as a biopolymeric matrix and nanocellulose as reinforcement were developed. The nanocelluloses produced in the first stage were

incorporated in three different amounts (1.5, 2, or 2.5 % (w/w) of Ch) and the bionanocomposites properties were studied and compared with an unreinforced chitosan film and with a bionanocomposite reinforced with commercial nanocellulose. The bionanocomposites were successfully produced and demonstrated similar optical properties, exhibiting a slightly yellowish color and high levels of transparency. Despite the low opacity to visible light, samples with 2.5 % CNCs developed an effective barrier against ultraviolet radiation. These results were important if it is intended to apply the bionanocomposites in food packaging, since these allow the consumer to have visual access to the product while at the same time protecting it from UV light, possibly delaying the degradation process by lipid oxidation. Through the chemical and crystallinity analysis, it was verified that a good interaction between chitosan and nanocellulose was established. However, it was also morphologically noted that during the drying process there was some aggregation of CNCs in the bottom of the bionanocomposite layer, being necessary to optimize the nanofillers dispersion process in the biopolymer matrix to further improve its reinforcing capacity. The nanocellulose introduction was preponderant in the improvement of the film's physical properties, mainly in the percentage of 2.5 %. The nanocelluloses did not show significant differences among themselves, but the reinforced bionanocomposites with CNCs derived from giant reed fiber were the ones that came closest to the bionanocomposites reinforced with commercial CNCs. At the mechanical level, it was verified that the nanoparticles increased the film's thickness and the values of strength and stiffness but reduced their ductility. Regarding the wettability and barrier properties, it was verified that the nanocellulose made the Ch films more hydrophobic, constituting an extra barrier to the passage of oxygen and water vapor. Moreover, the bionanocomposites also demonstrated greater thermal stability and lower mass loss amounts.

The improvement accomplished in the Ch films properties with the nanocellulose incorporation proved and increased the potential to employ this biomaterial in future active food packaging systems. However, the bionanocomposites were produced at a laboratory level, and their ability to be manufactured on a large scale has not been evaluated. There are still constraints associated with the bionanocomposite assemble methodology that must be overcome to be plausible for the industry to elaborate a clear bet on these materials. For example, in this work, the film-forming solutions were dried by the solvent casting method, something that is difficult to apply at an industrial level due to time and production volume constraints. Additionally, it would also be interesting to study the incorporation of cellulose nanocrystals in a dry format by the Freeze-Drying technique, replacing the controlled drying technique in an oven. This technique will bring a much higher yield potential at an industrial level, as it is already possible to consult in some literature. The affinity for water presented by the bionanocomposites is also a parameter that must be optimized. Although the nanocellulose

has created more blockages in the polymeric network that hindered the water intake, high values of swelling and solubility were still observed, which may prove to be problematic if this material is exposed to an environment with elevated moisture levels. Therefore, it is required to modify the bionanocomposite structure without severely affecting biodegradation, transforming them into thermoplastic, to be possible to pelletize and extrude them in large quantities. The bionanocomposites stability at freezing temperatures is also a critical aspect that requires thorough investigation, since freezing conditions pose challenges to bionanocomposites, such as ice crystal formation, homogeneity and dispersion, biopolymer-nanoparticle interaction, thermal properties, and processing techniques.

The prefix bio alone does not always imply that something is sustainably feasible. In the future, to introduce this novel material on the market, it is also crucial to carry out a detailed analysis of its biodegradation in different media, following the ISO and ASTM standards that are being developed for bioplastics, to define their compostability and biodegradability rates. At the laboratory level, it is possible to make a preliminary assessment of the compostability and biodegradability of bionanocomposites through visual evaluation and direct analysis of mass loss, however, to achieve completed outcomes, this analysis requires specific environmental conditions that are difficult to recreate at a laboratory level, and it is a time-consuming procedure, which was not possible to run during this experimental doctoral work. Accompanied by this, it is essential to perform an economic, ecotoxicological and life cycle assessment of the product, to guarantee that these bionanocomposites have a sustainable value chain, with lower environmental impacts to those existing for traditional plastics.

In the third stage of this doctoral work, the bionanocomposites developed with the best percentage of nanoreinforcement (2.5 %) were directly applied to a perishable food matrix, fresh poultry meat, with the aim of evaluating the biomaterial ability to act as an active element of a food package. To optimize the bionanocomposites antimicrobial and antioxidant activity, novel formulations were also developed in which sage essential oil was incorporated. Compared to unwrapped meat, it was observed that meat samples protected by the bionanocomposites had improved physicochemical parameters, thus justifying the improvements recorded by delaying the degradation phenomena. Chitosan, derived from its intrinsic antimicrobial activity, was largely responsible for inhibiting microbial proliferation since nanocellulose alone does not own this capacity. Nevertheless, as observed in the previous stage, the nanocellulose had a pivotal impact on increasing the film's barrier properties. Consequently, there was less gas exchange between the inside and outside of the packaging, helping to further delay the meat degradation processes. Once again, the results obtained with the films reinforced with the three extracted CNCs did not show substantial differences that deserved to be highlighted and were similar to those obtained for the specimens with commercial

nanocellulose. The incorporation of sage essential oil did not register significant improvements in the antimicrobial and antioxidant activity of the bionanocomposites, as was predicted by reviewing other similar works, yet interfered directly with the meat's color as it migrated to its surface. Through the "*in vitro*" migration assay, it was verified that the SEO had a more gradual with higher release rate of phenolic compounds for the dairy products simulating media (ethanol 50 %) than for the fatty acid products simulating media (ethanol 95 %). This behavior can be justified by the intrinsic properties of the chitosan film, which is more easily degraded in systems that contain a greater water content, thus causing the migration of higher amounts of oil. Consequently, a higher percentage of DPPH radical inhibition was detected for ethanol 50 %. It should be noted that these inhibition values never exceeded the 5 % for both media, which corresponds to only a slight antioxidant activity. Furthermore, this analysis proved that nanocellulose, incorporated into the film after the essential oil, was capable of delaying the migration of SEO to the outside, reducing the effect caused on the meat's color and on the pro-oxidant activity recorded in the TBARS assay. The encapsulating effect attributed to CNCs is important to praise since it may have the potential to help in the controlled migration of active agents in food packaging, which could also be applied in other areas, like the controlled release of drugs. It was then proved that it is possible to extend the shelf life of a perishable food matrix by packaging it in a chitosan/nanocellulose bionanocomposite, showing the potential of this bioproduct to be incorporated in active food packaging.

Despite the promising results, there is still a long way to go, and it is important in future works to complement this data already achieved with other analyses. For example, to obtain results closer to the shelf life of the food, it would be interesting to carry out a long-term permeability study on the package. The chemical characterization of sage essential oil is also crucial to understanding which components migrate to each type of simulant media as well as the specific antioxidant activity of each one. Complementarily, an evaluation of the physical properties of the bionanocomposites with this essential oil should be conducted, to understand its interaction with the other compounds present in the film. It is essential to perform a sensory analysis of the food packed in these bionanocomposites to identify the levels of acceptance or rejection for each property (e.g. texture, flavor, taste, appearance, smell) by the consumer. However, before reaching this test, it is critical to ensure that the elements present in the bionanocomposites are safe for human consumption. Currently, to our knowledge, chitosan and nanocellulose still do not have an official GRAS status from FDA for materials in contact with food. Another key aspect to establish is which type of foods are most suitable for this innovative packaging. Due to the hydrophilic nature of the bionanocomposites, it was found that from the ninth day onwards in contact with the meat, it began to show high levels of degradation, becoming a gel that was difficult to separate from the food. Therefore, it would

be interesting to evaluate the packaging capacity in food matrices with lower water content, like cereals, bread, or dried fruits. Finally, in order to guarantee the safety of foods packaged in this type of bionanocomposites, it is essential to guarantee the stability of the packaging in various media, therefore it is necessary to study the behavior of the packaging at different temperatures and with different light intensities.

In conclusion, this doctoral thesis proved that it was possible to reuse lignocellulosic biomass from energy crops to isolate cellulose and convert it into nanocellulose, a value-added nanoproduct with high applicability in several technological areas. It also proved to be possible to employ this nanoparticle to reinforce chitosan films, giving rise to a functional, renewable, biodegradable bionanocomposite with active properties, with the potential to be used as an integral part of food packaging, replacing traditional plastics of fossil origin.

REFERENCES

Abbasi, A., Mohammad, K., Ahmad, M., Mohammad, A., Sourestani, M., 2021. Nutritive composition, growth, biochemical traits, essential oil content and compositions of Salvia officinalis L. Grown in different nitrogen levels in soilless culture. J Soil Sci Plant Nutr 21, 3320–3332. https://doi.org/10.1007/s42729-021-00608-8

Abdul, P.M., Jahim, J., Harun, S., Markom, M., Aminah, N., Hassan, O., Balan, V., Dale, B.E., Tusirin, M., Nor, M., 2016. Effects of changes in chemical and structural characteristic of ammonia fibre expansion (AFEX) pretreated oil palm empty fruit bunch fibre on enzymatic saccharification and fermentability for biohydrogen. Bioresour Technol 211, 200–208. https://doi.org/10.1016/j.biortech.2016.02.135

Abreu, M., Ribeiro, B., Ferreira, A., Paix, S.M., Carvalheiro, F., Duarte, C., Fernando, A.L., Reis, A., Francisco, G., 2022. Low Indirect Land Use Change (ILUC) Energy Crops to Bioenergy and Biofuels—A Review. Energies (Basel) 15, 1–68.

Abushammala, H., Krossing, I., Laborie, M., 2015. Ionic liquid-mediated technology to produce cellulose nanocrystals directly from wood. Carbohydr Polym 134, 609–616. https://doi.org/10.1016/j.carbpol.2015.07.079

Ahankari, S.S., Subhedar, A.R., Bhadauria, S.S., Dufresne, A., 2021. Nanocellulose in food packaging: A review. Carbohydr Polym 255, 117479. https://doi.org/10.1016/j.carbpol.2020.117479

Akyüz, E., Başkan, K.S., Tütem, E., Apak, R., 2017. Novel protein-based solid-biosensor for determining pro-oxidant activity of phenolic compounds. J Agric Food Chem 65, 5821–5830. https://doi.org/10.1021/acs.jafc.7b01649

Akyuz, L., Kaya, M., Mujtaba, M., Ilk, S., Sargin, I., Salaberria, A.M., Labidi, J., Cakmak, Y.S., Islek, C., 2018. Supplementing capsaicin with chitosan-based films enhanced the antiquorum sensing, antimicrobial, antioxidant, transparency, elasticity and hydrophobicity. Int J Biol Macromol 115, 438–446. https://doi.org/10.1016/j.ijbiomac.2018.04.040

Albarelli, J., Paidosh, A., Santos, D.T., Maréchal, F., Meireles, M.A.A., 2016. Environmental, energetic and economic evaluation of implementing a supercritical fluid-based nanocellulose production process in a sugarcane biorefinery. Chem Eng Trans 47, 49–54. https://doi.org/10.3303/CET1647009

Al-Dulaimi, A.A., Wanrosli, W.D., 2017. Isolation and characterization of nanocrystalline cellulose from totally chlorine Free oil palm empty fruit bunch pulp. J Polym Environ 25, 192–202. https://doi.org/10.1007/s10924-016-0798-z

Alexandropoulou, M., Antonopoulou, G., Fragkou, E., Ntaikou, I., Lyberatos, G., 2017. Fungal pretreatment of willow sawdust and its combination with alkaline treatment for enhancing biogas production. J Environ Manage 203, 704–713. https://doi.org/10.1016/j.jenvman.2016.04.006

Alexopoulou, E., Cosentino, S.L., Danalatos, N., Picco, D., Lips, S., Berg, D. van den, Fernando, A.L., Monti, A., Tenorio, J.L., Kipriotis, E., Cadoux, S., Cook, S., 2013. New insights from the BIOKENAF Project, in: Monti, A., Alexopoulou, E. (Eds.), Kenaf: A Multi-Purpose Crop for Several Industrial Applications. Springer, pp. 177–203. https://doi.org/https://doi.org/10.1111/j.1744-7348.2010.00419.x

Ali, A., Ahmed, S., 2018. A review on chitosan and its nanocomposites in drug delivery. Int J Biol Macromol 109, 273–286. https://doi.org/10.1016/j.ijbiomac.2017.12.078

Aljohani, W., Wajid, M., Zhang, X., 2018. Bioprinting and its applications in tissue engineering and regenerative medicine. Int J Biol Macromol 107, 261–275. https://doi.org/10.1016/j.ijbiomac.2017.08.171

Altun, E., Çelik, E., Ersan, H.Y., 2020. Tailoring the microbial community for improving the biodegradation of chitosan films in composting environment. J Polym Environ 1–12. https://doi.org/10.1007/s10924-020-01711-0

Alves, V.L.C.D., Rico, B.P.M., Cruz, R.M.S., Vicente, A.A., Khmelinskii, I., Vieira, M.C., 2018. Preparation and characterization of a chitosan film with grape seed extract- carvacrol microcapsules and its effect on the shelf-life of refrigerated Salmon (Salmo salar). LWT - Food Science and Technology 89, 525–534. https://doi.org/10.1016/j.lwt.2017.11.013

André, da C., João, K.G., Rubik, D.F., Bogel-łukasik, E., Duarte, L.C., Andreaus, J., Bogel-łukasik, R., 2013. Pre-treatment of lignocellulosic biomass using ionic liquids: Wheat straw fractionation. Bioresour Technol 142, 198–208. https://doi.org/10.1016/j.biortech.2013.05.032

Angelini, L.G., Ceccarini, L., Nassi, N., Bonari, E., 2009. Long-term evaluation of biomass production and quality of two cardoon (Cynara cardunculus L.) cultivars for energy use. Biomass Bioenergy 33, 810–816. https://doi.org/10.1016/j.biombioe.2008.12.004

Anraku, M., Gebicki, J.M., Iohara, D., Tomida, H., Uekama, K., Maruyama, T., Hirayama, F., Otagiri, M., 2018. Antioxidant activities of chitosans and its derivatives in in vitro and in vivo studies. Carbohydr Polym 199, 141–149. https://doi.org/10.1016/j.carbpol.2018.07.016

AOAC, 2016. Official methods of analysis of the association of official analytical chemists, 20th ed. Rockville, Maryland, USA.

ASTM International, 2018. ASTM D882-18, Standard Test Method for Tensile Properties of Thin Plastic Sheeting. West Conshohocken, PA.

ASTM International, 2016. ASTM D6866-16, Standard test methods for determining the bi-obased content of solid, liquid, and gaseous samples using radiocarbon analysis. West Conshohocken, PA.

ASTM International, 2012. ASTM D883-00, Standard terminology relating to plastics. West Conshohocken, PA.

Azeredo, H.M.C., Mattoso, L.H.C., Avena-Bustillos, R.J., Filho, G.C., Munford, M.L., Wood, D., McHugh, T.H., 2010. Nanocellulose reinforced chitosan composite films as affected by nanofiller loading and plasticizer content. J Food Sci 75, 1–7. https://doi.org/10.1111/j.1750-3841.2009.01386.x

Babaee, M., Jonoobi, M., Hamzeh, Y., Ashori, A., 2015. Biodegradability and mechanical properties of reinforced starch nanocomposites using cellulose nanofibers. Carbohydr Polym 132, 1–8. https://doi.org/10.1016/j.carbpol.2015.06.043

Babaei-Ghazvini, A., Acharya, B., 2022. Influence of cellulose nanocrystal aspect ratio on shear force aligned films: Physical and mechanical properties. Carbohydrate Polymer Technologies and Applications 3, 100217. https://doi.org/10.1016/j.carpta.2022.100217

Babicka, M., Wo, M., Bartkowiak, M., Pepli, B., Waliszewska, H., Zborowska, M., Borysiak, S., Ratajczak, I., 2022. Miscanthus and Sorghum as sustainable biomass sources for nanocellulose production. Ind Crops Prod 186, 115177. https://doi.org/10.1016/j.indcrop.2022.115177

Babu Perumal, A., Selvam, P., Nambiar, R.B., Rotimi, E., 2018. Development of polyvinyl alcohol/chitosan bio-nanocomposite films reinforced with cellulose nanocrystals isolated from rice straw. Appl Surf Sci 449, 591–602. https://doi.org/10.1016/j.apsusc.2018.01.022

Bano, S., Negi, Y.S., 2017. Studies on cellulose nanocrystals isolated from groundnut shells. Carbohydr Polym 157, 1041–1049. https://doi.org/10.1016/j.carbpol.2016.10.069

Barbanti, L., Grandi, S., Vecchi, A., Venturi, G., 2006. Sweet and fibre sorghum (Sorghum bicolor (L.) Moench), energy crops in the frame of environmental protection from excessive nitrogen loads. European Journal of Agronomy 25, 30–39. https://doi.org/10.1016/j.eja.2006.03.001

Barbosa, L.C. de A., 2007. Espectroscopia no infravermelho na caracterização de compostos orgânicos, 1ª Edição. ed. Editora UFV.

Bekhit, A.E.A., Holman, B.W.B., Giteru, S.G., Hopkins, D.L., 2021. Total volatile basic nitrogen (TVB-N) and its role in meat spoilage: A review. Trends Food Sci Technol 109, 280–302. https://doi.org/10.1016/j.tifs.2021.01.006

Bernstein, P., Moholkar, V.S., 2020. Insight into chemical pretreatment of hardwood (Arundo donax) for improvement of pyrolysis. Bioresour Technol Rep 11, 100545. https://doi.org/10.1016/j.biteb.2020.100545

Beroual, M., Mehelli, O., Boumaza, L., Trache, D., Tarchoun, A.F., Derradji, M., Khimeche, K., 2021. Synthesis and characterization of microcrystalline cellulose from giant reed using different delignification processes. Materials Research and Applications 173–187.

Bharimalla, A.K., Deshmukh, S.P., Vigneshwaran, N., Patil, P.G., Prasad, V., Deshmukh, S.P., Vigneshwaran, N., Patil, P.G., Prasad, V., 2017. Nanocellulose-polymer composites for applications in food packaging: Current status, future prospects and challenges. Polym Plast Technol Eng 56, 805–823. https://doi.org/10.1080/03602559.2016.1233281

Bhatnagar, P., Law, J.X., Ng, S.-F., 2021. Chitosan reinforced with kenaf nanocrystalline cellulose as an effective carrier for the delivery of platelet lysate in the acceleration of wound healing. Polymers (Basel) 13, 4392.

Boluk, Y., Lahiji, R., Zhao, L., Mcdermott, M.T., 2011. Suspension viscosities and shape parameter of cellulose nanocrystals (CNC). Colloids Surf A Physicochem Eng Asp 377, 297–303. https://doi.org/10.1016/j.colsurfa.2011.01.003

Bonilla, J., Vargas, M., Atarés, L., 2014. Effect of chitosan essential oil films on the storage-keeping quality of pork meat products. Food Bioproc Tech 7, 2443–2450. https://doi.org/10.1007/s11947-014-1329-3

Bozin, B., Mimica-Dukic, N., Samojlik, I., Jovin, E., 2007. Antimicrobial and antioxidant properties of rosemary and sage (Rosmarinus officinalis L. and Salvia officinalis L., Lamiaceae) essential oils. J Agric Food Chem 55, 7879–7885.

Brandt, A., Gräsvik, J., Hallett, J.P., Welton, T., 2013. Deconstruction of lignocellulosic biomass with ionic liquids. Green Chemistry 9262, 537–848. https://doi.org/10.1039/c2gc36364j

Branislav, Š., Pavlić, B., Zeković, Z., Tomović, V., Ikonić, P., Džinić, N., 2018. The effect of essential oil and extract from sage (Salvia officinalis L.) herbal dust (food industry by-product) on the oxidative and microbiological stability of fresh pork sausages. LWT - Food Science and Technology 89, 749–755. https://doi.org/10.1016/j.lwt.2017.11.055

Bras, J., Viet, D., Bruzzese, C., Dufresne, A., 2011. Correlation between stiffness of sheets prepared from cellulose whiskers and nanoparticles dimensions. Carbohydr Polym 84, 211–215. https://doi.org/10.1016/j.carbpol.2010.11.022

Brigham, C., 2018. Biopolymers: biodegradable alternatives to traditional plastics, in: Green Chemistry: An Inclusive Approach. Elsevier Inc., pp. 753–770. https://doi.org/10.1016/B978-0-12-809270-5.00027-3

Brinchi, L., Cotana, F., Fortunati, E., Kenny, J.M., 2013. Production of nanocrystalline cellulose from lignocellulosic biomass: Technology and applications. Carbohydr Polym 94, 154–169. https://doi.org/10.1016/j.carbpol.2013.01.033

Buonocore, G.G., Nobile, M.A. Del, Panizza, A., Corbo, M.R., Nicolais, L., 2003. A general approach to describe the antimicrobial agent release from highly swellable films intended for food packaging applications. Journal of Controlled Release 90, 97–107.

Cano, A.I., Cháfer, M., Chiralt, A., González-Martínez, C., 2016. Biodegradation behavior of starch-PVA films as affected by the incorporation of different antimicrobials. Polym Degrad Stab 132, 11–20. https://doi.org/10.1016/j.polymdegradstab.2016.04.014

Cardoso, G.P., Dutra, M.P., Fontes, P.R., Ramos, A. de L.S., Gomide, L.A. de M., Ramos, E.M., 2016. Selection of a chitosan gelatin-based edible coating for color preservation of beef in retail display. Meat Sci 114, 85–94. https://doi.org/10.1016/j.meatsci.2015.12.012

Cegielka, A., Hac-Szymanczuk, E., Piwowarek, K., Dasiewicz, K., Slowinski, M., Wronska, K., 2019. The use of bioactive properties of sage preparations to improve the storage stability of low-pressure mechanically separated meat from chickens. Poult Sci 98, 5045–5053. https://doi.org/10.3382/ps/pez242

Celebi, H., Kurt, A., 2015. Effects of processing on the properties of chitosan/cellulose nanocrystal films. Carbohydr Polym 133, 284–293. https://doi.org/10.1016/j.carbpol.2015.07.007

Chaichi, M., Hashemi, M., Badii, F., Mohammadi, A., 2017. Preparation and characterization of a novel bionanocomposite edible film based on pectin and crystalline nanocellulose. Carbohydr Polym 157, 167–175. https://doi.org/10.1016/j.carbpol.2016.09.062

Chakrabarty, A., Teramoto, Y., 2018. Recent advances in nanocellulose composites with polymers: A guide for choosing partners and how to incorporate them. Polymers (Basel) 10, 517. https://doi.org/10.3390/polym10050517

Chan, C.H., Chia, C.H., Zakaria, S., Ahmad, I., Dufresne, A., 2013. Production and characterisation of cellulose and nano-crystalline cellulose from kenaf core wood. Bioresources 8, 785–794.

Chandra Pandey, V., Bajpai, O., Singh, N., 2016. Energy crops in sustainable phytoremediation. Renewable and Sustainable Energy Reviews 54, 58–73. https://doi.org/10.1016/j.rser.2015.09.078

Chauhan, S.S., Lemaster, M.N., Clark, D.L., Foster, M.K., Miller, C.E., England, E.M., 2019. Glycolysis and pH decline terminate prematurely in oxidative muscles despite the

presence of excess glycogen. Meat and Muscle Biology 3, 254–264. https://doi.org/10.22175/mmb2019.02.0006

Chen, H., 2014. Chemical composition and Structure of natural lignocellulose, in: Biotechnology of Lignocellulose: Theory Practice. Springer, pp. 25–71. https://doi.org/10.1007/978-94-007-6898-7

Chen, Y., Gan, L., Huang, J., Dufresne, A., 2019. Reinforcing mechanism of cellulose nanocrystals in nanocomposites, in: Huang, J., Dufresne, A., Lin, N. (Eds.), Nanocellulose: From Fundamentals to Advanced Materials. Wiley Online Library, pp. 201–249. https://doi.org/https://doi.org/10.1002/9783527807437.ch7

Cheng, Y., Hu, J., Wu, S., 2021. Chitosan based coatings extend the shelf-life of beef slices during refrigerated storage. LWT 138, 110694. https://doi.org/10.1016/j.lwt.2020.110694

Chitbanyong, K., Pitiphatharaworachot, S., Pisutpiched, S., Khantayanuwong, S., Puangsin, B., 2018. Characterization of bamboo nanocellulose prepared by TEMPO-mediated oxidation. Bioresources 13, 4440–4454.

Chu, Y., Sun, Y., Wu, W., Xiao, H., 2020. Dispersion properties of nanocellulose: A review. Carbohydr Polym 250, 116892. https://doi.org/10.1016/j.carbpol.2020.116892

Chung, D., Papadakis, S.E., Yam, K.L., 2002. Simple models for assessing migration from food-packaging. Food Addit Contam 19, 611–617. https://doi.org/10.1080/0265203021012638

Cinelli, P., Seggiani, M., Mallegni, N., Gigante, V., Lazzeri, A., 2019. Processability and degradability of PHA-based composites in terrestrial environments. Int J Mol Sci 20, 284. https://doi.org/10.3390/ijms20020284

Clifton-Brown, J., Stampfl, P., Jones, M., 2004. Miscanthus biomass production for energy in Europe and its potential contribution to decreasing fossil fuel carbon emissions. Glob Chang Biol 10, 509–518. https://doi.org/https://doi.org/10.1111/j.1529-8817.2003.00749.x

Çoban, O.E., Patir, B., Özpolat, E., Kuzgun, N.K., 2016. Improving the quality of fresh rainbow trout by sage essential oil and packaging treatments. J Food Saf 36, 299–307. https://doi.org/10.1111/jfs.12242

Collazo-Bigliardi, S., Ortega-Toro, R., Chiralt, A., 2018. Isolation and characterisation of microcrystalline cellulose and cellulose nanocrystals from co ff ee husk and comparative study with rice husk. Carbohydr Polym 191, 205–215. https://doi.org/10.1016/j.carbpol.2018.03.022

Commission, E., 2005. COMMISSION REGULATION (EC) No 2073/2005 of 15 November 2005 on microbiological criteria for foodstuffs.

Contini, L., Souza, T. De, Isadora, Z., Brazolin, F., Wesley, J., Mariangela, S., Silva, F., Lopes, P.S., Araújo, K., Rosemary, S., Carvalho, A. De, Cecília, A., Maria, C., Yoshida, P., 2021.

Antioxidant chitosan film containing lemongrass essential oil as active packaging for chicken patties. J Food Process Preserv 46, 1–14. https://doi.org/10.1111/jfpp.16136

Córdova, A., Afewerki, S., 2016. Environmentally friendly process for the preparation of nanocellulose and derivatives thereof. US2018346607 (A1).

Corsello, F.A., Bolla, P.A., Anbinder, P.S., Serradell, M.A., Amalvy, J.I., Peruzzo, P.J., 2017. Morphology and properties of neutralized chitosan-cellulose nanocrystals biocomposite films. Carbohydr Polym 156, 452–459. https://doi.org/10.1016/j.carbpol.2016.09.031

Costa, S.M., Ferreira, D.P., Teixeira, P., Ballesteros, L.F., Teixeira, J.A., Fangueiro, R., 2021. Active natural-based films for food packaging applications: The combined effect of chitosan and nanocellulose. Int J Biol Macromol 177, 241–251. https://doi.org/10.1016/j.ijbiomac.2021.02.105

Cuceu, A.P., Tofană, M., Socaci, S.A., Vârban, D., Nagy, M., Borş, M.-D., Fărcaş, A., 2015. Essential oil composition, phenolic content and antioxidant activity in Romanian Salvia officinalis L. Journal of Agroalimentary Processes and Technologies 21, 241–246.

Cui, S., Zhang, S., Ge, S., Xiong, L., Sun, Q., 2016. Green preparation and characterization of size-controlled nanocrystalline cellulose via ultrasonic-assisted enzymatic hydrolysis. Ind Crops Prod 83, 346–352. https://doi.org/10.1016/j.indcrop.2016.01.019

Daicho, K., Saito, T., Fujisawa, S., Isogai, A., 2018. The crystallinity of nanocellulose: Dispersion-induced disordering of the grain boundary in biologically structured cellulose. ACS Appl Nano Mater 1, 5774–5785. https://doi.org/10.1021/acsanm.8b01438

Dave, D., Ghaly, A.E., 2011. Meat spoilage mechanisms and preservation techniques: A critical review. Am J Agric Biol Sci 6, 486–510.

Deepa, B., Abraham, E., Cordeiro, N., Mozetic, M., Mathew, A.P., Oksman, K., Faria, M., Thomas, S., Pothan, L.A., 2015. Utilization of various lignocellulosic biomass for the production of nanocellulose: a comparative study. Cellulose 22, 1075–1090. https://doi.org/10.1007/s10570-015-0554-x

Dehghani, S., Vali, S., Regenstein, J.M., 2018. Edible films and coatings in seafood preservation : A review. Food Chem 240, 505–513. https://doi.org/10.1016/j.foodchem.2017.07.034

Dehnad, D., Emam-djomeh, Z., Mirzaei, H., 2014. Optimization of physical and mechanical properties for chitosan – nanocellulose biocomposites. Carbohydr Polym 105, 222–228. https://doi.org/10.1016/j.carbpol.2014.01.094

Dicastillo, C.L. de, Nerín, C., Alfaro, P., Catalá, R., Gavara, R., Hernández-Munoz, P., 2011. Development of new antioxidant active packaging films based on ethylene vinyl alcohol copolymer (EVOH) and green tea extract. J Agric Food Chem 59, 7832–7840.

Dien, L.Q., Cuong, T.D., Thi, N., Phuong, M., Huy, P., 2019. Nanocellulose fabrication from Oryza sativa L. rice straw using combined treatment by hydrogen peroxide and dilute sulfuric acid solution. Energy Sources, Part A: Recovery, Utilization, and Environmental Effects 1–10. https://doi.org/10.1080/15567036.2019.1687617

Ditzel, F.I., Prestes, E., Carvalho, B.M., Demiate, I.M., Pinheiro, L.A., 2017. Nanocrystalline cellulose extracted from pine wood and corncob. Carbohydr Polym 157, 1577–1585. https://doi.org/10.1016/j.carbpol.2016.11.036

Du, X., Zhang, Z., Liu, W., Deng, Y., 2017. Nanocellulose-based conductive materials and their emerging applications in energy devices - A review. Nano Energy 35, 299–320. https://doi.org/10.1016/j.nanoen.2017.04.001

Duan, C., Meng, X., Meng, J., Khan, I.H., Dai, L., Khan, A., An, X., 2019. Chitosan as A Preservative for Fruits and Vegetables : A Review on Chemistry and Antimicrobial Properties. Journal of Bioresources and Bioproducts 4, 11–21. https://doi.org/10.21967/jbb.v4i1.189

Dubois, J.-L., 2011. Requirements for the development of a bioeconomy for chemicals. Curr Opin Environ Sustain 3, 11–14. https://doi.org/10.1016/j.cosust.2011.02.001

Dufresne, A., 2013. Nanocellulose: a new ageless bionanomaterial. Materials Today 16, 220–227. https://doi.org/10.1016/j.mattod.2013.06.004

Ehsani, A., Hashemi, M., Afshari, A., Aminzare, M., Raeisi, M., Zeinali, T., 2020. Effect of different types of active biodegradable films containing lactoperoxidase system or sage essential oil on the shelf life of fish burger during refrigerated storage. LWT - Food Science and Technology 117, 108633. https://doi.org/10.1016/j.lwt.2019.108633

Ehsani, A., Hashemi, M., Aminzare, M., Raeisi, M., Afshari, A., Mirza, A., Mohammadreza, A., 2019. Comparative evaluation of edible films impregnated with sage essential oil or lactoperoxidase system: Impact on chemical and sensory quality of carp burgers. J Food Process Preserv 43, 1–10. https://doi.org/10.1111/jfpp.14070

El Achaby, M., El, N., Aboulkas, A., Zahouily, M., Bilal, E., Barakat, A., Solhy, A., 2017. Processing and properties of eco-friendly bio-nanocomposite films filled with cellulose nanocrystals from sugarcane bagasse. Int J Biol Macromol 96, 340–352. https://doi.org/10.1016/j.ijbiomac.2016.12.040

El-Hack, M.E.A., El-Saadony, M.T., Sha, M.E., Zabermawi, N.M., Arif, M., Elsaber, G., Khafaga, A.F., El-hakim, Y.M.A., Al-sagheer, A.A., 2020. Antimicrobial and antioxidant properties of chitosan and its derivatives and their applications: A review. Int J Biol Macromol 164, 2726–2744. https://doi.org/10.1016/j.ijbiomac.2020.08.153

Elias, N., Chandren, S., Attan, N., Mahat, N.A., Ilyana, F., Razak, A., Jamalis, J., Wahab, R.A., 2017. Structure and properties of oil palm-based nanocellulose reinforced chitosan

nanocomposite for efficient synthesis of butyl butyrate. Carbohydr Polym 176, 281–292. https://doi.org/10.1016/j.carbpol.2017.08.097

Elsabee, M.Z., Abdou, E.S., 2013. Chitosan based edible films and coatings : A review. Materials Science & Engineering C 33, 1819–1841. https://doi.org/10.1016/j.msec.2013.01.010

Emadian, S.M., Onay, T.T., Demirel, B., 2017. Biodegradation of bioplastics in natural environments. Waste Management 59, 526–536. https://doi.org/10.1016/j.wasman.2016.10.006

Errokh, A., Magnin, A., Sami, J.P., 2018. Morphology of the nanocellulose produced by periodate oxidation and reductive treatment of cellulose fibers. Cellulose 25, 3899–3911. https://doi.org/10.1007/s10570-018-1871-7

Esparza, I., Cimminelli, M.J., Moler, J.A., Jiménez-Moreno, N., Ancín-Azpilicueta, C., 2020. Stability of Phenolic Compounds in Grape Stem Extracts. Antioxidants 9, 1–14.

Espinoza-Acosta, J.L., Torres-Chávez, P.I., Carvajal-Millán, E., Ramírez-Wong, B., Bello-Pérez, L.A., Montaño-Leyva, B., 2014. Ionic liquids and organic solvents for recovering lignin from lignocellulosic biomass. Bioresources 9, 3660–3687.

EU, 2019. Directive (EU) 2019/904 of the European Parliament and of the Council of 5 June 2019 on the reduction of the impact of certain plastic products on the environment. Brussels.

European Bioplastics, 2016. What are bioplastics? [WWW Document]. URL https://www.european-bioplastics.org/bioplastics/ (accessed 2.17.20).

Fabra, M.J., Falcó, I., Randazzo, W., Gloria, S., López-Rubio, A., 2018. Antiviral and antioxidant properties of active alginate edible films containing phenolic extracts. Food Hydrocoll 81, 96–103. https://doi.org/10.1016/j.foodhyd.2018.02.026

Fan, M., 2016. Method of producing nanocellulose. WO2016/055782 (A1).

Faradilla, R.H.F., Lee, G., Rawal, A., Hutomo, T., Stenzel, M.H., Arcot, J., 2016. Nanocellulose characteristics from the inner and outer layer of banana pseudo-stem prepared by TEMPO-mediated oxidation. Cellulose 23, 3023–3037. https://doi.org/10.1007/s10570-016-1025-8

FDA, 2021. Use of recycled plastics in food packaging (chemistry considerations): Guidance for industry. Rockville, MD, USA.

Fernandes, E.M., Pires, R.A., Mano, J.F., Reis, R.L., 2013. Bionanocomposites from lignocellulosic resources: Properties, applications and future trends for their use in the biomedical field. Prog Polym Sci 38, 1415–1441. https://doi.org/10.1016/j.progpolymsci.2013.05.013

Fernandez-saiz, P., Soler, C., Lagaron, J.M., Ocio, M.J., 2010. Effects of chitosan films on the growth of Listeria monocytogenes, Staphylococcus aureus and Salmonella spp . in laboratory media and in fish soup. Int J Food Microbiol 137, 287–294. https://doi.org/10.1016/j.ijfoodmicro.2009.11.016

Fernando, A., Costa, J., Barbosa, B., Monti, A., Rettenmaier, N., 2018. Environmental impact assessment of perennial crops cultivation on marginal soils in the Mediterranean Region. Biomass Bioenergy 111, 174–186. https://doi.org/10.1016/j.biombioe.2017.04.005

Fernando, A.L., Boléo, S., Barbosa, B., Costa, J., Duarte, M.P., Monti, A., Fernando, A.L., 2015. Perennial grass production opportunities on marginal mediterranean land. Bioenergy Res 8, 1523–1537. https://doi.org/10.1007/s12155-015-9692-0

Ferreira, C.S.R., Henrique, B., Saqueti, F., Daniele, P., Martins, J., Ant, M., Carla, A., Martha, J., Mikcha, G., Oliveira, O., 2022. Effect of salvia (Salvia officinalis) on the oxidative stability of salmon hamburgers. LWT 154, 112867.

Ferreira, A.R. V, Torres, C.A. V, Freitas, F., Sevrin, C., Grandfils, C., Reis, M.A.M., Alves, V.D., Coelhoso, I.M., 2016. Development and characterization of bilayer films of FucoPol and chitosan. Carbohydr Polym 147, 8–15. https://doi.org/10.1016/j.carbpol.2016.03.089

Ferreira, F. V, Mariano, M., Rabelo, S.C., Gouveia, R.F., Lona, L.M.F., 2018. Isolation and surface modification of cellulose nanocrystals from sugarcane bagasse waste: From a micro- to a nano-scale view. Appl Surf Sci 436, 1113–1122. https://doi.org/10.1016/j.apsusc.2017.12.137

Ferrer, A., Pal, L., Hubbe, M., 2017. Nanocellulose in packaging: Advances in barrier layer technologies. Ind Crops Prod 95, 574–582. https://doi.org/10.1016/j.indcrop.2016.11.012

Flórez, M., Guerra-Rodríguez, E., Cazón, P., Vásquez, M., 2022. Chitosan for food packaging: Recent advances in active and intelligent films. Food Hydrocoll 124, 107328. https://doi.org/10.1016/j.foodhyd.2021.107328

Fortunati, E., Luzi, F., Yang, W., Kenny, J.M., Torre, L., Puglia, D., 2018. Bio-based nanocomposites in food packaging, in: Nanomaterials for Food Packaging. Elsevier, pp. 71–110. https://doi.org/10.1016/b978-0-323-51271-8.00004-8

Foster, E.J., Moon, R.J., Agarwal, U.P., Bortner, M.J., Bras, J., Camarero-espinosa, S., Chan, K.J., Clift, M.J.D., Cranston, E.D., Eichhorn, S.J., Fox, D.M., Hamad, W.Y., Heux, L., Jean, B., Korey, M., Nieh, W., Ong, K.J., Reid, M.S., Renneckar, S., Roberts, R., Shatkin, A., Moon, R.J., Nieh, W., Foster, E.J., 2018. Current characterization methods for cellulose nanomaterials. Chem Soc Rev 47, 2609–2679. https://doi.org/10.1039/c6cs00895j

Gamelas, J.A.F., Pedrosa, J., Lourenço, A.F., Mutjé, P., González, I., Chinga-carrasco, G., Singh, G., Ferreira, P.J.T., 2015. On the morphology of cellulose nanofibrils obtained by TEMPO-mediated oxidation and mechanical treatment. Micron 72, 28–33. https://doi.org/10.1016/j.micron.2015.02.003

Gan, P.G., Sam, S.T., Faiq, M., Omar, M.F., 2020. Thermal properties of nanocellulose-reinforced composites: A review. J Appl Polym Sci 137, 48544. https://doi.org/10.1002/app.48544

García, A., Gandini, A., Labidi, J., Belgacem, N., Bras, J., 2016. Industrial and crop wastes: A new source for nanocellulose biorefinery. Ind Crops Prod 93, 26–38. https://doi.org/10.1016/j.indcrop.2016.06.004

García, M.A., Rodríguez, M., Castro, C., De, N., 2020. Water vapor permeability of chitosan/zeolite composite films as affected by biopolymer and zeolite microparticle concentrations. J Packag Technol Res 4, 157–169. https://doi.org/10.1007/s41783-020-00092-y

Garrison, T.F., Murawski, A., Quirino, R.L., 2016. Bio-Based Polymers with Potential for Biodegradability. Polymers (Basel) 8, 262. https://doi.org/10.3390/polym8070262

George, T.S., Parambath, B., Texin, K., Dominic, M., Dominic, C., George, N., Balachandrakurupp, V., John, H., 2022. Isolation of high crystalline nanocellulose from Mimosa pudica plant fibres with potential in packaging applications. Packaging Technology and Science 35, 163–174. https://doi.org/10.1002/pts.2617

Geun Yoo, C., Pu, Y., Ragauskas, A.J., 2017. Ionic liquids: Promising green solvents for lignocellulosic biomass utilization. Curr Opin Green Sustain Chem 5, 5–11. https://doi.org/10.1016/j.cogsc.2017.03.003

Godinho, M.H., Almeida, P.L., Figueirinhas, J.L., 2014. From cellulosic based liquid crystalline sheared solutions to 1D and 2D soft materials. materials 7, 4601–4627. https://doi.org/10.3390/ma7064601

Gomes, L., Costa, J., Moreira, J., Cumbane, B., Abias, M., Santos, F., Zanetti, F., Monti, A., Fernando, A.L., 2022. Switchgrass and Giant Reed Energy Potential when Cultivated in Heavy Metals Contaminated Soils. Energies (Basel) 15. https://doi.org/10.3390/en15155538

Gomes, V.G.L., Rodrigues, C., Ferreira, L., Pires, J.R.A., Duarte, M.P., Coelhoso, I., Fernando, A.L., 2019. In vitro bioactivity of novel chitosan bionanocomposites incorporated with different essential oils. Ind Crops Prod 140, 111563. https://doi.org/10.1016/j.indcrop.2019.111563

Gopi, S., Amalraj, A., Jude, S., Thomas, S., Guo, Q., 2019. Bionanocomposite films based on potato, tapioca starch and chitosan reinforced with cellulose nanofiber isolated from turmeric spent. J Taiwan Inst Chem Eng 96, 664–671. https://doi.org/10.1016/j.jtice.2019.01.003

Grabka-Zasadzinska, A., Skrzypczak, A., Borysiak, S., 2019. The influence of the cation type of ionic liquid on the production of nanocrystalline cellulose and mechanical properties of chitosan-based biocomposites. Cellulose 26, 4827–4840. https://doi.org/10.1007/s10570-019-02412-1

Grashorn, M.A., 2010. Research into poultry meat quality. Br Poult Sci 51, 60–67. https://doi.org/10.1080/00071668.2010.506761

Graveson, I., English, R., 2015. Low energy method for the preparation of non-derivatized nanocellulose. US2015158955 (A1).

Gupta, K.M., Jiang, J., 2015. Cellulose dissolution and regeneration in ionic liquids: A computational perspective. Chem Eng Sci 121, 180–189. https://doi.org/10.1016/j.ces.2014.07.025

Hafemann, E., Battisti, R., Marangoni, C., Machado, R.A.F., 2019. Valorization of royal palm tree agroindustrial waste by isolating cellulose nanocrystals. Carbohydr Polym 218, 188–198. https://doi.org/10.1016/j.carbpol.2019.04.086

Haghighi, H., Licciardello, F., Fava, P., Wilhelm, H., Pulvirenti, A., 2020. Recent advances on chitosan-based films for sustainable food packaging applications. Food Packag Shelf Life 26, 100551. https://doi.org/10.1016/j.fpsl.2020.100551

Halkman, H.B.D., Halkman, A.K., 2014. Indicator Organisms, in: Batt, C.A., Tortorello, M. Lou (Eds.), Encyclopedia of Food Microbiology (Second Edition). Elsevier Ltd., pp. 358–363.

Harrison, J.P., Boardman, C., Callaghan, O., Delort, A., Song, J., Harrison, J.P., 2018. Biodegradability standards for carrier bags and plastic films in aquatic environments: a critical review. R Soc Open Sci 5, 171792. https://doi.org/https://doi.org/10.1098/rsos.171792

Hendriks, A.T.W.M., Zeeman, G., 2009. Pretreatments to enhance the digestibility of lignocellulosic biomass. Bioresour Technol 100, 10–18. https://doi.org/10.1016/j.biortech.2008.05.027

Hietala, M., Sain, S., Oksman, K., 2017. Highly redispersible sugar beet nanofibers as reinforcement in bionanocomposites. Cellulose 24, 2177–2189. https://doi.org/10.1007/s10570-017-1245-6

Higueras, L., López-carballo, G., Cerisuelo, J.P., Gavara, R., 2013. Preparation and characterization of chitosan/HP-β-cyclodextrins composites with high sorption capacity for carvacrol. Carbohydr Polym 97, 262–268. https://doi.org/10.1016/j.carbpol.2013.04.007

Hoeng, F., Denneulin, A., Bras, J., 2016. Use of nanocellulose in printed electronics: a review. Nanoscale 8, 13131–13154. https://doi.org/10.1039/c6nr03054h

Holtzapple, M.T., 2003. Cellulose, in: Caballero, B. (Ed.), Encyclopedia of Food Sciences and Nutrition. Elsevier, pp. 998–1007.

Hosseinnejad, M., Mahdi, S., 2016. Evaluation of different factors affecting antimicrobial properties of chitosan. Int J Biol Macromol 85, 467–475. https://doi.org/10.1016/j.ijbiomac.2016.01.022

Hu, L., Zheng, G., Yao, J., Liu, N., Weil, B., Eskilsson, M., Karabulut, E., Ruan, Z., Fan, S., Bloking, J.T., McGehee, M.D., Wagberg, L., Cui, Y., 2013. Transparent and conductive

paper from nanocellulose fibers. Energy Environ Sci 6, 513–518. https://doi.org/10.1039/c2ee23635d

Hubbe, M., Ferrer, A., Tyagi, P., Yin, Y., Salas, C., Pal, L., Rojas, O.J., 2017. Nanocellulose in thin films, coatings, and plies for packaging applications: A review. Bioresources 12, 2143–2233. https://doi.org/10.1016/B978-0-08-100957-4.00008-5

Hughes, J.M., Oiseth, S.K., Purslow, P.P., Warner, R.D., 2014. A structural approach to understanding the interactions between colour, water-holding capacity and tenderness. Meat Sci 98, 520–532. https://doi.org/10.1016/j.meatsci.2014.05.022

ICCT, 2018. Defining low and high indirect land-use change biofuels in european union policy.

Ilyas, R.A., Sapuan, S.M., Ishak, M.R., 2018. Isolation and characterization of nanocrystalline cellulose from sugar palm fibres (Arenga Pinnata). Carbohydr Polym 181, 1038–1051. https://doi.org/10.1016/j.carbpol.2017.11.045

Im, W., Lee, S., Rajabi, A., Hye, A., Youn, J., 2018. Optimization of carboxymethylation reaction as a pretreatment for production of cellulose nanofibrils. Cellulose 25, 3873–3883. https://doi.org/10.1007/s10570-018-1853-9

Ioelovich, M., 2017. Characterization of Various Kinds of Nanocellulose, in: Hanieh Kargarzadeh, Ishak Ahmad, Sabu Thomas, A.D. (Ed.), Handbook of Nanocellulose and Cellulose Nanocomposites, Volume 1. Wiley Online Library, pp. 51–100.

Irastorza, A., Zarandona, I., Andonegi, M., Guerrero, P., Caba, K. de la, 2021. The versatility of collagen and chitosan: From food to biomedical applications. Food Hydrocoll 116, 106633.

Islam, S., Kao, N., Bhattacharya, S.N., Gupta, R., Choi, H.J., 2018. Potential aspect of rice husk biomass in Australia for nanocrystalline cellulose production. Chin J Chem Eng 26, 465–476. https://doi.org/10.1016/j.cjche.2017.07.004

Ismail, M.Y., Patanen, M., Antti, J., Visanko, M., Ohigashi, T., 2019. Hybrid films of cellulose nano fibrils, chitosan and nanosilica — Structural, thermal, optical, and mechanical properties. Carbohydr Polym 218, 87–94. https://doi.org/10.1016/j.carbpol.2019.04.065

ISO, 2019. ISO 17410:2019 Microbiology of the food chain — Horizontal method for the enumeration of psychrotrophic microorganisms.

ISO, 2017. ISO 21528-2:2017 Microbiology of the food chain — Horizontal method for the detection and enumeration of Enterobacteriaceae — Part 2: Colony-count technique.

ISO, 2013. ISO 4833-1:2013 Microbiology of the food chain - Horizontal method fot the enumeration of microorganisms - Part 1: Colony count at 30 degrees C by the pour plate technique.

Isogai, A., Saito, T., Fukuzumi, H., 2011. Tempo-oxidized cellulose nanofibers. Nanoscale 3, 71–85. https://doi.org/10.1039/c0nr00583e

Isogai, A., Zhou, Y., 2019. Diverse nanocelluloses prepared from TEMPO-oxidized wood cellulose fibers: Nanonetworks, nano fibers, and nanocrystals. Curr Opin Solid State Mater Sci 23, 101–106. https://doi.org/10.1016/j.cossms.2019.01.001

Izawa, H., Toyoshima, Y., Morimoto, M., Saimoto, H., Ifuku, S., 2021. Surface wrinkles induced on oriented chitosan films via horseradish peroxidase-catalyzed reaction and drying. Chem Lett 50, 252–255. https://doi.org/10.1246/cl.200740

Jacob, J., Peter, G., Thomas, S., Haponiuk, J.T., Gopi, S., 2019. Chitosan and polyvinyl alcohol nanocomposites with cellulose nano fibers from ginger rhizomes and its antimicrobial activities. Int J Biol Macromol 129, 370–376. https://doi.org/10.1016/j.ijbiomac.2019.02.052

Jannatyha, N., Shojaee-aliabadi, S., Moslehishad, M., Moradi, E., 2020. Comparing mechanical, barrier and antimicrobial properties of nanocellulose/CMC and nanochitosan/CMC composite films. Int J Biol Macromol 164, 2323–2328. https://doi.org/10.1016/j.ijbiomac.2020.07.249

Jonoobi, M., Harun, J., Tahir, P., Shakeri, A., Saifulazry, S., 2011. Physicochemical characterization of pulp and nanofibers from kenaf stem. Mater Lett 65, 1098–1100. https://doi.org/10.1016/j.matlet.2010.08.054

Jonoobi, M., Oladi, R., Davoudpour, Y., 2015. Different preparation methods and properties of nanostructured cellulose from various natural resources and residues: a review. Cellulose 22, 935–969. https://doi.org/10.1007/s10570-015-0551-0

Jorfi, M., Foster, E.-J., 2015. Recent advances in nanocellulose for biomedical applications. J Appl Polym Sci 132.

Kallel, F., Bettaieb, F., Khiari, R., García, A., Bras, J., 2016. Isolation and structural characterization of cellulose nanocrystals extracted from garlic straw residues. Ind Crops Prod 87, 287–296. https://doi.org/10.1016/j.indcrop.2016.04.060

Kamireddy, S.R., Li, J., Tucker, M., Degestein, J., Ji, Y., 2013. Effects and mechanism of metal chloride salts on pretreatment and enzymatic digestibility of corn stover. Ind Eng Chem Res 52, 1775–1782.

Karan, H., Funk, C., Grabert, M., Oey, M., Hankamer, B., 2019. Green bioplastics as part of a circular bioeconomy. Trends Plant Sci 24, 237–249. https://doi.org/10.1016/j.tplants.2018.11.010

Kargarzadeh, H., Ioelovich, M., Ahmad, I., Thomas, S., Dufresne, A., 2017. Methods for extraction of nanocellulose from various sources, in: Handbook of Nanocellulose and Cellulose Nanocomposites, Volume 1. Wiley Online Library, pp. 1–49. https://doi.org/10.1002/9783527689972

Karimi, S., Tahir, P., Karimi, A., Dufresne, A., Abdulkhani, A., 2014. Kenaf bast cellulosic fibers hierarchy: A comprehensive approach from micro to nano. Carbohydr Polym 101, 878–885.

Kassab, Z., Abdellaoui, Y., Hamid, M., Bouh, R., El, A., Qaiss, K., El, M., 2020. Micro- and nanocelluloses derived from hemp stalks and their effect as polymer reinforcing materials. Carbohydr Polym 245, 116506. https://doi.org/10.1016/j.carbpol.2020.116506

Ke, C.-L., Deng, F.-S., Chuang, C.-Y., Lin, C.-H., 2021. Antimicrobial actions and applications of chitosan. Polymers (Basel) 13, 904.

Kedare, S.B., Singh, R.P., 2011. Genesis and development of DPPH method of antioxidant assay. J Food Sci Technol 48, 412–422. https://doi.org/10.1007/s13197-011-0251-1

Kenar, M., Ozogul, F., Kuley, E., 2010. Effects of rosemary and sage tea extracts on the sensory, chemical and microbiological changes of vacuum-packed and refrigerated sardine (Sardina pilchardus) fillets. Int J Food Sci Technol 45, 2366–2372. https://doi.org/10.1111/j.1365-2621.2010.02414.x

Khalil, H.P.S.A., Davoudpour, Y., Islam, N., Mustapha, A., Sudesh, K., Dungani, R., Jawaid, M., 2014. Production and modification of nanofibrillated cellulose using various mechanical processes: A review. Carbohydr Polym 99, 649–665. https://doi.org/10.1016/j.carbpol.2013.08.069

Khan, A., Khan, R.A., Salmieri, S., Le, C., Riedl, B., Bouchard, J., Tan, V., Kamal, M.R., Lacroix, M., 2012. Mechanical and barrier properties of nanocrystalline cellulose reinforced chitosan based nanocomposite films. Carbohydr Polym 90, 1601–1608. https://doi.org/10.1016/j.carbpol.2012.07.037

Kian, L.K., Jawaid, M., Ariffin, H., Karim, Z., 2018. Isolation and characterization of nanocrystalline cellulose from roselle-derived microcrystalline cellulose. Int J Biol Macromol 114, 54–63. https://doi.org/10.1016/j.ijbiomac.2018.03.065

Kim, D., 2018. Physico-Chemical Conversion of Lignocellulose : Inhibitor Effects and Detoxification Strategies : A Mini Review. Molecules 23, 309. https://doi.org/10.3390/molecules23020309

Kim, D.-Y., Lee, B.-M., Koo, D.H., Kang, P.-H., Jeun, J.-P., 2016. Preparation of nanocellulose from a kenaf core using E-beam irradiation and acid hydrolysis. Cellulose 23, 3039–3049. https://doi.org/10.1007/s10570-016-1037-4

Kim, Joo-hyung, Shim, B.S., Kim, H.S., Lee, Y., Min, S., Jang, D., Abas, Z., Kim, Jaehwan, 2015. Review of nanocellulose for sustainable future materials. International Journal of Precision Engineering and Manufacturing-Green Technology 2, 197–213. https://doi.org/10.1007/s40684-015-0024-9

Kininge, M.M., Gogate, P.R., 2022. Intensification of alkaline delignification of sugarcane bagasse using ultrasound assisted approach. Ultrason Sonochem 82, 105870. https://doi.org/10.1016/j.ultsonch.2021.105870

Klemm, D., Cranston, E.D., Fischer, D., Gama, M., Kedzior, S.A., Kralisch, D., Kramer, F., Kondo, T., Lindström, T., Nietzsche, S., Petzold-welcke, K., Rauchfuß, F., Association, P.J., 2018. Nanocellulose as a natural source for groundbreaking applications in materials science : Today's state. Materials Today 21, 720–748. https://doi.org/10.1016/j.mattod.2018.02.001

Knorr, D., 1991. Recovery and utilization of chitin and chitosan in food processing waste management. Food technology (Chicago) 45, 114–122.

Ko, J.K., Kim, Y., Ximenes, E., Landisch, M.R., 2015. Effect of liquid hot water pretreatment severity on properties of hardwood lignin and enzymatic hydrolysis of cellulose. Biotechnol Bioeng 112, 252–262.

Koçar, G., Civa, N., 2013. An overview of biofuels from energy crops: Current status and future prospects. Renewable and Sustainable Energy Reviews 28, 900–916. https://doi.org/10.1016/j.rser.2013.08.022

Kontturi, E., Meriluoto, A., Penttila, P.A., Baccile, N., Malho, J.-M., Potthast, A., Rosenau, T., Ruokolainen, J., Serimaa, R., Laine, J., Sixta, H., 2016. Degradation and Crystallization of Cellulose in Hydrogen Chloride Vapor for High-Yield Isolation of Cellulose Nanocrystals. Angewandte Chemie 55, 14455–14458. https://doi.org/https://doi.org/10.1002/anie.201606626

Kou, S.G., Peters, L., Mucalo, M., 2022. Chitosan: A review of molecular structure, bioactivities and interactions with the human body and micro-organisms. Carbohydr Polym 282, 119132. https://doi.org/10.1016/j.carbpol.2022.119132

Kumar, R., Rai, B., Kumar, G., 2019. A simple approach for the synthesis of cellulose nanofiber reinforced Chitosan/PVP bio nanocomposite film for packaging. J Polym Environ 27, 2963–2973. https://doi.org/10.1007/s10924-019-01588-8

Kumar, S., Mukherjee, A., Dutta, J., 2020. Chitosan based nanocomposite films and coatings: Emerging antimicrobial food packaging alternatives. Trends Food Sci Technol 97, 196–209. https://doi.org/10.1016/j.tifs.2020.01.002

Laborie, M.P., Abushammala, H., 2018. Ionic-liquid mediated production of cellulose nanocrystals directly from wood, grass or bioresidues. US2018037702 (A1).

Lambert, S., Wagner, M., Wagner, M., 2017. Environmental performance of bio-based and biodegradable plastics : the road ahead. Chem Soc Rev 46, 6855–6871. https://doi.org/10.1039/C7CS00149E

Lan, W., Wang, S., Zhang, Z., Liang, X., Liu, X., Zhang, J., 2021. Development of red apple pomace extract/chitosan-based films reinforced by TiO2 nanoparticles as a multifunctional packaging material. Int J Biol Macromol 168, 105–115. https://doi.org/10.1016/j.ijbiomac.2020.12.051

Langerwall, J., Schutz, C., Salajkova, M., Noh, J., Park, J.H., Scalia, G., Bergstrom, L., 2014. Cellulose nanocrystal-based materials: from liquid crystal self-assembly and glass formation to multifunctional thin films. NPG Asia Mater 1–12. https://doi.org/10.1038/am.2013.69

Lau, W., Shiran, Y., Bailey, R.M., Cook, E., Stuchtey, M.R., Koskella, J., Velis, C.A., Godfrey, L., Boucher, J., Murphy, M.B., Thompson, R.C., Jankowska, E., Castillo, A.C., Pilditch, T.D., Dixon, B., Koerselman, L., Kosior, E., Favoino, E., Gutberlet, J., Baulch, S., Atreya, M.E., Fischer, D., He, K.K., Petit, M.M., Sumaila, U.R., Neil, E., Bernhofen, M. V., Lawrence, K., Palardy, J.E., 2020. Evaluating scenarios toward zero plastic pollution. Science (1979) 369, 1455–1461. https://doi.org/10.1126/science.aba9475

Lavric, G., Oberlintner, A., Filipova, I., Novak, U., Likozar, B., Urska, V.-B., 2021. Functional nanocellulose, alginate and chitosan nanocomposites designed as active film packaging materials. Polymers (Basel) 13, 2523.

Lee, H. V, Hamid, S.B.A., Zain, S.K., 2014. Conversion of Lignocellulosic Biomass to Nanocellulose: Structure and Chemical Process. The Scientific World Journal 2014. https://doi.org/https://doi.org/10.1155/2014/631013

Li, J., Gao, R., Xiao, S., Gan, W., 2017. Preparation method of super-hydrophobic and oil-absorption nanocellulose aerogel material. CN107199020 (A).

Liimatainen, H., Visanko, M., 2013. Sulfonated cellulose nanofibrils obtained from wood pulp through regioselective oxidative bisulfite pre-treatment. Cellulose 20, 741–749. https://doi.org/10.1007/s10570-013-9865-y

Lin, N., Dufresne, A., 2014. Nanocellulose in biomedicine: Current status and future prospect. Eur Polym J 59, 302–325. https://doi.org/10.1016/j.eurpolymj.2014.07.025

Liu, X., Jiang, Y., Qin, C., Yang, S., Song, X., 2018. Enzyme-assisted mechanical grinding for cellulose nanofibers from bagasse: energy consumption and nanofiber characteristics. Cellulose 25, 7065–7078. https://doi.org/10.1007/s10570-018-2071-1

Long, L., Tian, D., Hu, J., Wang, F., Saddler, J., 2017. A xylanase-aided enzymatic pretreatment facilitates cellulose nanofibrillation. Bioresour Technol 243, 898–904. https://doi.org/10.1016/j.biortech.2017.07.037

López-Bellido, L., Wery, J., López-Bellido, R.J., 2014. Energy crops: Prospects in the context of sustainable agriculture. European Journal of Agronomy 60, 1–12. https://doi.org/10.1016/j.eja.2014.07.001

Luzi, F., Fortunati, E., Jiménez, A., Puglia, D., Pezzolla, D., Gigliotti, G., Kenny, J.M., Chiralt, A., Torre, L., 2016. Production and characterization of PLA_PBS biodegradable blends reinforced with cellulose nanocrystals extracted from hemp fibres. Ind Crops Prod 93, 276–289. https://doi.org/10.1016/j.indcrop.2016.01.045

Lv, S., Zhang, Y., Gu, J., Tan, H., 2018. Soil burial-induced chemical and thermal changes in starch/poly (lactic acid) composites. Int J Biol Macromol 113, 338–344. https://doi.org/10.1016/j.ijbiomac.2018.02.139

Lv, W., Xia, Z., Song, Y., Wang, P., Liu, S., Zhang, Y., Ben, H., Han, G., Jiang, W., 2021. Using microwave assisted organic acid treatment to separate cellulose fiber and lignin from kenaf bast. Ind Crops Prod 171, 113934. https://doi.org/10.1016/j.indcrop.2021.113934

Ma, Z., Garrido-maestu, A., Casey, K., 2017. Application , mode of action , and in vivo activity of chitosan and its micro- and nanoparticles as antimicrobial agents : A review. Carbohydr Polym 176, 257–265. https://doi.org/10.1016/j.carbpol.2017.08.082

Makkar, H., Becker, K., 2009. Jatropha curcas, a promising crop for the generation of biodiesel and value-added coproducts. European Journal of Lipid Science and Technology 111, 773–787. https://doi.org/https://doi.org/10.1002/ejlt.200800244

Malucelli, L.C., Lacerda, L.G., Aure, M., 2017. Preparation, properties and future perspectives of nanocrystals from agro-industrial residues: a review of recent research. Rev Environ Sci Biotechnol 16, 131–145. https://doi.org/10.1007/s11157-017-9423-4

Mandal, A., Chakrabarty, D., 2011. Isolation of nanocellulose from waste sugarcane bagasse (SCB) and its characterization. Carbohydr Polym 86, 1291–1299. https://doi.org/10.1016/j.carbpol.2011.06.030

Mangaraj, S.., Yadav, A., Dash, S.K., Mahanti, N.K., 2018. Application of biodegradable polymers in food packaging industry: A comprehensive review. J Packag Technol Res 3, 77–96. https://doi.org/10.1007/s41783-018-0049-y

Mao, H., Li, S., Tong, S., Hua, F., Chen, J., Meng, Y., Long, J., 2016. Production method of lithium ion battery separator paper. CN105926347 (A).

Mao, H., Wei, C., Gong, Y., Wang, S., Ding, W., 2019. Mechanical and water-resistant properties of eco-friendly chitosan membrane reinforced with cellulose nanocrystals. Polymers (Basel) 11, 166. https://doi.org/10.3390/polym11010166

Maria Pelissari, F., Andrade-Mahecha, M.M., José, P., Cecilia, F., 2017. Nanocomposites based on banana starch reinforced with cellulose nanofibers isolated from banana peels. J Colloid Interface Sci 505, 154–167. https://doi.org/10.1016/j.jcis.2017.05.106

Mariani, C., Cabrini, R., Danin, A., Piffanelli, P., Fricano, A., Gomarasca, S., Dicandilo, M., Grassi, F., Soave, C., 2010. Origin, diffusion and reproduction of the giant reed (Arundo

donax L.): a promising weedy energy crop. Annals of Applied Biology 157, 191–202. https://doi.org/https://doi.org/10.1111/j.1744-7348.2010.00419.x

Marmion, M., Ferone, M.T., Whyte, P., Scannell, A.G.M., 2021. The changing microbiome of poultry meat; from farm to fridge. Food Microbiol 99, 103823. https://doi.org/10.1016/j.fm.2021.103823

Martínez-Sanz, M., Erboz, E., Fontes, C., López-Rubio, A., 2018. Valorization of Arundo donax for the production of high performance lignocellulosic films. Carbohydr Polym 199, 276–285. https://doi.org/10.1016/j.carbpol.2018.07.029

Matarneh, S.K., England, E.M., Scheffler, T.L., Gerrard, D.E., 2017. The conversion of muscle to meat, in: Toldrá, F. (Ed.), Lawrie's Meat Science. Woodhead Publishing, pp. 159–185.

Matei, P.M., Buzón-Durán, L., Pérez-Lebeña, E., Martín-Gil, J., Iacomi, B.M., Ramos-Sánchez, M.C., Martín-Ramos, P., 2020. In vitro antifungal activity of chitosan-polyphenol conjugates against Phytophthora cinnamomi. AgriEngineering 2, 72–77.

Mehdizadeh, T., Langroodi, A.M., 2019. Chitosan coatings incorporated with propolis extract and Zataria multi flora Boiss oil for active packaging of chicken breast meat. Int J Biol Macromol 141, 401–409. https://doi.org/10.1016/j.ijbiomac.2019.08.267

Mehdizadeh, T., Tajik, H., Jafarie, S., Kaboudari, A., 2019. Effect of Salvia officinalis L. extract on chemical, microbial, sensory and shelf life of rainbow trout fillet. Food Sci Biotechnol 28, 1499–1506. https://doi.org/10.1007/s10068-019-00575-y

Mehrabi, F.A., Sharifi, A., Ahvazi, M., 2021. Effect of chitosan coating containing Nepeta pogonosperma extract on shelf life of chicken fillets during chilled storage. Food Sci Nutr 9, 4517–4528. https://doi.org/https://doi.org/10.1002/fsn3.2429

Messa, L.L., Faez, R., 2020. Spray-dried chitosan/nanocellulose microparticles: synergistic effects for the sustained release of NPK fertilizer. Cellulose 27, 10077–10093. https://doi.org/10.1007/s10570-020-03482-2

Miao, C., Hamad, W.Y., 2013. Cellulose reinforced polymer composites and nanocomposites: A critical review. Cellulose 20, 2221–2262. https://doi.org/10.1007/s10570-013-0007-3

Mir, N.A., Rafiq, A., Kumar, F., Singh, V., Shukla, V., 2017. Determinants of broiler chicken meat quality and factors affecting them: a review. J Food Sci Technol 54, 2997–3009. https://doi.org/10.1007/s13197-017-2789-z

Mishra, V., Jana, A.K., Maiti, M., Gupta, A., 2017. Enhancement in multiple lignolytic enzymes production for optimized lignin degradation and selectivity in fungal pretreatment of sweet sorghum bagasse. Bioresour Technol 236, 49–59. https://doi.org/10.1016/j.biortech.2017.03.148

Miteluț, A.C., Popa, E.E., Popescu, P.A., Rapa, M., Popa, M.E., 2019. Soil ecotoxicity assessment after biodegradation of some polymeric materials. Agronomy Series of Scientific Research/Lucrari Stiintifice Seria Agronomie 61, 538–543.

Mohaiyiddin, M.S., Lin, O.H., Owi, W.T., Chan, C.H., Chia, C.H., Zakaria, S., Villagracia, A.R., Akil, H.M., 2016. Characterization of nanocellulose recovery from Elaeis guineensis frond for sustainable development. Clean Technol Environ Policy 18, 2503–2512. https://doi.org/10.1007/s10098-016-1191-2

Mohaiyiddin, M.S., Ong, H.L., Othman, M.B.H., Julkapli, N.Muhd., Villagracia, A.R.C., Akil, H.Md., 2018. Swelling behavior and chemical stability of chitosan/nanocellulose biocomposites. Polym Compos 39, E561–E572. https://doi.org/https://doi.org/10.1002/pc.24712

Mondragon, G., Santamaria-Echart, A., Hormaiztegui, M.E.V., Arbelaiz, A., Peña-Rodriguez, C., Mucci, V., Corcuera, M., Aranguren, M.I., Eceiza, A., 2018. Nanocomposites of Waterborne Polyurethane Reinforced with Cellulose Nanocrystals from Sisal Fibres. J Polym Environ 26, 1869–1880. https://doi.org/10.1007/s10924-017-1089-z

Montero, Y., Souza, A.G., Oliveira, É.R., Rosa, S., 2021. Nanocellulose functionalized with cinnamon essential oil: A potential application in active biodegradable packaging for strawberry. Sustainable Materials and Technologies 29, e00289. https://doi.org/10.1016/j.susmat.2021.e00289

Morais, J.P.S., Freitas, M. De, De, M., Souza, M. De, Dias, L., Magalhães, D., Ribeiro, A., 2013. Extraction and characterization of nanocellulose structures from raw cotton linter. Carbohydr Polym 91, 229–235. https://doi.org/10.1016/j.carbpol.2012.08.010

Morán, J.I., Alvarez, V.A., Cyras, V.P., Vásquez, A., 2008. Extraction of cellulose and preparation of nanocellulose from sisal fibers. Cellulose 15, 149–159. https://doi.org/10.1007/s10570-007-9145-9

Mora-Pale, M., Meli, L., Doherty, T. V., Linhardt, R.J., Dordick, J.S., 2011. Room temperature ionic liquids as emerging solvents for the pretreatment of lignocellulosic biomass. Biotechnol Bioeng 108, 1229–1245.

Morone, A., Chakrabarti, T., Pandey, R.A., 2017. Assessment of alkaline peroxide-assisted wet air oxidation pretreatment for rice straw and its effect on enzymatic hydrolysis. Cellulose 24, 4885–4898. https://doi.org/10.1007/s10570-017-1451-2

Mujtaba, M., Morsi, R.E., Kerch, G., Elsabee, M.Z., Kaya, M., Labidi, J., Mahmood, K., 2019. Current advancements in chitosan-based fi lm production for food technology ; A review. Int J Biol Macromol 121, 889–904. https://doi.org/10.1016/j.ijbiomac.2018.10.109

Mujtaba, M., Salaberria, A.M., Andres, M.A., Kaya, M., Gunyakti, A., Labidi, J., 2017. Utilization of flax (Linum usitatissimum) cellulose nanocrystals as reinforcing material for

chitosan films. Int J Biol Macromol 104, 944–952. https://doi.org/10.1016/j.ijbiomac.2017.06.127

Muxika, A., Etxabide, A., Uranga, J., Guerrero, P., Caba, K. De, 2017. Chitosan as a bioactive polymer : Processing , properties and applications. Int J Biol Macromol 105, 1358–1368. https://doi.org/10.1016/j.ijbiomac.2017.07.087

Naderi, A., Lindstrom, T., Sundstrom, J., 2014. Carboxymethylated nanofibrillated cellulose: rheological studies. Cellulose 21, 1561–1571. https://doi.org/10.1007/s10570-014-0192-8

Naduparambath, S., T.V., J., Shaniba, V., M.P., S., Balan, A.K., Purushothaman, E., 2018. Isolation and characterisation of cellulose nanocrystals from sago seed shells. Carbohydr Polym 180, 13–20. https://doi.org/10.1016/j.carbpol.2017.09.088

Nair, J.R., Bella, F., Angulakshmi, N., Manuel, A., Gerbaldi, C., 2016. Nanocellulose-laden composite polymer electrolytes for high performing lithium – sulphur batteries. Energy Storage Mater 3, 69–76. https://doi.org/10.1016/j.ensm.2016.01.008

Nascimento, D.M., Nunes, Y.L., Figueirêdo, M.C.B., Azeredo, H.M.C. de, Aouada, F.A., Feitosa, J.P.A., Rosa, M.F., Dufresne, A., 2018. Nanocellulose nanocomposite hydrogels:technological and environmental issues. Green Chemistry 20, 2428–2448. https://doi.org/10.1039/c8gc00205c

Nasri-Nasrabadi, B., Behzad, T., Bagheri, R., 2014. Extraction and characterization of rice straw cellulose nanofibers by an optimized chemomechanical method. J Appl Polym Sci 131, 40063. https://doi.org/10.1002/app.40063

Nechyporchuk, O., Belgacem, M.N., Bras, J., 2016. Production of cellulose nanofibrils: A review of recent advances. Ind Crops Prod 93, 2–25. https://doi.org/10.1016/j.indcrop.2016.02.016

Nelson, K., Banerjie, A.K., Retsina, T., 2017. Nanocellulose-polystyrene composites. US2017015822 (A1).

Ng, H.-M., Sin, L.T., Bee, S.-T., Tee, T.-T., Rahmat, A.R., 2017. Review of Nanocellulose Polymer Composites Characteristics and Challenges. Polymer - Plastics Technology and Engineering 56, 687–731. https://doi.org/10.1080/03602559.2016.1233277

Noguchi, Y., Homma, I., Matsubara, Y., 2017. Complete nanofibrillation of cellulose prepared by phosphorylation. Cellulose 24, 1295–1305. https://doi.org/10.1007/s10570-017-1191-3

Norrrahim, M.N.F., Nurazzi, N.M., Jenol, M.A., Farid, M.A.A., Janudin, N., Ujang, F.A., Yasim-Anuar, T.A.T., Najmuddin, S.U.F.S., Ilyas, R.A., 2021. Emerging development of nanocellulose as an antimicrobial material: an overview. Mater Adv 2, 3538–3551. https://doi.org/10.1039/d1ma00116g

Noshirvani, N., Ghanbarzadeh, B., Rezaei, R., Hashemi, M., 2017. Novel active packaging based on carboxymethyl cellulose-chitosan -ZnO NPs nanocomposite for increasing the shelf life of bread. Food Packag Shelf Life 11, 106–114. https://doi.org/10.1016/j.fpsl.2017.01.010

Nouri, A., Yaraki, M.T., Ghorbanpour, M., Agarwal, S., Gupta, V.K., 2017. Enhanced Antibacterial effect of chitosan film using Montmorillonite/CuO nanocomposite. Int J Biol Macromol 109, 1219–1231. https://doi.org/10.1016/j.ijbiomac.2017.11.119

O'Neil, M.J., 2013. The Merck Index - An Encyclopedia of Chemicals, Drugs, and Biologicals, 15th ed. Chemistry, Royal Society of, Cambridge, UK.

Onkarappa, H.S., Prakash, G.K., Pujar, G.H., Kumar, C.R.R., Latha, M.S., Betageri, V.S., 2020. Hevea brasiliensis mediated synthesis of nanocellulose: Effect of preparation methods on morphology and properties. Int J Biol Macromol 160, 1021–1028. https://doi.org/10.1016/j.ijbiomac.2020.05.188

Otoni, C.G., Azeredo, H.M.C., Mattos, B.D., Beaumont, M., Correa, D.S., Rojas, O.J., 2021. The food–materials nexus: Next generation bioplastics and advanced materials from agri-food residues. Advanced Materials 33, 2102520. https://doi.org/10.1002/adma.202102520

Oun, A.A., Rhim, J.W., 2015. Preparation and characterization of sodium carboxymethyl cellulose/cotton linter cellulose nanofibril composite films. Carbohydr Polym 127, 101–109. https://doi.org/10.1016/j.carbpol.2015.03.073

Öztürk, İ., Irmak, S., Hesenof, A., Erbatur, O., 2010. Hydrolysis of kenaf (Hibiscus cannabinus L.) stems by catalytical thermal treatment in subcritical water. Biomass Bioenergy 34, 1578–1585. https://doi.org/10.1016/j.biombioe.2010.06.005

Pacáková, V., Virt, J., 2005. Plastics, in: Worsfold, P., Townshend, A., Poole, C. (Eds.), Encyclopedia of Analytical Science. Elsevier B.V, pp. 180–187. https://doi.org/https://doi.org/10.1016/B0-12-369397-7/00467-2

Paomephan, P., Assavanig, A., Chaturongakul, S., 2018. Insight into the antibacterial property of chitosan nanoparticles against Escherichia coli and Salmonella Typhimurium and their application as vegetable wash disinfectant. Food Control 86, 294–301. https://doi.org/10.1016/j.foodcont.2017.09.021

Pateiro, M., Munekata, P.E.S., Sant´Ana, A.S., Domínguez, R., Rodríguez-Lázaro, D., Lorenzo, J.M., 2021. Application of essential oils as antimicrobial agents against spoilage and pathogenic microorganisms in meat products. Int J Food Microbiol 337, 108966. https://doi.org/10.1016/j.ijfoodmicro.2020.108966

Patel, D.K., Dutta, S.D., Ganguly, K., Lim, K., 2021. Multifunctional bioactive chitosan/cellulose nanocrystal scaffolds eradicate bacterial growth and sustain drug delivery. Int J Biol Macromol 170, 178–188. https://doi.org/10.1016/j.ijbiomac.2020.12.145

Peng, B.L., Dhar, N., Liu, H.L., Tam, K.C., 2011. Chemistry and applications of nanocrystalline cellulose and its derivatives: A nanotechnology perspective. Can J Chem Eng 89, 1191–1206. https://doi.org/https://doi.org/10.1002/cjce.20554

Pereda, M., Dufresne, A., Aranguren, M.I., Marcovich, N.E., 2014. Polyelectrolyte films based on chitosan/olive oil and reinforced with cellulose nanocrystals. Carbohydr Polym 101, 1018–1026. https://doi.org/10.1016/j.carbpol.2013.10.046

Phanthong, P., Guan, G., Ma, Y., Hao, X., Abudula, A., 2016. Effect of ball milling on the production of nanocellulose using mild acid hydrolysis method. J Taiwan Inst Chem Eng 60, 617–622. https://doi.org/10.1016/j.jtice.2015.11.001

Phan-Xuan, T., Thuresson, A., Skepo, M., Labrador, A., Bordes, R., Matic, A., 2016. Aggregation behavior of aqueous cellulose nanocrystals: the effect of inorganic salts. Cellulose 23, 3653–3663. https://doi.org/10.1007/s10570-016-1080-1

Pires, J.R.A., de Souza, V.G.L., Fernando, A.L., 2019a. Production of nanocellulose from lignocellulosic biomass wastes: Prospects and limitations, Lecture Notes in Electrical Engineering. https://doi.org/10.1007/978-3-319-91334-6_98

Pires, J.R.A., de Souza, V.G.L., Fernando, A.L., 2018. Chitosan/montmorillonite bionanocomposites incorporated with rosemary and ginger essential oil as packaging for fresh poultry meat. Food Packag Shelf Life 17. https://doi.org/10.1016/j.fpsl.2018.06.011

Pires, J.R.A., Paula, C.D. De, Gomes, V.G.L., Fernando, A.L., Coelhoso, I., 2021. Understanding the barrier and mechanical behavior of different nanofillers in chitosan films for food packaging. Polymers (Basel) 13, 721. https://doi.org/10.3390/polym13050721

Pires, J.R.A., Souza, V.G.L., Fernando, A.L., 2019b. Valorization of energy crops as a source for nanocellulose production – Current knowledge and future prospects. Ind Crops Prod 140. https://doi.org/10.1016/j.indcrop.2019.111642

Pires, J.R.A., Souza, V.G.L., Fernando, A.L., 2019c. Ecofriendly strategies for the production of nanocellulose from agro-industrial wastes. European Biomass Conference and Exhibition Proceedings 1781–1784.

Pires, João R. A., Souza, V.G.L., Fernando, A.L., 2019. Valorization of energy crops as a source for nanocellulose production – Current knowledge and future prospects. Ind Crops Prod 140, 111642. https://doi.org/10.1016/j.indcrop.2019.111642

Pires, J.R.A., Souza, V.G.L., Fuciños, P., Pastrana, L., Fernando, A.L., 2022a. Methodologies to assess the biodegradability of bio-based polymers — Current knowledge and existing

gaps. Polymers (Basel) 14, 1359. https://doi.org/https://doi.org/10.3390/polym14071359

Pires, J.R.A., Souza, V.G.L., Gomes, L.A., Coelhoso, I.M., Godinho, M.H., Fernando, A.L., 2022b. Micro and nanocellulose extracted from energy crops as reinforcement agents in chitosan films. Ind Crops Prod 186, 115247. https://doi.org/10.1016/j.indcrop.2022.115247

Plackett, D. V, Letchford, K., Jackson, J.K., Burt, H.M., Jackson, J., Burt, H., 2014. A review of nanocellulose as a novel vehicle for drug delivery. Nord Pulp Paper Res J 29, 105–118.

Pola, L., Collado, S., Oulego, P., Díaz, M., 2022. Kraft black liquor as a renewable source of value-added chemicals. Chemical Engineering Journal 448, 137728. https://doi.org/10.1016/j.cej.2022.137728

Poletto, M., Zattera, A.J., Forte, M.M.C., Santana, R.M.C., 2012. Thermal decomposition of wood: Influence of wood components and cellulose crystallite size. Bioresour Technol 109, 148–153. https://doi.org/10.1016/j.biortech.2011.11.122

Poonguzhali, R., Basha, S.K., Kumari, V.S., 2017. Synthesis and characterization of chitosan-PVP-nanocellulose composites for in-vitro wound dressing application. Int J Biol Macromol 105, 111–120. https://doi.org/10.1016/j.ijbiomac.2017.07.006

Qazanfarzadeh, Z., Kadivar, M., 2016. Properties of whey protein isolate nanocomposite films reinforced with nanocellulose isolated from oat husk. Int J Biol Macromol 91, 1134–1140. https://doi.org/10.1016/j.ijbiomac.2016.06.077

Qian, S., Zhang, H., Yao, W., Sheng, K., 2018. Effects of bamboo cellulose nanowhisker content on the morphology, crystallization, mechanical, and thermal properties of PLA matrix biocomposites. Composites Part B 133, 203–209. https://doi.org/10.1016/j.compositesb.2017.09.040

Qin, Y., Li, P., 2020. Antimicrobial chitosan conjugates: Current synthetic strategies and potential applications. International Journal of Molecular Science 21, 499.

Qin, Z.-H., Mou, J., Chao, C.Y.H., Chopra, S.S., Daoud, W., Leu, S., Ning, Z., Tso, C.Y., Chan, C.K., Tang, S., Hathi, Z.J., Haque, M.A., Wang, X., Lin, C.S.K., 2021. Biotechnology of plastic waste degradation, recycling, and valorization: current advances and future perspectives. ChemSusChem 14, 4103–4114. https://doi.org/10.1002/cssc.202100752

Rahman, M., Mosta, S.B., Paatero, J. V, Lahdelma, R., 2014. Extension of energy crops on surplus agricultural lands: A potentially viable option in developing countries while fossil fuel reserves are diminishing. Renewable and Sustainable Energy Reviews 29, 108–119. https://doi.org/10.1016/j.rser.2013.08.092

Rambabu, N., Panthapulakkal, S., Sain, M., Dalai, A.K., 2016. Production of nanocellulose fibers from pinecone biomass: Evaluation and optimization of chemical and mechanical

treatment conditions on mechanical properties of nanocellulose films. Ind Crops Prod 83, 746–754. https://doi.org/10.1016/j.indcrop.2015.11.083

Rashid, S., Dutta, H., 2020. Characterization of nanocellulose extracted from short, medium and long grain rice husks. Ind Crops Prod 154, 112627. https://doi.org/10.1016/j.indcrop.2020.112627

Rauchfuss, U., Settmacher, D., Klemm, W., Fried, T., Richter, K., Petzold-Welke, R., 2018. Medical implant based on nanocellulose. US2018221129 (A1).

Ravindran, R., Jaiswal, A.K., 2016. A comprehensive review on pre-treatment strategy for lignocellulosic food industry waste: Challenges and opportunities. Bioresour Technol 199, 92–102. https://doi.org/10.1016/j.biortech.2015.07.106

Ribeiro-Santos, R., Melo, N.R. de, Andrade, M., Sanches-Silva, A., 2017. Potential of migration of active compounds from protein-based films with essential oils to a food and a food simulant. Packaging Technology and Science 30, 791–798.

Rizzieri, R., Mahadevan, L., Vaziri, A., Donald, A., 2006. Superficial wrinkles in stretched, drying gelatin films. Langmuir 22, 3622–3626.

Robertson, G.L., 2013. Packaging of flesh foods, in: Food Packaging: Principles and Practice. CRC Press, pp. 445–476.

Rong, S.Y., Mubarak, N.M., Tanjung, F.A., 2017. Structure-property relationship of cellulose nanowhiskers reinforced chitosan biocomposite films. J Environ Chem Eng 5, 6132–6136. https://doi.org/10.1016/j.jece.2017.11.054

Rosenboom, J., Langer, R., Traverso, G., 2022. Bioplastics for a circular economy. Nat Rev Mater 7, 117–137. https://doi.org/10.1038/s41578-021-00407-8

Rosmini, M.R., Perlo, F., Pérez-Alvarez, J.A., Pagán-Moreno, M.J., Gago-Gago, A., López-Santoveña, F., Aranda-Catalá, V., 1996. TBA test by an extractive method applied to 'paté.' Meat Sience 42, 103–110. https://doi.org/10.1016/0309-1740(95)00010-0

Saito, T., Kimura, S., Nishiyama, Y., Isogai, A., 2007. Cellulose nanofibers prepared by TEMPO-mediated oxidation of native cellulose. Biomacromolecules 8, 2485–2491. https://doi.org/10.1021/bm0703970

Salamon, D., 2014. Chapter 6 - Advanced Ceramics, in: Shen, J.Z., Kosmač, T. (Eds.), Advanced Ceramics for Dentistry. Elsevier B.V, pp. 103–122. https://doi.org/https://doi.org/10.1016/C2011-0-07169-7

Salari, M., Sowti, M., Rezaei, R., Ghanbarzadeh, B., 2018. Development and evaluation of chitosan based active nanocomposite fi lms containing bacterial cellulose nanocrystals and silver nanoparticles. Food Hydrocoll 84, 414–423. https://doi.org/10.1016/j.foodhyd.2018.05.037

Salehpour, S., Jonoobi, M., Ahmadzadeh, M., Siracusa, V., Rafieian, F., Oksman, K., 2018. Biodegradation and ecotoxicological impact of cellulose nanocomposites in municipal solid waste composting. Int J Biol Macromol 111, 264–270. https://doi.org/10.1016/j.ijbiomac.2018.01.027

Samapundo, S., Baenst, I. De, Aerts, M., Cnockaert, M., Devlieghere, F., Damme, P. Van, 2019. Tracking the sources of psychrotrophic bacteria contaminating chicken cuts during processing. Food Microbiol 81, 40–50. https://doi.org/10.1016/j.fm.2018.06.003

Sánchez-González, L., Cháfer, M., González-Martínez, C., Chiralt, A., Desobry, S., 2011a. Study of the release of limonene present in chitosan films enriched with bergamot oil in food simulants. J Food Eng 105, 138–143. https://doi.org/10.1016/j.jfoodeng.2011.02.016

Sánchez-González, L., Cháfer, M., Hernández, M., Chiralt, A., 2011b. Antimicrobial activity of polysaccharide fi lms containing essential oils. Food Control 22, 1302–1310. https://doi.org/10.1016/j.foodcont.2011.02.004

Santmartí, A., Lee, K.-Y., 2018. Crystallinity and thermal stability of nanocellulose, in: Nanocellulose and Sustainability. CRC Press, pp. 67–86.

Seabra, A.B., Bernardes, J.S., Fávaro, W.J., Paula, A.J., 2018. Cellulose nanocrystals as carriers in medicine and their toxicities: A review. Carbohydr Polym 181, 514–527. https://doi.org/10.1016/j.carbpol.2017.12.014

Sedlaříková, J., Doležalová, M., Egner, P., Pavlačková, J., Krejčí, J., Rudolf, O., Peer, P., 2017. Effect of Oregano and Marjoram Essential Oils on the Physical and Antimicrobial Properties of Chitosan Based Systems. Int J Polym Sci. https://doi.org/https://doi.org/10.1155/2017/2593863

Shankar, S., Rhim, J., 2018. Bionanocomposite films for food packaging applications. Reference Module in Food Science 1–10. https://doi.org/10.1016/B978-0-08-100596-5.21875-1

Sharma, B., Malik, P., Jain, P., 2018. Biopolymer reinforced nanocomposites : A comprehensive review. Mater Today Commun 16, 353–363. https://doi.org/10.1016/j.mtcomm.2018.07.004

Sharma, H.K., Xu, C., Qin, W., 2019. Biological pretreatment of lignocellulosic biomass for biofuels and bioproducts : An overview. Waste Biomass Valorization 10, 235–251. https://doi.org/10.1007/s12649-017-0059-y

Sharma, S., Barkauskaite, S., Jaiswal, A.K., Jaiswal, S., 2021. Essential oils as additives in active food packaging. Food Chem 343, 128403.

Shirkavand, E., Baroutian, S., Gapes, D.J., Young, B.R., 2017. Pretreatment of radiata pine using two white rot fungal strains Stereum hirsutum and Trametes versicolor. Energy Convers Manag 142, 13–19. https://doi.org/10.1016/j.enconman.2017.03.021

Shojaee-aliabadi, S., Amin, M., Hosseini, H., 2014. Characterization of nanobiocomposite kappa-carrageenan film with Zataria multiflora essential oil and nanoclay. Int J Biol Macromol 69, 282–289. https://doi.org/10.1016/j.ijbiomac.2014.05.015

Silvério, H.A., Neto, W.P.F., Dantas, N.O., Pasquini, D., 2013. Extraction and characterization of cellulose nanocrystals from corncob for application as reinforcing agent in nanocomposites. Ind Crops Prod 44, 427–436. https://doi.org/10.1016/j.indcrop.2012.10.014

Sims, R., Hastings, A., Schlamadinger, B., Taylor, G., Smith, P., 2006. Energy crops: Current status and future prospects. Glob Chang Biol 12, 2054–2076. https://doi.org/https://doi.org/10.1111/j.1365-2486.2006.01163.x

Sindhu, R., Binod, P., Pandey, A., 2016. Biological pretreatment of lignocellulosic biomass – An overview. Bioresour Technol 199, 76–82. https://doi.org/10.1016/j.biortech.2015.08.030

Singh, J., Suhag, M., Dhaka, A., 2015. Augmented digestion of lignocellulose by steam explosion, acid and alkaline pretreatment methods: A review. Carbohydr Polym 117, 624–631. https://doi.org/10.1016/j.carbpol.2014.10.012

Singh, P., Wani, A.A., Saengerlaub, S., Langowski, H.-C., 2011. Understanding critical factors for the quality and shelf-life of MAP fresh meat: A Review. Crit Rev Food Sci Nutr 51, 146–177. https://doi.org/10.1080/10408390903531384

Singh, S., Bharadwaja, S.T.P., Yadav, P.K., Moholkar, V.S., Goyal, A., 2014. Mechanistic investigation in ultrasound-assisted (Alkaline) delignification of Parthenium hysterophorus biomass. Ind Eng Chem Res 53, 14241–14252.

Singleton, V.L., Orthofer, R., Lamuela-Raventós, R.M., 1999. Analysis of total phenols and other oxidation substrates and antioxidants by means of folin-ciocalteu reagent, in: Methods in Enzymology. Elsevier B.V, pp. 152–178.

Sirviö, J.A., Visanko, M., Liimatainen, H., 2015. Deep eutectic solvent system based on choline chloride-urea as a pre-treatment for nanofibrillation of wood cellulose. Green Chemistry 17, 3401–3406. https://doi.org/10.1039/c5gc00398a

Slavutsky, A.M., Bertuzzi, M.A., 2014. Water barrier properties of starch films reinforced with cellulose nanocrystals obtained from sugarcane bagasse. Carbohydr Polym 110, 53–61. https://doi.org/10.1016/j.carbpol.2014.03.049

Soest, P.J. Van, 1963. Use of detergents in the analysis of fibrous feeds. 2. A rapid method for the determination of fiber and lignin. Journal of the Association of Official Agricultural Chemists 46, 829–835.

Song, L., Yu, H., Zhang, X., 2013. Biological pretreatment under non-sterile conditions for enzymatic hydrolysis of corn stover. Bioresources 8, 3802–3816.

Souza, A.G. De, Rocha, D.B., Kano, F.S., Rosa, S., 2019. Valorization of industrial paper waste by isolating cellulose nanostructures with different pretreatment methods. Resour Conserv Recycl 143, 133–142. https://doi.org/10.1016/j.resconrec.2018.12.031

Souza, V.G.L., 2015. Thesis plan proposal: Development of a noval bionanocomposite based on Chitosan/MMT with antioxidant activity for food appliance.

Souza, V.G.L., Alves, M.M., Santos, C.F., Ribeiro, I.A.C., Rodrigues, C., Coelhoso, I., Fernando, A.L., 2021. Biodegradable chitosan films with ZnO nanoparticles and characterization. Coatings 11, 646.

Souza, V.G.L., Fernando, A.L., 2016. Nanoparticles in food packaging: Biodegradability and potential migration to food — A review. Food Packag Shelf Life 8, 63–70. https://doi.org/10.1016/j.fpsl.2016.04.001

Souza, V.G.L., Fernando, A.L., Pires, J.R.A., Rodrigues, P.F., Lopes, A.A.S., Fernandes, F.M.B., 2017. Physical properties of chitosan films incorporated with natural antioxidants. Ind Crops Prod 107. https://doi.org/10.1016/j.indcrop.2017.04.056

Souza, V.G.L., Mello, I.P., Khalid, O., Pires, J.R.A., Rodrigues, C., Alves, M.M., Santos, C., Luisa Fernando, A., Coelhoso, I., 2022. Strategies to improve the barrier and mechanical properties of pectin films for food packaging: Comparing nanocomposites with bilayers. Coatings 12, 108.

Souza, V.G.L., Pires, J.R.A., Rodrigues, C., Coelhoso, I.M., Fernando, A.L., 2020a. Novel approaches for chitin/ chitosan composites in packaging industry, in: Chitin-and Chitosan-Based Biocomposites for Food Packaging. CRC Press, p. 87. https://doi.org/10.1201/9780429299605-8

Souza, V.G.L., Pires, J.R.A., Rodrigues, C., Coelhoso, I.M., Fernando, A.L., 2020b. Chitosan composites in packaging industry — Current trends and future challenges. Polymers (Basel) 12, 417. https://doi.org/10.3390/polym12020417

Souza, V.G.L., Pires, J.R.A., Rodrigues, C., Rodrigues, P.F., Lopes, A., Silva, R.J., Caldeira, J., Duarte, M.P., Fernandes, F.B., Coelhoso, I.M., Fernando, A.L., 2019a. Physical and morphological characterization of chitosan/montmorillonite films incorporated with ginger essential oil. Coatings 9. https://doi.org/10.3390/coatings9110700

Souza, V.G.L., Pires, J.R.A., Rodrigues, P.F., Lopes, A.A.S., Fernandes, F.M.B., Duarte, M.P., Coelhoso, I.M., Fernando, A.L., 2018a. Bionanocomposites of chitosan/montmorillonite incorporated with Rosmarinus officinalis essential oil: Development and physical characterization. Food Packag Shelf Life 16. https://doi.org/10.1016/j.fpsl.2018.03.009

Souza, Victor G. L., Pires, J.R.A., Torrico, É., Coelhoso, I.M., Paula Duarte, M., Luisa Fernando, A., 2019. Activity of chitosan-montmorillonite bionanocomposites incorporated with

rosemary essential oil: From in vitro assays to application in fresh poultry meat. Food Hydrocoll 89, 241–252. https://doi.org/10.1016/j.foodhyd.2018.10.049

Souza, V.G.L., Pires, J.R.A., Vieira, É.T., Coelhoso, I.M., Duarte, M.P., Fernando, A.L., 2019b. Activity of chitosan-montmorillonite bionanocomposites incorporated with rosemary essential oil: From in vitro assays to application in fresh poultry meat. Food Hydrocoll 89. https://doi.org/10.1016/j.foodhyd.2018.10.049

Souza, V.G.L., Pires, J.R.A., Vieira, É.T., Coelhoso, I.M., Duarte, M.P., Fernando, A.L., 2018b. Shelf life assessment of fresh poultry meat packaged in novel bionanocomposite of chitosan/montmorillonite incorporated with ginger essential oil. Coatings 8. https://doi.org/10.3390/coatings8050177

Souza, V.G.L., Rodrigues, C., Valente, S., Pimenta, C., Pires, J.R.A., Alves, M.M., Santos, C.F., Coelhoso, I.M., Fernando, A.L., 2020c. Eco-Friendly ZnO/Chitosan bionanocomposites films for packaging of fresh poultry meat. Coatings 10, 110. https://doi.org/10.3390/coatings10020110

Souza, Victor G. L., Rodrigues, P.F., Duarte, M.P., Fernando, A.L., 2018. Antioxidant migration studies in chitosan films incorporated with plant extracts. J Renew Mater 6, 548–558. https://doi.org/10.7569/JRM.2018.634104

Sukyai, P., Anongjanya, P., Bunyahwuthakul, N., Kongsin, K., Harnkarnsujarit, N., Sukatta, U., Sothornvit, R., Chollakup, R., 2018. Effect of cellulose nanocrystals from sugarcane bagasse on whey protein isolate-based films. Food Research International 107, 528–535. https://doi.org/10.1016/j.foodres.2018.02.052

Sundqvist-Andberg, H., Åkerman, M., 2021. Sustainability governance and contested plastic food packaging - An integrative review. J Clean Prod 306, 127111. https://doi.org/10.1016/j.jclepro.2021.127111

Sung, S.H., Chang, Y., Han, J., 2017. Development of polylactic acid nanocomposite films reinforced with cellulose nanocrystals derived from coffee silverskin. Carbohydr Polym 169, 495–503. https://doi.org/10.1016/j.carbpol.2017.04.037

Suranjoy, S., Lim, L., Manickavasagan, A., 2020. Ultrasound-assisted alkali-urea pre-treatment of Miscanthus × giganteus for enhanced extraction of cellulose fiber. Carbohydr Polym 247, 116758. https://doi.org/10.1016/j.carbpol.2020.116758

Surendhiran, D., Chandra, V., Park, J., Chun, B., 2022. Fabrication of chitosan-based food packaging film impregnated with turmeric essential oil (TEO)-loaded magnetic-silica nanocomposites for surimi preservation. Int J Biol Macromol 203, 650–660. https://doi.org/10.1016/j.ijbiomac.2022.01.178

Szymanska-Chargot, M., Ciesla, J., Chylinska, M., Gdula, K., Pieczywek, P.M., Koziol, A., Cieslak, K.J., Zdunek, A., 2018. Effect of ultrasonication on physicochemical properties of

apple based nanocellulose-calcium carbonate composites. Cellulose 25, 4603–4621. https://doi.org/10.1007/s10570-018-1900-6

Talebi, H., Ghasemi, F.A., Ashori, A., 2021. The effect of nanocellulose on mechanical and physical properties of chitosan-based biocomposites. Journal of Elastomers & Plastics 1–20. https://doi.org/10.1177/00952443211017169

Talón, E., Trifkovic, K.T., Nedovic, V.A., Bugarski, B.M., Vargas, M., Chiralt, A., González-martínez, C., 2017. Antioxidant edible films based on chitosan and starch containing polyphenols from thyme extracts. Carbohydr Polym 157, 1153–1161. https://doi.org/10.1016/j.carbpol.2016.10.080

Tarchoun, A.F., Trache, D., Klapotke, T.M., Derradji, M., Bessa, W., 2019. Ecofriendly isolation and characterization of microcrystalline cellulose from giant reed using various acidic media. Cellulose 26, 7635–7651. https://doi.org/10.1007/s10570-019-02672-x

Thakur, M., Sharma, A., Ahlawat, V., Bhattacharya, M., Goswami, S., 2020. Process optimization for the production of cellulose nanocrystals from rice straw derived a-cellulose. Mater Sci Energy Technol 3, 328–334. https://doi.org/10.1016/j.mset.2019.12.005

Thakur, S., Chaudhary, J., Sharma, B., Verma, A., Tamulevicius, S., Thakur, V.K., 2018. Sustainability of bioplastics: opportunities and challenges. Curr Opin Green Sustain Chem 13, 68–75. https://doi.org/10.1016/j.cogsc.2018.04.013

Thomas, B., Raj, M.C., Athira, K.B., Rubiyah, M.H., Joy, J., Moores, A., Drisko, G.L., 2018. Nanocellulose, a Versatile Green Platform: From Biosources to Materials and Their Applications. Chem Rev 118, 11575–11625. https://doi.org/10.1021/acs.chemrev.7b00627

Trache, D., Tarchoun, A.F., Derradji, M., Hamidon, T.S., 2020. Nanocellulose: From fundamentals to advanced applications. Front Chem 8, 392. https://doi.org/10.3389/fchem.2020.00392

Trifol, J., Plackett, D., Sillard, C., Hassager, O., Daugaard, A.E., Bras, J., Szabo, P., 2015. A comparison of partially acetylated nanocellulose, nanocrystalline cellulose, and nanoclay as fillers for high-performance polylactide nanocomposites. J Appl Polym Sci 133.

Tsalagkas, D., Borcsok, Z., Pasztory, Z., Gogate, P., Csoka, L., 2021. Assessment of the papermaking potential of processed Miscanthus × giganteus stalks using alkaline pre-treatment and hydrodynamic cavitation for delignification. Ultrason Sonochem 72, 105462.

Tyl, C., Sadler, G.D., 2017. pH and Titratable Acidity, in: Nielsen, S.S. (Ed.), Food Analysis. Springer, pp. 389–406. https://doi.org/https://doi.org/10.1007/978-3-319-45776-5_22

UN, 2015. Transforming our world: the 2030 agenda for sustainable development.

Ünal, K., Babaoglu, A.S., Karakaya, M., 2014. Effect of oregano, sage and rosemary essential oils on lipid oxidation and color properties of minced beef during refrigerated storage.

Journal of Essential Oil Bearing Plants 17, 797–805. https://doi.org/10.1080/0972060X.2014.956803

USFDA, 2013. GRAS notice inventory N°443, GNR.

Vasylieva, V.A., Barbash, V.O., Yashchenko, O.A., 2020. Preparation and application of nanocellulose from Miscanthus × giganteus to improve the quality of paper for bags. SN Appl Sci 2, 1–12. https://doi.org/10.1007/s42452-020-2529-2

Velmurugan, R., Incharoensakdi, A., 2018. Nanoparticles and Organic Matter: Process and Impact, in: Tripathi, D.K., Ahmad, P., Sharma, S., Chauhan, D.K., Dubey, N.K. (Eds.), Nanomaterials in Plants, Algae, and Microorganisms. Elsevier, pp. 407–428. https://doi.org/https://doi.org/10.1016/C2016-0-00176-6

Velmurugan, R., Muthukumar, K., 2012. Ultrasound-assisted alkaline pretreatment of sugarcane bagasse for fermentable sugar production: Optimization through response surface methodology. Bioresour Technol 112, 293–299. https://doi.org/10.1016/j.biortech.2012.01.168

Verlee, A., Mincke, S., Stevens, C. V, 2017. Recent developments in antibacterial and antifungal chitosan and its derivatives. Carbohydr Polym 164, 268–283. https://doi.org/10.1016/j.carbpol.2017.02.001

Ververis, C., Georghiou, K., Christodoulakis, N., Santas, P., Santas, R., 2004. Fiber dimensions, lignin and cellulose content of various plant materials and their suitability for paper production. Ind Crops Prod 19, 245–254. https://doi.org/10.1016/j.indcrop.2003.10.006

Vilarinho, F., Silva, A.S., Vaz, M.F., Farinha, J.P., Vilarinho, F., Silva, A.S., Vaz, M.F., Farinha, J.P., 2018. Nanocellulose in green food packaging. Crit Rev Food Sci Nutr 58, 1526–1537. https://doi.org/10.1080/10408398.2016.1270254

Vishu, A.B., Varadaraj, M.C., Gowda, L.R., Tharanathan, R.N., 2007. Low molecular weight chitosans — Preparation with the aid of pronase , characterization and their bactericidal activity towards Bacillus cereus and Escherichia coli 1770, 495–505. https://doi.org/10.1016/j.bbagen.2006.12.003

Viuda-Martos, M., Navajas, Y.R., Zapata, E.S., Fernández-López, J., Pérez-Álvarez, J.A., 2009. Antioxidant activity of essential oils of five spice plants widely used in a Mediterranean diet. Flavour Fragr J 25, 13–19. https://doi.org/10.1002/ffj

Vizireanu, S., Panaitescu, D.M., Nicolae, C.A., Frone, A.N., Chiulan, I., Ionita, M.D., Satulu, V., Carpen, L.G., Petrescu, S., Birjega, R., Dinescu, G., 2018. Cellulose defibrillation and functionalization by plasma in liquid treatment. Sci Rep 1–14. https://doi.org/10.1038/s41598-018-33687-2

Wahba, M.I., 2020. Enhancement of the mechanical properties of chitosan. J Biomater Sci Polym Ed 31, 350–375. https://doi.org/10.1080/09205063.2019.1692641

Walker, S., Rothman, R., 2020. Life cycle assessment of bio-based and fossil-based plastic: A review. J Clean Prod 261, 121158. https://doi.org/10.1016/j.jclepro.2020.121158

Wan, A., Xu, Q., Sun, Y., Li, H., 2013. Antioxidant activity of high molecular weight chitosan and N,O-quaternized chitosans. J Agric Food Chem 61, 6921–6928.

Wang, W., Yuan, T., Wang, K., Cui, B., Dai, Y., 2012. Combination of biological pretreatment with liquid hot water pretreatment to enhance enzymatic hydrolysis of Populus tomentosa. Bioresour Technol 107, 282–286. https://doi.org/10.1016/j.biortech.2011.12.116

Wang, Z., Carlsson, D.O., Tammela, P., Hua, K., Zhang, P., Nyholm, L., Strømme, M., Al, W.E.T., 2015. Surface modified nanocellulose fibers yield conducting polymer-based flexible supercapacitors with enhanced capacitances. ACS Nano 9, 7563–7571.

Wang, Z., Yao, Z., Zhou, J., He, M., Jiang, Q., Li, S., Ma, Y., 2019. Isolation and characterization of cellulose nanocrystals from pueraria root residue. Int J Biol Macromol 129, 1081–1089. https://doi.org/10.1016/j.ijbiomac.2018.07.055

Wardhono, E.Y., Pinem, M.P., Kustiningsih, I., Agustina, S., Oudet, F., Lefebvre, C., Clausse, D., Saleh, K., Guénin, E., 2019. Cellulose nanocrystals to improve stability and functional properties of emulsified film based on chitosan nanoparticles and beeswax. Nanomaterials 9, 1–17.

Warner, R.D., 2017. The Eating Quality of Meat—IV Water-Holding Capacity and Juiciness, in: Toldra, F. (Ed.), Lawrie's Meat Science. Woodhead Publishing, pp. 419–459.

Woranuch, S., Yoksan, R., 2013. Eugenol-loaded chitosan nanoparticles: I. Thermal stability improvement of eugenol through encapsulation. Carbohydr Polym 96, 578–585. https://doi.org/10.1016/j.carbpol.2012.08.117

Xu, K., Liu, C., Kang, K., Zheng, Z., Wang, S., 2018. Isolation of nanocrystalline cellulose from rice straw and preparation of its biocomposites with chitosan: Physicochemical characterization and evaluation of interfacial compatibility. Compos Sci Technol 154, 8–17. https://doi.org/10.1016/j.compscitech.2017.10.022

Xu, Y., Atrens, A., Stokes, J.R., 2020. A review of nanocrystalline cellulose suspensions: Rheology , liquid crystal ordering and colloidal phase behaviour. Adv Colloid Interface Sci 275, 102076. https://doi.org/10.1016/j.cis.2019.102076

Xu, Yang, Xu, Yongjian, Chen, H., Gao, M., Yue, X., Ni, Y., 2022. Redispersion of dried plant nanocellulose: A review. Carbohydr Polym 294, 119830. https://doi.org/10.1016/j.carbpol.2022.119830

Yadav, M., Behera, K., Chang, Y.H., Chiu, F.C., 2020. Cellulose nanocrystal reinforced chitosan based UV barrier composite films for sustainable packaging. Polymers (Basel) 12. https://doi.org/10.3390/polym12010202

Yahya, M., Lee, H. V, Zain, S.K., Hamid, S.B.A., Lefakane, T.E., Ndibewu, P.P., Netshiozwi, T.E., Nuradibah, M.A., Sam, S.T., Noriman, N.Z., Samera, S.S., Ismail, H., Nasir, R., Mukhtar, H., Man, Z., Zailani, M., Bakar, A., Ng, P., Chia, C.H., Zakaria, S., Gan, S., Kaco, H., Nadia, F., Padzil, M., Chook, S.W., Toh, G.Y., Lin, O.H., Lim, H.N., Huang, N.M., 2015. Chemical conversion of palm-based lignocellulosic biomass to nano-cellulose: Review. Polymers Research 9, 385. https://doi.org/10.1007/s13398-014-0173-7.2

Yalkowsky, S.H., He, Y., Jain, P., 2010. Handbook of Aqueous Solubility Data, 2nd ed. CRC Press.

Yang, H., Yan, R., Chen, H., Zheng, C., Lee, D.H., Uni, V., V, N.D., March, R. V, Re, V., Recei, M., September, V., 2006. In-depth investigation of biomass pyrolysis based on three major components: Hemicellulose, cellulose and lignin. Energy & Fuels 388–393.

Yang, J., Wang, X., Shen, B., Hu, Z., Xu, L., Yang, S., 2020. Lignin from energy plant (Arundo donax): Pyrolysis kinetics, mechanism and pathway evaluation. Renew Energy 161, 963–971. https://doi.org/10.1016/j.renene.2020.08.024

Yang, X., Han, F., Xu, C., Jiang, S., Huang, L., Liu, L., 2017. Effects of preparation methods on the morphology and properties of nanocellulose (NC) extracted from corn husk. Ind Crops Prod 109, 241–247. https://doi.org/10.1016/j.indcrop.2017.08.032

Yoo, Y., Youngblood, J., 2019. Functionalized cellulose nanocrystal materials and methods of preparation. US2019092926 (A1).

Youssef, A.M., El-sayed, S.M., 2018. Bionanocomposites materials for food packaging applications : Concepts and future outlook. Carbohydr Polym 193, 19–27. https://doi.org/10.1016/j.carbpol.2018.03.088

Yousuf, B., Sha, O., Kumar, A., 2018. Recent developments in shelf-life extension of fresh-cut fruits and vegetables by application of di ff erent edible coatings : A review. LWT - Food Science and Technology 89, 198–209. https://doi.org/10.1016/j.lwt.2017.10.051

Yu, J., Zhang, J., He, J., Liu, Z., Yu, Z., 2009. Combinations of mild physical or chemical pretreatment with biological pretreatment for enzymatic hydrolysis of rice hull. Bioresour Technol 100, 903–908. https://doi.org/10.1016/j.biortech.2008.07.025

Yuan, G., Chen, X., Li, D., 2016. Chitosan films and coatings containing essential oils: The antioxidant and antimicrobial activity, and application in food systems. Food Research International 89, 117–128. https://doi.org/10.1016/j.foodres.2016.10.004

Yuan, X., Ma, L., Wen, B., Zhou, D., Kuang, M., Yang, W., Cui, Z., 2016. Enhancing anaerobic digestion of cotton stalk by pretreatment with a microbial consortium (MC1). Bioresour Technol 207, 293–301. https://doi.org/10.1016/j.biortech.2016.02.037

Zhang, W., Li, X., Jiang, W., 2020. Development of antioxidant chitosan film with banana peels extract and its application as coating in maintaining the storage quality of apple. Int J Biol Macromol 154, 1205–1214. https://doi.org/10.1016/j.ijbiomac.2019.10.275

Zhang, X., Ismail, B.B., Cheng, H., Jin, T.Z., Qian, M., Ali, S., Liu, D., Guo, M., 2021a. Emerging chitosan-essential oil films and coatings for food preservation - A review of advances and applications. Carbohydr Polym 273, 118616. https://doi.org/10.1016/j.carbpol.2021.118616

Zhang, X., Li, Y., Guo, M., Jin, T.Z., Arabi, S.A., He, Q., Ismail, B.B., Hu, Y., Liu, D., 2021b. Antimicrobial and UV Blocking Properties of Composite Chitosan Films with Curcumin Grafted Cellulose Nanofiber. Food Hydrocoll 112, 106337. https://doi.org/10.1016/j.foodhyd.2020.106337

Zhang, X., Liu, Y., Yong, H., Qin, Y., Liu, Jing, Liu, Jun, 2019. Development of multifunctional food packaging films based on chitosan, TiO2 nanoparticles and anthocyanin-rich black plum peel extract. Food Hydrocoll 94, 80–92. https://doi.org/10.1016/j.foodhyd.2019.03.009

Zhang, X., Yuan, Q., Cheng, G., 2017. Deconstruction of corncob by steam explosion pretreatment: Correlations between sugar conversion and recalcitrant structures. Carbohydr Polym 156, 351–356. https://doi.org/10.1016/j.carbpol.2016.09.044

Zhong, L., Fu, S., Peng, X., Zhan, H., Sun, R., 2012. Colloidal stability of negatively charged cellulose nanocrystalline in aqueous systems. Carbohydr Polym 90, 644–649. https://doi.org/10.1016/j.carbpol.2012.05.091

Zhu, Y., Romain, C., Williams, C.K., 2016. Sustainable polymers from renewable resources. Nature 540, 354–362. https://doi.org/10.1038/nature21001